UNIVERSITÀ DEGLI STUDI DELL'INSUBRIA

PhD Program in Chemical and Environmental Sciences (XXXIII Cycle)

Reconstruction of deglaciation history of Central Italian Alps since Last Glacial Maximum

PhD Thesis

Supervisor: **Prof. Mauro Guglielmin**

Candidate: **Alessandro Longhi**

N°: 720397

ABSTRACT

The analysis and reconstruction of glacial fluctuations after the last glacial maximum and, in particular, during the Holocene allow us to better understand the environmental and climatic changes that have occurred since the Last Glacial Maximum. The knowledge about the timing and extent of the deglaciation after the Last Glacial Maximum in the mountain areas of the European Alps is still limited. For these reasons, 4 study areas have been chosen in the Italian Central Alps to carry out the project: the Forni Area, the Gavia Pass Area, the Stelvio Pass Area, and the Viola Pass Area.

Multiple approaches have been used in the areas in order to obtain deglaciation ages and past glacier extents. The applied methods are the use of Iron Crystallinity Ratio (CRF) of podzols and its calibration in absolute ages, the Schmidt's Hammer R-values on roches moutonneés and its calibration in absolute ages, the cosmogenic techniques dating, and the analysis of peatland cores.

First, a total of 29 podzols were dug, described, and sampled on the flat top of morainic ridges: 13 in the Stelvio Pass Area, 6 in the Viola Pass Area, 8 in the Gavia Area, and 2 in the Forni Area. Whenever possible, samples of undisturbed soil were taken with Kubiëna Boxes. Soil routine analysis (water content, pH, particle size distribution, and LOI) have been processed on the sampled horizons of every soil profile. In addition, chemical analyses were focused on Fe: it has been extracted both with standard dithionite extraction and standard oxalate extraction, and its total content was calculated with a SEM-EDX system. The crystallinity ratio (CRF), a soil weathering index, has been then calculated as $CRF = \frac{Fe_d - Fe_o}{Fe_{tot}}$, where Fed is the iron fraction extracted with dithionite, Feo is the iron fraction extracted with oxalate, and Fetot is the total iron content and calibrated with absolute ages following a logarithmic regression. Applying the calibration curve, it was possible to calculate ages for all soil profiles and different glacial phases. From the undisturbed samples collected in Kubiëna boxes, glass-covered soil thin sections were prepared through impregnation with polystyrene. Thin

sections were described and very high importance was given to micromorphologies related to the presence of permafrost or ice lenses, as this could be related to the origin of podzols.

The absolute ages used in the calibration were mostly derived from peatland and lakes sediment radiocarbon dating and from historical maps.

A second method, the Schmidt's Hammer R-value, has been measured with 25 reads on a total of 400 stations on roches moutonnées: 90 stations in the Forni Area, 171 stations in the Gavia Pass Area, and 139 stations in the Stelvio Pass Area dividing the areas into different geomorphological units. Calibration curves were calculated both in the Forni Area and in the Gavia Pass Area: in the Gavia Pass Area, 4 different curves have been extracted to evaluate the best fitting between the curves calculated using R25 and R5 values from the single station closest to the site of the 14C-dated samples and with the mean R25 and R5 values for all stations within in the unit containing the 14C sample site. In the Forni Area, the calibration curve has been calculated using the R25 values for all stations within the unit containing the 14C sample sites. In both sites, the confidence interval was calculated by applying a linear regression between the maximum and minimum of the R-value (R±Std. Dv.) and the maximum and minimum of the 14C ages.

The third planned method was the dating of the deglaciation of roches moutonneés and of the landslides in Viola Pass Area with cosmogenic techniques. 15 samples have been collected and prepared for 10Be cosmogenic analysis, but due to the Covid-19 outbreak results are not available at the moment.

Moreover, two peatland cores were then further analysed in order to try to extract some paleoclimate informations. To achieve this goal each core was sampled taking out three samples of 1 cm^3 with a vertical span of 1 cm. On these samples routine analysis (water content, pH, particle size distribution, and LOI), together with the analysis of macroremains and mineralogical/petrographical composition analysis were done on the samples. Three absolute ages have been then obtained with 14C on three different cores: RT in the Gavia Pass Area with an age of 5091-4990 cal. BP, TBG1 in the Gavia Pass

Area with an age of 8010-7029 cal. BP, and TBS1 in the Stelvio Pass Area with an age of 7271-7125 cal. BP.

Here, it has been demonstrated how a multidisciplinary approach is needed to understand glacial processes involved in response to past climate change in different and close locations as both the CRF and the SH have been demonstrated suitable methods for dating the glacial history.

Concerning the CRF, it has been demonstrated as a suitable method for dating soils and to have a potential in the reconstruction of glacial phase boundaries, especially if calculated on the Bs horizon because morphological or pedogenetic processes in the A horizon may lead to errors in calculated age. Concerning the SH instead, the calibration curve produced in the Gavia Pass Area suggested that also the SH is a suitable method of reconstructing exposure ages and glacial history even if the SH calibration curve is not universal: the local variation in calibration parameters may be due to site-specific temperature and precipitation. The best calibration curve is calculated using the R25 values for all stations within in the unit containing the 14C sample sites. In the Gavia Pass Area can date glacially-polished bedrock of Late Pleistocene age until 15ka, even if the method generally underestimates the ages when compared to the CRF index of soils and the available 14C dates.

Combining all methods, eleven successive glacial events have been identified and dated before the LIA: 16.7-14.7 ka, 13.7 ka, 12.3-11.8 ka, 11 ka, 10.2-9.5 ka, 9 ka, 7.5ka, 5.5 ka, 4.1 ka, 3.2 ka, and 1.9-1.5 ka. These events were not ubiquitarian, and happened differently in each different study area. In detail, in the Stelvio Pass Area, five successive glacial events have been identified and dated before the LIA: 12.3 ka, 11 ka, 10-9.7 ka, 9 ka, and 7.5ka. In the Viola Pass Area, four successive glacial events have been identified and dated before the LIA instead: 16.7-14.7 ka, 12.3 ka, 11 ka, and 9 ka. Moving to the Gavia Pass Area, seven successive glacial events have been identified and dated before the LIA: 14.7 ka, 13.7 ka, 12.2-11.8 ka, 10.2-9.7 ka, 7.5 ka, 5.5 ka, and 1.9 ka, but the evolution was asynchronous between Mt. Gavia Glacier and Lake Bianco Glacier. Finally, a total of six different glacial phases were identified and dated for the Forni Area before the LIA: 15 ka, 12.2 ka, 9.5 ka, 4.1

ka, 3.2 ka, and 1.5 ka. Some of these events are synchronous in the four study areas, but the extent is different. Comparisons with other glaciers in the Alps showed that the morphology of the catchments (i.e., area, slope, aspect, and maximum altitudes) was more important than proximity in the glacial evolution during the Holocene. Indeed, while in similar glaciers even if located on a different sector of the Alps like the Forni glacier and Triftjegletscher the LIA is the second most expanded advance during all the Holocene in the adjacent Gavia Pass Area its extent is definitely smaller than every other Holocene advances.

Moreover, in the Forni Valley, the LIA was almost equal to the 9.5 Ka phase and therefore a large part of the roches moutonnées were re-covered by ice during the LIA, so that it was possible to date the maximum of the LIA expansion in 1810 AD and to underline probably during that time the glacier was cold-based.

The thin section analysis, in particular the depth of the microfeatures related to permafrost condition and their frequency, allowed us to determine the lowest limit of past permafrost at 2228m a.s.l. in Stelvio Pass area and 2347m a.s.l. in Val Viola and Val Cantone area, respectively ca. 400 m and 330m lower than today.

Moreover, the analysis of precipitation and temperature derived from various proxy data allowed us to identify four different phases of podzolization dated to: 13.5-11.5ka (I phase), 11-9.7ka (II phase), 9.3-8ka (III phase), and 7.7-7.3ka (IV phase). Reconstructed paleoprecipitation and paleotemperature of the four phases of podzolization also allowed us to determine that in Val Cantone there were two different permafrost aggradation periods that were synchronous to podzolization while in Stelvio Pass area (11-9.7ka and 9.3-8ka) and one additional permafrost aggradation period that occurred at 7.7-7.3ka.

The glacial evolution of the four close different areas has been different in time and space, even if some similarities have been shown: it is clear that to better reconstruct the glacial evolution of the Alps, more local data are needed as the deglaciation pattern is not the same everywhere.

INDEX

DISSERTATION STRUCTURE 9
1. INTRODUCTION 10
1.1. PREFACE 10
1.2. STATE OF THE ARTS 11
1.2.1. Paleoclimate after the LGM 11
1.2.2. Glacial Evolution after the LGM in the Alps 14
1.2.3. Absolute dating techniques 17
1.2.4. Relative dating techniques 20
1.3. AIMS 23
1.4. CONTRIBUTION TO SCIENTIFIC PAPERS 24
2. STUDY AREA 25
2.1. FORNI GLACIER AREA 25
2.1.1. Geography and Climate 25
2.1.2. Geology and Geomorphology 27
2.2. GAVIA PASS AREA 29
2.2.1. Geography and Climate 29
2.2.2. Geology and Geomorphology 30
2.3. STELVIO PASS AREA 32
2.3.1. Geography and Climate 32
2.3.2. Geology and Geomorphology 33
2.4. VIOLA PASS AREA 36
2.4.1. Geography and Climate 36
2.4.2. Geology and Geomorphology 37
3. METHODS 40
3.1. FIELD DATA COLLECTION 40
3.1.1. Podzol mapping and site selection 40
3.1.2. Soil Profile description and sampling 41
3.1.3. Lakes sediments collection 44
3.1.4. Schmidt's Hammer 46
3.1.5. Cosmogenic sample collection 47
3.2. LABORATORY ANALYSES 50
3.2.1. Soil Routine Analyses 50
3.2.2. Soil Iron Analysis 51
3.2.3. Soil Macroremains 52

3.2.4. Soil Micromorphology 53
3.2.5. Cores Routine Analyses 53
3.2.6. Cores Macroremains 54
3.2.7. Cores Sand Mineralogical Composition 55
3.2.8. Radiocarbon Datings 56
3.2.9. Cosmogenic Sample Preparation 57
3.3. DATA ANALYSIS 59
3.3.1. Iron Crystallinity Ratio Calibration 59
3.3.2. Schmidt's Hammer R-Values Calibration 61
3.3.3. Glacial Reconstruction 63
4. RESULTS 64
4.1. THE USE OF IRON CHEMICAL ANALYSIS OF PODZOLS TO DATE THE LATE PLEISTOCENE-HOLOCENE DEGLACIATION HISTORY OF THE CENTRAL ITALIAN ALPS 64
4.2. SOIL MICROMORPHOLOGY AS TOOL FOR THE PAST PERMAFROST RECONSTRUCTION AND PALEOCLIMATIC VARIATIONS 79
4.2.1. Abstract 79
4.2.2. Introduction 80
4.2.3. Study Area 81
4.2.3.1. Stelvio Pass 82
4.2.3.2. Val Cantone 82
4.2.4. Methods 83
4.2.4.1. Field Work 83
4.2.4.2. Laboratory Work: Microscopic Analyses 84
4.2.4.3. Climatic Reconstruction and Soil Dating 84
4.2.5. Results 84
4.2.5.1. Soil Description 84
4.2.5.2. Micromorphology 85
4.2.6. Discussion 87
4.2.6.1. Evidences of Cryogenic Processes 87
4.2.6.2. Podzol and Climatic Conditions 88
4.2.7. Conclusions 91
4.2.8. Acknowledgements 91
4.2.9. References 92
4.2.10. Pictures and Tables 99

4.3. RECONSTRUCTION OF THE GLACIAL HISTORY AFTER THE LAST GLACIAL MAXIMUM IN THE ITALIAN CENTRAL ALPS USING SCHMIDT'S HAMMER R-VALUES AND CRYSTALLINITY RATIO INDICES OF SOILS. 107
4.4. THE GLACIAL HISTORY SINCE THE LAST GLACIAL MAXIMUM IN THE FORNI VALLEY (ITALIAN CENTRAL ALPS). RECONSTRUCTION BASED ON SCHMIDT'S HAMMER R-VALUES AND CRYSTALLINITY RATIO INDICES OF SOILS. 116
4.4.1. Abstract 116
4.4.2. Introduction 117
4.4.3. Study Area 118
4.4.4. Methods 119
4.4.4.1. Soil Analysis 119
4.4.4.2. Schmidt's Hammer Measurements 120
4.4.4.3. Absolute ages for Schmidt's Hammer Calibration 121
4.4.4.4. LIA dating 122
4.4.5. Results 123
4.4.5.1. Soil Description and Characteristics 123
4.4.5.2. Schmidt-Hammer Measurements 123
4.4.5.3. Schmidt-Hammer Calibration 123
4.4.5.4. Units exposure age 124
4.4.6. Discussion 124
4.4.6.1. The glacial history of the Forni Glacier 124
4.4.6.2. Glacier fluctuations in the Alps 126
4.4.7. Conclusion 129
4.4.8. Acknowledgements 130
4.4.9. References 131
4.4.10. Pictures and Tables 138
4.5.LAKES SEDIMENT ANALYSIS 143
5. CONCLUSION 153
6. ACKNOWLEDGMENTS 157
7. REFERENCES 158

DISSERTATION STRUCTURE

This dissertation is structured as follows:

1. INTRODUCTION. After a brief preface that gives the rationale of the thesis, I present the aims of the Ph.D. project. Subsequently, the state of the art is treated. The existing knowledge about the glacial history in the Late Pleistocene and Holocene is treated and the different methods to reconstruct it are shown in terms of definitions and explanation of the most recent researches present in literature. Then the contribution of the project in scientific papers is proposed.

2. STUDY AREA. It describes in terms of geography, climate, geology, and geomorphology the four main investigated valleys in the Alps: the Forni Glacier Area, the Gavia Pass Area, the Stelvio Pass Area, and the Viola Pass Area.

3. METHODS. Here all the materials and methods used for data acquisition and analysis are listed and grouped in sub-sections related to fieldwork, laboratory work, and data analysis.

4. RESULTS. In this section, the results are presented as published papers and submitted manuscripts. The results of the lake sediment analysis occupies a single different section.

5. CONCLUSION. Here all the results found are summarized and linked and suggestions for future perspectives are given.

6. ACKNOWLEDGMENTS. In this part, a series of important people are thanked for their support to the thesis.

7. REFERENCES. In this section, all the references of citations that are not comprehended in the submitted or published papers are listed.

1. INTRODUCTION

1.1.PREFACE

In recent years a general awareness of the fact that the earth's climate is changing was born, and, already in 1988, the establishment of an international committee of experts to assess the relevance, the speed, and possible response strategies has been founded by the General Assembly of the United Nations, called IPCC (International Panel on Climate Change). In this context of climate change, paleoclimatic studies have assumed particular relevance as they can provide us with useful information to discriminate climatic variations due to natural causes from those of Anthropocenic origin. Paleoclimatic reconstructions also make up for the lack of climatic data based on instrumental measurements that are spatially and temporally limited.

The analysis and reconstruction of glacial fluctuations that occurred after the last glacial maximum and in particular during the Holocene represents a topic of great interest as it allows to understand the environmental and climatic changes that have occurred so far, and therefore to interpret both the current situation and future trends.

Phases of glacial advance mainly occur in response to periods of climatic deterioration and leave traces that can be identified through their moraines: their dating, therefore, allows us to reconstruct both the history of the glacier and that of the corresponding climatic changes.

This dissertation takes place in this context of comprehension of paleoclimate related to geomorphological reading and landscape evolution.

1.2.STATE OF THE ARTS

1.2.1. Paleoclimate after the LGM

The period after the Last Glacial Maximum has been widely discussed and many classifications have been made to better describe the climatic evolution through time, such as the INTIMATE event stratigraphy (*Rasmussen et al*., 2014), the biostratigraphic division (*Iversen*, 1954), and the European pollen zones (*Iversen*, 1954) (Fig. 1).

The INTIMATE (INTegration of Ice-core, MArine and TErrestrial records) event stratigraphy (*Rasmussen et al*., 2014) is the result of a project that following strict protocols provides a formal definition and an ordinal numbering of the sequence of Greenland Stadials (GS) and Greenland Interstadials (GI) based on a combination of stable-oxygen isotope ratios of the ice ($\delta^{18}O$) and calcium ion concentrations, reworked on a synchronization of the NGRIP, GRIP, and GISP2 ice-core records (*Rasmussen et al*., 2014).

The biostratigraphic division, proposed by Iversen (1954), is a classification of the period between 15ka CalBP to present based on layers of peat bogs in Denmark.

Matching these periods, pollen zones are a classification system used to subdivide paleoclimate of the last glacial period and the Holocene, using data from pollen cores. Iversen (1954) defined the current classification following the works of Von Post, the founder of modern palynology.

The oldest pollen zone (Ia) matches with the Oldest Dryas biostratigraphic division (*Iversen*, 1954) and correspond to the end of the GS-2 (*Rasmussen et al*., 2014). Glaciological modeling shows a lower summer temperature of about 10°C relative to mean 20th-century values and precipitation reduced to 30% of present-day amounts (*Kerschner and Ivy-Ochs*, 2007; *Kerschner*, 2009) in this period. Around 14.7ka years CalBP an increase of 2-3°C in summer temperatures recorded by lake sediment proxies (*Heiri et al.*, 2014) brought the stable Stadial to end in the GH-1 (*Rasmussen et al*.,

2014). Climate during the GH-1 Interstadial wasn't steady so that the INTIMATE event stratigraphy subdivides it into 5 different events (GH-1e, GH-1d, GH-1c, GH-1b, and GH-1a respectively) alternating warming and cooling periods. Pollen zone and biostratigraphic division (*Iversen*, 1954) are more confusing in this period: the first one relates the pollen zone Ib to the GH-1e, the pollen zone Ic to the GH-1d, and the pollen zone II to the remaining GH-1c/b/a; the second one associates the Bølling/Allerød to the whole GH-1 event.

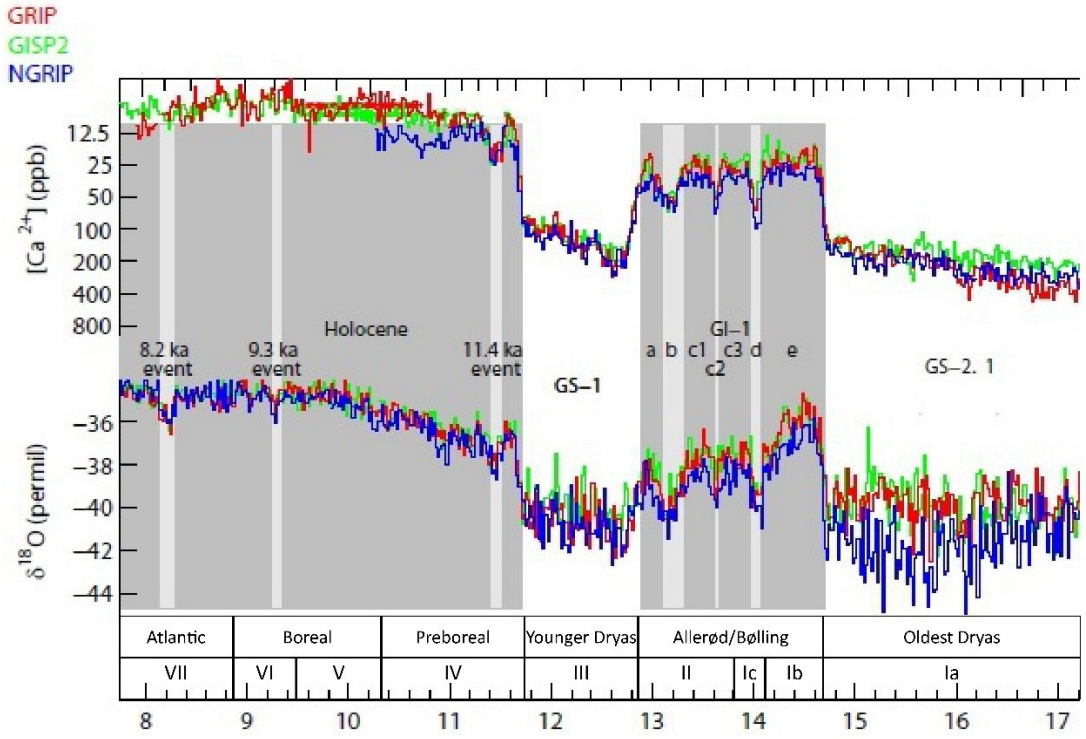

Figure 1: NGRIP, GRIP, and GISP2 $\delta^{18}O$ and Ca^{2+} concentration (*Rasmussen et al.*, 2014), INTIMATE event chronology (*Rasmussen et al.*, 2014), and European pollen zones and biostratigraphic division (*Iversen*, 1954) between 17ka and 8ka.

A rapid cooling in temperatures (*Walker et al.*, 2009) introduced the beginning of a new Stadial (GS-1), the most recent one. The stadial is related to the pollen zone III, the Younger Dryas biostratigraphic division (*Iversen*, 1954), when in most of the Alps the temperatures remained low and the conditions were dry (*Kerschner et al.*,2000; *Walker et al.*, 2009). Subsequently, 11.7ka years CalBP has been

defined as the onset of the Holocene (*Walker et al.*, 2009), with the beginning of the Preboreal biostratigraphic division, pollen zone IV (*Iversen*, 1954). All the remaining pollen zones (V, VI, VII, VIII, and IX) and biostratigraphic divisions (Boreal, Atlantic, Subboreal, and Subatlantic) are referred to different periods in the Holocene (*Iversen*, 1954). From a climatic point of view, the Holocene can be divided into three parts (*Wanner et al.*, 2013):

- a first deglacial phase, between 11.7ka and 7ka, characterized by a temperate climate in North America and Eurasia (*Renssen et al.*, 2009) and by high monsoon activity in Africa (*de Menocal et al.*, 2000);
- the Holocene Thermal Optimum, between around 7ka and 4.2ka, characterized by higher summer temperatures than in the pre-industrial period in the medium and high latitudes of the Northern Hemisphere (*Alverson et al.*, 2003);
- the Neoglacial, after 4.2ka, dominated by a lowering in summer temperatures in Northern Hemisphere due to a decrease in insolation during the boreal summer (*Denton and Karlèn*, 1973).

Despite this general trend, the climatic variability of the Holocene period is testified by three big cold events registered in the Greenland cores, respectively at around 11.4ka, 9.3, and 8.2ka (*Walker et al.*, 2009). Since the late 1990s, many studies have tried to reconstruct the instability of the Holocene. Renssen et al. (2009) firstly highlighted cooling events in surficial water assuming changes in the North Atlantic ocean circulation with a related glacier advance at 10.3, 9.4, 8.1, 5.9, 4.2, 2.8, 1.4, and 0.4ka CalBP. Wanner et al. (2011), based on a statistical analysis applied on different proxy data, suggest the existence of 6 different significative cold events: 8.2, 6.3, 4.7, 2.7, 1.55, and 0.55ka cal BP. The most recent phase is the so-called "Little Ice Age" (LIA), in which happened an irregular decrease of temperatures of 0.2°C in the Northern Hemisphere, with a global increase of glacier volume best represented in the Alps and Scandinavia (*Nesje and Dahl*, 2003). The complex spatial and temporal pattern of these cold events is difficult to explain with a single process and probably

depended on a combination of different processes and feedbacks may have played a very important role (*Wanner et al.*, 2011).

1.2.2. Glacial Evolution after the LGM in the Alps

Knowledge about deglaciation within the mountain area of Alps after the Last Glacial Maximum (LGM) remains limited (*Tremblay et al.*, 2019): a summary of the current chronological knowledge is reported in Table 1.

Cosmogenic nuclide analysis places the limit of the Last Glacial Maximum within Swiss Alps between 21.1 and 19.1 ka (*Ivy-Ochs et al.*, 2004; *Ivy-Ochs*, 2015); by 18 ka, more than 80% of the ice volume had melted (*Ivy-Ochs et al.*, 2008; *Ivy-Ochs, 2015*; *Wuthrich et al.*, 2018). A series of Late Pleistocene-Holocene glacial advances have been identified throughout the Alps based on local type glacier. However, the time and extent of these successive phases are regionally variable, and every valley has its own evolution. Generally, glaciers re-advanced with a maximum around 17 ka and a stabilization ca. 15.4 ka (*Ivy-Ochs et al.*, 2008; *Ivy-Ochs*, 2015; *Wuthrich et al.*, 2018) during the so-called Gschnitz stadial following a cooling period after an Early Lateglacial decay (*Ivy-Ochs et al.*, 2006). Next came the Clavadel/Senders with a maximum around 15ka, and then came the Daun around 14.7ka, which both occurred before the Bølling/Allerød (*Ivy-Ochs et al.*, 2006). Successive phases of glacier advance occurred around 12.3ka, (Egesen I stadial: e.g. *Kershner et al.*, 2000; *Bohlert et al.*, 2011; *Ivy-Ochs*, 2015) and around 11.3 (Egesen II stadial: e.g. *Zoller et al.*,1998; *Ivy-Ochs et al.*, 2006; *Ivy-Ochs et al.*, 2008), the first one in the middle of the Younger Dryas, while the second on the border between Younger Dryas and the Preboreal.

Name	Age	Citation
Last Glacial Maximum	~21ka	Ivy-Ochs et al., 2006
Early Lateglacial Decay	18-19ka	Ivy-Ochs et al., 2006
Gschnitz	>15ka	Ivy-Ochs et al., 2006
Clavedel/Senders	15ka	Ivy-Ochs et al., 2006
Daun	14.7ka	Ivy-Ochs et al., 2006
Egesen I	12.3ka	Ivy-Ochs et al., 2006
Egesen II	11.3ka	Ivy-Ochs et al., 2006
Kartell	10.8ka	Ivy-Ochs et al., 2006
Kromer	~9ka	Ivy-Ochs et al., 2006
Mount Minè	8ka	Nicolussi and Schlucther, 2012
Tsidjore	3.8ka	Schimmelpfenning et al., 2012-2014
Göshen I	3-2.3ka	Boxleitner et al., 2019
Göshen II	1.8-1.1ka	Boxleitner et al., 2019

Table 1: timing of known glacial phases after the Last Glacial Maximum.

During the Holocene, glaciers throughout Alps were probably smaller than their present extent *(Ivy-Ochs et al.*, 2009), at least before the Middle Holocene (*Walker et al.*, 2009; *Walker et al.*, 2012). Despite this, more glacial phases have been identified, among which the oldest one is the Kartell Stadial around 10.8ka (*Ivy-Ochs* et al., 2006) followed by the Kromer Stadiar around 9ka (*Ivy-Ochs* et al., 2006). At around 8ka Nicolussi and Schlucter (2012) detected a glacial pulsation at the Mont

Minè glacier that is the last detectable for a long time, as the following one is the Tsidjiore Glacier one at 3.8ka (*Schimmelpfenning et al.*, 2012; *Schimmelpfenning et al.*, 2014). Two more Stadial are described for the Göshenen Valley, Göshenen I at 3-2.3ka, and Göshenen II at around 1.8-1.1ka (*Boxleitner et al.*, 2019). Between these phases and the LIA, many glacier advances are recorded in historical time around 527-578AD, 820-834AD, 1100AD, and 1340AD (*Holzhause et al.*, 2005).

In the Italian Alps, most prior studies evaluated low elevation sites and set the ultimate LGM culmination between 26 ka and 17 ka (*Comerci et al.*, 2007; *Ravazzi et al.*, 2012; *Pini et al.*, 2016; *Ravazzi et al.*, 2014*; Ivy-Ochs*, 2018). At high elevations, the latest LGM culmination is placed before 17 ka (*Favilli et al.*, 2008) in Eastern Alps; recalculation of moraine boulder exposure rates within the Maritime Alps sets the LGM around 24 ka (*Federici et al.,* 2016). In the latter, the Bühl stadial was dated around 18.5 ka, and then the Egesen stadial around 13.5 ka (*Federici et al.,* 2016). Within the Garda Basin, a regressive phase interrupted forest growth between 16.4 and 15.5 ka (*Ravazzi et al.*, 2012).

Beyond these studies, knowledge related to the LGM and successive glacial phases in the Italian Central Alps is still scarce. Scotti et al. (2017) registered a glacial advance that left morainic ridges at the bottom of Dosè Valley around 11.4ka and referred it to the Kartell Stadial. The finding of a mummified prehistoric man (the Neolithic Iceman 'Otzi') dated 5300-5050 Cal BP in the Ötztaler Alps (*Bonani et al.*, 1984), and chironomid (*Ilyashuk et al.*, 2011) and pollen records (*Ortu et al.*, 2008) in Alpine lakes suggest a cooling around 5.2 ka that was probably accompanied by a rapid glacier expansion. Around 4.4ka a glacial advance is supposed in the Forni Valley (*Pelfini et al.*, 2014) as the possible event that buried a log in a peat. Further advances are not contemporary and local, confusing the reconstruction of a pattern of glaciation for the Alpine Mountain Chain.

1.2.3. Absolute dating techniques

Among the different techniques to reconstruct deglaciation and subsequent glacial advances, cosmogenic dating has received the greatest consideration (e.g., *Chenet et al.*, 2016; *Moran et al.*, 2016; *Wuthrich et al.*, 2018; *Rolland et al.*, 2020). Cosmic radiation, a high-energy radiation produced mainly by supernovas, can reach the Earth with trajectories deflected by the Sun's forces and a path that depends upon the angle of entry the Earth's magnetic field (*Von Blanckenburg and Willenbring*, 2014), Cosmogenic nuclides are particles produced by the interaction of cosmic radiation (comprised mostly of protons and neutrons) with atoms in the upper atmosphere. This interaction generates a cascade of nuclear reactions that produce particles that can proceed all the way to the Earth's surface (*Von Blanckenburg and Willenbring*, 2014). There are two main types of cosmogenic nuclides, the meteoric and the in situ. The spallation is the main process that creates cosmogenic nuclides such as ^{10}Be, ^{14}C, ^{26}Al, and ^{36}Cl: it happens in the atmosphere and can reach the Earth's surface, penetrating even a few meters of rocks (*Von Blanckenburg and Willenbring*, 2014). Once they have entered the rocks and mineral of the surface, they start to interact and produce in situ cosmogenic nuclides within the crystalline structure, but some noble gasses do diffuse out of the mineral structure. Cosmogenic nuclides may be stable or they may decay if they are radioactive nuclides.

The sites and distribution of meteoric cosmogenic nuclides depend upon air pressure and circulation (*Willenbring and von Blanckenburg*, 2010). The in situ production of cosmogenic nuclides at the Earth's surface depends on the entire mass of atmosphere within the overlying air column (*Stone*, 2000), and hence depends on altitude. Production is further modified by the geomagnetic field strength and therefore depends on latitude. Thus, the intensity of production of both meteoric and in situ cosmogenic nuclides is a function of variations in the Earth's magnetic field (*Von Blanckenburg and Willenbring*, 2014). Atmospheric cosmogenic nuclides are produced at much greater rates than the nuclides formed in situ in minerals at the Earth's surface (*Willenbring and von Blanckenburg*,

2010). These cosmogenic nuclides could exist in minerals before the exposure to cosmic radiation or before meteoric nuclides accumulate on the surface and they accumulate over time so they can provide exposure ages (*Von Blanckenburg and Willenbring*, 2014). The differential equation governing the calculus for exposure age (*Lal*, 1991) considering no initial amount of nuclide due to a prior exposure is:

$$N(\varepsilon, t) = \frac{P}{(\lambda + {\varepsilon}/{\Lambda})} * (1 - e^{-(\lambda + {\varepsilon}/{\Lambda})t}$$

Where:

t ≡ exposure ages [yr];

N ≡ number of cosmogenic atoms found [at];

P ≡ production rates for the sample [at/g*yr];

ε ≡ erosion rate [g/cm^2*yr];

Λ ≡ attenuation length of production rate [g/cm^2];

λ ≡ decay rate of nuclide (1/yr).

Every cosmogenic nuclide has its own half-life, so any single nuclide has a range of age in which it applicable (*Von Blanckenburg and Willenbring*, 2014)

Particularly, the formation of ^{14}C is the result of the cosmic ray bombardment of ^{14}N in the upper troposphere and stratosphere as:

$$^{14}N + {}^{1}n \rightarrow {}^{14}C + {}^{1}p^{+}$$ (*Törnqvist et al*., 2015).

This particular nuclide has a great potential because it can be used to date buried organic matter: the fundamental assumption is that any organism used for radiocarbon dating was in equilibrium with the atmosphere at the time of death in terms of ${}^{14}C/{}_{12}C$ ratio (*Törnqvist et al*., 2015). The ultimately accepted half-life of ^{14}C is 5730 a ^{14}C (*Godwin*, 1962) but for radiocarbon dating the use of the "Libby half-life" of 5568 a ^{14}C (*Libby*, 1952) is suggested.

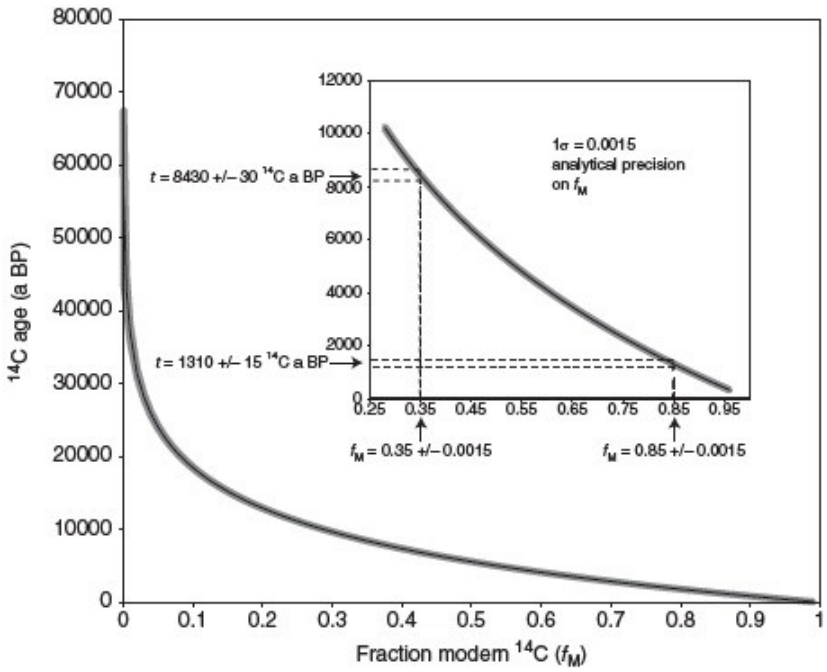

Figure 2: Relationship between f_M and ^{14}C age with an error envelope that reflects the typical analytical precision of f_M of 1.5‰. The inset illustrates in more detail how uncertainties in f_M translate to the analytical ^{14}C age error. Also note that as the curve becomes steeper when f_M approaches zero, this analytical error translates not only to larger but also increasingly asymmetric ^{14}C age errors. Image from Törnqvist et al. (2015).

For the age calculation, it is necessary to introduce the concept of fraction modern ^{14}C (f_M) as the ratio $^{14}C/_{12}C$ in the sample divided by the same ratio in wood from 1950 AD (generally the normalization is now based on secondary standards) (*Törnqvist et al.*, 2015). The age is then obtainable with the following equation:

$$t = -8033 * \ln(f_M) \text{ (Fig. 2)}$$

Where 8033 is that the mean lifetime of ^{14}C supported by the "Libby half-life" (*Törnqvist et al.*, 2015).

1.2.4. Relative dating techniques

Cosmogenic dating techniques are not always feasible due to logistical and economic constraints, even if they have received great consideration in the reconstruction of deglaciation and subsequent glacial advances (e.g., *Chenet et al.*, 2016; *Moran et al.*, 2016; *Wuthrich et al.*, 2018). For this reason, different index and relative methods to obtain ages have been developed. Jenny (1941) proposed its equation describing soils as a function of climate, organisms, relief, parent material, and time (S=f(cl, o, r, p, t,…). Soils developed on glacial and periglacial features, such as late-glacial moraines and rock glaciers, provide the opportunity to date deglaciation or to investigate subsequent geomorphological modification (e.g. *Favilli et al.*, 2008) as they allow to choose profile where climate, organisms, relief, and parent material may be considered the same, isolating time in Jenny's equation (*Jenny*, 1941). The first author who tried to create a soil development index was Harden (1982) in order to measure quantitatively the degree of soil profile development. This original soil development index combines eight soil properties that can be calculated on field: clay films, texture plus wet consistency, rubification (color hue and chroma), structure, dry consistency, moist consistency, colour value, and pH (*Harden*, 1982). The quantification of these properties is based on the model proposed by Bilzi and Ciolkosz (1977) that assign points for differences between each horizon and the parent material and the developed soil horizons but modified as the incremental differences between each horizon ad the parent material are arbitrarily assigned to 10 points (*Harden*, 1982). For each horizon, the result of every property is then normalized to a number between 0 and 1, summed, and finally divided by the number of properties to obtain the horizon index (*Harden*, 1982). This horizon index is then multiplied by the horizon thickness, and the product of each horizon is summed to obtain the soil development index (*Harden*, 1982). The index has been applied in many recent studies (e.g., *Huges et al.*, 2006; *Hannah et al.*, 2017) but in recent times great attention has been given to indexes that remove the arbitrariness using calculated values (e.g. *Birkeland*, 1999; *Egli*

et al., 2003; *Egli et al.*, 2006; *Egli et al.*, 2010; *Egli et al.*, 2015; *Maejima et al.*, 2002). Several of these indexes share a similar general principle that is based on the ratio of the base cations (Ca, Mg, K, Na) to Al and/or Si. Kronberg and Nesbitt (1981) proposed two indexes still used (*Egli et al.*, 2010; *Egli et al.*, 2015), the A and B indexes, defined as the molar ratio of:

$$A = \frac{SiO_2 + CaO + K_2O + Na_2O}{Al_2O_3 + SiO_2 + CaO + K_2O + Na_2O}$$

$$B = \frac{CaO + K_2O + Na_2O}{Al_2O_3 + CaO + K_2O + Na_2O}$$

Other proposed weathering indexes of soil are the CIA and the CIW (*Hamois*, 1988; *Nesbitt and Young*, 1989), defined as:

$$CIA = \frac{Al_2O_3}{Al_2O_3 + CaO + K_2O + Na_2O}$$

$$CIW = \frac{Al_2O_3}{Al_2O_3 + CaO + Na_2O}$$

Egli et al. (2015) proposed the use of the dating method applied for rock varnish in semi-arid to arid regions (*Harrington and Whitney*, 1987), defined as the molar ratio (K+Ca)/Ti, as Ti is considered to be an immobile element. Particularly in Podzols for their own nature, iron is a crucial element; therefore, the iron crystallinity ratio has been proposed as an index of soil development (*Arduino et al*., 1984; *Maejima et al.,* 2002). The iron crystallinity ratio is calculated as $CRF = \frac{Fe_d - Fe_o}{Fe_{tot}}$, where Fe_d is the iron fraction extracted with dithionite, Fe_o is the iron fraction extracted with oxalate, and Fe_{tot} is the total iron content.

Soils are not the only way to obtain indexes of relative ages. Since the 1980s, Schmidt's hammer has been used in studies of glacial and periglacial environments, in particular for the relative dating of the surface of moraines (e.g., *Mccarrol*, 1989; *Shakesby et al.*, 2006), of rock glaciers and deglaciated surfaces (*Scapozza et al.*, 2010), landslides and rock avalanches (*Clark et al.*, 2004; *Dawson et al.*, 1986). The rebound value, defined as R, is proportional to the compressive strength of the rock surface

and, with the same mineralogical composition and climatic conditions, it is proportional to the degree of alteration of the rock and therefore to its age of exposure (*Mccarroll*, 1989; *Laustela et al.*, 2003). All the described indexes can be mathematically translated in absolute ages with calibration based on regression with known absolute ages.

1.3. AIMS

The general context of the thesis is to understand how deglaciation of high elevation and amphitheater area in the Central Italian Alps occurred since the Last Glacial Maximum. All the analyses were processed in different valleys, as the deglaciation could have been different in timing, extent, and spatial pattern.

A more detailed list of the objectives is:

a) Apply one of the relative dating methods, the iron crystallinity ratio (*Arduino et al*., 1984; *Maejima et al.,* 2002), and evaluate of the possibility of using it as an absolute dating method for deglaciation within a sector of the Central Italian Alps (Upper Valtellina);
b) Reconstruction of the glacial evolution of the Gavia Pass area and the Forni Valley area after the LGM using Schmidt Hammer R-values and Crystallinity Ratio indices of soils;
c) compare the efficiency of the Schmidt Hammer R-values and of the Crystallinity Ratio indices of soils as dating methods;
d) Evaluation of the effect of the following glacier advance on the exposure age of previously exposed roches moutonnée in terms of Schmidt Hammer R-values;
e) Reconstruction of permafrost present or past distribution related to soil micromorphology;
f) Paleoclimatic and Paleoenvironmental reconstruction based on lake cores analysis.

1.4. CONTRIBUTION TO SCIENTIFIC PAPERS

This dissertation contributed to the preparation of 4 manuscripts, aimed to be published in different scientific journals:

- Longhi A., Monticelli D., Guglielmin M., 2020. The use of iron chemical analysis of Podzols to date the Late Pleistocene-Holocene deglaciation history of the Central Italian Alps. Journal of Quaternary Science 35, 1021-1035.
- Longhi A., Trombino L., Guglielmin. Soil micromorphology as tool for the past permafrost reconstruction and paleoclimatic variatons. Manuscript submitted to Catena for publication.
- Longhi A., Guglielmin M., 2020. Reconstruction of the glacial history after the Last Glacial Maximum in the Italian Central Alps using Schmidt's hammer R-values and crystallinity ratio indices of soils. Quaternary International 558, 19-27.
- Longhi A., Guglielmin M. The glacial history after the Last Glacial Maximum in the Italian Central Alps (Forni Valley). Manuscript submitted to Geomorphology for publication.

2. STUDY AREA

The study area is located in Upper Valtellina, Central Italian Alps. Within this sector of Valtellina, four main valleys were selected: the Forni Glacier area, the Gavia Pass area, the Stelvio Pass area, and the Viola Pass area.

These areas were selected so that, representing glacier with various exposition and catchment's morphology (i.e., area, slopes, aspects, and altitude) at similar elevation and close to each other, it could be possible to find differences in glacial evolution and relate them to a property of the area. The dimension of the area and their characteristics (presence/absence of suitable morphologies, soils, and striated roches moutonnée) allowed us to select the best approach to use in each area.

Moreover, we selected areas already well known (Forni Glacier area, Stelvio Pass area) to have a good comparison and to confirm the findings even in not so studied areas (Gavia Pass area, Viola Pass area).

2.1.FORNI GLACIER AREA

2.1.1. Geography and Climate

The Forni Glacier Area (Fig. 3) is located in the Central Italian Alps, in Upper Valtellina, within the Lombardy sector of the Stelvio National Park. The area is located in the Frodolfo Basin, a tributary of the Adda, between 2150m a.s.l. around the Forni Hut (46.42N, 10.55E) and 3600m a.s.l. of the P. Cadini (46.37N, 10.60E). Throughout the E-W directed main valley, a lot of side valleys like the Rosole Valley, the Cedèc Valley, and the S. Giacomo Valley are evident. The Northern and Eastern limits of the area border with Trentino Alto Adige in a series of high elevation peaks, like the highest

and most known Cevedale (46.44N, 10.62E, 3758m a.s.l.). The western limit corresponds with the Zebrù valley, to which the area is connected by the Zebrù Pass (46.46N, 10.56E, 3031m a.s.l.). In the Southern part of the valley, a small road connects the Forni Hut to Santa Caterina Valfurva, the nearest city to the area.

In the area, the Forni Glacier was once the greatest alpine glacier in Italy originated from three different basins with three different tongues connected around 3000m a.s.l. (*Pelfini*, 1992). Since 2015, the Eastern tongue detached from the main glacier, and actually, the glacier has an extension of about 11.3 km² (*Smiraglia and Diolaiuti*, 2015).

The study area is recognized as a site of community importance (SIC "Valle e Ghiacciaio dei Forni – Val Cedèc – Gran Zebrù – Cevedale") by the European Union in the frame of "Nature 2000" established under the Habitats Directive (92/4/EEC) (*Malfasi*, 2018).

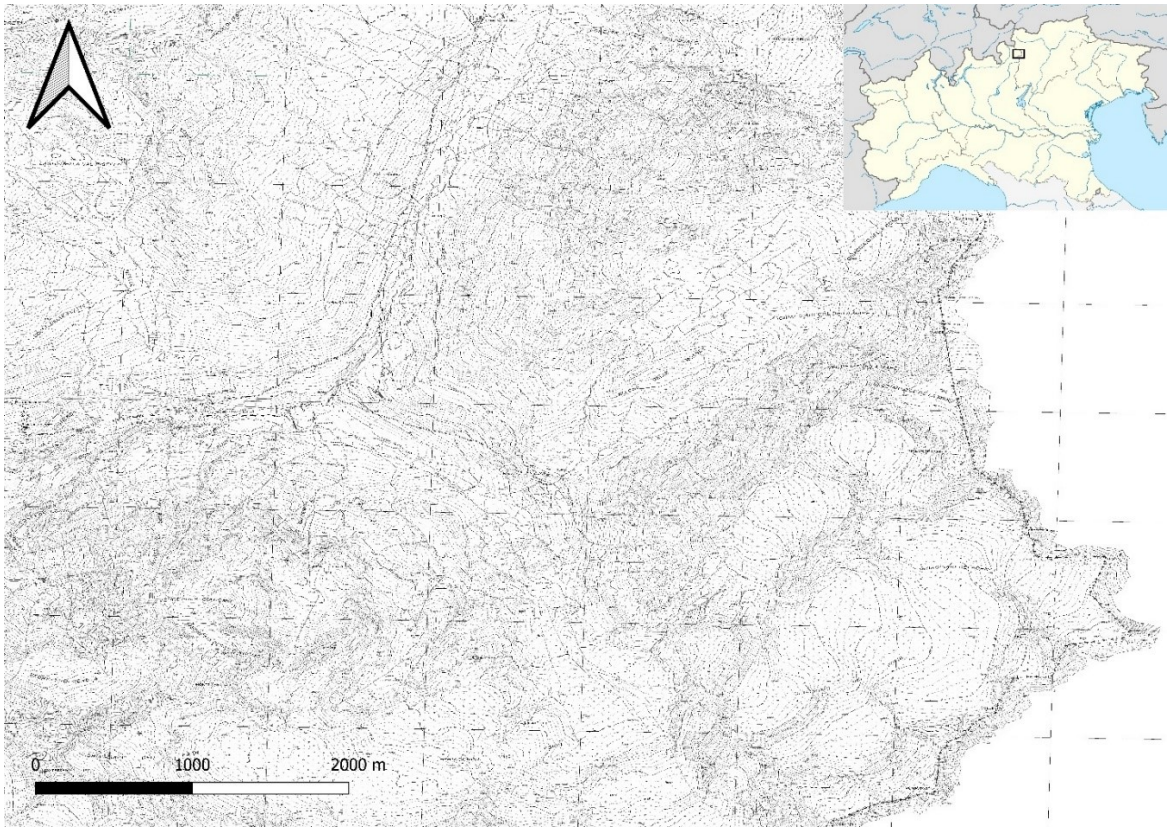

Figure 3: Reference map of site location (Forni Valley).

The climate is characterized by a continental regime (*Ceriani and Carelli*, 2000): the mean annual precipitation calculated between 1972 and 1982 at the Forni San Giacomo weather station (2750m a.s.l.) is 1241 mm/year (*Ceriani and Carelli*, 2000). On a longer time scale, the mean annual precipitation calculated between 1927 and 1990 at the Forni Prese weather station (2165m a.s.l.) is 811 mm/year. The mean annual air temperature, calculated between 2006 and 2010 from the AWS1 Forni weather station at 2631m a.s.l., is -1.4°C (*Senese et al*., 2012).

2.1.2. Geology and Geomorphology

The geology and lithology of the area are complex, but the bedrock is mainly acidic, mostly characterized by chlorite and sericite micaschists, and banded paragneiss (*Montrasio et al.*, 2012). The valley bottom shows clear evidence of glacial activity, with many striated roches moutonnée. The valley sides are mainly covered by ablation till with several moraine ridges deposited by different glacial phases. The valley sides are also characterized by gravitational processes like landslides and debris flows.

In the upper forefield area, soils mostly correspond to Leptosols (*ERSAF*, 2012), with very shallow A horizons over a deeper and extremely stony deposit (*Pelfini et al.*, 2014; *FAO*, 2006). On the contrary, the lower part of the Forni Valley, where a forest is present, is characterized by coniferous forest soils (*ERSAF*, 2012), i.e., Podzols (*Pelfini et al.*, 2014; *FAO*, 2006; *Duchaufour*, 1983).

The Forni Glacier recent fluctuations are well documented by its moraine apparatus, and the post-LIA advances are evident in 1904 AD, 1926 AD, and 1981 AD (*Pelfini et al.*, 2014). The orthophotos (1950, 1998, 2003, 2007, 2014) provided by Geoportale Regione Lombardia allows a further comprehension of the even more recent glacier dynamic. Given the great expansion of the glacier advance during the LIA, evidence of smaller past advances have been eroded and just two glacial advances have been identified during the Holocene: the first one around 4400 years CalBP, obtained

by radiocarbon dating a buried log under glacial till (*Pelfini et al.*, 2014); the second one radiocarbon dating the base of a small peat dammed by a morain around 2800 years CalBP (*Pelfini et al.*, 2014). Permafrost is present in favorable conditions above 2450m a.s.l. in the South-Eastern and North-faced area, while above 2650m a.s.l. in the North-Eastern and South-faced area (*Boeckli et al.*, 2012) while its maximum Holocene expansion is above 2100m a.s.l. (*Guglielmin and Siletto*, 2000).

2.2.GAVIA PASS AREA

2.2.1. Geography and Climate

The Gavia Pass area is located in Upper Valtellina, within the Central Italian Alps (Fig. 4) within the Lombardy sector of the Stelvio National Park. The area is located in the Gavia basin, a tributary of Frodolfo Creek, between 2300m a.s.l. at the confluence with the dell'Alpe Valley (46.38N, 10.49E) and 3360m a.s.l. of the Tre Signori Horn (46.34N, 10.52E). The main valley is South-North oriented and a little further downstream from the Berni Hut (46.36N, 10.50E, 2511m a.s.l.) on the hydrological right the main valley merges with a lateral West/East oriented valley, the Dosegù Valley. The area border in the Western part, above Mount Gavia, with dell'Alpe Valley, while in the Eastern side the Tre Signori Horn signs the border with the Trentino Alto Adige (Palù Valley). From North to South the SS36 crosses the valley and connects Santa Caterina Valfurva to Ponte di Legno across the Gavia Pass, which sign the limit between Sondrio and Brescia province and connect the Gavia Valley to the Camonica Valley.

Currently, two glaciers still exist in the area: the Mount Gavia Glacier with a mean front elevation of 2980m a.s.l. and the Sforzellina Glacier with a mean front elevation of 2790m a.s.l. (*Smiraglia and Diolaiuti*, 2015). The Lake Bianco Glacier was declared extinct in 1985 by the Comitato Glaciologico Italiano Bulletin instead.

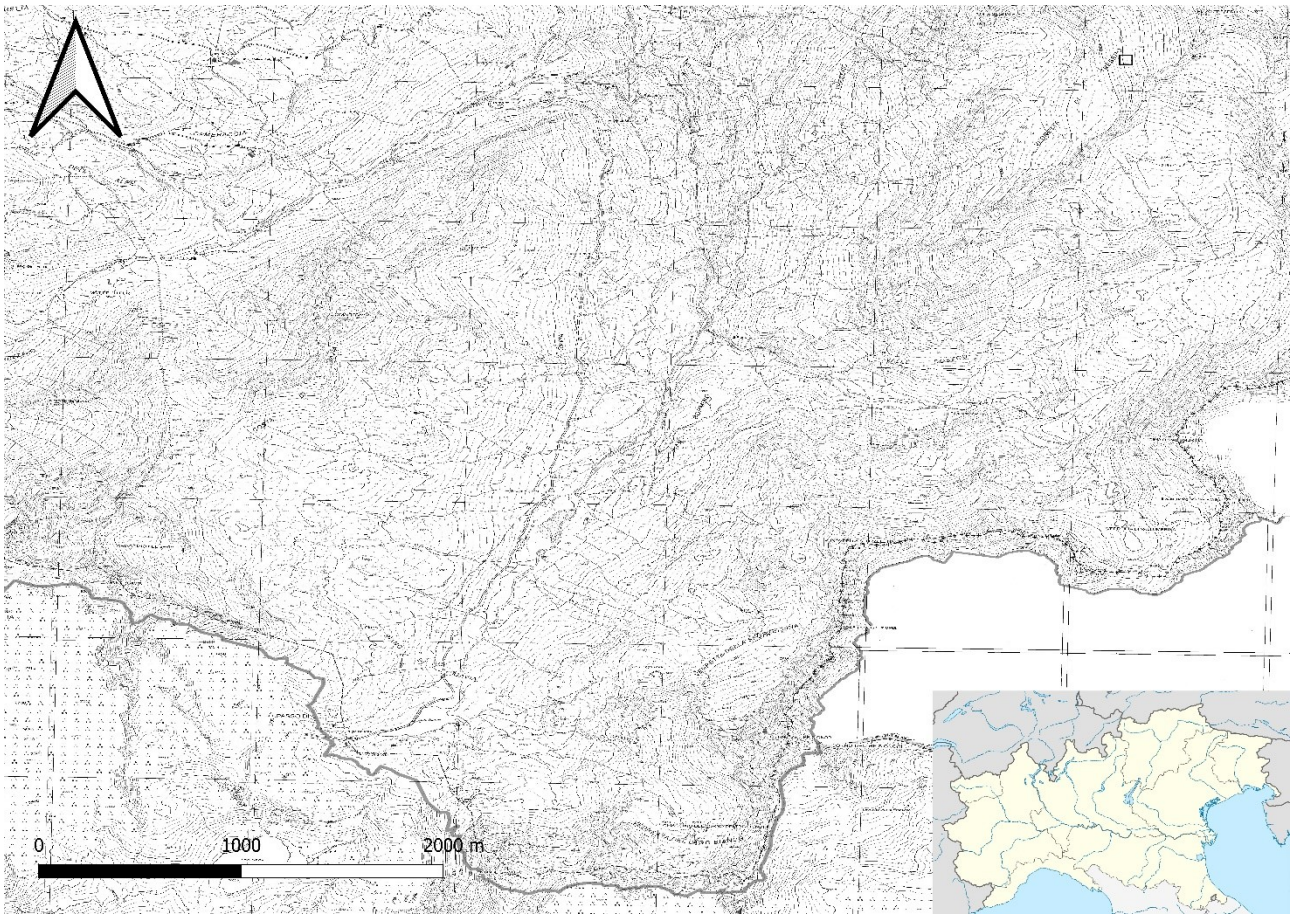

Figure 4: Reference map of site location (Gavia Pass Area).

The climate is characterized by a continental regime (*Ceriani and Carelli*, 2000): the mean annual precipitation calculated between 1927 and 1982 at the Gavia lower weather station (2210m a.s.l.) is 1310 mm/year (*Ceriani and Carelli*, 2000). The mean annual temperature is calculated between +1°C and -1.4°C (*Hijmans et al.*, 2005).

2.2.2. Geology and Geomorphology

The geology and lithology of the area are characterized by orthogneiss, paragneiss, and quartz-phyllites, mostly strongly retrogressed varieties of earlier medium-grade paraschists (*Dal Piaz et al.*, 1988). The valley bottom is mainly rocky with clear evidence of glacial erosion, including roches

moutonnées with several ponds in between. The valley sides are mainly covered by ablation till with several moraine ridges deposited by different lateral glaciers. A few rock glaciers and many small periglacial landforms, such as earth hummocks and gelifluction/solifluction lobes, are also present.

In the upper area in the Eastern side, soils mostly correspond to Leptosols (*ERSAF*, 2012) at least down to 2700m a.s.l., with very shallow A horizons over a deeper deposit (*Pelfini et al.*, 2014; *FAO*, 2006). The lower part and the Western side of the Gavia Valley is characterized by coniferous forest soils (*ERSAF*, 2012), mainly Podzols (*Carta pedologica Regione Lombardia*).

The Mount Gavia Glacier and the Lake Bianco Glacier recent fluctuations are easy to reconstruct from the orthophotos (1950, 1998, 2003, 2007, 2014) provided by Geoportale Regione Lombardia and the Comitato Glaciologico Italiano Bulletins allow an even further comprehension of the more recent glacier dynamic. The Holocene glacial history of the area may be complex, as in a pass area the glacier flow may have changed across the Gavia Pass, but there is no prior knowledge about the timing and the extension of the glacial phases. However, lithic industry in the Dosso Gavia area, at 2360m a.s.l. indicates that the Alpe Valley was glacier free, at least in the Boreal division (*Angelucci et al.*, 1992). Moreover, in the area close to Lake Nero, there is evidence of more intense periglacial processes and expansion of natural meadows around 7ka (*Ravazzi and Aceti*, 2004).

Permafrost is present in favorable conditions above 2700m a.s.l. in the West-faced Lake Bianco side, while above 2750m a.s.l. in the East-faced Mount Gavia area (*Boeckli et al.*, 2012), while its maximum Holocene expansion is above 2200m a.s.l. (*Guglielmin and Siletto*, 2000).

2.3.STELVIO PASS AREA

2.3.1. Geography and Climate

The Stelvio Pass area is located in Upper Valtellina, within the Central Italian Alps (Fig. 5) within the Lombardy sector of the Stelvio National Park. Along the Braulio Valley, runs the upper part of the Stelvio National road (SS38 “dello Stelvio"), built at the beginning of the XIX century to connect Lombardy and Tyrol territories through the Stelvio Pass (46.53N, 10.45E, 2757m a.s.l.) (*Malfasi*, 2018). The area is located in the Braulio Basin, a tributary of the Adda, between 2230m a.s.l. above the Seconda Cantoniera (46.52N, 10.41E) and 3095m a.s.l. of the Mount Scorluzzo (46.53N, 10.44E). The Nort-Eastern edge of the area is connected by the SS38 to Venosta Valley and the province of Bolzano through the Stelvio Pass, while at the North-West corner the Umbrail Pass (46.45N, 10.43E, 2503m a.s.l.) connects the area to the Müstair Valley and the Swiss Confederation. At the Western border, the area confines to the Forcola Valley, while in the Southern part the SS38 connects the Stelvio Pass to Bormio, the nearest city to the area.

Glaciers disappeared from the study area in 1952 (*Guglielmin et al.*, 2001).

The study area is recognized as a site of community importance (SIC “Valle del Braulio – Cresta di Reit”) by the European Union in the frame of “Nature 2000” established under the Habitats Directive (92/4/EEC) (*Malfasi*, 2018).

The climate is characterized by a continental regime (*Ceriani and Carelli*, 2000): the mean annual precipitation calculated between 1877 and 1990 at 2328m a.s.l. is 1138 mm/year (*Ceriani and Carelli*, 2000). The mean annual air temperature calculated between 1978 and 2015 from data from the nearest available meteorological station at Cancano (46.51N, 10.32E, 1948m a.s.l., 9 km to E-SE) is +3.3°C (*Ponti*, 2018). Previous studies in the area indicate the mean annual air temperature in the area as between +1°C and -3°C (*Cannone et al.,* 2007).

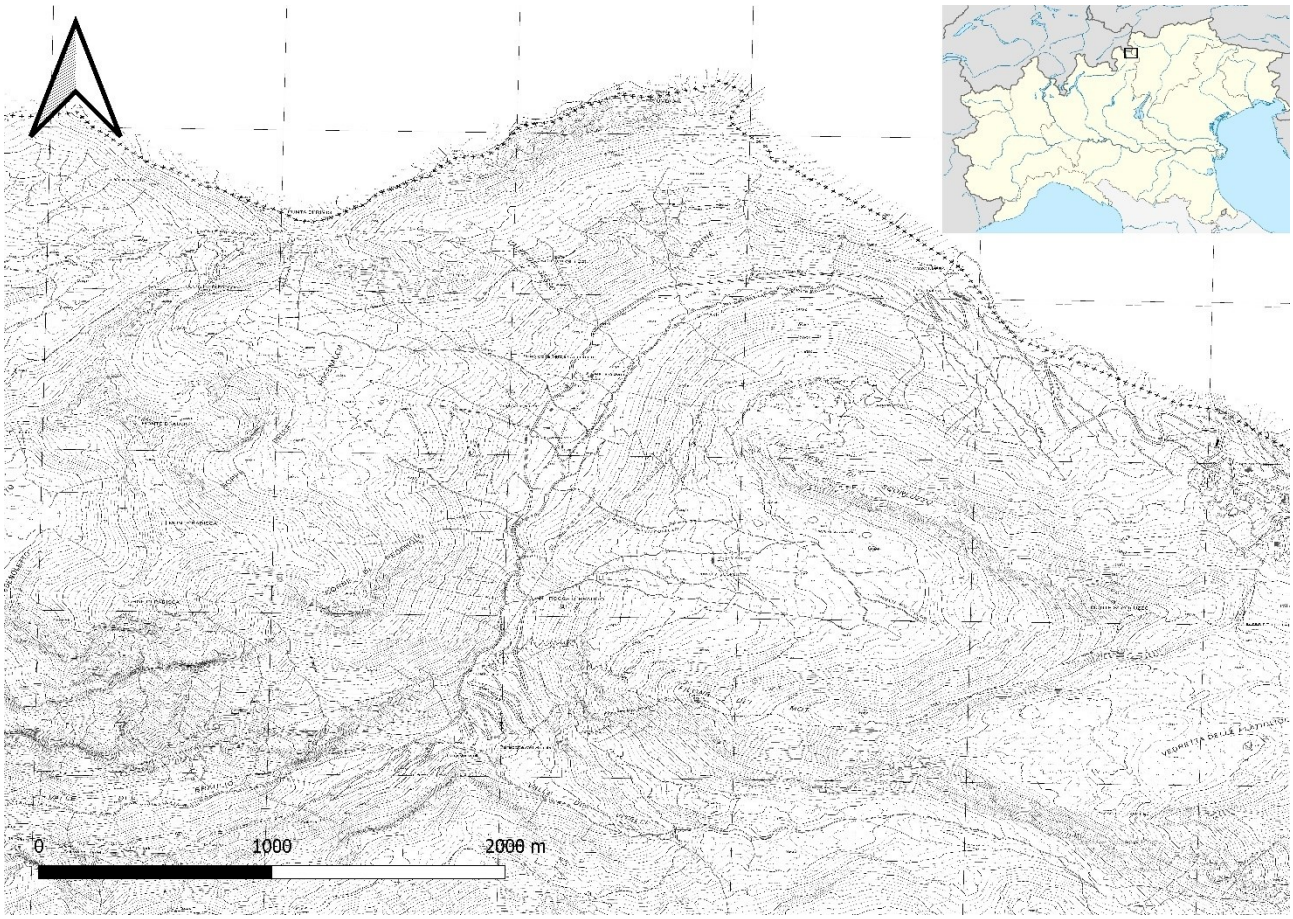

Figure 5: Reference map of site location (Stelvio Pass Area).

2.3.2. Geology and Geomorphology

The geology and the lithology of the Stelvio Pass area is complex as units of the Upper Austroalpine domain overlay and interact in this part of the Central Alps (*Montrasio et al.*, 2012; *Malfasi*, 2018). The study area is part of the Umbrail-Chavalatsch fault belonging to the Upper Austroalpine domain (*Ponti*, 2018). The bedrock is mainly acidic, composed by granitic and granodioritic orthogneiss, and by biotitic or two micas paragneiss, presenting outcrops of dolomite in the south-west corner of the area, from Bocca del Braulio (2280m a.s.l.) upward to the south slope of Filone dei Mot *(Giacomini and Pignatti*, 1955; *Guglielmin and Tellini*, 1992) and a local outcrop of andesite-basalts about 700m West from Mount Scorluzzo (*Montrasio et al.*, 2012). Glacial deposits, mainly composed of ablation

till, are common and widespread up to 2850m a.s.l., whereas inactive eluvial-colluvial and fluvial-stream deposits are mainly located below 250 m a.s.l. (*Ponti*, 2018; *Malfasi*, 2018). The landscape records its glacial, paraglacial, and periglacial history; roches moutonées, morainic ridges, rock glaciers, and protalus ramparts are common also as gelifluction lobes and terracettes. Several debris flows, scree slopes, and deep slope deformations are among common gravitational features in the area.

The soils are mainly Podzols, with only localized areas with Leptosols, Regosols, and mixed soils underneath the dolomite deposits and along the ridges that bring to Mt. Scorluzzo, respectively (*Carta pedologica Regione Lombardia*; *FAO*, 2006).

Even if historical documents are pretty abundant for the area, the Holocene glacial evolution of the Stelvio Pass area is still not well known. Historical reconstruction reports that Platigliole and Vedretta Piana glaciers were joint until 1872 (*Hoffmann and Haushofer*, 1872). The minimum elevation of the Little Ice Age (LIA) ice borders was 2780m a.s.l. in the Platigliole Valley and 2680m a.s.l. in the Trafoi Valley. Notwithstanding the impossibility of dating the glacier advance with absolute methods (^{14}C or cosmogenic nuclides) or relative methods, Cardassi (1995) obtained the ^{14}C age of 1580 AD for the contiguous glacier of Trafoi Valley and provides an approximate date for the Vedretta Piana glacier maximum during the LIA. During the Holocene, the glacier maximum extension was 2610m a.s.l. (*Cannone et al.*, 2003) and during this phase, the Vedretta Piana glacier crossed the Stelvio pass and joined with Scorluzzo glacier. A frontal morainic ridge at 2690m a.s.l. represents the maximum advance of the Scorluzzo glacier during the LIA (*Ponti*, 2018; *Malfasi*, 2018). Scorluzzo glacier remained in the northern cirque until 1937 when the front reached a minimum altitude of 2820m a.s.l. (*Pelfini*, 1992) and around 1910 two small tongues reached 2720m a.s.l. and 2730m a.s.l. In the western glacial cirque of Mt. Scorluzzo, the presence of a glacier is documented until 1872 and it was further substituted by the actual active rock glacier (*Guglielmin*, 2007).

Permafrost in the area has a patchy and discontinuous distribution (*Guglielmin and Siletto*, 2000; *Guglielmin et al.*, 2001; *Cannone et al.*, 2003). Permafrost distribution in the Stelvio pass area was little known before the PACE European Permafrost Monitoring Network project (*Harris et al.*, 2001) commenced at Stelvio-Livrio area in 1998 (*Guglielmin et al.*, 2001; *Malfasi*, 2018). The areas with actual potential permafrost occurrence are above 2500-2600m a.s.l., and the potential maximum Holocene permafrost expansion is between 2300-2500m a.s.l. (*Guglielmin and Siletto*, 2000).

2.4. VIOLA PASS AREA

2.4.1. Geography and Climate

The Val Viola and Val Cantone (Fig. 6) area is located in the upper part of the Viola Creek basin, a tributary to the Adda River, between 2120m a.s.l. at the Altumeira Hut (46.43N, 10.19E) and 3150m a.s.l. of Corno Dosè (46.41N, 10.17E). The Viola Pass (46.41N, 10.15E, 2471m a.s.l.) connects Italy to Switzerland and was important for strategical reasons during recent history. The Northern border of the area is represented by the Val Cantone cirque, while the Southern by the Corno Dosdè (46.41N, 10.17E, 3152m a.s.l.). The main valley is ENE-WSW oriented and is crossed by two main tributary valleys: from North by the Cantone Valley and from South by the Cantone di Dosdè Valley. The trail conducting to the Eastern side of the area down from the Altumeira Hut connects the area to Arnoga, a small district of Valdidentro, the closest municipality.

The glaciers of the area are relegated to the upper part of the Val Cantone di Dosdè area, where a once big glacier now shattered into ten glaciers covers the area of 1.88km² (*Scotti et al.*, 2013).

The study area is recognized as a site of community importance (SIC "Val Viola Bormina-Ghiacciaio di Cima dei Piazzi") by the European Union in the frame of "Nature 2000" established under the Habitats Directive (92/4/EEC).

The climate is characterized by a continental regime (*Ceriani and Carelli*, 2000): the mean annual precipitation calculated between 1927 and 1987 at 2000m a.s.l. is 1097 mm/year with a maximum of 2020mm/year (*Ceriani and Carelli*, 2000). The mean annual air temperature is between 3°C and -4°C calculated from the Arnoga weather station.

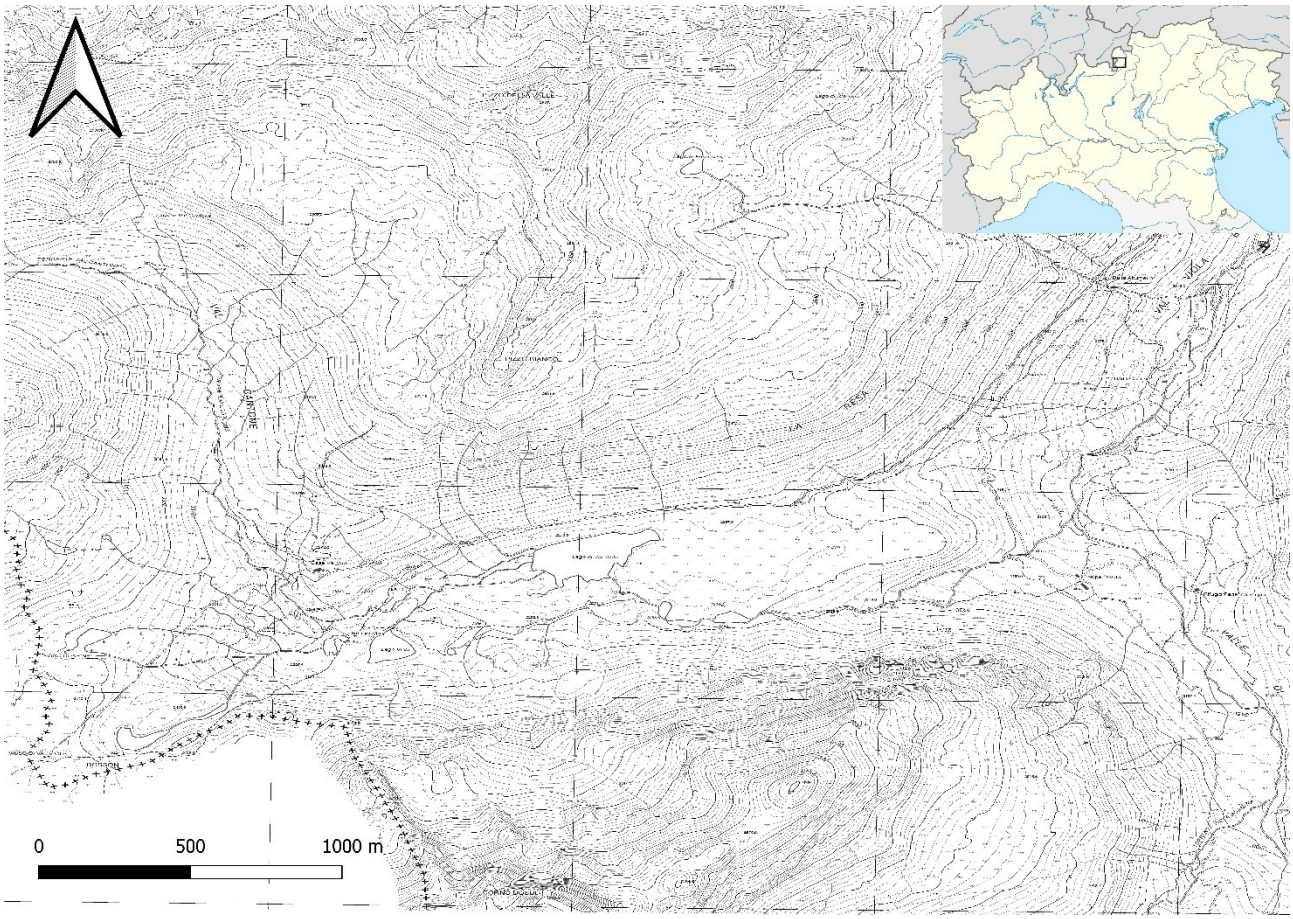

Figure 6: Reference map of site location (Viola Pass Area).

2.4.2. Geology and Geomorphology

The Viola Valley is aligned ENE-WSW, corresponding to the strike of the overthrust between the Campo Unit and the Grosina Unit, both pertinent to the Austroalpine domain (*Notapietro and De Capitani, 1985*).

The Austroalpine mostly consists of terrigenous sediments and intrusive bodies metamorphosed starting from the Hercynian orogeny (probably aged between 290 and 270 Ma BP, up to a maximum of 450 Ma BP) and not metamorphosed carbonatic sediments from the Mesozoic age. The rocks constituting the Austro-Alpine units have undergone several deformation events, schistogenesis, crystallization, and recrystallization during their history, and can therefore be considered

polymetamorphic (*Notapietro and De Capitani, 1985*). The most ancient lithologies of the Austroalpine have been placed in the Ordovician thanks to radiometric investigations; in particular, orthogneisses are identified as metamorphosed Ordovician granite intrusions and have been attributed to an age of 440-450 Ma (*Notapietro and De Capitani, 1985*).

The Campo Unit includes, in the study area, paragneisses and micaschists of high metamorphic grade, with intercalations of amphibolites and orthogneiss; in correspondence with Pizzo Bianco, Passo della Val Viola, and the valley bottom of the Alta Val Viola intrusive lithologies emerge with a granitic, granodioritic, and dioritic compositions, respectively. The granite of Pizzo Bianco has been attributed to the late Hercynian magmatic cycle (*Notapietro and De Capitani*, 1985).

The Grosina Unit, which constitutes the Northside of the Corno di Dosdè, is mainly composed of orthogneiss, migmatites, and paragneiss.

There is clear evidence of glacial, paraglacial, and periglacial processes in this area. Several morainic ridges, along with some subglacial features like possible fluted moraines and eskers, are present along the Viola Valley. Roches moutonées are also common, sometimes with striae. Rock glaciers, protalus ramparts, earth hummocks, gelifluction/solifluction lobes, and unsorted polygons are also also present. A large rock avalanche characterizes a wide section of the Viola Valley (*Hormes et al.*, 2008), while debris flows and scree slopes are widespread.

During the LGM, the upper Val Viola was covered by ice up to an elevation of about 2800m a.s.l. (*Bini et al.*, 2009). Deglaciation in the basins occurred no later than ~17.7 ka before the Gschnitz stadial re-advance (17-16 ka) (*Wirsig et al.*, 2016). Burga (1987) documented two Gschnitz glacier advances respectively at 1250m a.s.l. (Gschnitz I) and 1400m a.s.l. (Gschnitz II) in Val Viola. Morainic systems particularly well preserved in the mid and upper Val Viola have been associated to the Daun stadial (14.7 ka) at 1820m a.s.l. and to the Egesen/Younger Dryas stadial (13.0-11.7 ka) at 2010 m a.s.l., based on the dating of a peat bog (*Burga*, 1987). LIA moraines are well preserved in the upper portion of the Cantone di Dosdè Valley (*Scotti et al.*, 2017), and more recent fluctuations

are easy to reconstruct from the orthophotos (1950, 1998, 2003, 2007, 2014) provided by Geoportale Regione Lombardia and the Comitato Glaciologico Italiano Bulletins.

According to the Alpine Permafrost Index (*Boeckli et al.*, 2012), areas with permafrost are located above 2750m a.s.l. and the maximum Holocene permafrost expansion is above about 2200m a.s.l. (*Guglielmin and Siletto*, 2000).

3. METHODS

3.1.FIELD DATA COLLECTION

3.1.1. Podzol mapping and site selection

The first part of the work was focused on the selection of the soil profile locations. In order to select a suitable location, a total of 108 soil cores were analyzed (*Longhi*, 2017): 41 in the Stelvio Pass Area, 36 in the Viola Pass Area, 20 in the Gavia Pass Area, and 11 in the Forni Area. The corings were performed with a hand auger following transects across the valleys, taking into consideration the various geomorphological units present based on the CARG Regione Lombardia, sheet of Bormio 024 and sheet of Ponte di Legno 041, scale 1: 10000 in each area. The morphological analysis was also facilitated by the use of orthophotos from the Geoportale Regione Lombardia and satellite images from Google Earth and Bing. For each core, a double description is given: the first one of the station and the second one of the structure of the core itself.

For the station, in addition to the coordinates identified with a GPS, elevation, aspect, and slope are given, being careful to take the most horizontal planes possible. Furthermore, a percentage estimate of the vegetation cover and the stoniness is established as a percentage of the non-vegetated area; for the vegetation cover, the presence of herbaceous vegetation, lichens, and mosses is also indicated in percentage, while the stoniness is described as its composition in terms of gravel, sand and any clasts.

For the core, first of all, the length of each extracted section and the depth reached at each extraction must be registered, so that corrections can then be made in case of any compressions or expansions due to errors inherent in the instrument itself. Then the cores are divided into horizons and, for each horizon, the description followed the *Guidelines for soil description* (*FAO*, 2006): the depth in cm,

the colour using the Munsell tables, an estimate of the granulometry by field method, the distinctness of the limits (Abrupt, Clear, Gradual, Diffuse), and as far as possible their topography (Smooth, Wavy, Irregular, Broken).

The selection of the location of the profiles was based only on Podzols and on the previous work phase in order to analyze:

- Podzols placed on all the geomorphological forms analyzed and comparable, as well as at least one comparison in the valley floor;
- The podzols found at the highest altitudes;
- The podzols with greater depth up to the Bs or Bhs horizon;
- Podzols with interesting particularities and / or singular traits.

3.1.2. Soil Profile description and sampling

The soil survey involved the excavation of a total of 29 soil profiles: 13 in the Stelvio Pass Area, 6 in the Viola Pass Area, 8 in the Gavia Area, and 2 in the Forni Area (Figure 7).

Each soil profile is given an excavation suitable to exceed the depth of any Bhs or Bs horizons: the excavations must be completed only once the C horizon is reached and never less than 50cm deep.

The field analysis consisted of two different descriptions, that of the pedological station and that of the soil. The first one involved observing the surroundings of the profile to provide essential information for the subsequent data analysis:

- Date;
- Coordinates;
- Elevation;
- Aspect and slope (always less than 10°);

- Stoniness (described as a percentage of the non-vegetated area);
- Vegetational coverage (described as the percentage of cover between herbaceous vegetation, lichens, and mosses).

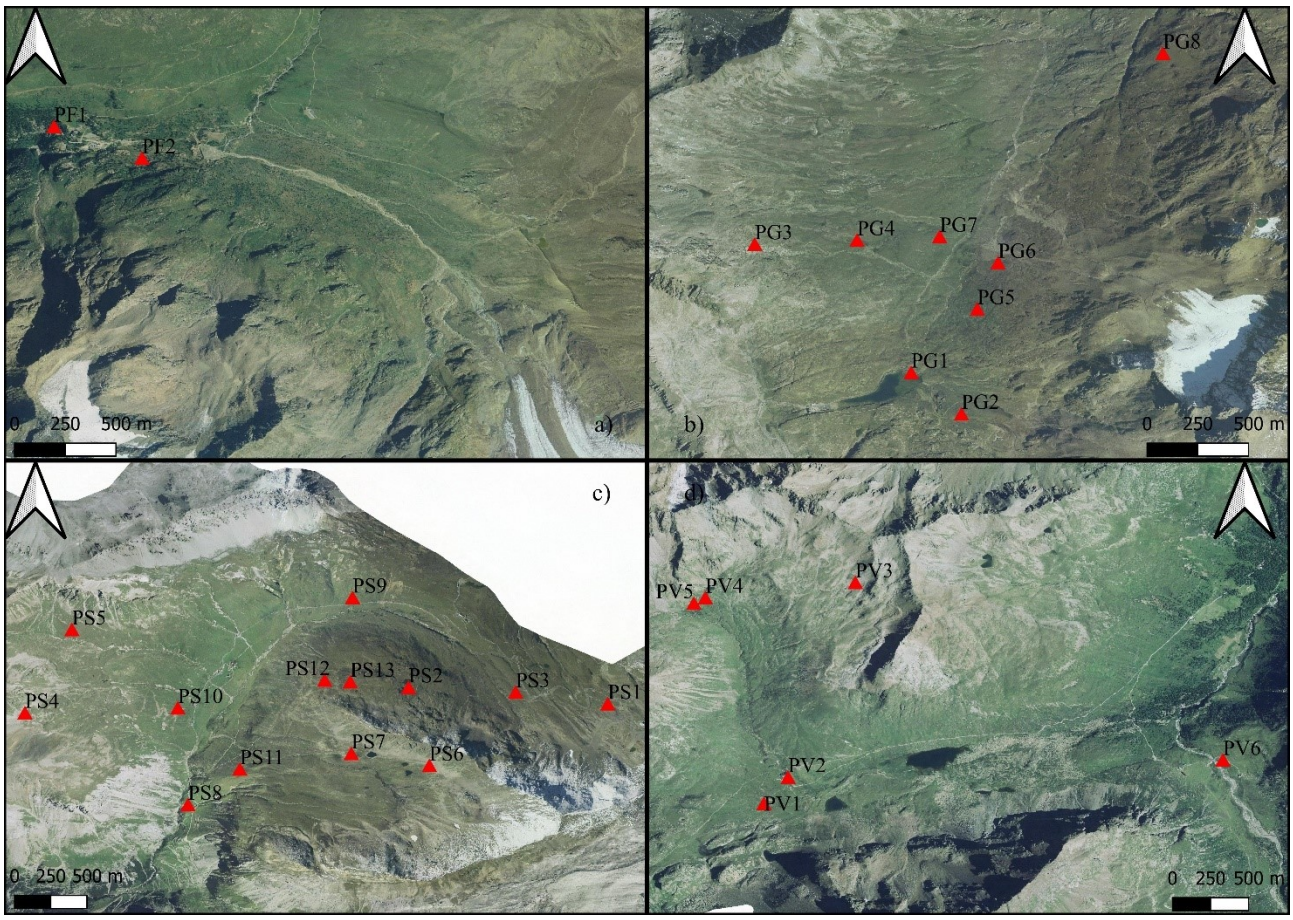

Figure 7: Distribution of the soil profile in the study areas (a) Forni Area; b) Gavia Pass Area; c) Stelvio Pass Area; d) Viola Pass Area).

The description of the soil instead consisted of its subdivision into horizons and, for each horizon, the description following *Guidelines for Soil Description* (*FAO*, 2006):

- Depth in cm;
- Distinctness of the limits (abrupt, clear, gradual, diffuse);
- Limits topography (smooth, wavy, irregular, broken);

- Shape of the aggregates (prismatic, polyhedral, granular, lamellar);
- Size of the aggregates (very fine, fine, medium, large);
- Colour (through the Munsell Tables);
- Granulometry (percentage of gravel, sand, silt, and clay);
- Root frequency (abundant, frequent, common, scarce, absent);
- Root size (very fine, fine, medium, large);
- Presence of cryoturbation.

Each profile is photographed and the photo is subsequently reworked through the GIMP software, in order to highlight the various horizons with their name directly in the photo (Figure 8). Soils were then classified using the *World reference base for soil resources 2014: International soil classification system for naming soils and creating legends for soil maps* (F.A.O., 2014).

Figure 8: PS2, an example of Skeletic Podzol.

About 1kg of sample is taken from each horizon A, Bhs, Bh, and from horizon E, if well developed and collectible. The samples were stored closed in plastic bags, subsequently weighed and reopened to be used in the following chemical and macroremains analyzes.

If buried organic matter or coals are found within any profile, cautions not to contaminate with new organic matter have been taken, and then the samples have been stored in aluminum paper at -4 ° C for future analysis.

Whenever possible, samples are taken with Kubiena boxes: this sampling method allows to obtain an undisturbed soil sample which is then used for the preparation of thin soil sections. For each profile described, samples are taken in interesting situations, mainly where the Bs horizon is particularly developed or at the contact between the E horizon and the Bs horizon.

3.1.3. Lakes sediments collection

Three peatlands sediments were sampled with an Eijkelkamp piston sampler 01.09 to obtain basal radiocarbon ages. Since all peatlands and lakes were dammed by morainic ridges or located in depressions between roches moutonées geomorphologically contemporary to the morainic ridges containing the soil profiles, the basal radiocarbon ages represent the minimum age of soil profile formation and give information about the deglaciation ages. The three sampled peatlands (Figure 9) are:

- RT in the Gavia Pass Area (46.35N, 10.48E, 2704m a.s.l.);
- TBG1 in the Gavia Pass Area (46.34N, 10.49E, 2657m a.s.l.);
- TBS1 in the Stelvio Pass Area (46.54N, 10.44E, 2565m a.s.l.).

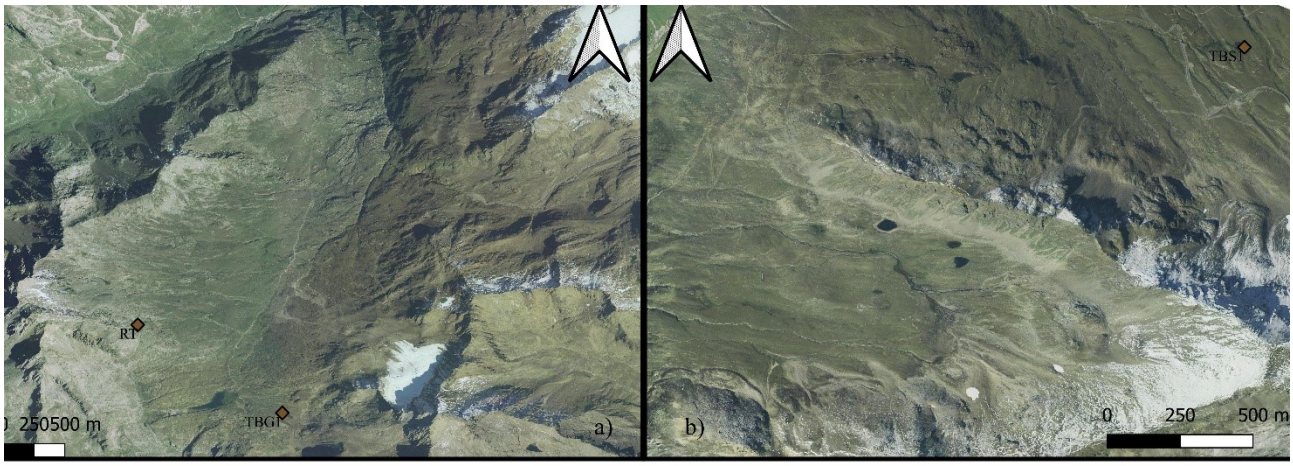

Figure 9: Distribution of the cores in the study areas (a) Gavia Pass Area; b) Stelvio Pass Area).

The cores (Figure 10) were described following the stratigraphy dividing them into segments and giving the segments' depth (in cm), colour (with the Munsell Tables), and particle size distribution. The taken samples were left to dry covered inside an aluminum foil, being careful not to let them contaminate by contact with the outside. Once dried, they were stored in the freezer at -20 ° C to avoid the formation of mold, and to conserve them for radiocarbon dating and further analysis.

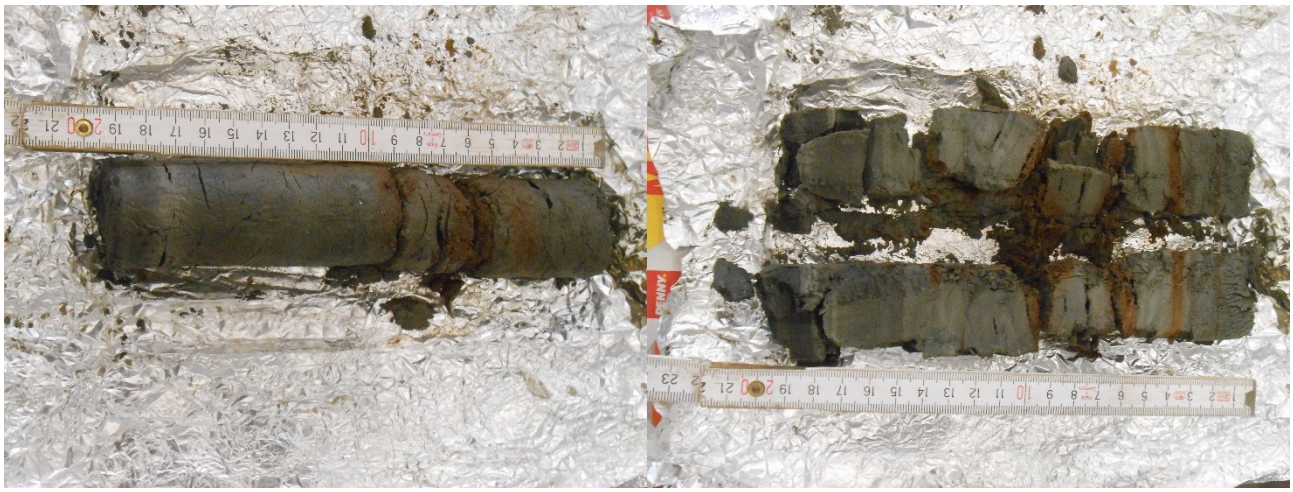

Figure 10: an example of the same sample as it is extracted (on the left) and just opened (on the right) of the TBG1 core.

3.1.4. Schmidt's Hammer

A Schmidt-Hammer type N with an impact pressure of 2.207 Nm, which is particularly suited for hard rock (*Guglielmin et al.*, 2012) has been used in three of the study areas: the Forni Area, the Gavia Pass Area, and the Stelvio Pass Area.

In order to avoid potential errors associated with the method, several precautions were taken.

First, large, flat, horizontal, or sub-horizontal surfaces of roches moutonnées were selected, possibly characterized by low roughness, to ensure a homogeneous weathering of crystals over the entire surface (*Williams and Robinson*, 1983; *Owen et al.*, 2007). Second, measurements were taken in dry conditions during summer to avoid the effects of moisture on the rocks (*Sumner and Nel*, 2002).

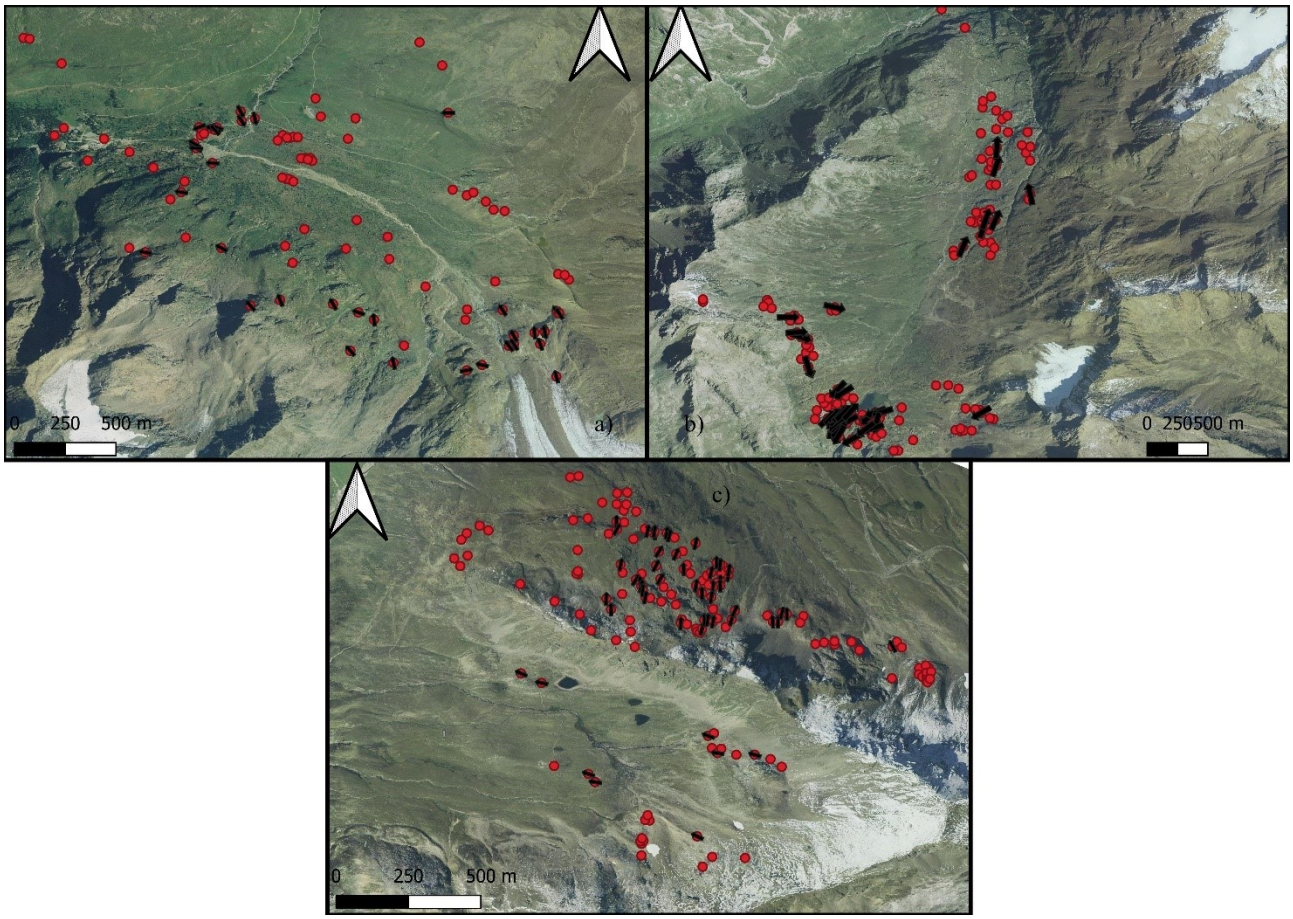

Figure 11: Distribution of the Schmidt Hammer Stations in the study areas (a) Forni Area; b) Gavia Pass Area; c) Stelvio Pass Area).

Third, lichen-covered surfaces (*McCarrol*, 1991) were intentionally avoided. Given the homogeneity of the chosen surfaces, 25 readings at each of the roches moutonnées stations were made, which Matthews and Owen (2010) consider statistically significant. Moreover, we considered the mean R-values of the 5 highest measurements (*Evans et al*., 1999; *Guglielmin et al.*, 2012) as the minimal exposure age of each tested surface. Striae orientation over roches moutonnées was also recorded in order to help in the reconstruction of the glacial flow directions.

A total of 400 stations were analyzed (Figure 11), divided as follows: 90 stations in the Forni Area, 171 stations in the Gavia Pass Area, and 139 stations in the Stelvio Pass Area.

3.1.5. Cosmogenic sample collection

The cosmogenic sample collection followed two distinct objectives. The first idea was to have absolute ages for roches moutonnées deglaciation to reconstruct glacial dynamic in three of the study areas. The general idea over the site selection was to draw an elevational transect on striated roches moutonnées in different morphological units so that the results should be related to different glacial phases. For this objective, 12 rock samples were sampled on top of the highest possible and flat roches moutonnées: 5 in the Gavia Pass Area, 4 in the Stelvio Pass Area, and 3 from the Viola Pass Area (Figure 12).

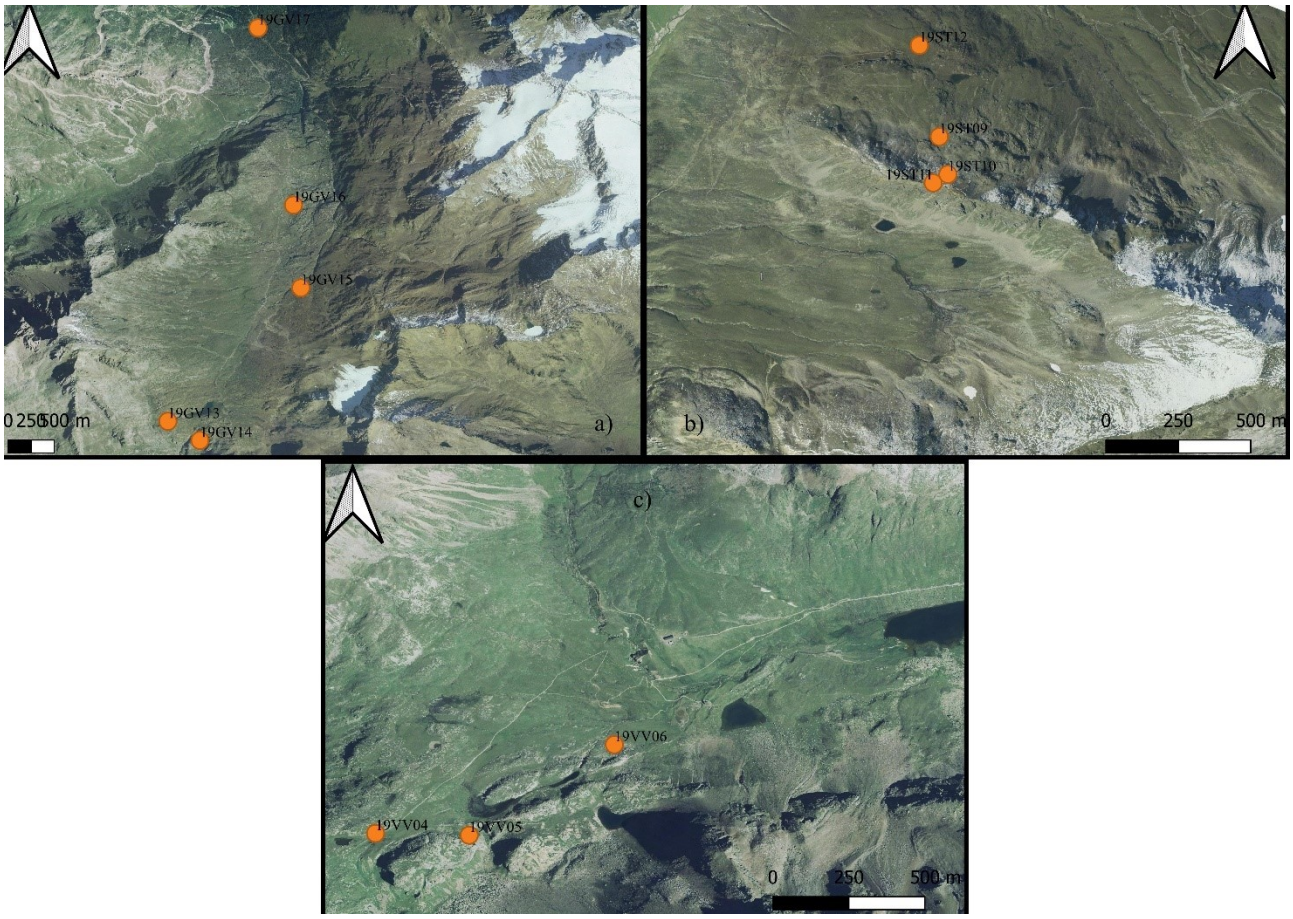

Figure 12: Distribution of the cosmogenic samples sites in the study areas (a) Gavia Pass Area; b) Stelvio Pass Area; c) Viola Pass Area).

The site characteristics are important for the future conversion of ^{10}Be concentration in exposure age, so for each site, a series of data have been collected (*Stone et al.*, 2000):

- Date and time;
- Latitude and Longitude;
- Elevation;
- Pressure;
- Temperature;
- Thickness;
- Skyline (Figure 13).

Figure 13: On-field description of the skyline using two different compasses.

The second idea was related to the Val Viola landslide: a previous work of thesis (*Longhi*, 2015) already divided the big landslide into different units with different ages and different lithologies using the Schmidt Hammer R-values. The idea was to verify this partition and the units' age: 3 boulders were sampled on Orthogneiss units and 2 boulders were sampled on Paragneiss units (Figure 14). The same site characteristics as the previous point have been registered.

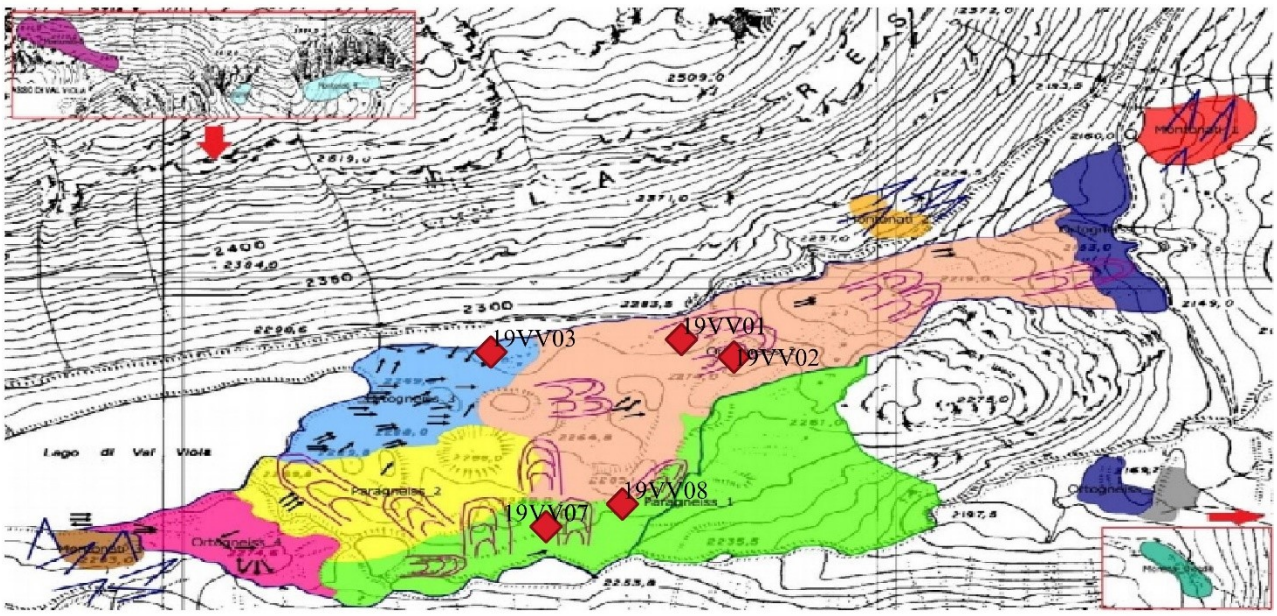

Figure 14: Distribution of the cosmogenic samples sites based on the units from Longhi (2015).

3.2.LABORATORY ANALYSES

3.2.1. Soil Routine Analyses

Routine soil analyses were performed on all the horizons sampled in the field.

The water content was calculated the percentage in water, the whole soil sample is weighed with a balance with a precision of one-tenth of a gram and is left in the dryer for 24 hours at 105° C. Then it is weighed again: the percentage in water is given by the normalized loss by weight between wet weight and dry weight (*Gardner,* 1986).

The particle size distribution was calculated stirring the sample in a series of sieves (weighted as tare) with the following openings: 25mm, 12.5mm, 9.5mm, 6.3mm, 4.7mm, 2.36mm, 2mm, 1.18mm, 0.6mm, 0.425mm, 0.3mm, 0.18mm, 0.15mm, 0.106mm, and 0.075mm for at least 20 minutes. At the end of the shaking, each sieve and the lower plate are weighed: by subtracting the tare and knowing the total dry weight, the percentage for each granulometry analyzed can be obtained. The particle size distribution was then classified according to ASTM classification (*ASTM*, 2007).

Soil pH (in H_2O) was determined on an oven-dried fine earth sample using a 1:1 soil:water ratio (*Kalra,* 1995). 50g of dry soil were weighed and placed in a 100ml beaker with 50ml of distilled water, mixed with a glass rod, and left to stand for 30 minutes, stirring the suspension every 10 minutes during this period. Subsequently, after an hour, the suspension is stirred again and the electrode is introduced for at least 3cm: after at least 30 seconds the reading is recorded.

Organic matter content was determined with LOI (loss-on-ignition) (*Blume et al.*, 1990; *Nelson and Sommers*, 1996). First, about 5g of fine earth were weighed and heated in a dryer at 105° C for 12 hours to remove the soil moisture. Subsequently, the samples were placed in a muffle at 440° C for 8 hours and left to rest so that they could not in any way moisten overnight. The samples are then

weighed again and the total organic matter is calculated as the percentage of weight lost during combustion:

$$SOM_{LOI} = \left(\frac{W_{105°C} - W_{440° C}}{W_{105°C}}\right) \times 100$$

where $W_{105°C}$ represents the sample weight at 105° C e $W_{440°C}$ represents the sample weight at 440° C.

3.2.2. Soil Iron Analysis

The standard procedure (*Mehra and Jackson*, 1960; *Jackson*, 1986) has been followed halving all the quantities for the dithionite extraction. About 2.5g of soils, ground to 0.06mm nominal pore size, were transferred in a 50mL polypropylene centrifuge tube. 20mL of 0.3M sodium citrate and 2.5mL of 1M sodium bicarbonate were added to the tube, then shook and heated to 78°C. At this point, 0.5g of sodium dithionite were added and the solution was stirred for about a minute and then intermittently for 5 minutes. This step was repeated a second time and at the end of the 5 minutes, 5mL of saturated NaCl solution were added to promote flocculation. The solution was then centrifuged at 2500 rpm for 20 minutes, then diluted in 2% nitric acid for ICP analysis.

The standard procedure (*Schwertmann*, 1964; *McKeague and Day*, 1966) have been followed for the oxalate extraction. 500 mg of soil, ground to 0.06mm nominal pore size, were transferred in a 50mL polypropylene centrifuge tube. 30mL of pH 3.0 ammonium oxalate solution were added to the tube that was immediately put in a light-proof container. The samples were then agitated for 2 hours on a reciprocating shaker and centrifuged at 2500rpm for 20 minutes, then diluted in 2% nitric acid for ICP analysis.

Two spoonfuls of 0.06mm grounded soil were pressured to create thin pads, then analyzed with an SEM-EDX system to calculate the total iron content of each sample.

3.2.3. Soil Macroremains

50 cm^3 of the sample were sieved at 2mm by manual sieving with the aid of distilled water.

The first phase, the macroremains research one, involved the use of a stereomicroscope with a maximum magnification of 4x. A portion of the previously sieved sample is placed in a petri dish with distilled water and, by observation under the stereomicroscope, the macroremains were identified and stored in another petri dish are isolated with the aid of entomologist tweezers. Once the operation is complete on the whole sample, the petri dish containing the macroremains of the horizon being analyzed is closed and stored at -4° C, moving on to the next sample.

Once all the macroremains have been isolated, the second phase consisted in the identification of the macroremains. The previously sampled macroremains were analyzed under a microscope with magnifications of 10x, 20x, 40x, and 100x and compared with images of reference books, in order to trace the possible species:

- A simplified seed identification key for nine species of Pinus based on morphological and anatomy characters, Paliwal et al., 1984;
- Samen un Fructe, Schlichtherle, 1985;
- Blattoberfla¨chen mitteleuropa¨ischer laubgeho¨ lze: Leaf surfaces of central European woody plants. Atlas and Keys, Westercamp and Demmelmeyer, 1997;
- Macrofossils as records of assemblages from sites at different altitudes in the SwissAlps - implications on climate and environment. Palaeo-plant responses to rapid Late Glacial climatic changes at three sites in the Swiss Alps, Tobolski and Ammann, 2000;
- Mire and peat macros, Van Geel and Mauquoy, 2007;
- Late-glacial vegetation development in Denmark – new evidence based on macrofossils and pollen from Slotseng, a small-scale site in southern Jutland, Mortensen et al., 2011;

- Impact of Holocene climate changes on alpine and treeline vegetation at Sanetsch Pass, Bernese Alps, Switzerland, Berthel et al., 2012.

3.2.4. Soil Micromorphology

From the undisturbed samples collected in Kubiëna boxes, glass-covered soil thin sections were prepared through impregnation with polystyrene. Micromorphological study of these thin sections employed an optical petrographic microscope Leica Laborlux 12pol (from 16x to 100× magnifications), equipped with an Olympus C4040 digital camera. Micropedological observations were carried out in plane polarized light (PPL), crossed polarized light (XPL), and oblique incident light (OIL). In thin sections descriptions, the terminology of Bullock et al. (1985) and Stoops (2003) was mainly used; specific references are given each time a different vocabulary is employed. Interpretation is mostly based on and Stoops et al. (2018). Very high importance is given to micromorphologies related to the presence of permafrost or ice lenses, as this could be related to the origin of podzols.

3.2.5. Cores Routine Analyses

On TBG1 and TBS1, after a by sight description of the colour (with the Munsell tables) and the difference in texture, samples have been taken every cm with a 1 cm^3 sampler (two samples every cm). On one of the samples, routine analyses have been carried on through the whole core. The water content was calculated the percentage in water, the whole soil sample is weighed with a balance with a precision of one-tenth of a gram and is left in the dryer for 24 hours at 105° C. Then it is weighed again: the percentage in water is given by the normalized loss by weight between wet weight and dry weight (*Gardner,* 1986).

The particle size distribution was calculated stirring the sample in a series of sieves (weighted as tare) with the following openings: 25mm, 12.5mm, 9.5mm, 6.3mm, 4.7mm, 2.36mm, 2mm, 1.18mm, 0.6mm, 0.425mm, 0.3mm, 0.18mm, 0.15mm, 0.106mm, and 0.075mm for at least 20 minutes. At the end of the shaking, each sieve and the lower plate are weighed: by subtracting the tare and knowing the total dry weight, the percentage for each granulometry analyzed can be obtained. The particle size distribution was then classified according to ASTM classification (*ASTM*, 2007).

Organic matter content was determined with LOI (loss-on-ignition) (*Blume et al.*, 1990; *Nelson and Sommers*, 1996). First, the samples were weighed and heated in a dryer at 105° C for 12 hours to remove the soil moisture. Subsequently, the samples were placed in a muffle at 440° C for 8 hours and left to rest so that they could not in any way moisten overnight. The samples are then weighed again and the total organic matter is calculated as the percentage of weight lost during combustion:

$$SOM_{LOI} = \left(\frac{W_{105°C} - W_{440° C}}{W_{105°C}}\right) \times 100$$

where $W_{105°C}$ represents the sample weight at 105° C e $W_{440°C}$ represents the sample weight at 440° C.

3.2.6. Cores Macroremains

The second of the 1 cm³ sample were sieved at 2mm by manual sieving with the aid of distilled water. The first phase, the macroremains research one, involved the use of a stereomicroscope with a maximum magnification of 4x. A portion of the previously sieved sample is placed in a petri dish with distilled water and, by observation under the stereomicroscope, the macroremains were identified and stored in another petri dish are isolated with the aid of entomologist tweezers. Once the operation is complete on the whole sample, the petri dish containing the macroremains of the horizon being analyzed is closed and stored at -4° C, moving on to the next sample.

Once all the macroremains have been isolated, the second phase consisted in the identification of the macroremains. The previously sampled macroremains were analyzed under a microscope with magnifications of 10x, 20x, 40x, and 100x and compared with images of reference books, in order to trace the possible species:

- A simplified seed identification key for nine species of Pinus based on morphological and anatomy characters, Paliwal et al., 1984;
- Samen un Fructe, Schlichtherle, 1985;
- Blattoberfla¨chen mitteleuropa¨ischer laubgeho¨ lze: Leaf surfaces of central European woody plants. Atlas and Keys, Westercamp and Demmelmeyer, 1997;
- Macrofossils as records of assemblages from sites at different altitudes in the SwissAlps - implications on climate and environment. Palaeo-plant responses to rapid Late Glacial climatic changes at three sites in the Swiss Alps, Tobolski and Ammann, 2000;
- Mire and peat macros, van Geel and Mauquoy, 2007;
- Late-glacial vegetation development in Denmark – new evidence based on macrofossils and pollen from Slotseng, a small-scale site in southern Jutland, Mortensen et al., 2011;
- Impact of Holocene climate changes on alpine and treeline vegetation at Sanetsch Pass, Bernese Alps, Switzerland, Berthel et al., 2012.

The results were then represented as number of macroremains of each species over depth with the software Tilia.

3.2.7. Cores Sand Mineralogical Composition

Half of the core was then subdivided in units: most of them were of 10cm (if the core didn't show any difference in stratigraphy), the other were depending of the depth of the layer. In the study, the

method proposed by Dell (1959) was followed on the units to describe the mineralogical composition of the sands of cores TBG1 and TBS1. After the removal of organic matter with hydrogen peroxide and the following cleaning with distilled water, the sample was divided into the desired fraction (from 0.075mm to 2.0mm) by sieving. The grains were then mounted on slides and identified using a petrographic microscope (from 16x to 100× magnifications) out in plane polarized light (PPL), crossed polarized light (XPL), and oblique incident light (OIL). The sands were then classified following the classification proposed by Pettijohn (1975) based on the percentages of quartz, feldspar, and lithic fragments.

3.2.8. Radiocarbon Datings

The basal cm of RT, TBG1, and TBS1 was reunited, sealed in aluminum foil, and frozen at -20°C. Concerning TBG1, after searching for macroremains of terrestrial plants, macroremains of a *Kalmia procumbens* leaf and a fragment of *Plantago alpine* were found. The material was insufficient for dating, so radiocarbon dating was performed on the bulk sediment including the plant fragments. . Concerning RT, after searching for macroremains of terrestrial plants, just a single fragment of a leaf of *Kalmia procumbens* was found, which was insufficient material for dating. The age was consequently obtained from bulk sediment including the leaf fragment. TBS1 had no macroremains, so the age was consequently obtained from bulk sediment. The samples were kept frozen until being sent to Beta Analytic Laboratories for radiocarbon dating. After pre-treatment, samples for radiocarbon dating were prepared for AMS by converting them into graphite. Calibrated ages were calculated with the software OxCal 4.2 using the INTCAL13 ^{14}C dataset (*Reimer et al.*, 2013). Radiocarbon age data are reported as conventional radiocarbon years BP (^{14}C yr BP) and as calibrated age ranges with a 2σ error (95.4%) (cal. yr BP; relative to AD 1950).

3.2.9. Cosmogenic Sample Preparation

The sample preparation for cosmogenic analysis followed a revised protocol from Wang et al. (2014) aiming to obtain about 10 g of pure quartz. The rocks were crushed and sieved to have grains between 250μm and 500 μm, starting from about 100 g; the sample was then cleared of the slimes rinsing it with water and in the sonic bath, and finally treated with 5% nitric acid and 5% hydrochloric acid for further cleaning and to remove any carbonate present. A surfactant separation was then performed as follows to separate minerals that fracture (quartz) from those that have cleavage planes (such as feldspar, micas, pyroxenes, and amphiboles). The rock was leached in 1% hydrofluoric acid for 30 minutes to fluorinate quartz surfaces and clean up other grain surfaces. Subsequently, 10 drops of dodecylamine solution and 10 drops of tea tree oil were added and mixed with the rock. Fluent water was flowed in the jar and abruptly stopped not to break up the foam layer formed on the surfaces: the feldspar and mica, attached to the foam, were then poured off into a different plastic tube. Then few drops of 5% hydrofluoric acid, 10 drops of dodecylamine solution, and 10 drops of eucalyptus oil were added again and the process was repeated. After 2 or 3 times, a clean pile of quartz was collected on the floor of the jar: all samples were etched in 2% hydrofluoric acid for three days a minimum of two times, and then was rinsed again to remove any hydrofluoric acid present.

Before the cosmogenic content analysis, the quartz underwent an aluminum check to evaluate the purity of the sample. 0.25g of each sample were transferred to the bottom of a clean vial beaker, and 5ml of 48%/50% hydrofluoric acid (Figure 15) and 1ml of 10% sulfuric acid were added.

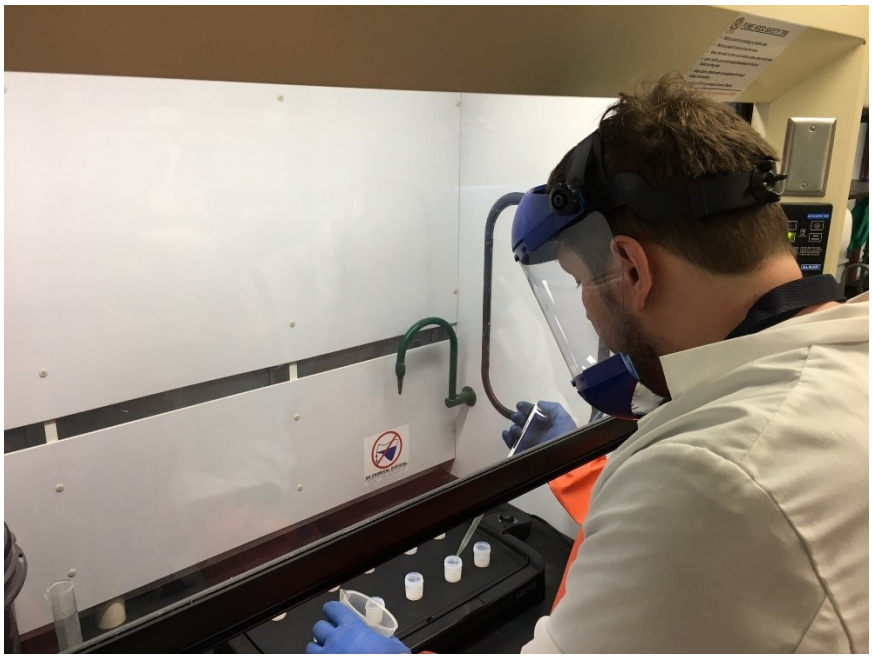

Figure 15: Adding 48%/50% hydrofluoric acid for quartz dissolution.

The vials were posed on a hotplate set to 120° C and left to dissolve and evaporate overnight. If the samples have dissolved and evaporated as expected, in the cooled vial 10ml of 1% nitric acid were added and the samples were analyzed for Al, Fe, and Ti in an ICP-OES: if the samples have less than 150ppm Al, they were clean enough for cosmogenic analysis. Even if Fe or Ti concentration were higher than 300ppm the sample was treated as failed. If samples failed, they underwent additional mineral separations, including heavy liquids with lithium heteropolytungstate (LST), magnetic separation on a Frantz separator, additional surfactant separations, treatment with 3M potassium hydroxide, and additional treatments with 1% hydrofluoric acid / 1% nitric acid.

Unfortunately, even if the samples were ready for cosmogenic analysis, due to Covid-19 outburst, all analyses were delayed and no data are available at the moment of the writing of this dissertation.

3.3.DATA ANALYSIS

3.3.1. Iron Crystallinity Ratio Calibration

The crystallinity ratio of free iron oxides (CRF) was calculated as $CRF = \frac{Fe_d - Fe_o}{Fe_{tot}}$ (*Arduino et al.*, 1984; *Arduino et al.*, 1986; *Maejima et al.,* 2002), where Fe_d is the iron fraction extracted with dithionite, Fe_o is the iron fraction extracted with oxalate, and Fe_{tot} is the total iron content.

Five absolute ages were used to determine the relationship between CRF and soil formation age. Because the A horizon may be the result of an integrated soil type that forms when a podzol develops into a new kind of soil (*Maejima et al.,* 2002), different calibrations were performed for the A and Bs horizons. Differences between the results may then permit the evaluation of the calibration curves' reliability. The calibration consisted of a logarithmic regression between CRF and the mean value of the absolute ages and the confidence interval of the curves was calculated with a logarithmic regression between CRF and the maximum and minimum of the absolute ages. The logarithmic regression was chosen because the CRF depends on the alteration of iron: as time passes, the not altered iron decrease and so the logarithmic function is the most representative for this phenomenon. The five absolute ages used in the calibration were the following (Figure 16):

- The basal age of TBG1 was considered the minimum age of formation for profile PG2 because the drilled pond containing TBG1 is dammed by the morainic ridge containing PG2.
- The minimum formation age of profile PG3 is considered the basal age of RT, as the drilled pond lies in a depression among some roches moutonées in the same geomorphological unit as the profile.
- The basal age of TBS1 was considered the minimum age of formation for profile PS1, as the pond is within a depression among some roches moutonées in close proximity to profile PS1.

- The lake “Laghetto Alto”, cored in a previous thesis, is within a depression among some rochees moutonneès very close to profile PS2. The age of the basal lacustrine sediment was considered the minimal age of profile PS2.
- In addition to these four radiocarbon dates, one ^{10}Be age of 15661-12049 cal. BP (*Scotti et al.*, 2017) for a granitic boulder in the morainic ridge containing soil profile PV6 was used as minimum formation age for the soil profile.

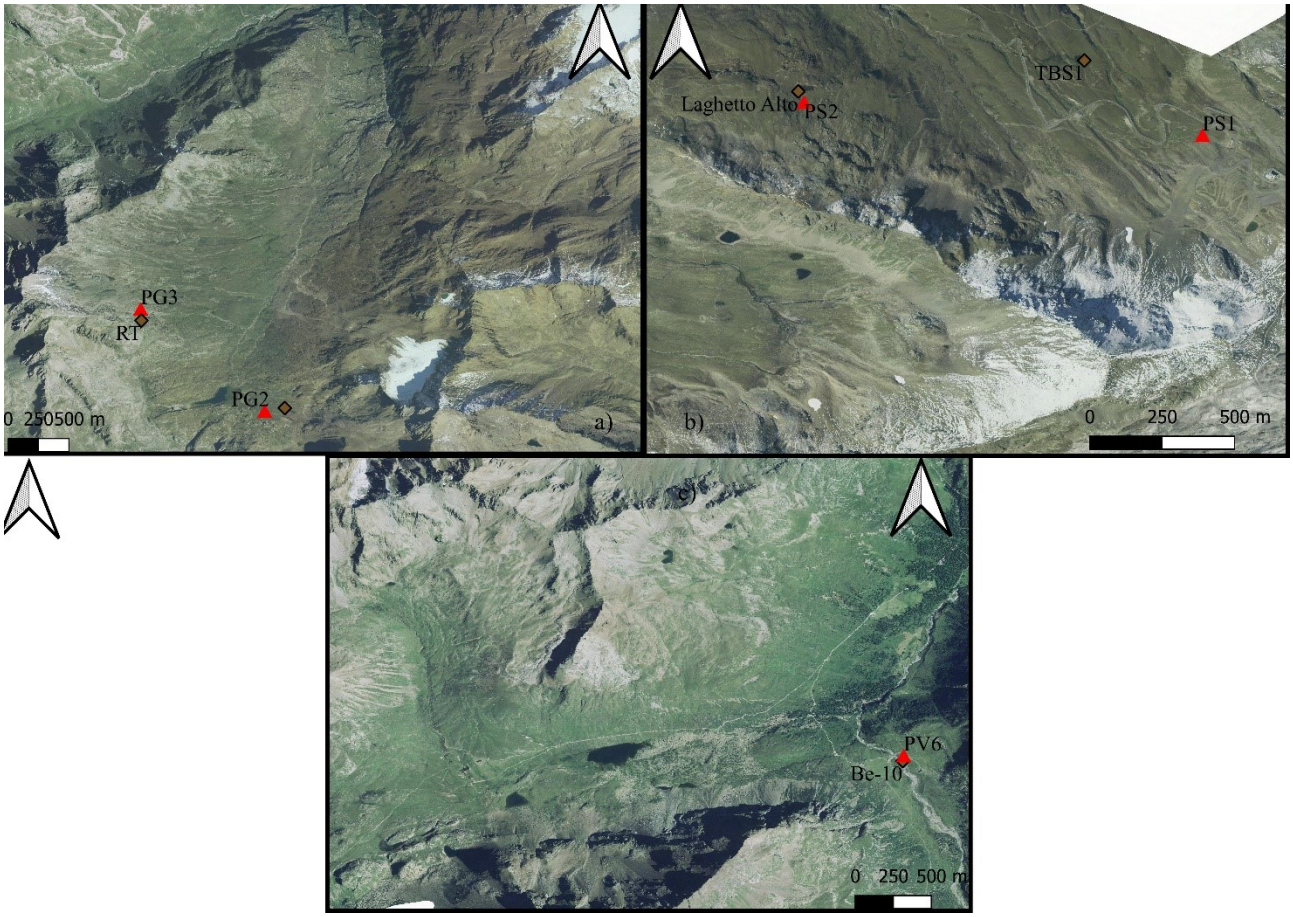

Figure 16: Distribution of soil profiles and relative absolute ages for the calibration in the study areas (a) Gavia Pass Area; b) Stelvio Pass Area; c) Viola Pass Area).

3.3.2. Schmidt's Hammer R-Values Calibration

A different approach was used in the Gavia Pass Area and in the Forni Area.

In the Gavia Pass Area, three different rock types were analyzed: orthogneiss, paragneiss, and micaschists. However, an evaluation of the description in the geological map suggested not consider orthogneiss as the mineralogical composition is very different. To test the difference in weathering between paragneiss and micaschists in this area, Unit 7b, where both lithologies were present in nearly the same percentage, was further investigated. R-value and its standard deviation on the 30 stations of micaschists and on the 34 stations of paragneiss were calculated and compared to evaluate if measurements from both lithologies could be correctly used jointly in the study area. Three ^{14}C ages and one historical age were used for the calibration of Schmidt's Hammer R-values (Figure 17b). The first age corresponds to the base of Core RT, drilled in a relict pond dammed by a morainic ridge close to site MGV108 (Unit 4a); this, therefore, represents its minimal exposure age. The second age corresponds to a paleosol buried in front of a rock glacier located at the base of C.rno dei Tre Signori, in the Lake Bianco catchment, and represents the minimal exposure age of Site MGV87 (Unit 2b). The third ^{14}C age corresponds to the base of Core TBG1 and represents the minimal exposure age of MGV161 (Unit 5b). The historical ages were calculated from overlaying the orthophotos (2000 and 1975, provided by Geoportale Regione Lombardia); this constrains the minimal exposure age of MGV110 (Unit 1a). Four calibration curves were generated with a linear regression using the R25 (the mean R-value considering all 25 the readings of every site) and R5 (considering the highest 5 R values from the reading of every site) values from the single station closest to the site of the ^{14}C-dated samples and with the mean R25 and R5 values for all stations within in the unit containing the ^{14}C sample site. For each calibration curve, the confidence interval was calculated by applying a linear regression between the maximum and minimum of the R-value (R±Std. Dv.) and the maximum and minimum of the ^{14}C ages.

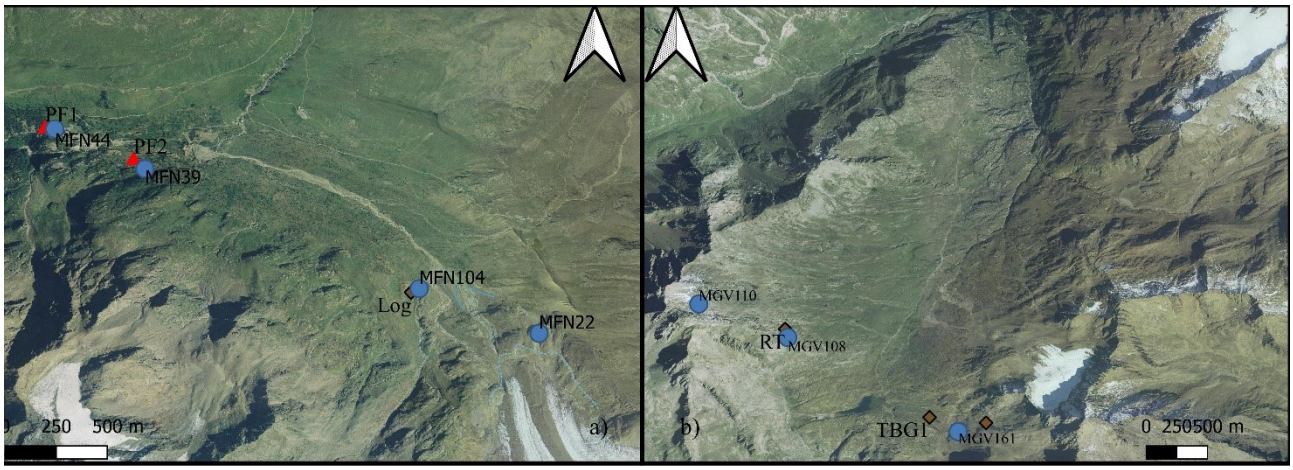

Figure 17: Distribution of roches moutonneés and relative ages for the calibration in the study areas (a) Forni Area; b) Gavia Pass Area).

In the Forni Area, the Schmidt's Hammer measurements were on a single lithology, micaschists, so all the data were comparable. Two CRF calculated age on soil, one ^{14}C age, and one historical age were used for the calibration of Schmidt's Hammer R-values (Figure 17a). The oldest age corresponds to the age of the dated soil PF1, dug on a morainic ridge close to site 44 (Unit 7); this, therefore, represents its minimal exposure age of unit 7 because the soil can be developed after some decades after the glacier advance. The second age corresponds to the age of PF2, soil pit opened on a morainic ridge close to site 39 (Unit 6), and also in this case, therefore, represents the minimal exposure age of Unit 6. The only ^{14}C age available, corresponds to the age of a Pinus cembra log (*Pelfini et al.*, 2014) found close to site 104 (Unit 5), and dated 4117 Cal BP, representing its minimal exposure age. Finally, the historical age was calculated from overlaying the orthophotos (1998 and 1981, provided by Geoportale Regione Lombardia); this constrains the minimal exposure age of the whole Unit 2. The calibration curve was calculated on the mean of the 25 values of all the stations containing the absolute age and the confidence interval was calculated by applying a linear regression between the maximum and minimum of the R-value (R±Std. Dv.) and the maximum and minimum of the absolute ages.

3.3.3. Glacial Reconstruction

The final step was to reconstruct the different phases of deglaciation with the aim of the software QGIS 3.16. All the ^{14}C age, the soil ages obtained via the CRF calibration curves, the exposure ages obtained via the Schmidt's Hammer calibration curves, the geomorphological evidence of glaciation (mainly morainic ridges and the striae on roches moutonnées), and the historical position obtained from maps and orthophotos were combined to obtain deglaciation phases. Different phases were then confronted between themselves in the four study areas and were then referenced to post-LGM glacial advances in the most proximal location from previous studies (*Burga*, 1987; *Ivy-Ochs et al.*, 2006; *Hormes et al.*, 2008; *Chenet et al.*, 2016; *Moran et al.*, 2016; *Scotti et al.*, 2017; *Kronig et al.*, 2018) and related to lake sediment records (*Heiri et al.*, 2014; *Ilyashuk et al.*, 2011; *Lauterbach et al.*, 2011; *Ortu et al*., 2008), the INTIMATE event stratigraphy (*Rasmussen et al.*, 2014), the NGRIP $\delta^{18}O$ (*Walker et al.*, 2009; *Walker et al.*, 2012), the biostratigraphic division (*Iversen*, 1954), and the European pollen zones (*Iversen*, 1954).

4. RESULTS

4.1. THE USE OF IRON CHEMICAL ANALYSIS OF PODZOLS TO DATE THE LATE PLEISTOCENE-HOLOCENE DEGLACIATION HISTORY OF THE CENTRAL ITALIAN ALPS

JOURNAL OF QUATERNARY SCIENCE (2020) **35**(8) 1021–1035 ISSN 0267-8179. DOI: 10.1002/jqs.3253

JQS Journal of Quaternary Science QRA

The use of iron chemical analysis of podzols to date the Late Pleistocene–Holocene deglaciation history of the Central Italian Alps

ALESSANDRO LONGHI,[1] DAMIANO MONTICELLI[2] and MAURO GUGLIELMIN[1]*
[1]Department of Theoretical and Applied Sciences, Insubria University, Varese, Italy
[2]Department of Science and High Technology, Insubria University, Como, Italy

Received 22 May 2020; Revised 21 August 2020; Accepted 21 September 2020

ABSTRACT: Podzols that have developed on glacial and periglacial features provide the opportunity to reconstruct glacial evolution after the Last Glacial Maximum (LGM) using different soil indices. Analysing 17 soils classified as podzol, we used the crystallinity ratio of free iron oxides (CRF) on both the A and Bs horizons, and absolute ages for the same landforms containing the soil profile, to create dating curves. Two equations were generated: age = 4566.9 × ln (CRF) + 1760 (1), and age = 3907 × ln (CRF) + 3508.2 (2). The reliability of the curves was evaluated with the Fe_o/Fe_d ratio, and with the difference of ages calculated using both equations. Equation (2) is considered more reliable because the A horizon may be influenced by new pedogenesis on the pre-existing podzol, leading to the development of a new type of soil. By dating the soils, we reconstructed the glacial history of the three main upper branches of the LGM Adda Glacier in the Central Italian Alps, specifically the Stelvio Pass area (ST), Gavia Pass area (GV), and the Val Viola valley (VV). Seven glacial advances were identified at 16.7–14.7 ka (phase I), 12.3 ka (phase II), 11 ka (phase III), 10–9.7 ka (phase IV), 9 ka (phase V), 7.5 ka (phase VI) and 5.3 ka (phase VII). The first five phases are chronologically similar to the main Late Pleistocene–Early Holocene phases recorded in the Central European Alps. The last two Holocene phases, which are both longer in duration than the Little Ice Age, are recorded in ST and GV. Interestingly, these phases generally are not recorded in the rest of the Central European Alps, where the late Holocene glaciers were smaller than their present size. Copyright © 2020 John Wiley & Sons, Ltd.

KEYWORDS: glacial reconstruction; Holocene; Italian Alps; Late Pleistocene; soils

INTRODUCTION

Knowledge about deglaciation after the Last Glacial Maximum (LGM) in the mountain areas of the Alps is still limited (Tremblay *et al.*, 2019). Cosmogenic nuclide analysis places the limit of the LGM in the Swiss Alps between 21.1 and 19.1 ka (Ivy-Ochs *et al.*, 2004, 2015); by 18 ka, more than the 80% of the ice volume had melted (Ivy-Ochs *et al.*, 2008, 2015; Wuthrich *et al.*, 2018). Subsequently, glaciers re-advanced, reaching a maximum at around 17 ka and a stabilisation ca. 15.4 ka (Ivy-Ochs *et al.*, 2008, 2015; Wuthrich *et al.*, 2018). Successive phases of glacier advance occurred between 13.5 and 12 ka, (Egesen stadial: e.g. Kerschner *et al.*, 2000; Bohlert *et al.*, 2011; Ivy-Ochs, 2015) and between 11.3 and 10 ka (Zoller *et al.*, 1998; Ivy-Ochs *et al.*, 2006, 2008).

In the Italian Alps, most prior studies evaluated low elevation sites and set the latest LGM culmination between 26 ka and 17 ka (Comerci *et al.*, 2007; Ravazzi *et al.*, 2012, 2014; Pini *et al.*, 2016; Ivy-Ochs *et al.*, 2018). At high elevations, the latest LGM culmination is placed before 17 ka (Favilli *et al.*, 2008) in the Eastern Alps; recalculation of moraine boulder exposure rates in the Maritime Alps places the LGM around 24 ka (Federici *et al.*, 2016). In the latter, the Bühl stadial was dated around 18.5 ka and the Egesen stadial around 13.5 ka (Federici *et al.*, 2016). In the Garda Basin, a regressive phase interrupted forest growth between 16.4 and 15.5 ka (Ravazzi *et al.*, 2012).

Beyond these studies, knowledge related to the LGM and successive glacial phases in the Italian Central Alps is still scarce.

Soils that have developed on glacial and periglacial features, such as late-glacial moraines and rock glaciers, provide the opportunity to date deglaciation or to investigate subsequent geomorphological modification (e.g. Favilli *et al.*, 2008). The original soil profile development index proposed by Harden (1982), based on quantification of field information, has been applied in many recent studies (e.g. Huges *et al.*, 2006; Hannah *et al.*, 2017). Other well-known soil age indicators include soil pH, rubification, or transformation of pedogenic Fe and Al (e.g. Birkeland, 1999, Egli *et al.*, 2003, 2006, 2010, 2015), but these give relative instead of absolute ages. The present study aims to apply one of these relative dating methods, the iron crystallinity ratio (Arduino *et al.*, 1984; Maejima *et al.*, 2002), and evaluate the possibility of using it as an absolute dating method for deglaciation in a sector of the Central Italian Alps (Upper Valtellina). If successful, the method could then be used as a template for reconstructing the deglaciation history of other Alpine areas.

*Correspondence: M. Guglielmin, as above.
E-mail: mauro.guglielmin@uninsubria.it

STUDY AREA

The study area is located in Upper Valtellina, Central Italian Alps. Our sample sites are divided among the region's three main valleys: the Stelvio Pass area (ST), the Gavia Valley (GV), and the Val Viola – Val Cantone area (VV). (Fig. 1)

Stelvio Pass (ST)

The Stelvio Pass area is located in the Braulio basin, a tributary of the Adda River, between 2200 and 2704 m asl. The most common lithologies in the area are granitic and granodioritic orthogneiss and biotitic paragneiss. Geomorphologically, the landscape records its glacial, paraglacial and periglacial history; roches moutonées, morainic ridges, rock glaciers and protalus ramparts are common, as well as gelifluction lobes

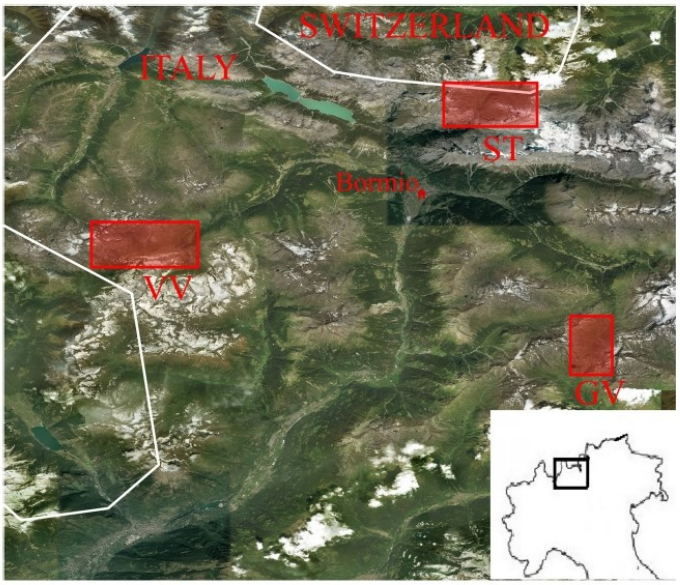

Figure 1. Reference map for site location: GV = Gavia Valley, ST = Stelvio Pass area, VV = Val Viola–Val Cantone. [Color figure can be viewed at wileyonlinelibrary.com].

and terracettes. Several deep slope deformations, debris flows, and scree slopes are among the more common gravitational features. Glaciers have been completely absent from the study area since 1952 (Guglielmin *et al.*, 2001). The mean annual air temperature in the area is between +1 °C and −3 °C (Cannone *et al.*, 2007), and the mean annual precipitation is 1310 mm/a.

Gavia Valley (GV)

The GV is located in the Gavia basin, a tributary to Frodolfo Creek, between 2500 and 2784 m asl. The most common lithologies in the area are orthogneiss, paragneiss and quartz-phyllites, mostly strongly retrogressed varieties of medium-grade paraschist (Dal Piaz *et al.*, 1988). The valley bottom is mainly rocky with clear evidence of glacial erosion, including roches moutonées and several ponds among these. The valley sides are mainly covered by ablation till with several morainic ridges from the different lateral glaciers. A few rock glaciers and many small periglacial landforms such as earth hummocks and gelifluction/solifluction lobes are also present. Currently, two glaciers still exist in the area with mean front elevations of 2980 m asl and 2790 m asl. The mean annual temperature is between +1 °C and −1.4 °C (Hijmans *et al.*, 2005), and the mean annual precipitation is 1150 mm/a.

Val Viola – Val Cantone (VV)

The Val Viola – Val Cantone area is located in the upper part of the Viola Creek basin, a tributary to the Adda River, between 2100 and 2740 m asl. The Viola Valley is aligned ENE–WSW, corresponding to the strike of the overthrust between the Campo Unit and the Grosina Unit. The lower unit (Campo Unit) is characterised by paragneiss and micaschists, with anphibolites and orthogneiss intercalations, while the upper (Grosina Unit) is mainly composed of orthogneiss, migmatites, and higher-grade paragneiss. Some late Varisican intrusive granitic, granodioritic and dioritic bodies crop out near Pizzo Bianco and the Val Viola Pass.

There is clear evidence of glacial, paraglacial and periglacial processes in this area. Several morainic ridges, along with some subglacial features like possible fluted moraines and eskers, are present along the Viola Valley. Roches moutonées are also common, sometimes with striae. Rock glaciers, protalus ramparts, gelifluction/solifluction lobes, earth hummocks and unsorted polygons are also present. A large rock avalanche characterises a part of the Viola Valley (Hormes *et al.*, 2008), while debris flows and scree slopes are widespread. The mean annual air temperature is between 3 °C and −4 °C, and the mean annual precipitation is between 700 mm and 1900 mm (data from the Arnoga meteorological station, ARPA Regione Lombardia).

METHODS

Field data

In order to select the soil profile locations, we first cored the soils with a hand auger to check for the presence of podzols. For each core, the site characteristics (coordinates, elevation, aspect, slope, vegetational coverage, dominant vegetation, and stoniness) and the soil characteristics (horizon sequence, colour, texture, structure, characteristics of the boundaries, and eventual cryoturbations) were described following the *Guidelines for Soil Description* (FAO, 2006). At sites where podzols were identified, profiles were dug on the flat top of morainic ridges in order to reconstruct the different glacial phases. The number of examined profiles in every study area was proportional to their extent. A total of 17 soil profiles were opened: eight for ST, six for VV, and three for GV. All soil profiles were described through the C horizon and to a minimum depth of 50 cm. For each soil profile, the site characteristics (coordinates, elevation, aspect, slope, vegetational coverage, dominant vegetation and stoniness) and the soil characteristics (horizon sequence, colour, texture, structure, characteristics of the boundaries and eventual cryoturbations) were described following the *Guidelines for Soil Description* (FAO, 2006). Moreover, approximately 1 kg of soil was sampled from the A, B and (when possible) E horizons.

Soils were then classified using the *World reference base for soil resources 2014: International soil classification system for naming soils and creating legends for soil maps* (FAO, 2014).

Some peatlands and lake sediments were sampled with an Eijkelkamp piston sampler 01.09 to obtain basal radiocarbon ages. Since all peatlands and lakes were dammed by morainic ridges or located in depressions between roches moutonées geomorphologically contemporary to the morainic ridges containing the soil profiles, the basal radiocarbon ages represent the minimum age of soil profile formation and give information about the deglaciation ages.

Routine soil analysis

Routine soil analyses were performed on the 39 horizons sampled in the field. Water content was calculated with weight loss by oven-drying the soil at 105 °C (Gardner, 1986). Soil pH (in H_2O) was determined on an oven-dried fine earth sample using a 1:1 soil:water ratio (Kalra, 1995). The particle size distribution was measured using a series of sieves (25 mm, 12.5 mm, 9.5 mm, 6.3 mm, 4.7 mm, 2.36 mm, 2 mm, 1.18 mm, 0.6 mm, 0.425 mm, 0.3 mm, 0.18 mm, 0.15 mm, 0.106 mm and 0.075 mm) and classified according to the ASTM classification (ASTM, 2007). Organic matter content was determined with LOI (loss-on-ignition) on 5 g of fine earth heated to 400 °C for 8 hours (Blume *et al.*, 1990; Nelson and Sommers, 1996).

Soil chemical analysis

The standard procedure for dithionite extraction (Mehra and Jackson, 1960; Jackson *et al.*, 1986) was followed with half of the reagent quantities on about 2.5 g of ground soil.

The standard procedure for oxalate extraction (Schwertmann, 1964; McKeague and Day, 1966) was applied to 500 mg of ground soil. Both extraction procedures were tested for reproducibility by repeating the analysis three times on three random samples.

Two spoonfuls of 0.06 mm ground soil were pressured to create thin pads, then analysed with a SEM-EDX system to calculate the total iron content of each sample.

The crystallinity ratio (CRF) was calculated as $Cr = \frac{Fe_d - Fe_o}{Fe_{tot}}$ (Arduino *et al.*, 1984, 1986; Maejima *et al.*, 2002), where Fe_d is the iron fraction extracted with dithionite, Fe_o is the iron fraction extracted with oxalate, and Fe_{tot} is the total iron content.

Radiocarbon dating

The basal cm of each peat or lacustrine sediment core was sampled, sealed in aluminium foil, and frozen at −20 °C. The samples were kept frozen until being sent to Beta Analytic Laboratories for radiocarbon dating. After pre-treatment, samples for radiocarbon dating were prepared for AMS by converting them into graphite. Calibrated ages were calculated with the software OxCal 4.2 using the INTCAL13 ^{14}C dataset (Reimer *et al.*, 2013). Radiocarbon age data are reported as conventional radiocarbon years BP (^{14}C yr BP) and as calibrated age ranges with a 2σ error (95.4%) (cal yr BP; relative to AD 1950).

CRF–age calibration and glacial reconstruction

Five absolute ages were used to determine the relationship between CRF and soil formation age. Since the A horizon may be the result of an integrated soil type that forms when a podzol develops into a new kind of soil (Maejima *et al.*, 2002), different calibrations were performed for the A and Bs horizons. Differences between the results may then permit evaluation of the calibration curves' reliability. The calibration consisted of a logarithmic regression between CRF and the mean value of the absolute ages. The confidence interval of the curves was calculated with a logarithmic regression between CRF and the maximum and minimum of the absolute ages.

Finally, we combined the ^{14}C ages, the soil ages obtained via the CRF calibration curves, and the geomorphological evidence of glaciation (mainly the morainic ridges and the striae on some roche moutonnée) to reconstruct the different phases of deglaciation in QGIS 3.16.

RESULTS

Soil description

The main site characteristics and soil classification are synthesised in Table 1, while soil characteristics described in the field are listed in Table 2.

The soil profiles were collected at elevations between 2126 m (PV6 in VV) and 2789 m (PG3 in GV), and all the three study areas contained podzols up to at least 2704 m. All the analysed sites had more than 70% vegetational coverage; generally, herbaceous plants typical of natural Alpine meadows. In contrast, PV3 and PG3 were dominated by lichens, whereas mosses were the dominant vegetation at PG2 and PS6. None of the soils were very developed, and the thickness of A + B was always less than 60 cm. The thinnest soil profile was PV5 with only 25 cm, and the thickest was PS8 with 56 cm. Twelve profiles displayed an E horizon associated with diagnostic Albic material (PG1, PG3, PS1, PS2, PS3, PS4, PS5, PS6, PS7, PS8, PV1 and PV4); this horizon was always present in ST. The diagnostic Spodic horizon was present in all soil profiles with a thickness of between 10 cm (PV5) and 28 cm (PV1).

All the described soils are classified as podzols (see example in Fig. 2); eight were classified as Albic podzols, five as Skeletic podzols, three as Entic podzols, and one as a Gelic podzol. All three study areas present Albic soils characterised by an evident E Albic horizon.

Charcoals were found in profile PV6 at 8–10 cm and 13–14 cm depth.

Cryoturbations were found in several profiles: PG3 and PS2 between the B and C horizons, PS4 between the E and B horizons, and PS7 and PV3 between the B and B/C horizons.

Soil laboratory results

The main soil characteristics determined by laboratory analysis are reported in Table 3. The silt and clay fraction is always <10% (Table 3), reaching its highest values in the Bs horizon of PV3 (9.03%) and in the Bhs horizon of PG2 (8.54%). On average, the Stelvio area's A and Bs horizons are the most skeletic and sand-poor profiles, whereas the Val Viola area is the opposite.

The pH is fairly acidic in every horizon, ranging between 3.7 in PG3-A and 4.64 in PG1-Bs. The Stelvio and Gavia areas have the same mean pH of 4.18, whereas the Val Viola area has a slightly higher mean pH (4.28 ± 0.17). In every profile, the B horizon is more acidic than the corresponding A horizon, with the exception of profile PS3.

The LOI ranges between 5.23% in PG1-Bs and 22.43% in PV4-A. The A and Bs horizons from the Val Viola area have the highest mean LOI, whereas the Gavia area has the lowest. The A horizon has a higher LOI value than the B horizon as expected in every profile with the exception of profile PS1.

Table 1. Site description and soil classification.

Profile ID	X	Y	Elevation (m a.s.l.)	Aspect (°)	Slope (°)	Vegetational coverage	Dominant vegetation	Stoniness	Horizon sequence	Soil classification	Depth (cm)
PG1	46.34586	10.49383	2602	5	2	70%	Herbaceous	30%	O-A-E-Bs-C	Albic podzol	36
PG2	46.34295	10.49696	2641	230	2	100%	Mosses	0%	O-A-Bhs-Bs-C	Entic podzol	44
PG3	46.35523	10.48203	2789	112	3	60%	Lichens	40%	O-A-E-Bs-C	Albic podzol	35
PS1	46.53214	10.44636	2655	240	2	80%	Herbaceous	20%	O-A1-A2-E-Bs-B/C-C	Albic podzol	48
PS2	46.53441	10.42816	2588	338	2	90%	Herbaceous	10%	O-A-E-Bs-C	Skeletic podzol	38
PS3	46.53280	10.43835	2534	274	3	100%	Herbaceous	0%	O-A-E-Bs-B/C-C	Skeletic podzol	35
PS4	46.53158	10.39423	2700	98	4	90%	Herbaceous	10%	O-A-E-Bs-B/C-C	Gelic podzol	48
PS5	46.53849	10.39837	2610	180	4	80%	Herbaceous	20%	O-A-E-Bs-B/C-C	Albic podzol	45
PS6	46.5263	10.42936	2630	250	1	75%	Mosses	25%	O-A-E-Bhs-Bs-C	Skeletic podzol	40
PS7	46.52733	10.42352	2647	301	0	70%	Herbaceous	30%	O-A-E-Bs-B/C-C	Albic podzol	48
PS8	46.52228	10.40879	2228	356	4	95%	Herbaceous	5%	O-A-E-Bhs-Bs-C	Albic podzol	56
PV1	46.41917	10.15708	2347	126	0	60%	Herbaceous	40%	O-A-E-Bs-C	Albic podzol	48
PV2	46.42117	10.15922	2359	152	4	95%	Herbaceous	5%	O-A-E-Bs-C	Albic podzol	45
PV3	46.43767	10.16492	2740	256	0	60%	Lichens	40%	O-A-Bs-B/C-C	Skeletic podzol	40
PV4	46.43666	10.15191	2564	160	4	90%	Herbaceous	10%	O-A-Bs-B/C-C	Skeletic podzol	45
PV5	46.43594	10.15129	2525	141	3	90%	Herbaceous	10%	O-A-Bs-B/C-C	Entic podzol	25
PV6	46.42268	10.19662	2126	151	3	100%	Herbaceous	0%	O-A-Bs1-Bs2-B/C-C	Entic podzol	37

Soil iron content

The quantification of soil iron content with dithionite, oxalate, and total Fe analysis was performed on the A, B and E (when sampled) horizons for a total of 36 samples. The VV soils were richer in Fe than the GV and ST samples (Table 4). In the available E horizons (PS8 and PV1), total Fe and its ratio is very low, as expected in eluvial horizons. The ratio Fe_o/Fe_d, known as the index of pedogenetic state (Schwertmann and Taylor, 1989; Zanelli *et al.*, 2007), is generally close to 0.5 and always <1 in our study area. The value 0.5 is the threshold of a very active pedogenetic state, with high intensity of weathering and a high release rate of metal cations and pedogenetic oxides (Schwertmann and Taylor, 1989; Zanelli *et al.*, 2007). The upper limit of Fe_o/Fe_d occurs for profiles PS7 and PV2, in which the A horizon displays its highest recorded value. In these cases, the A horizon may be the result of new pedogenesis on a pre-existing podzol, leading to the development of a new kind of soil (Maejima *et al.*, 2002).

The test for the dithionite extraction was replicated three times on samples PG1-A, PS1-Bs and PV1-Bs to evaluate its reproducibility. The extraction returned values of 62.76, 63.33 and 63.15 for sample PG1-A, with a mean result of 63.08 ± 0.29. PS1-Bs returned values of 38.61, 38.38 and 39.17, with a mean result of 38.72 ± 0.41; PV1-Bs returned values of 89.04, 89.80 and 89.24, with a mean result of 89.36 ± 0.39. The test for the oxalate extraction was replicated three times on samples PS7-A, PS7-Bs and PV2-A. PS7-A returned values of 36.86, 36.18 and 36.28, with a mean result of 36.44 ± 0.37; PS7-Bs returned values of 38.63, 38.89 and 39.18, with a mean result of 38.90 ± 0.28; and PV2-A returned values of 41.80, 41.74 and 41.20, with a mean result of 41.58 ± 0.33. These results demonstrate the reproducibility of both extraction methods and support the effectiveness of the calibration procedure described in the following section.

Soils as a proxy for the deglaciation age

The base of TBG1 was dated at 8010–7029 cal BP (Table 5). This represents the minimum age of formation for profile PG2 because the drilled pond containing TBG1 is dammed by the morainic ridge containing PG2.

In the same valley, the minimum formation age of profile PG3 is 5091–4990 cal BP (Table 5), considering that the drilled pond (RT1) lies in a depression among some roches moutonées in the same geomorphological unit as the profile.

In the ST area, a pond within a depression among some roches moutonées was cored (TBS1) in close proximity to profile PS1 (Table 5). The deepest centimetre of sediment from TBS1 was dated at 7271–7125 cal BP.

Finally, in the ST area the lacustrine sediments of a small lake named Laghetto Alto were cored. The lake is within a depression among some rochees moutonnées very close to profile PS2. The age of the basal lacustrine sediment was 11 137–10 852 cal BP, which represents the minimum age of profile PS2 (Table 5).

In addition to these four radiocarbon dates, our absolute age dataset includes one ^{10}Be age of 15 661–12 049 cal. BP for a granitic boulder in the morainic ridge containing soil profile PV6 (Scotti *et al.*, 2017; see Table 5). We used these five absolute ages to calibrate the iron crystallinity ratio index of the A and B horizons for use as a dating proxy.

The calibration for the A horizon gave the curve age = $4566.9 \times \ln(\text{CRF}) + 1760$ (Equation 1; grey) with an $R^2 = 0.9469$. Using the B horizon produced the relationship age = $3907 \times \ln(\text{CRF}) + 3508.2$ (Equation 2; red) with an $R^2 = 0.9539$. These are shown in Fig. 3 with their respective range of uncertainty. In both

Table 2. Characteristics of soil profiles as recorded in the field.

Profile Id	Depth	Horizon	Lower boundary	Aggregates	Colour	Cryoturbation (cm)
PG1	0–1	O	Abrupt wavy	Granular fine	10YR 2/1	Not found
	1–8	A	Clear wavy	Granular medium	7.5YR 2.5/1	Not found
	4–8	E	Clear wavy	Prismatic fine	5YR 8/2	Not found
	12–36	Bs	Clear wavy	Granular medium	5YR 3/4	Not found
	36–50	C	Unknown	Granular coarse	10YR 4/6	Not found
PG2	0–2	O	Abrupt smooth	Granular fine	10YR 2/1	Not found
	2–12	A	Clear wavy	Granular fine	7.5YR 2.5/2	Not found
	12–30	Bhs	Clear wavy	Granular medium	5YR 3/3	Not found
	30–44	Bs	Abrupt wavy	Granular fine	7.5YR 3/3	Not found
	44–55	C	Unknown	Granular fine	10YR 5/6	Not found
PG3	0–1	O	Clear smooth	Granular medium	10YR 2/2	Not found
	1–8	A	Clear wavy	Granular medium	7.5YR 3/2	Not found
	8–10	E	Clear wavy	Granular medium	7.5YR 7/3	Not found
	8/10–35	Bs	Clear wavy	Granular fine	5YR 4/4	3–5
	35–53	C	Unknown	Blocky medium	10YR 5/3	5
PS1	0–1	O	Abrupt smooth	Poliedric fine	7.5YR 2.5/1	Not found
	1–3	A	Abrupt wavy	Poliedric medium	10YR 4/2	Not found
	3–8.5	A1	Abrupt wavy	Poliedric fine	7.5YR 4/2	Not found
	8.5–11	E	Abrupt wavy	Poliedric fine	10YR 8/2	Not found
	11–30	Bs	Clear wavy	Granular medium	7.5YR 4/4	Not found
	30–48	B/C	Abrupt wavy	Granular medium	10YR 6/2	Not found
	48–50	C	Unknown	Granular coarse	10YR 5/1	Not found
PS2	0–2	O	Abrupt wavy	Granular fine	10YR 2/1	Not found
	2–15	A	Abrupt wavy	Granular medium	10YR 2/2	Not found
	15–20	E	Clear wavy	Blocky medium	10YR 7/1	Not found
	20–38	Bs	Abrupt wavy	Granular fine	7.5YR 4/4	5–6
	38–50	C	Unknown	Granular medium	7.5YR 5/3	4
PS3	0–1	O	Abrupt smooth	Granular fine	10YR 2/2	Not found
	1–6	A	Abrupt wavy	Granular fine	7.5YR 3/1	Not found
	6–10	E	Abrupt wavy	Granular fine	5YR 7/2	Not found
	10–25	Bs	Clear wavy	Granular medium	5YR 3/2	Not found
	25–35	B/C	Clear wavy	Blocky fine	7.5YR 4/2	Not found
	35–50	C	Unknown	Blocky medium	10YR 6/2	Not found
PS4	0–1	O	Abrupt smooth	Blocky fine	10YR 2/2	Not found
	1–8	A	Abrupt smooth	Granular fine	7.5YR 3/1	Not found
	8–15	E	Clear wavy	Granular fine	5YR 7/2	3
	15–35	Bs	Clear wavy	Granular medium	5YR 3/2	6–7
	35–48	B/C	Abrupt smooth	Granular fine	7.5YR 5/4	Not found
	48–50	C	Unknown	Granular medium	10yR 7/4	Not found
PS5	0–2	O	Abrupt wavy	Blocky fine	7.5YR 2.5/2	Not found
	2–7	A	Clear wavy	Blocky medium	10YR 2/2	Not found
	7–13	E	Clear wavy	Granular fine	7.5YR 7/2	Not found
	13–36	Bs	Gradual wavy	Granular fine	7.5YR 4/4	Not found
	36–45	B/C	Abrupt wavy	Granular medium	10YR 6/6	Not found
	45–50	C	Unknown	Granular medium	10YR 6/2	Not found
PS6	0–2	O	Abrupt wavy	Granular fine	7.5YR 2.5/1	Not found
	2–8/9	A	Clear wavy	Granular medium	7.5YR 3/1	Not found
	8/9–13	E	Clear wavy	Blocky fine	7.5YR 8/3	Not found
	13–25	Bhs	Abrupt wavy	Granular fine	5YR 3/3	Not found
	25–40	Bs	Clear wavy	Granular fine	5YR 4/4	Not found
	40–50	C	Unknown	Prismatic medium	10YR 3/4	Not found
PS7	0–1	O	Abrupt smooth	Granular fine	7.5YR 2.5/1	Not found
	1–9	A	Abrupt wavy	Granular fine	7.5YR 2.5/1	Not found
	9–12	E	Clear wavy	Granular medium	7.5YR 8/2	Not found
	12–38	Bs	Gradual wavy	Granular medium	5YR 3/3	5
	38–48	B/C	Clear wavy	Blocky fine	7.5YR 5/4	5–7
	48–54	C	Unknown	Blocky medium	10YR 7/3	Not found
PS8	0–1	O	Abrupt wavy	Blocky fine	10YR 2/2	Not found
	1–14	A	Abrupt wavy	Blocky medium	10YR 2/1	Not found
	14–16	E	Clear wavy	Granular fine	7.5YR 7/3	Not found
	16–31	Bhs	Clear wavy	Granular fine	5YR 3/1	Not found
	31–56	Bs	Gradual wavy	Granular fine	5YR 4/4	Not found
	56–60	C	Unknown	Blocky medium	10YR 4/3	Not found
PV1	0–1	O	Abrupt smooth	Granular fine	7.5YR 2.5/1	Not found
	1–9/12	A	Clear wavy	Granular fine	7.5YR 2.5/3	Not found
	9/12–20	E	Clear wavy	Granular fine	7.5YR 8/2	Not found
	20–48	Bs	Gradual wavy	Blocky medium	7.5YR 5/3	Not found
	48–60	C	Unknown	Granular medium	10YR 7/8	Not found

(*Continued*)

Table 2. (*Continued*)

Profile Id	Depth	Horizon	Lower boundary	Aggregates	Colour	Cryoturbation (cm)
PV2	0–1	O	Abrupt wavy	Granular fine	7.5YR 2.5/1	Not found
	1–20	A	Clear wavy	Granular medium	10YR 2/1	Not found
	20–22	E	Clear wavy	Granular fine	7.5YR 7/2	Not found
	22–45	Bs	Gradual wavy	Granular fine	5YR 4/4	Not found
	45–50	C	Unknown	Blocky medium	10YR 6/4	Not found
PV3	0–1	O	Abrupt smooth	Granular fine	10YR 2/2	Not found
	1–16/18	A	Clear wavy	Blocky fine	7.5YR 2.5/3	Not found
	16/18–24/30	Bs	Clear wavy	Granular fine	5YR 4/3	8
	24/30–40	B/C	Clear wavy	Granular fine	7.5YR 6/2	3–5
	40–50	C	Unknown	Blocky medium	10YR 6/4	Not found
PV4	0–1	O	Abrupt wavy	Granular fine	10YR 2/1	Not found
	1–14	A	Clear wavy	Granular medium	10YR 2/2	Not found
	14–29	Bs	Clear wavy	Granular fine	5YR 4/2	Not found
	29–45	B/C	Gradual wavy	Prismatic fine	7.5YR 6/3	Not found
	45–50	C	Unknown	Prismatic fine	10YR 6/2	Not found
PV5	0–2	O	Abrupt smooth	Blocky fine	10YR 2/1	Not found
	2–15	A	Clear wavy	Blocky fine	7.5YR 2.5/1	Not found
	15–25	Bs	Clear wavy	Granular medium	5YR 4/4	Not found
	25–40	B/C	Abrupt smooth	Granular medium	10YR 6/3	Not found
	40–50	C	Unknown	Granular fine	10YR 7/1	Not found
PV6	0–3	0	Abrupt smooth	Granular fine	10YR 2/2	Not found
	3–8	A	Abrupt wavy	Granular fine	7.5YR 2.5/1	Not found
	8–10	Carbons	Abrupt wavy	Undefinable	Undefinable	Not found
	10–13	Bs1	Abrupt wavy	Granular medium	5YR 4/4	Not Found
	13–14	Carbons	Abrupt wavy	Undefinable	Undefinable	Not Found
	14–24	Bs2	Clear wavy	Granular medium	5YR 4/6	Not Found
	24–37	B/C	Clear wavy	Granular fine	5YR 3/4	Not Found
	37–50	C	Unknown	Locally cemented	10YR 6/2	Not found

Equation (1) and Equation (2), the uncertainty is low when the soil profile is young and increases as the profile gets older. This is most likely due to the uncertainty of the radiocarbon dating rather than an error in the CRF index. By applying these equations, a range of ages for each horizon in all soil profiles was calculated.

DISCUSSION

The CRF crystallinity ratio of free iron for soil dating

The CRF (crystallinity ratio of free iron oxides) gradually increases with the stage of soil development and displays a

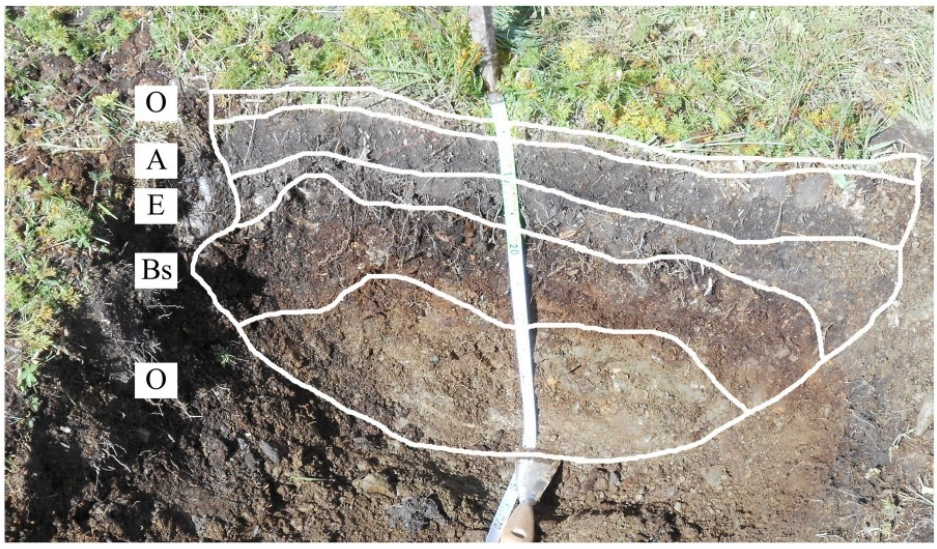

Figure 2. PS2, an example of Skeletic Podzol. [Color figure can be viewed at wileyonlinelibrary.com].

Table 3. Soil characteristics. The grain size classes (skeleton, sands, silt+clay), the water content, and the LOI are in % while the pH is in pH unit.

Profile Id	Horizon	Skeleton	Sands	Silt + clay	Water content	pH	LOI
PG1	O	N.A.	N.A.	N.A.	N.A.	N.A.	N.A.
	A	34.47	62.94	2.59	26.74	4.07	14.98
	E	N.A.	N.A.	N.A.	N.A.	N.A.	N.A.
	Bs	40.26	58.88	0.86	15.73	4.64	5.23
	C	N.A.	N.A.	N.A.	N.A.	N.A.	N.A.
PG2	O	N.A.	N.A.	N.A.	N.A.	N.A.	N.A.
	A	21.09	76.81	2.1	23.84	3.77	17.28
	Bhs	39.35	55.43	5.22	16.18	4.39	5.73
	Bs	45.94	45.52	8.54	15.08	4.36	11.12
	C	N.A.	N.A.	N.A.	N.A.	N.A.	N.A.
PG3	O	N.A.	N.A.	N.A.	N.A.	N.A.	N.A.
	A	28.36	71.48	0.16	23.14	3.7	10.78
	E	N.A.	N.A.	N.A.	N.A.	N.A.	N.A.
	Bs	28.75	64.43	6.82	17.22	4.34	5.34
	C	N.A.	N.A.	N.A.	N.A.	N.A.	N.A.
PS1	O	N.A.	N.A.	N.A.	N.A.	N.A.	N.A.
	A	27.42	71.31	1.27	25.61	3.87	7.38
	A1	N.A.	N.A.	N.A.	N.A.	N.A.	N.A.
	E	N.A.	N.A.	N.A.	N.A.	N.A.	N.A.
	Bs	37.69	61.69	0.62	14.96	4.57	10.44
	B/C	N.A.	N.A.	N.A.	N.A.	N.A.	N.A.
	C	N.A.	N.A.	N.A.	N.A.	N.A.	N.A.
PS2	O	N.A.	N.A.	N.A.	N.A.	N.A.	N.A.
	A	37.23	62	0.77	22.09	4.01	18.87
	E	N.A.	N.A.	N.A.	N.A.	N.A.	N.A.
	Bs	61.97	37.38	0.65	18.42	4.13	9.34
	C	N.A.	N.A.	N.A.	N.A.	N.A.	N.A.
PS3	O	N.A.	N.A.	N.A.	N.A.	N.A.	N.A.
	A	30.13	69.14	0.73	32.66	4.36	17.47
	E	N.A.	N.A.	N.A.	N.A.	N.A.	N.A.
	Bs	18.42	78.03	3.55	28.57	4.24	8.84
	B/C	N.A.	N.A.	N.A.	N.A.	N.A.	N.A.
	C	N.A.	N.A.	N.A.	N.A.	N.A.	N.A.
PS4	O	N.A.	N.A.	N.A.	N.A.	N.A.	N.A.
	A	12.09	84.94	2.97	26.8	3.89	17.49
	E	N.A.	N.A.	N.A.	N.A.	N.A.	N.A.
	Bs	49.03	50.06	0.91	19.23	4.11	12.93
	B/C	N.A.	N.A.	N.A.	N.A.	N.A.	N.A.
	C	N.A.	N.A.	N.A.	N.A.	N.A.	N.A.
PS5	O	N.A.	N.A.	N.A.	N.A.	N.A.	N.A.
	A	23	71.59	5.41	26.41	4.03	13.78
	E	N.A.	N.A.	N.A.	N.A.	N.A.	N.A.
	Bs	49.18	49.98	0.84	17.62	4.2	10.12
	B/C	N.A.	N.A.	N.A.	N.A.	N.A.	N.A.
	C	N.A.	N.A.	N.A.	N.A.	N.A.	N.A.
PS6	O	N.A.	N.A.	N.A.	N.A.	N.A.	N.A.
	A	26.94	71.55	1.51	25.72	4.18	11.18
	E	N.A.	N.A.	N.A.	N.A.	N.A.	N.A.
	Bhs	50.1	47.86	2.04	20.25	4.3	9.68
	Bs	55.53	42.97	1.5	13.71	4.17	7.02
	C	N.A.	N.A.	N.A.	N.A.	N.A.	N.A.
PS7	O	N.A.	N.A.	N.A.	N.A.	N.A.	N.A.
	A	49.52	46.68	3.8	27.66	4.1	15.81
	E	N.A.	N.A.	N.A.	N.A.	N.A.	N.A.
	Bs	58.86	36.09	5.05	21.82	4.2	9.76
	B/C	N.A.	N.A.	N.A.	N.A.	N.A.	N.A.
	C	N.A.	N.A.	N.A.	N.A.	N.A.	N.A.
PS8	O	N.A.	N.A.	N.A.	N.A.	N.A.	N.A.
	A	25.84	71.91	2.25	26.22	4.02	16.26
	E	29.62	67.57	2.81	22.6	4.5	12.11
	Bhs	49.27	48.85	1.88	20.65	4.17	10.16
	Bs	43.89	53.7	2.41	18.56	4.41	6.01
	C	N.A.	N.A.	N.A.	N.A.	N.A.	N.A.
PV1	O	N.A.	N.A.	N.A.	N.A.	N.A.	N.A.
	A	5.98	86.3	7.72	26.75	4.33	11.73
	E	13.37	79.37	7.26	25.82	4.27	7.43
	Bs	7.78	85.99	6.23	25.28	4.51	8.75
	C	N.A.	N.A.	N.A.	N.A.	N.A.	N.A.

(*Continued*)

Table 3. (*Continued*)

Profile Id	Horizon	Skeleton	Sands	Silt + clay	Water content	pH	LOI
PV2	O	N.A.	N.A.	N.A.	N.A.	N.A.	N.A.
	A	12.86	84.62	2.52	29.27	3.92	18.65
	E	N.A.	N.A.	N.A.	N.A.	N.A.	N.A.
	Bs	50.57	48.83	0.6	25.93	4.07	15.05
	C	N.A.	N.A.	N.A.	N.A.	N.A.	N.A.
PV3	O	N.A.	N.A.	N.A.	N.A.	N.A.	N.A.
	A	57.01	35.76	7.23	27.76	4.18	15.99
	Bs	39.17	51.8	9.03	29.93	4.32	13.5
	B/C	N.A.	N.A.	N.A.	N.A.	N.A.	N.A.
	C	N.A.	N.A.	N.A.	N.A.	N.A.	N.A.
PV4	O	N.A.	N.A.	N.A.	N.A.	N.A.	N.A.
	A	35.32	62.36	2.32	25.96	4.27	22.34
	Bs	59.38	36.98	3.64	25.51	4.43	17.02
	B/C	N.A.	N.A.	N.A.	N.A.	N.A.	N.A.
	C	N.A.	N.A.	N.A.	N.A.	N.A.	N.A.
PV5	O	N.A.	N.A.	N.A.	N.A.	N.A.	N.A.
	A	25.51	73.46	1.03	22.85	4.2	17.34
	Bs	44.15	55.16	0.69	25.15	4.55	12.06
	B/C	N.A.	N.A.	N.A.	N.A.	N.A.	N.A.
	C	N.A.	N.A.	N.A.	N.A.	N.A.	N.A.
PV6	0	N.A.	N.A.	N.A.	N.A.	N.A.	N.A.
	A	16.98	80.2	2.82	28.25	4.29	18.28
	Carbons	N.A.	N.A.	N.A.	N.A.	N.A.	N.A.
	Bs1	N.A.	N.A.	N.A.	N.A.	N.A.	N.A.
	Carbons	N.A.	N.A.	N.A.	N.A.	N.A.	N.A.
	Bs2	35.24	62.12	2.64	18.25	4.32	6.88
	B/C	N.A.	N.A.	N.A.	N.A.	N.A.	N.A.
	C	N.A.	N.A.	N.A.	N.A.	N.A.	N.A.

N.A. = not analysed.

highly positive correlation with the absolute ages of soils. Similar trends have previously been identified in Northern Italy for soils developed between the Middle Pleistocene and the Holocene (Arduino *et al.*, 1984, 1986). Elsewhere in the world, a curve has been calculated over a longer time scale. Comparing this previous result with our mean calibration curves, we observe that the function reaches an asymptote at a younger age, indicating that it may be less reliable over a longer time scale (Maejima *et al.*, 2002) (Fig. 4). Using the Fe_d, Woodward *et al.* (1994) proposed a quantitative weathering index that is the product of the difference between the maximum Fe_d value and the least-altered or unweathered sample Fe_d value and the total thickness of the strongly weathered horizon. This approach implies a linear relationship between the weathering index and the profile age, but many studies emphasise that the weathering rate tends to decelerate through time (e.g. Birkeland, 1984; Maejima *et al.*, 2002). Therefore, in this study we prefer to apply only the logarithmic regression proposed by our CRF–age curves.

The soil formation ages calculated using the A horizon versus the B horizon are slightly different, especially for profiles PS7, PS5 and PV2. At these sample sites, the results calculated with Equation (1) are respectively 4271, 3784 and 4714 years younger than those obtained with Equation (2). Similar results have been reported by previous studies in Italy (Arduino *et al.*, 1986) and worldwide (Maejima *et al.*, 2002). A possible explanation for this discrepancy is that the soil we sampled is an integrated soil type that develops from podzol to a new kind of soil (Maejima *et al.*, 2002). This reinforces our interpretation of the Fe_o/Fe_d ratio, particularly for sites PS7 and PV2. In these two cases, we cannot eliminate the possibility that the A horizon developed on a sliding surface, although no discontinuities are visible in the sections. For this reason, even though R^2 is high for Equation (1), the glacial reconstruction proposed in this study will be based on soil ages calculated from Equation (2).

In ST, the oldest profiles are PS4 and PS5, which have similar ages of 10 828 ± 1243 and 11 791 ± 1380, respectively. Both profiles are located at approximately the same elevation (2700 m asl). The youngest profile at site ST is PS1, with an age of 6740 ± 46 and an elevation of 2655 m asl.

In GV, the oldest profile is PG1 with an age of 10 230 ± 947 (2602 m asl), while the youngest is PG3 with an age of 5490 ± 187 (2789 m asl).

In VV, the oldest profile is PV3 with an age of 14 669 ± 2008 (2740 m asl), while the youngest is PV5 with an age of 9088 ± 675 (2525 m asl).

The deglaciation of the Upper Valtellina and its relationship with glacier fluctuations in the Alps

Considering the similar elevations of sites VV, ST and GV, the development of podzols is remarkably different in the three areas. Specifically, the soils in VV were much older (16 700 cal year BP, at 2740 m asl) than the soils in ST (12 500 cal year BP at 2700 m asl). Both VV and ST were significantly older than the soils from a comparable elevation in GV (5300 cal year BP at 2780 m asl).

Combining the ^{14}C ages and the mean soil ages obtained with CRF, we identified seven glacial advance phases preceding the Little Ice Age (LIA). These phases have been dated as follows: 16.7–14.7 ka (phase I), around 12.3 ka (phase II), 11 ka (phase III), 10–9.7 ka (phase IV), 9 ka (phase V), 7.5 ka (phase VI) and 5.3 ka (phase VII). These phases were then referenced to post-LGM glacial advances in the most proximal location from previous studies (Burga, 1987; Ivy-Ochs *et al.*, 2006; Hormes *et al.*, 2008; Chenet *et al.*, 2016; Moran *et al.*, 2016;

Table 4. Results of soil iron extraction.

Profile Id	Horizon	Fe_d	Fe_o	Fe_{tot}	CRF
PG1	O	N.A.	N.A.	N.A.	N.A.
	A	63.08	41.11	3.73	5.89
	E	N.A.	N.A.	N.A.	N.A.
	Bs	44.11	30.61	2.11	6.39
	C	N.A.	N.A.	N.A.	N.A.
PG2	O	N.A.	N.A.	N.A.	N.A.
	A	53.69	40.72	4.47	2.90
	Bhs	N.A.	N.A.	N.A.	N.A.
	Bs	40.47	30.98	2.72	3.48
	C	N.A.	N.A.	N.A.	N.A.
PG3	O	N.A.	N.A.	N.A.	N.A.
	A	98.23	43.81	6.63	8.21
	E	N.A.	N.A.	N.A.	N.A.
	Bs	43.78	30.06	6.06	2.26
	C	N.A.	N.A.	N.A.	N.A.
PS1	O	N.A.	N.A.	N.A.	N.A.
	A	33.76	21.54	4.09	2.99
	A1	N.A.	N.A.	N.A.	N.A.
	E	N.A.	N.A.	N.A.	N.A.
	Bs	38.72	27.05	5.10	2.29
	B/C	N.A.	N.A.	N.A.	N.A.
	C	N.A.	N.A.	N.A.	N.A.
PS2	O	N.A.	N.A.	N.A.	N.A.
	A	36.61	27.59	1.90	4.75
	E	N.A.	N.A.	N.A.	N.A.
	Bs	52.64	30.58	5.50	4.01
	C	N.A.	N.A.	N.A.	N.A.
PS3	O	N.A.	N.A.	N.A.	N.A.
	A	69.84	56.20	2.96	4.60
	E	N.A.	N.A.	N.A.	N.A.
	Bs	83.27	55.67	5.86	4.71
	B/C	N.A.	N.A.	N.A.	N.A.
	C	N.A.	N.A.	N.A.	N.A.
PS4	O	N.A.	N.A.	N.A.	N.A.
	A	33.62	14.71	2.63	7.20
	E	N.A.	N.A.	N.A.	N.A.
	Bs	67.33	48.47	2.90	6.51
	B/C	N.A.	N.A.	N.A.	N.A.
	C	N.A.	N.A.	N.A.	N.A.
PS5	O	N.A.	N.A.	N.A.	N.A.
	A	31.82	24.29	1.92	3.93
	E	N.A.	N.A.	N.A.	N.A.
	Bs	54.73	35.19	2.35	8.33
	B/C	N.A.	N.A.	N.A.	N.A.
	C	N.A.	N.A.	N.A.	N.A.
PS6	O	N.A.	N.A.	N.A.	N.A.
	A	54.23	34.62	2.68	3.86
	E	N.A.	N.A.	N.A.	N.A.
	Bhs	N.A.	N.A.	N.A.	N.A.
	Bs	54.89	46.65	2.86	2.89
	C	N.A.	N.A.	N.A.	N.A.
PS7	O	N.A.	N.A.	N.A.	N.A.
	A	39.40	36.44	1.96	1.51
	E	N.A.	N.A.	N.A.	N.A.
	Bs	48.74	38.90	3.18	3.09
	B/C	N.A.	N.A.	N.A.	N.A.
	C	N.A.	N.A.	N.A.	N.A.
PS8	O	N.A.	N.A.	N.A.	N.A.
	A	58.62	47.69	2.55	4.29
	E	31.23	27.54	1.37	1.55
	Bhs	N.A.	N.A.	N.A.	N.A.
	Bs	92.09	61.50	5.36	5.71
	C	N.A.	N.A.	N.A.	N.A.
PV1	O	N.A.	N.A.	N.A.	N.A.
	A	149.64	49.40	8.43	11.89
	E	53.55	38.35	2.99	3.40
	Bs	89.69	28.86	5.71	10.66
	C	N.A.	N.A.	N.A.	N.A.
PV2	O	N.A.	N.A.	N.A.	N.A.
	A	115.96	107.65	8.45	2.51
	E	N.A.	N.A.	N.A.	N.A.
	Bs	62.23	41.58	2.29	9.03
	C	N.A.	N.A.	N.A.	N.A.
PV3	O	N.A.	N.A.	N.A.	N.A.
	A	105.01	42.53	4.64	13.47
	Bs	79.04	17.22	3.66	16.89
	B/C	N.A.	N.A.	N.A.	N.A.
	C	N.A.	N.A.	N.A.	N.A.
PV4	O	N.A.	N.A.	N.A.	N.A.
	A	97.88	84.13	1.75	7.84
	Bs	65.11	58.18	0.96	7.20
	B/C	N.A.	N.A.	N.A.	N.A.
	C	N.A.	N.A.	N.A.	N.A.
PV5	O	N.A.	N.A.	N.A.	N.A.
	A	71.66	43.40	6.11	4.62
	Bs	53.67	32.45	4.27	4.98
	B/C	N.A.	N.A.	N.A.	N.A.
	C	N.A.	N.A.	N.A.	N.A.
PV6	0	N.A.	N.A.	N.A.	N.A.
	A	87.97	47.66	3.97	10.16
	Carbons	N.A.	N.A.	N.A.	N.A.
	Bs1	N.A.	N.A.	N.A.	N.A.
	Carbons	N.A.	N.A.	N.A.	N.A.
	Bs2	60.67	32.48	2.54	11.09
	B/C	N.A.	N.A.	N.A.	N.A.
	C	N.A.	N.A.	N.A.	N.A.

Fed = dithionite extracted iron, (‰); Feo = oxalate extracted iron, (‰); Fetot = total iron content, (dg/g); CRF = crystallinity ratio, (pure number); N.A. = not analysed.

Scotti *et al.*, 2017) and related to lake sediment records (Heiri *et al.*, 2014; Ilyashuk *et al.*, 2011; Lauterbach *et al.*, 2011; Ortu *et al.*, 2008), the INTIMATE event stratigraphy (Rasmussen *et al.*, 2014), the NGRIP $\delta^{18}O$ (Walker *et al.*, 2009, 2012), the biostratigraphic division (Iversen, 1954) and the European pollen zones (Iversen, 1954).

The oldest glacial phase (phase I) is dated between 16.7 and 14.7 ka. It is recorded only in VV, in the eastern sector (P.zzo Della Valle Glacier) of the Val Cantone, where a small morainic ridge reached around 2700 m asl (Fig. 7). This phase may be chronologically referenced to the Gschnitz II stadial (Burga, 1987), which is related to the end of the GS-2 event of the INTIMATE stratigraphy (Rasmussen *et al.*, 2014) and is also detectable on the NGRIP $\delta^{18}O$ records (Walker *et al.*, 2009, 2012). Phase I falls within pollen zone Ia of the Oldest Dryas (Iversen, 1954), a period with cool summer temperatures that ends after 14.6 ka, when a rapid increase of 2–3 °C in summer temperatures is recorded by lake sediment proxies (Heiri *et al.*, 2014). Glaciological modelling at the Gschnitz-type locality shows a summer temperature lowering

Table 5. Absolute ages (cal BP) and the most proximal soil profile used for calibrating the relationship between iron content and soil profile age.

Name	Profile ID	Ages cal bp
TBG1	PG2	8010–7029
RT1	PG3	5091–4990
TBS1	PS1	7271–7125
Laghetto Alto	PS2	11 137–10 852
Scotti *et al.*	PV6	15 661–12 049

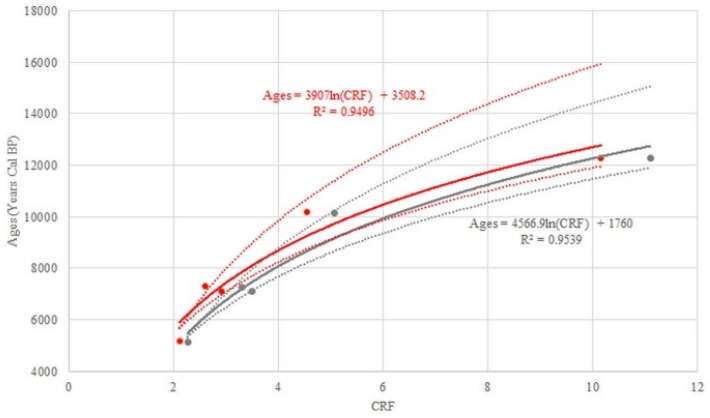

Figure 3. Curves relating CRF and soil age using the CRF values for the A horizon (grey) and for B horizon (red) with relative confidence intervals (dashed lines). [Color figure can be viewed at wileyonlinelibrary.com].

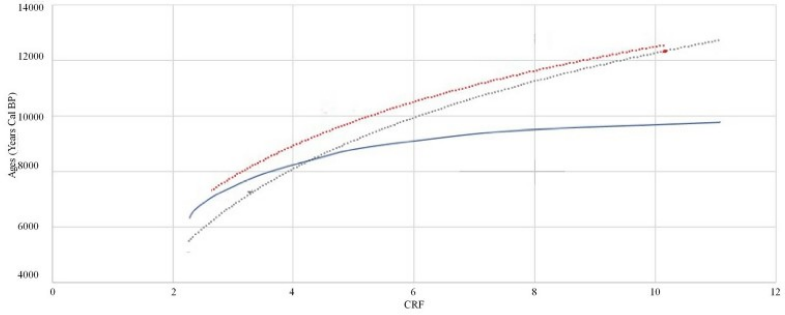

Figure 4. Comparison of Equation (1) (grey) and Equation (2) (red) with the curve from Maejima *et al.*, 2012 (blue). [Color figure can be viewed at wileyonlinelibrary.com].

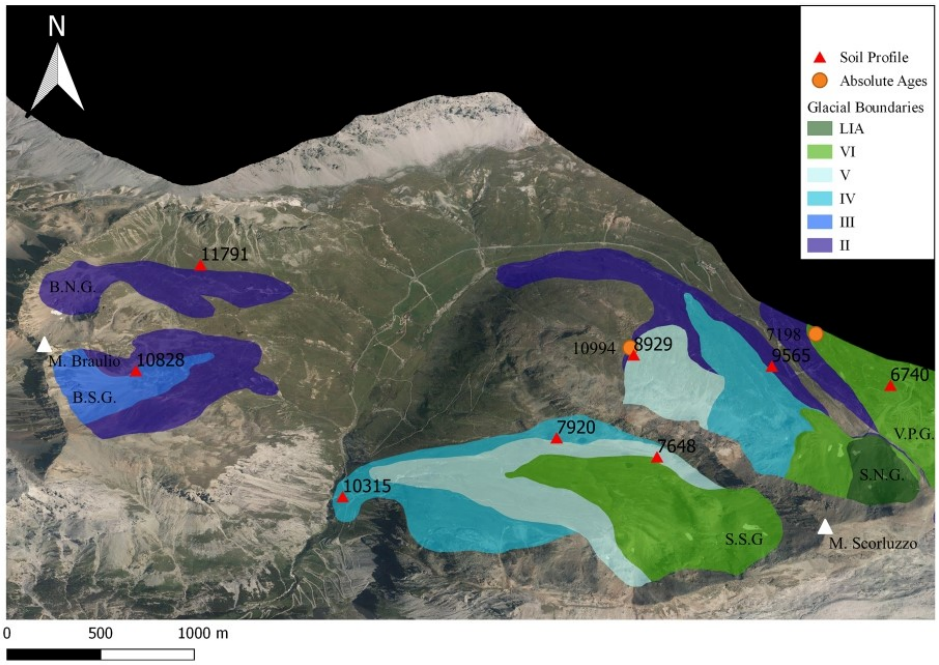

Figure 5. Soil ages and possible glacial reconstruction in ST. B.N.G.: Braulio N Glacier, B.S.G.: Braulio S Glacier, S.N.G.: Scorluzzo N Glacier, S.S.G.: Scorluzzo S Glacier, V.P.G.: Vedretta Piana – Platigliole Glacier. [Color figure can be viewed at wileyonlinelibrary.com].

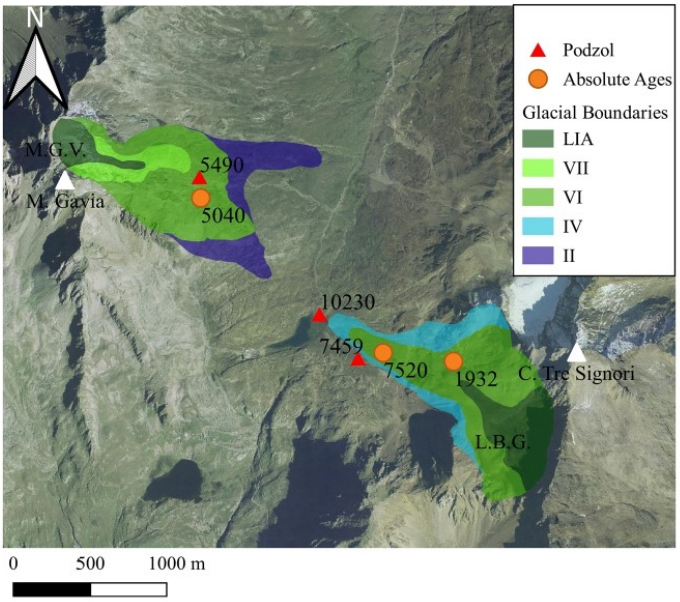

Figure 6. Soil ages and possible glacial reconstruction in GV. M.G.V.: M. Gavia Glacier, L.B.G.: Lago Bianco Glacier. [Color figure can be viewed at wileyonlinelibrary.com].

of about 10 °C relative to mean 20th century values and precipitation reduced to 30% of present-day amounts (Kerschner and Ivy-Ochs, 2007; Kerschner, 2009). This glacial phase was also recognised by Burga (1987) for the VV area but with a much larger extent. Indeed, according to Burga (1987), the VV glacier front was around 1420 m asl during this time period, which is almost 1300 m below the elevation of the frontal moraine soil dated here. In other areas of the Central and Eastern Alps (such as the Julier Pass and Ferwall), this glacial advance was dated to 14.4 ± 1.7 ka and 14.2 ± 1.2 ka, respectively (Ivy-Ochs *et al.*, 2006; Chenet *et al.*, 2016).

The second glacial advance (phase II) is dated to around 12.3 ka, and it is detectable in all the three study areas. In ST (Fig. 5), we reconstructed an asymmetrical deglaciation in the three main catchments (Scorluzzo N; Scorluzzo S; M. Braulio) during phase II. The Scorluzzo N glacier tongue reached the

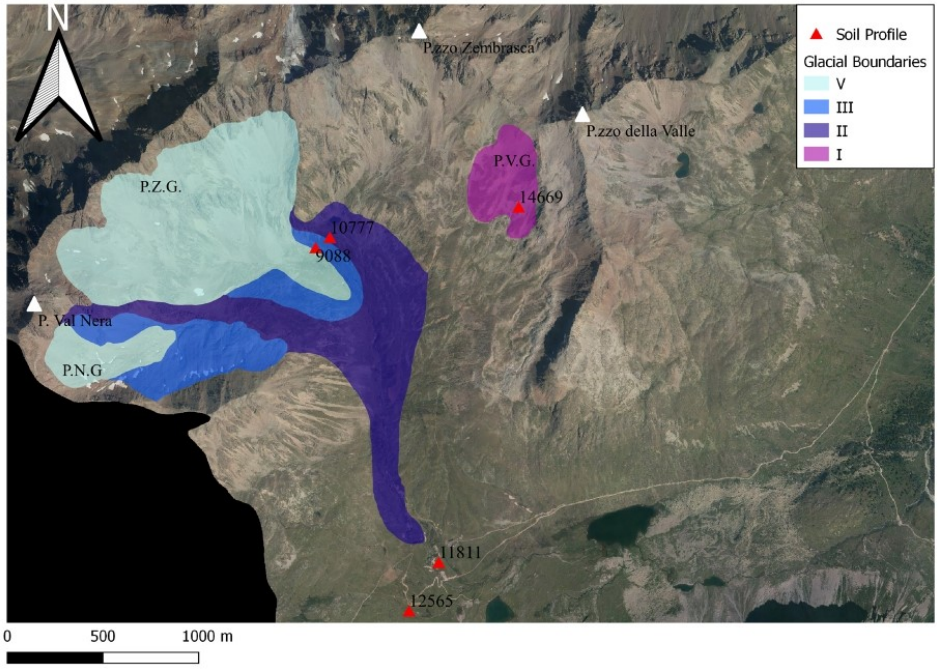

Figure 7. Soil ages and possible glacial reconstruction in VV. P.V.G.: P.zzo della Valle Glacier, P.Z.G.: P.zzo Zembrasca Glacier, P.N.G.: P. Val Nera Glacier. [Color figure can be viewed at wileyonlinelibrary.com].

valley bottom at 2340 m asl. The catchment of M. Braulio was already split into separate north and south units with their frontal moraines reaching 2500 m asl on M. Braulio N and around 2520 m asl on M. Braulio S. The Scorluzzo S glacier during phase II probably reached an elevation similar to its position during phase IV. In addition, during this episode across the Stelvio Pass the Vedretta Piana-Platigliole glacier flowed in this catchment reaching 2520 m asl. In the GV area (Fig. 6), remarkably, the two glaciers (M. Gavia and Lago Bianco) had a very different evolution despite their proximity and similar elevation. During this phase, the M. Gavia glacier left the GV bottom when its frontal moraine reached 2640 m asl, although the Lago Bianco glacier was still at a lower elevation. In VV (Fig. 7), the western sector of Val Cantone was largely glaciated with a well-developed tongue that reached an elevation of 2350 m asl near the confluence with the Val Viola Valley. This phase has been referenced to the Egesen II stadial (Burga, 1987) in VV, with a similar extent; Burga (1987) determined that the glacier front was around 2350 m asl, close to the elevation of the soil dated for the present study. In the Dosdè Valley, Egesen II moraines dated 12.2 ± 1.5 ka (Scotti *et al.*, 2017) indicate that the glacier reached 2180 m asl during the same period. In other sectors of the Central and Eastern Alps (Ivy-Ochs *et al.*, 2006; Chenet *et al.*, 2016; Moran *et al.*, 2016), the corresponding glacier advance was dated 12.6 ± 1.1 ka in Farwell, where a morainic ridge reached 2200 m asl (Ivy-Ochs *et al.*, 2006; Chenet *et al.*, 2016) and 11.7 ± 0.9 ka in Falgin cirque, when the glacier tongue was at 2460 m asl (Chenet *et al.*, 2016; Moran *et al.*, 2016). This phase may be associated with the second half of the Younger Dryas (Balco *et al.*, 2009) and the beginning of the Preboreal, when rock glacier activity ended at lower altitudes within the glacier-covered area (Ivy-Ochs, 2009). This advance is typical in pollen zone III (Iversen, 1954) when the temperature remained low and dry conditions were common in most of the Alps (Kerschner *et al.*, 2000; Walker *et al.*, 2009). A rapid cooling in summer temperature of about 1.5–3 °C has been reconstructed based on pollen, chironomids, and cladoceran records around 12.7 ka (Heiri *et al.*, 2014). The transition between GS-1 and Holocene II (Rasmussen *et al.*, 2014) also appears in the NGRIP $\delta^{18}O$ records (Walker *et al.*, 2009, 2012) as a rapid shift in precipitation of 2–2.5‰ (Lauterbach *et al.*, 2011).

The following event (phase III, around 11 ka) is only visible in VV and ST. In ST (Fig. 5) phase III is detectable only in the M. Braulio S catchment, where the glacier reached 2600 m asl, i.e. 150 m higher than a thousand years earlier. After this fluctuation on the M. Braulio catchment, there is no further evidence of glacial advance. Meanwhile, in VV (Fig. 7), the western sector of Val Cantone was characterised by the splitting of the glacier into two separate bodies; the northern body (P.zo Zembrasca Glacier) reached 2450 m asl, while the western (P. Val Nera Glacier) reached 2670 m asl. This phase may be chronologically referenced to the Kartell stadial (Ivy-Ochs *et al.*, 2006). In the Dosdè Valley, despite the opposite aspect the frontal moraine of the Dosdè glacier reached a similar elevation (2375 vs. 2384 m asl), suggesting that the cosmogenic age of 11 ± 1.4 ka could be more accurately referenced to the Egesen II stadial rather than the Kartell stadial reported in Scotti *et al.*, (2017). This glacier advance may be associated with the Preboreal Oscillation (Ivy-Ochs *et al.*, 2006) in pollen zone IV (Iversen, 1954), a period of transition towards warming conditions (Heiri *et al.*, 2014) in which several glacial oscillations were documented with extents larger than the LIA (Ivy-Ochs *et al.*, 2006; Heiri *et al.*, 2014). This glacial phase may be a result of the 11.4 ka cold event (Rasmussen *et al.*, 2014), which is also visible in the NGRIP $\delta^{18}O$ records (Walker *et al.*, 2009, 2012).

The next glacial phase (phase IV) is dated around 10 ka and is detectable in ST and GV. This phase was the most extensive for the Scorluzzo S in ST (Fig. 5), where a small tongue reached the valley bottom at around 2230 m asl. In contrast, the Scorluzzo N glacier reached only 2460 m asl. In GV (Fig. 6), at the same time, the Lago Bianco glacier reached the GV bottom with a frontal moraine deposited at 2610 m a.s.l. This phase may be associated with the Kromer Valley glacier advance (Moran *et al.*, 2016). In other areas of the Central Alps, like Ferwall, this glacial phase was identified at 2220 m asl and dated to 10.0 ± 0.7 ka (Ivy-Ochs *et al.*, 2006; Chenet *et al.*, 2016). This glacial advance is included in the Boreal biostratigraphic division, pollen zone V (Iversen, 1954). As for glacial phase III, temperature and precipitation variation are considerably difficult to track in lake sediment records (Heiri *et al.*, 2014). This advance also does not have a straightforward association with a climatic event, because the NGRIP $\delta^{18}O$ (Walker *et al.*, 2009, 2012) shows no evidence of a cold event before 9.3 ka (Rasmussen *et al.*, 2014). The relatively short duration of the phase, especially in ST, may suggest a rapid response to a small climatic forcing like a small drop in temperature around 10.1 ka visible in the NGRIP $\delta^{18}O$ (Walker *et al.*, 2009, 2012).

The glacier advance around 9 ka (phase V) is evident in ST and VV, but the glaciers were smaller and terminated at higher elevations relative to phase IV. In ST (Fig. 5), this phase occurred in both the Scorluzzo S and Scorluzzo N glaciers; the former reached 2340 m asl. The latter glacier split into two main bodies, but only the frontal moraine of the western body is preserved at 2490 m asl. The eastern body is not recorded in the geomorphology because a subsequent phase erased the evidence of phase V. During phase V, the transfluence of the Vedretta Piana–Platigliole glacier also presumably continued across the Stelvio Pass, although its deposits were erased during phase VI. In VV (Fig. 7), this advance is evident in both sectors with moraine ridges at 2480 m asl on the P.zo Zembrasca and at 2790 m asl on the P. Val Nera. This is the last detectable evidence of glaciation at P. Val Nera. This phase does not have a synchronous event in any other region of the Central and Eastern Alps. The phase is set between the Boreal and the Atlantic divisions, in pollen zone VI (Iversen, 1954). This was a period of general warming with some small fluctuations in temperature that are not evident in lacustrine sediments (Heiri *et al.*, 2014). Phase V may possibly be a consequence of a cold event recorded in the INTIMATE chronology at 9.3 ka (Rasmussen *et al.*, 2014) and also detectable in the NGRIP $\delta^{18}O$ (Walker *et al.*, 2009, 2012).

Subsequently, the continued trend of increasing temperatures favoured glacial retreat (Leutscher *et al.*, 2011). Glaciers throughout the Alps were probably smaller than their present extent (Ivy-Ochs *et al.*, 2009), at least before the first half of the Middle Holocene (Walker *et al.*, 2009, 2012).

Despite this regional trend of decreasing glacial extent, in ST and GV we found morainic ridges that are dated around 7.5 ka (phase VI). In ST (Fig. 5) this is the last detectable advance before the LIA. Scorluzzo S glacier reached an elevation only 40 m higher than during the previous fluctuation. The western side of the Scorluzzo N glacier reached 2620 m asl, and the eastern side reached 2575 m asl. A synchronous event can be detected in GV (Fig. 6), with the M. Gavia glacier reaching 2700 m asl, and the Lago Bianco glacier reaching 2620 m asl. During the Atlantic division, pollen zone VII (Iversen, 1954) was the best-known and most relevant cold event in the Holocene (8.2 ka event) (Rasmussen *et al.*, 2014). This pollen zone had temperature variations comparable to the Late-glacial ones. This cold event is also detectable in the NGRIP $\delta^{18}O$ (Walker *et al.*, 2009, 2012) and may be responsible for

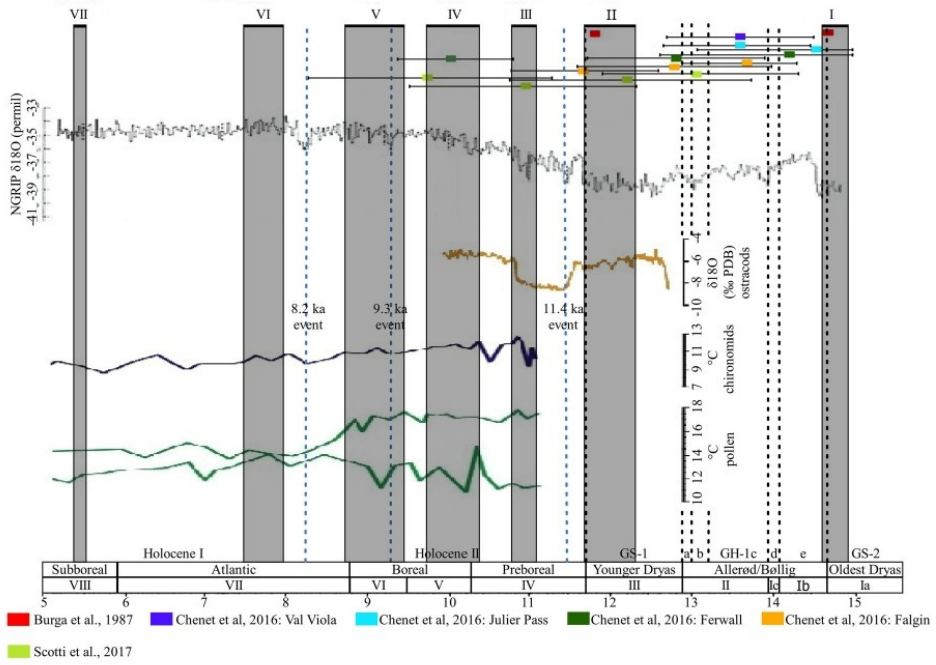

Figure 8. Relationship between calculated glacial phases, literature glacial phases, the NGRIP $\delta^{18}O$ (Walker *et al.*, 2009, 2012), INTIMATE event chronology (Rasmussen *et al.*, 2014), lake sediment proxies (Ostracods: Lauterbach *et al.*, 2011; Chironomids: Ilyashuk *et al.*, 2011; Pollen: Ortu *et al.*, 2008), and European pollen zones and biostratigraphic division (Iversen, 1954). [Color figure can be viewed at wileyonlinelibrary.com].

phase VI, especially considering that after 7.6 ka the trend shows a general cooling (Schimmelpfenning *et al.*, 2012). The pollen records from high Alpine lakes (Ortu *et al.*, 2008) also support this trend of cooling summer temperatures, with a lowering of about 3 °C between 7.9 and 7 ka.

Finally, in GV (Fig. 6), a final glacial phase (phase VII) is detectable around 5.3 ka. A further advance is visible up to 2770 m asl within the M. Gavia catchment, 70 m higher than the glacier's extent during the previous phase. This last phase may be associated with a small drop in temperature around 5.6 ka in NGRIP $\delta^{18}O$ within a trend of general cooling (Walker *et al.*, 2009, 2012). Not far from the study area, Calderoni *et al.* (1998) dated a permafrost aggradation phase responsible for the formation of some rock glaciers at around 2650 m asl, which further supports a cold phase in this region. Also, chironomid (Ilyashuk *et al.*, 2011) and pollen records (Ortu *et al.*, 2008) from the Swiss Alps suggest a cooling around 5.2 ka that was probably accompanied by a rapid glacier expansion; this is evidenced by the finding of a mummified prehistoric man (the Neolithic Iceman 'Otzi') dated 5300–5050 cal BP in the Ötztaler Alps (Bonani *et al.*, 1994).

In ST (Fig. 5), evidence of the LIA is limited to the Scorluzzo N. At this location, two frontal morainic ridges are present at 2690 and 2710 m asl, with the lower one datable to AD 1590 (Cannone *et al.*, 2003). In this area, a small glacier was documented until 1952 (Cannone *et al.*, 2003). In GV (Fig. 6), evidence of the LIA is present in both the M. Gavia and Lago Bianco glaciers; these glaciers reached 2864 and 2807 m asl, respectively, and date to around 1877 AD (Austro-Hungarian Monarchy. Militärgeographisches Institut, 1877; Pelfini, 1991).

The Egesen I phase is well-documented throughout the Central and Eastern Alps (Burga, 1987; Ivy-Ochs *et al.*, 2006; Hormes *et al.*, 2008; Chenet *et al.*, 2016; Moran *et al.*, 2016; Scotti *et al.*, 2017). However, none of our three study sites displays evidence of this phase (Fig. 8). It is possible that successive phases erased the records of the Egesen I phase at these locations. Alternatively, the difference in extension between the two phases in these areas may have been negligible. Moreover, sometimes the delineation of Egesen I and Egesen II stadial morainic ridges is supported by field-based differences in stratigraphic position, even though the ages are not statistically different (e.g. Ivy-Ochs *et al.*, 2006). Such differences were not detected in the present study.

CONCLUSIONS

The CRF calculated on both the A and Bs horizons has a good relationship with absolute age, and the trends are consistent with the results of previous studies (Arduino *et al.*, 1984, 1986; Maejima *et al.*, 2002). Although Equation (1) and Equation (2) can both be used date soil profiles in the study area, we recommend caution when interpreting results from the A horizon. Morphological or pedogenetic processes in the A horizon may lead to errors in calculated age, as demonstrated by the Fe_o/Fe_d ratio in PS7 and PV2, and by the age differences from PS5, PS7 and PV2 when both equations are applied. It is therefore preferable to use Equation (2), which was calibrated for the Bs horizon, to date the soils.

The podzol development was very different in the three study areas, despite their similar elevations.

The glacial advances after the LGM in ST and GV were asynchronous; in both cases, the western part of each area was deglaciated before its corresponding eastern part.

Seven successive events have been identified between 16.7 ka and the 5.3 ka, with a chronological sequence similar to other parts of the Central European Alps and with the few previous studies in study area VV (Burga, 1987; Ivy-Ochs *et al.*, 2006; Hormes *et al.*, 2008; Chenet *et al.*, 2016; Moran *et al.*, 2016; Scotti *et al.*, 2017). However, their extension was very different; this is evidenced by the reduced glacier extent in VV with respect to the previous reconstruction for the Gschnitz II stadial.

It is also remarkable that in this sector of the Central Alps, the glacial advances around 7.5 ka and 5.3 ka were more extended than during the LIA. In contrast, other Alpine valleys had smaller glaciers during these two time periods (Ivy-Ochs *et al.*, 2009).

Our data demonstrate the suitability of the CRF method for dating soils and its potential for use in reconstructing glacial phase boundaries from podzols at high elevations.

Acknowledgements. We want to thank the Stelvio National Park for their logistical support of our work in the Gavia Valley and Stelvio Pass areas, and the PRIN 2015 'Project Resacc' funded by the MUR. A special thanks to prof. Nicoletta Cannone and Dr Rachel Bain for their language revision. We want to thank also the two anonymous reviewers for their precious suggestions that significantly improved the paper.

Data availability statement

Data will be available on request to the corresponding author.

References

Arduino E, Barberis E, Marsan FA *et al.* 1986. Iron Indexes and clay minerals within profiles as indicators of soil age in Northern Italy. *Geoderma* **37**: 45–55.

Arduino E, Barberis E, Carraro F *et al.* 1984. Estimating relative ages from iron-oxides/total-iron ratios of soils in the western Po Valley, Italy. *Geoderma* **33**: 39–52.

ASTM. 2007. *Standard Test Method for Particle Size Analysis of soil*. ASTM D422-63.

Austro-Hungarian Monarchy. Militärgeographisches Institut. 1877. *Bormio und Passo Del Tonale*, Spezialkarte der osterreichisch-ungarischen Monarchie.

Balco G, Briner J, Finkel RC *et al.* 2009. Regional Beryllium-10 production rate calibration for late-glacial northeastern North America. *Quaternary Geochronology* **4**: 93–107.

Bohlert R, Mirabella A, Plotze M *et al.* 2011. Landscape evolution in Val Mulix, eastern Swiss Alps – soil chemical and mineralogical analyses as age proxies. *Catena* **87**: 313–325.

Birkeland PW. 1984. *Soil and Geomorphology*. Oxford University Press: New York.

Birkeland PW. 1999. *Soils and Geomorphology*. Oxford University Press: New York.

Blume LJ, Schumacher BA, Schaffer PW *et al.* 1990. *Handbook of Methods for Acid Deposition Studies Laboratory Analyses for Soil Chemistry*. EPA/600/4-90/023. U.S. Environmental Protection Agency: Las Vegas, NV.

Bonani G, Ivy SD, Hajdas I *et al.* 1994. AMS 14C age determinations of tissue, bone and grass samples from the Ötztal Ice Man, *Radiocarbon* **36**: 247–250.

Burga CA. 1987. Gletscher- und Vegetationsgeschichte der Südrätischen Alpen seit der Späteiszeit. *Denkschritfen der Schweizerischen Naturforschenden Gesellschraft* **101**.

Calderoni G, Guglielmin M, Tellini C. 1998. Radiocarbon dating and postglacial evolution, upper Valtellina and Livignese area (Sondrio, central Italian Alps). *Permafrost and Periglacial Processes* **9**: 275–284.

Cannone N, Sgorbati S, Guglielmin M. 2007. Unexpected impacts of climate change on alpine vegetation. *Frontiers in ecology and the environment* **5**: 360–364.

Cannone N, Guglielmin M, Hauck C *et al.* 2003. The impact of recent glacier fluctuation and human activities on permafrost distribution, Stelvio Pass (Italian Central-Eastern Alps). *Proceedings of the 8th International Conference on Permafrost, Zurich, Switzerland, 21–25 July 2003*, 125–130.

Chenet M, Brunstein D, Jomelli V *et al.* 2016. ^{10}Be cosmic-ray exposure dating of moraines and rock avalanches in the Upper Romanche Valley (French Alps): Evidence of two glacial advances during the Late-Glacial/Holocene Transition. *Quaternary Science Reviews* **148**: 209–221.

Comerci V, Capelletti S, Michetti AM *et al.* 2007. Land subsidence and Late Glacial environmental evolution of the Como urban area (Northern Italy). *Quaternary International* **173–174**: 67–86.

Dal Piaz GV, Del Moro A, Martin S *et al.* 1988. Post-Collisional magmatism in the Ortler-Cevedale Massif (Northern Italy). *Jahrbuch der Geologischen Bundesanstalt* **131**: 533–551.

Egli M, Lessovaia SN, Chistyakov K *et al.* 2015. Microclimate affects soil chemical and mineralogical properties of cold-alpine soils of the Altai Mountains (Russia). *Journals of soils and sediments* **15**: 1420–1436.

Egli M, Sartori G, Mirabella A *et al.* 2010. The effects of exposure and climate on the weathering of late Pleistocene and Holocene Alpine soils. *Geomorphology* **114**: 466–482.

Egli M, Wernli M, Kneisel C *et al.* 2006. Melting glaciers and soil development in the proglacial area Morteratsch (Swiss Alps): I. Soil type chronosequence. *Arctic, Antarctic, and Alpine Research* **38**: 499–509.

Egli M, Mirabella A, Sartori G *et al.* 2003. Weathering rates as a function of climate - results from a climosequence of the Val Genova (Trentino, Italian Alps). *Geoderma* **111**: 99–121.

FAO, 2006. Guidelines for soil description. Food and Agriculture Organization of the United Nations, Rome, 109.

Favilli F, Egli M, Mirabella A *et al.* 2008. High Alpine landscape evolution in Val di Sole (Trentino, Italy) during the Holocene based on charcoal, soil chemistry and mineralogy. Rothenbühler C. Klimaveränderungen auf der Spur. Samedan, 18–37.

Federici P, Ribolini A, Spagnolo M. 2016. Glacial history of the Maritime Alps from the Last Glacial Maximum to the Little Ice Age. *Geological Society, London* **433**: 137–159.

Gardner WA. 1986. Water Content. Methods of soil analysis, Part 1: Physical and Mineralogical Methods, American Society of Agronomy, Soil Society of America, 493–544.

Guglielmin M, Cannone N, Dramis F. 2001. Permafrost–glacial evolution during the Holocene in the Italian Central Alps. *Permafrost and periglacial processes* **12**: 111–124.

Hannah G, Hughes PD, Gibbard PL. 2017. Pleistocene plateau ice fields in the High Atlas, Morocco. In *Quaternary glaciation in the Mediterranean Mountains*, Hughes PD, Woodward JC (eds). Geological Society of London Special Publications 433: 25–53.

Harden JW. 1982. A Quantitative Index of Soil Development From Field Descriptions: Examples from a Chronosequence in Central California. *Geoderma* **28**: 1–28.

Heiri O, Koinig KA, Spotl C *et al.* 2014. Paleoclimate records 60-8ka in the Austrian and Swiss Alps and their forelands. *Quaternary Science Review* **106**: 186–205.

Hijmans RJ, Cameron SE, Parra JL *et al.* 2005. Very high resolution interpolated climate surfaces for global land areas. *International Journal of Climatology* **25**: 1965–1978.

Hormes A, Ivy-Ochs S, Kubik PW *et al.* 2008. Be-10 exposure ages of a rock avalanche and a late glacial moraine in Alta Valtellina, Italian Alps. *Quaternary International* **190**: 136–145.

Huges PD, Woodward JC, Gibbard PL *et al.* 2006. The glacial history of the Pindus Mountains, Greece. *Journal of Geology* **114**: 413–434.

Ilyashuk EA, Koinig KA, Heiri O *et al.* 2011. Holocene temperature variations at high-altitude site in Eastern Alps: a chironomid record from Schwarzsee ob Sölden, Austria. *Quaternary Science Review* **30**: 176–191.

Iversen J. 1954. The Late-Glacial flora of Denmark and its relation to climate and soil. *Danmarks Geologiske Undersøgelse II.række* **80**: 87–119.

Ivy-Ochs S, Lucchesi S, Baggio P *et al.* 2018. New geomorphological and chronological constraints for glacial deposits in the Rivoli-Avigliana end-moraine system and the lower Susa Valley (Western Alps, NW Italy). *Journal of Quaternary Science* **33**: 550–562.

Ivy-Ochs S. 2015. Glacier variations in the European Alps at the end of the last glaciation. *Cuadernos de Investigation Geografica* **41**: 295–315.
Ivy-Ochs S, Kerschner H, Maisch M *et al.* 2009. Latest Pleistocene and Holocene variations in the European Alps. *Quaternary Science Review* **28**: 2137–2149.
Ivy-Ochs S, Kerschner H, Reuther A *et al.* 2008. Chronology of the last glacial cycle in the European Alps. *Journal of Quaternary Sciences* **23**: 559–573.
Ivy-Ochs S, Kerschner H, Reuther A *et al.* 2006. The timing of glacier advances in the Northern European Alps based on surface exposure dating with cosmogenic 10Be, 26Al, 36Cl, and 21Ne. In situ-produced Cosmogenic Nuclides and Quantification of Geological Processes. *Geological Society of America special paper* 415: 43–60.
Ivy-Ochs S, Schafer G, Kubik PW *et al.* 2004. Timing of deglaciation on the northern Alpine foreland (Switzerland). *Eclogae Geologicae Helvetiae* **97**: 47–55.
Jackson ML, Lim CH, Zelazny LW. 1986. *Oxides, hydroxides, and aluminosilicates. Methods of Soil Analysis: Part 1. Physical and Mineralogical Methods*. American Society of Agronomy, Inc., Soil Science Society of America, Inc.: Madison, WI.
Kalra YP. 1995. Determination of Ph of soils by different methods: collaborative study. *Journal of AOAC International* **2**: 310–324.
Kerschner H. 2009. Gletscher und Klima im Alpinen Spätglazial und frühen Holozän. In *Klimawandel in Österreich. Die letzten 20.000 Jahre und ein Blick voraus*, Schmidt R, Matulla C, Psenner R (eds). Innsbruck University Press: Innsbruck; 5–26.
Kerschner H, Ivy-Ochs S. 2007. Palaeoclimate from glaciers: examples from the Eastern Alps during the Alpine Lateglacial and early Holocene. *Global and Planetary Change* **60**: 58–71.
Kerschner H, Kaser G, Sailer R. 2000. Alpine Younger Dryas glaciers as paleo precipitation gauges. *Annals of Glaciology* **31**: 80–84.
Lauterbach S, Brauer A, Andersen N *et al.* 2011. Environmental responses to Lateglacial climatic fluctuations recorded in the sediments of pre-Alpine Lake Mondsee (northeastern Alps). *Journal of Quaternary Science* **26**: 253–267.
Leutscher M, Hoffmann DL, Frisia S *et al.* 2011. Holocene glacier history from alpine speleotherms, Milchbach Cave, Switzerland. *Earth and Planetary Science Letters* **302**: 95–106.
Maejima J, Nagatsuka S, Higashi T. 2002. Application of the Crystallinity Ratio of Free Iron Oxides for Dating Soils Developed on the Raised Coral Reef Terraces of Kikai and Minami-Daito Islands, Southwest Japan. *The Quaternary Research* **41**: 485–493.
McKeague JA, Day DH. 1966. Dithionite- and Oxalate-Extractable Fe and Al as Aids in Differentiating Various Classes of Soils. *Canadian Journal of Soil Science* **46**: 13–22.
Mehra OP, Jackson ML. 1960. Iron Oxide Removal from Soils and Clay by a Dithionite-Citrate System Buffered with Sodium Bicarbonate. *Clays and Clay Minerals* **7**: 317–327.
Moran AP, Ivy-Ochs S, Schuh M *et al.* 2016. Evidence of central Alpine glacier advance during the Younger Dryas-early Holocene transition period. *Boreas* **45**: 398–410.
Nelson DW, Sommers LE. 1996. Total carbon, organic carbon, and organic matter. In *Methods of Soil Analysis, Part 2*, 2nd ed., Page AL, *et al.* (eds). *Agronomy* 9: 961–1010. American Society of Agronomy, Inc: Madison, WI.
Ortu E, Peyron O, Bordon A *et al.* 2008. Lateglacial and Holocene climate oscillations in the South-western Alps: an attempt at quantitative reconstruction. *Quaternary International* **190**: 71–88.
Pelfini M. 1991. Equilibrium Line Altitude (ELA) variations recorded by Ortles-Cevedale glaciers (Lombardy, Italy). From Little Ice Age to present. *Geografia Fisica e Dinamica Quaternaria* **17**: 194–206. Tesi di dottorato IV ciclo.
Pini R, Ravazzi C, Aceti A *et al.* 2016. Ecological changes and human interaction in Valcamonica, the rock art valley, since the Last Deglaciation. *Alpine and Mediterranean Quaternary* **29**: 19–34.
Rasmussen SO, Bigler M, Blockley SP *et al.* 2014. A stratigraphic framework for abrupt climatic changes during the Last Glacial period based on three synchronized Greenland ice-core records: refining and extending the INTIMATE event stratigraphy. *Quaternary Science Review* **106**: 14–28.
Ravazzi C, Pini R, Badino F. 2014. The latest LGM culmination of the Garda Glacier (Italian Alps) and the onset of glacial termination. Age of glacial collapse and vegetation chronosequence. *Quaternary Science Review* **105**: 26–47.
Ravazzi C, Badino F, Marsetti D. 2012. Glacial to paraglacial history and forest recovery in the Oglio glacier system (Italian Alps) between 26 and 15 ka cal BP. *Quaternary Science Reviews* **58**: 146–161.
Reimer PJ, Bard E, Bayliss A *et al.* 2013. IntCal13 and Marine13 radiocarbon age calibration curves 0–50,000 years cal BP. *Radiocarbon* **55**: 1869–1887.
Schimmelpfenning I, Schaefer JM, Akcar N *et al.* 2012. Holocene glacier culmination in the Western Alps and their hemispheric relevance. *Geology* **40**: 891–894.
Schwertmann U, Taylor RM. 1989. Iron oxides. In *Minerals in soil environments*, Dixon JB, Weed SB (eds). Soil Science Society of America: Madison; 379–438.
Schwertmann U. 1964. Differenzierung der Eisenoxide des Bodens durch Extraktion mit Ammonium-Lösung. *Z. Pflanzenemähr Düng Bodenk* **105**: 194–202.
Scotti R, Brardinoni F, Crosta GB *et al.* 2017. Time constraints for post-LGM landscape response to deglaciation in Val Viola, Central Italian Alps. *Quaternary Science Review* **177**: 10–33.
Tremblay MM, Shuster DL, Spagnolo M *et al.* 2019. Temperatures recorded by cosmogenic noble gasses since the Last Glacial Maximum in the Maritime Alps. *Quaternary Research* **91**: 829–847.
Walker MJC, Berkelhammer M, Björk S *et al.* 2012. Formal subdivision of the Holocene Series/Epoch: a discussion paper by a Working Group INTIMATE (Integration of ice-core, marine and terrestrial records) and the Subcommission on Quaternary Stratigraphy (International Commission on Stratigraphy). *Journal of Quaternary Science* **27**: 649–659.
Walker M, Johnsen S, Rasmussen So *et al.* 2009. Formal definition and dating of the GSSP (Global Stratotype Section and Point) for the base of the Holocene using the Greenland NGRIP ice core, and selected auxiliary records. *Journal of Quaternary Science* **24**: 3–17.
Woodward JC, Macklin MG, Lewin J. 1994. Pedogenic weathering and relative-age dating of Quaternary alluvial sediments in the Pindus Mountains of northwest Greece. In *Rock Weathering and Landform Evolution*, Robinson DA, Williams RBG (eds). Wiley, 259–283.
Wuthrich L, Morabito EG, Zech J *et al.* 2018. Be-10 surface exposure dating of the last deglaciation in the Aare Valley, Switzerland. *Swiss Journal of Geosciences* **111**: 295–303.
Zanelli R, Egli M, Mirabella A *et al.* 2007. Vegetation effects on pedogenetic forms of Fe, Al and Si and on clay minerals in soils in southern Switzerland and northern Italy. *Geoderma* **141**: 119–129
Zoller H, Athanasiadis N, Heitz-Waniger A. 1998. Late-glacial and Holocene vegetation and climate change at Palu glacier, Bernina Pass, Grisons Canton, Switzerland. *Vegetation History and Archaeobotany* **7**: 241–249.

4.2. SOIL MICROMORPHOLOGY AS TOOL FOR THE PAST PERMAFROST RECONSTRUCTION AND PALEOCLIMATIC VARIATIONS

Longhi A.[1], Trombino L. [2], Guglielmin M.[1*]

[1] Department of Theoretical and Applied Sciences, Insubria University, Varese, Italy.

[2] Department of Earth Sciences, University of Milan, Milan, Italy.

4.2.1. Abstract

Podzols developed on glacial and periglacial features provide the opportunity to reconstruct permafrost past limits and related paleoclimatic variations using micromorphological analysis. Analyzing 10 thin sections on 8 soils classified as Podzol in two study areas in the Central Italian Alps (Stelvio Pass area and Val Cantone area), we have been able to find different microstructures or pedofeatures (i.e., granular, platy, subangular blocky microstructures, silt cappings on coarse mineral grains) induced by processes related to permafrost conditions like gelifluction and ice lenses segregation. The type and the frequency of these micropedological traits allowed us to determine the lowest limit of past permafrost at 2228m a.s.l. in Stelvio Pass area and 2347m a.s.l. in Val Cantone area, respectively ca. 400 m and 330m lower than today.

Moreover, the analysis of precipitation and temperature derived from various proxy data allowed us to identify four different phases of podzolization dated to: 13.5-11.5ka (I phase), 11-9.7ka (II phase), 24 9.3-8ka (III phase), and 7.7-7.3ka (IV phase).

Reconstructed paleoprecipitation and paleotemperature of the four phases of podzolization also allowed us to determine that in Val Cantone there were two different permafrost aggradation periods that were synchronous to podzolization (11-9.7ka and 9.3-8ka) while in Stelvio Pass area one additional permafrost aggradation period occurred at 7.7-7.3ka.

Keywords: Podzol; Soil Micromorphology; Permafrost; Holocene; Italian Alps

4.2.2. Introduction

Soils need time for their development, and traces of the past effects of climate and vegetation cover can persist through time (*Antisari et al.*, 2018; *Karmakar et al.*, 2016) in the so-called "soil memory" (*Targulian and Goryachkin*, 2004). Recorded in “soil memory” are the in-situ interaction of so-called flux-factors (climate and biota) with the site factors of the land surface-parent rocks, both consolidated and unconsolidated, in each given geomorphic position during time. Such in-situ exogenic atmo-hydro-bio-litho-interactions gradually transform the solid-phase substances of parent material by weathering, leaching, aggregation, etc., and create some new substances which were absent in parent material (*Targulian and Goryachkin*, 2004).

Among atmo-hydro interactions, the effects of frost action in permafrost can be observed at both the macroscale and microscale (*Szymanski et al.*, 2015). At the macroscale, for example, the sight of cryoturbations (*Ping et al.*, 1998), vertical orientation of rock fragments in soil profiles (*Bockheim et al.*, 2006), ice wedge pseudomorphs (*Murton*, 2013), or sand wedge casts (*Murton et al.*, 2000) suggests the presence of permafrost. The application of micromorphology on frost affected soils started during the 1950s (for a complete review see Van Vliet-Lanoë and Fox, 2018). Today, the relevance of a micromorphological approach to identify frost action is very well assessed and the frost-related micropedological features cover the main aspects of the soil thin section description (i.e. microstructure, groundmass, and pedofeatures) including: coatings and infillings of iron oxides clays (e.g. *Rellini et al.*, 2014; *Szymanski et al.*, 2015), vertical orientation of grains and minerals (e.g. *Rellini et al.*, 2014; *Szymanski et al.*, 2015), net planes (e.g. *Rellini et al.*, 2014), dehydration cracks (e.g. *Bunting*, 1983), frost cracked quartz (e.g. *Egli et al.*, 2015), slightly humified organic matter (e.g. *Egli et al.*, 2015), normal nodules of iron and manganese (e.g. *Szymanski et al.*, 2015), and subhorizontal planes (e.g. *Kovda et al.*, 2017). Moreover, the frost-related micropedological features are very distinctive and persistent (e.g. *Van Vliet-Lanoë and Fox*, 2018) and are widely used as indicators of relict frost related process, inactive for short- or long-time spans, in various

environmental contexts (e.g., not an exhaustive list: *Menzies and Maltman,* 1992; *Laafar et al*, 1996; *Todisco and Bhiry*, 2008; *Kovda and Lebedeva*, 2013; *D'Amico et al.*, 2019). In addition, the frost related micropedological features pinpoint the ice segregation phenomenon (*Van Vliet-Lanoë and Fox*, 2018 and references therein) and, in terms of environmental reconstruction, support the presence of frost activity in space (i.e. variable depth) and time (i.e. variable duration). Thus, the use of soil micromorphology as a tool for past permafrost reconstructions cannot be constrained only to pure cryogenic fabrics, but must also involve other micromorphological features related to environmental changes (such as the spodic features in this study case), allowing for a more comprehensive reconstruction of the complex pedogenic settings (e.g. *Kovda et al.*, 2009; *Egli et al.*, 2015; *Sedov et al.*, 2016; *Sheinkman et al.*, 2016; *Kovda et al.*, 2017; *DiPietro et al.*, 2018) in which cryogenic fabrics were/are developed.

Podzols occur mainly in cool humid climates (*McKeague et al.*, 1983) under forest (*Sheinkman et al.*, 2016) or heath vegetation in medium textured to coarse material (*Steila and Pond*, 1989) or in Subarctic Tundra and Polar Desert in permafrost conditions (*Pitkaranta*, 2009). Podzolization occurs mainly in soils developed from acidic, highly leached, and, often, coarse-textured parent materials in areas that remain under the influence of humid climate conditions and where forest or heath vegetation supply enough organic matter to form organic horizons on the surface of mineral soils (*Musielok et al.*, 2021).

The study aims to use soil micromorphology to reconstruct the past permafrost distribution and compare paleo-precipitation and temperature with permafrost distribution and podzolization processes, to reconstruct the paleoclimate of the area during the Holocene.

4.2.3. Study Area

The study area is located in Upper Valtellina, Central Italian Alps. Within this sector of Valtellina, our study sites are along 2 main valleys: the Stelvio area and the Val Cantone area. (Fig. 1)

4.2.3.1. Stelvio Pass

This area (Fig. 2a) is located in the Braulio basin, a tributary of the Adda river, between 2208m a.s.l. and 2647m a.s.l. The geological substratum is constituted by granitic and granodioritic orthogneiss and biotitic paragneiss. The landscape of the valley was influenced by a complex glacial, paraglacial, and periglacial history: roches moutonées, morainic ridges, rock glaciers, and protalus ramparts are common, as well as gelifluction lobes and terracettes. Several deep gravitational slope deformations and debris flows, as well as scree slopes, are common gravitational features.

Glaciers had completely disappeared from this part of the study area by 1952 (*Guglielmin et al.*, 2001).

Present day permafrost is identified above 2640m a.s.l. (*Boeckli et al.*, 2012) while relict permafrost is reported above 2100m a.s.l. (*Guglielmin and Siletto*, 2000).

The soils reported by Soil Map of Regione Lombardia at 1:250:000 (*ERSAF*, 1990) are mainly Regosols, with some localized areas with Leptosols overlying the dolomite and limestones outcroppings and along the ridges that bring to Mt. Scorluzzo, respectively

The mean annual air temperature in the area ranges between +1°C and -3°C (*Cannone et al.*, 2007), and the mean annual precipitation is about 1300 mm/year.

4.2.3.2. Val Cantone

The area (Fig. 2b) is a tributary valley to the Val Viola in the upper part of the Viola creek basin, a tributary to the Adda river, and has an altitude between 2347m a.s.l. and 2564m a.s.l.

The Val Cantone shows a main direction N-S and intersects the Val Viola that is aligned accordingly with the overthrust between the Campo Unit and the Grosina Unit due to its ENE-WSW direction.

The lower unit (Campo Unit) is characterized by paragneiss and micaschists with anfibolites and orthogneiss intercalations, while the upper one (Grosina Unit) is mainly composed by orthogneiss, migmatites, and higher grade-paragneiss. Some late Varisican intrusive granitic, granodioritic, and dioritic bodies outcrop near Pizzo Bianco (*Notapietro and De Capitani*, 1985).

There is clear evidence of the glacial, paraglacial, and periglacial history in this valley including several morainic ridges and some subglacial features like fluted moraines and esker, which are present along the Viola Valley, and common roches moutonneés with striae. Rock glaciers and protalus ramparts as gelifluction/solifluction lobes, earth hummocks, and unsorted polygons are also present. A large rock avalanche characterizes a part of the Viola Valley (*Hormes et al.*, 2008) while debris flows and scree slopes are widespread.

Present day permafrost is recognized above 2680m a.s.l. (*Boeckli et al.*, 2012) while the whole area was affected by relict permafrost (*Guglielmin and Siletto*, 2000).

The soils reported at scale 1:25000 are mainly Regosols with some higher elevation areas characterized by Leptosols (*ERSAF*, 1990).

The mean annual air temperature is between 3°C and -4°C and the mean annual precipitation is 1097 mm/year with a maximum of 2020mm/year (*Ceriani and Carelli*, 2000).

4.2.4. Methods

4.2.4.1. Field Work

A total of 8 soil profiles were dug: 5 for Stelvio Pass area and 3 for Val Cantone area; podzols were identified both in the current permafrost area (*Boeckli et al.*, 2012) and in the relict permafrost area (*Guglielmin and Siletto*, 2000), the number of profiles in the two study areas is proportional to their extent. All soil profiles were already described in Longhi et al., (2020) through the C horizon. Here, we reported only the site characteristics (coordinates, elevation, aspect, slope, vegetational coverage, dominant vegetation, and stoniness).

Soils were then classified according to the World reference base for soil resources 2014: International soil classification system for naming soils and creating legends for soil maps (*F.A.O.*, 2014). Ten micropedological undisturbed samples from selected horizons were collected in Kubiëna boxes. For each described profile, one sample was collected at the transition between the B and A horizons or the B and E horizons, with the exception of PS5 and PS8 profiles, where two samples were collected.

4.2.4.2. Laboratory Work: Microscopic Analyses

Glass covered soil thin sections were prepared through impregnation with polystyrene. Micromorphological study of these thin sections employed an optical petrographic microscope Leica Laborlux 12pol (from 16x to 100× magnifications), equipped with an Olympus C4040 digital camera. Micropedological observations were carried out in plane polarized light (PPL), crossed polarized light (XPL), and oblique incident light (OIL). In thin sections descriptions, the terminology of Bullock et al. (1985) and Stoops (2003) was mainly used; specific references are given each time a different vocabulary is employed. Interpretation is mostly based on and Stoops et al. (2018).

4.2.4.3. Climatic Reconstruction and Soil Dating

The relative ages of soils, which were used to date podzolization and/or permafrost aggradation phases, were calculated on the basis of CRF (Crystallinity Ratio of Free Iron Oxides), as stated in Longhi et al., 2020.

For the supposed podzolization and/or permafrost aggradation phases, paleoprecipitation and paleotemperatures have been reconstructed on the basis of different proxy data.

Precipitation reconstructions were based on the core analyzed by Finsinger and Tinner (2007) at 2143m a.s.l. in the Swiss Alps at Lac de Fully, the closest elevation possible to our sites (Fig. 1).

The mean air temperature was obtained from alpine lake cores (*Furlanetto et al.*, 2018; *Heiri et al.*, 2014; Tab. 1) and then multiplied by a temperature gradient to obtain the temperature at the phase elevation. The gradient was calculated from the air temperature between 2007 and 2017 at the closest available weather stations: Cancano (1948m a.s.l.), Oga (2300m a.s.l.), and Vallaccia (2660m a.s.l.). The same gradient (0.3°C/100 m) was also used in each phase to determine the elevation of the -2°C isotherm.

4.2.5. Results

4.2.5.1. Soil Description

The main site characteristics and soil classification are synthesized in Table 2.

All the described soils are Podzols: 4 of them are Albic Podzols, 3 are Skeletic Podzols, and 1 is an Entic Podzol.

The soil profiles were opened between 2228m (PS8 in Stelvio Pass area) and 2647m (PS7 in Stelvio Pass area), but both study areas showed podzols up to at least 2800m. All the analyzed sites have more than 60% herbaceous vegetational cover. Differently, PS6 showed mosses as the dominant vegetation. All soils are not very developed and the solum (*Soil Survey Staff*, 2003) is always lower than 56cm. The thinnest solum is in soil profile PV5 with only 25cm and the thickest in PS8 (56cm). 6 profiles (PS3, PS5, PS6, PS7, PS8, and PV1) display an E horizon.

Cryoturbation evidences have been identified in PS4 profile, at the transition between E and Bs horizon, and in PS7 profile, at the transition between the Bs and the B/C horizon, both as undulations or individual folds of relatively small amplitude (in the range of decimeters) (*Vandenberghe*, 2007).

4.2.5.2. Micromorphology

The described thin sections, pertaining to profiles of both the Stelvio Pass and Val Cantone areas, shows several common traits including: i) the high porosity and the various morphology of voids (i.e. packing voids, channel, chambers, vughs, and planes, in decreasing occurrence order); ii) the nature of the mineral coarse material (i.e. metamorphic rocks fragments, up to gravel size, together with quartz grain and mica flakes, up to sand size); iii) the grain size and nature of the mineral fine material (i.e. an admixture of clay and fine silt, brownish to reddish in colour, showing a weak to undifferentiated b-fabric); and iv) the ubiquitarian presence of vegetal fragments (i.e. organs and tissues) of different sizes. The other micromorphological descriptive criteria are regarded, they are summarised in the qualitative Table 3 and described as follows.

In the Val Cantone area, the thin sections of the profiles PV4 and PV5 (both referring to the Bs horizons) are very similar, above all as regards the groundmass, with a similar c/f5µm ratio (2:3 to 1:1), the porphyric c/f related distribution, and the presence of polymorphic (*De Coninck et al.*, 1974)

fine organic material. Also, the granular microstructure (Fig 3a-1) is shared by the two thin sections, even if in the PV4 profile a coarser level of aggregation (i.e. lenticular platy to subangular blocky - Fig. 3a-2) is locally developed by the coalescence of granular (micro)aggregates. Finally, only very few pedofeatures are present in form of silt capping, sometimes downturned (*Van Vliet-Lanoë and Fox*, 2018) in PV5. On the contrary, the latter pedofeatures are more frequent in the PV1 thin section (Fig 3a-3) which also show a coarser groundmass (c/f5µm ratio 7:3) inducing a grain dominated microstructure (from pellicular to bridged grain - Fig. 3a-4) and a secondary coarser level of aggregation (subangular blocky); also in this case, polymorphic (*De Coninck et al.*, 1974) fine organic material is present.

For the Stelvio Pass area, seven thin sections pertaining to five profiles have been described; some of the thin sections have been sampled at the boundary between different horizons. For this reason, micromorphological characteristics are described according to the horizon type among different profiles, instead of according to a single profile.

Eluvial E horizons have been sampled at the top of the PS3 and PS8-1 thin sections and in the whole PS5-1 thin section. As expected, these thin sections lack of identifiable pedofeatures except for very few reworked aggregates of soil material (i.e. pedorelicts - *Brewer*, 1964) in PS3; the organic fine material is not identifiable, while mineral fine material is common; as regards of the microstructure, spheroidal aggregates are not identifiable (except in PS5-1, which probably is an EA horizon), while coarser subangular blocky peds and platy aggregates are present, the latter only in PS5-1 and PS8-1 (Fig. 3b-2).

Bh horizons have been sampled at the top of the PS6 and at the base of the PS8-1 thin sections: both thin sections are dominated by granular to crumby aggregates and show a significant amount of coarse material allowing the development of grain dominated c/f related distribution (as enaulic and chitonic); the lack of identifiable pedofeatures is also a recurring aspect of the two thin sections, together with the presence of polymorphic (*De Coninck et al.*, 1974) fine organic material (Fig. 3b-

2). Moreover, in PS8-1 also monomorphic (*De Coninck et al.*, 1974) fine organic material is locally present.

Bs horizons have been sampled at the base of the PS3 and PS6 thin sections and in the PS5-2, PS7 and PS8-2 thin sections. Spheroidal aggregates are present in all the profiles (except PS5) and coarse lenticular to platy aggregates (Fig. 3b-3) have been identified in all profiles (except PS8, when they become subangular). The c/f5µm ratio is quite homogeneous in all profiles, ranging from 2:3 to 1:1 to 3:2; polymorphic (*De Coninck et al.*, 1974) fine organic material is always present, while monomorphic (*De Coninck et al.*, 1974) fine organic material is locally (frequently in PS8 - Fig.3b-4) present, except in PS3. Among the pedofeatures, silt cappings, sometimes downturned (*Van Vliet-Lanoë and Fox*, 2018 - Fig. 3b-5) or fragmented (in PS3 and PS7 - Fig. 3b-6) have been described in all profiles, and amorphous hypocoatings, are present except in PS3.

4.2.6. Discussion

4.2.6.1. Evidences of Cryogenic Processes

The granular microstructure is a micromorphological feature characteristic of the active layer and the upper portion of permafrost (*Van Vliet-Lanoë*, 1998), while platy aggregates are associated with freezing/thawing and the growth of ice lenses (*Dumanski and St. Arnaud*, 1966; *Pawluk and Brewer*, 1975; *Mermut and St. Arnaud*, 1981; *Van Vliet-Lanoë*, 1988, 1998; *Fitzpatrick*, 1993). Also, the presence of subangular blocky aggregates is associated with freezing/thawing, but is formed by reticulate ice due to severely obstructed soil water migration in the fine-grained sediments (*Van Vliet-Lanoë*, 1988, 1998; *Fitzpatrick*, 1993). The presence of silt cappings over coarse grains is characteristic of the active layer and of the upper portion of permafrost (*Van Vliet-Lanoë*, 1998) as these features suggest disaggregation and illuviation of coarse particles in response to freeze/thaw cycles and percolation of seasonal melt-water (*Scarciglia et al.*, 2003). The fact that the silt cappings

are sometimes downturned may be the result of the traction exerted 228 by the growing ice lenses on rigid fragments in a frost-susceptible matrix (*Pissart*, 1969).

In the Val Cantone area (Fig. 4), PV1 has the lowest elevation (2347m a.s.l.) and the greatest thickness among the soils analyzed. This may be reflected in the more accentuate characterization of the cryogenic features related to gelifluction in the lower horizon. PV5 also shows micromorphological aspects in the Bs horizon at 2525m a.s.l. indicating gelifluction. PV4 instead is representative of a time of ice lens formation at 2564m a.s.l. with the Bs horizon. Since the three profiles are in an area where permafrost is absent according to Boeckli et al. (2012) and the permafrost related features are all in the deep horizons, we can assume that permafrost was present sometime in the area at least above 2347m a.s.l.. This finding confirms the limit of relict permafrost proposed by Guglielmin and Siletto (2000) based on the distribution of relict rock glaciers and protalus ramparts.

In the Stelvio Pass area (Fig. 5), the upper part of every profile shows no significant features related to permafrost condition, at least down to the Bs horizon. The soil profiles PS3, PS5, PS6, and PS7 show features related to ice lens formation at 2534m a.s.l., 2610m a.s.l., 2630m a.s.l., and 2647m a.s.l., respectively. Soil profile PS8 interestingly shows evidence of a gelifluction period and of a time of ice lens formation at the lower elevation (2228m a.s.l.). All the soil profiles are in an area where permafrost is absent according to Boeckli et al. (2012) with the exception of PS6, but are within the area with relict permafrost proposed by Guglielmin and Siletto (2000) which reached 2228m a.s.l. in this area. Although PS6 may be less indicative of permafrost extent than the other soil profiles since the micropedological features are present in the Bs and Bh horizon, the silt cappings are downturned, and it lies in an area where permafrost exists in only very favourable conditions, we can assume its relevance in the interpretation.

4.2.6.2. Podzol and Climatic Conditions

Podzolization occurs mainly in soils developed from highly leached and coarse-textured parent materials in areas that remain under the influence of humid climate conditions and where forest or

heath vegetation supply enough organic matter to form organic horizons on the surface of mineral soils (*Musielok et al.*, 2021). The soil map of the two areas 254 reports a wide distribution of Leptosols and Regosols, so the occurrence of podzol could be explained in light of past pedogenesis events. Indeed, field and micropedological features account for podzolization processes active in the area, leaving clear evidences on studied soil profiles. Moreover, from the micromorphological point of view, the podzolic traits show different aspects of the podzolization process, mainly dealing with the presence of polymorphic and/or monomorphic fine organic material (*De Coninck et al.*, 1974). According to Van Ranst et al. (2018), polymorphic fine organic material is common in well-aerated horizons, while monomorphic fine organic material is the most common form of organic material in hydromorphic Podzols. The presence of monomorphic fine organic material (associated with polymorphic material) has been recorded in PS5, PS6, PS7 and PS8 profiles. All the horizons (except PS8 Bh) show monomorphic fine organic material and very few amorphous hypocoatings have been described, which account for waterlogging phenomena. It is therefore possible to state that some of the studied podzols developed in slight hydromorphic conditions could be related to the occurrence of a permafrost table that normally acted as an impermeable layer.

Longhi et al. (2020) previously dated the analyzed soils as reported in Table 4 and it was possible to identify 4 possible pedogenesis phases at around 13.5-11.5ka (I phase), 11-9.7ka (II phase), 9.3-8ka (III phase), and 7.7-7.3ka (IV phase). It was possible to reconstruct the climate conditions and determine if they were favourable for permafrost aggradation using the scheme proposed by Haeberli and Burn (2002) (Fig. 6) and for podzolization following the climatic constraints proposed by Lundström (2000) by re-analysing data from precipitation [lake sediments (*Lauterbach et al.*, 2011; *Furlanetto et al.*, 2018), speleothem (*Mangini*, 2005), and lakes levels (*Furlanetto et al.*, 2018)] and temperature [INTIMATE event stratigraphy (*Rasmussen et al.*, 2014), the NGRIP $\delta^{18}O$ in the Greenland Ice Core (*Walker et al.*, 2009; *Walker et al.*, 2012), the $\delta^{18}O$ in speleotherms (*Mangini*, 2005), and lake sediments records (*Heiri et al.*, 2014). It is crucial to understand if the presence of

permafrost, possible in all hypothesized phases (Fig. 6), may be synchronous to the podzolization (*Lundström*, 2000).

PS6, dated 7.5±0.2 ka (IV phase, *Longhi et al.*, 2020), was under the glacier before its genesis (Tab. 4) so the permafrost must be syngenetic to the pedogenesis because successive climatic conditions, including during the LIA, were not compatible with permafrost aggradation. It is therefore possible to assume that during IV phase, podzolization and permafrost conditions were synchronous even if following the scheme proposed by Haeberli and Burn (2002) permafrost was discontinuous.

PS7 and PV5, both attributed to III phase and dated 8.2±0.2ka and 9.1±0.8ka, respectively (*Longhi et al.*, 2020), were under their respective glaciers before the beginning of their formation (Tab. 4).

The permafrost aggradation in PV5 can be reasonably synchronous to the podzolization because the successive permafrost phase (IV) reached a lower limit of 2569m a.s.l compared to the 2525m a.s.l of the soil. Differently, PS7 is located at 2647m a.s.l. and was potentially affected by permafrost aggradation during both III and IV phases, although it may have been in exceptional condition and under the timberline following the scheme proposed by Haeberli and Burn (2002).

PV4, PS3, and PS8, dated at 10.7±0.7ka, 9.7±0.5ka, and 10.3±0.6ka, respectively (*Longhi et al.*, 2020), and are attributed to II phase. These soil profiles were buried by the ice of their respective glaciers before the pedogenesis so permafrost aggradation could not have taken place prior to their formation (Tab. 4). Considering that the later phases of permafrost aggradation reached lower limits of 2597m a.s.l. and 2569 m asl, these three profiles were reasonably synchronous to the II phase when permafrost should have been continuous.

PV1 and PS5, dated at 12.5±1.0ka and 12±0.8ka, respectively (*Longhi et al.*, 2020), were attributed to I phase. It is impossible to say if PS5 was covered by the glacier before its formation, as the oldest recognizable glacial phase in the area is 12.5ka (*Longhi et al.*, 2020). Concerning PV1, some authors (Burga, 1987) record that the area was covered by the glacier even in the Daun stadial (14.7 ka). Both soil profiles are above the lower boundary of permafrost from the previous II phase, so it is not

possible to determine if podzolization occurred in the same period of the permafrost aggradation, even if the precipitation and temperature conditions allowed the permafrost to be continuous following the scheme proposed by Haeberli and Burn (2002).

In summary, in Val Cantone, two different permafrost aggradation periods have been found at 11-9.7ka, and 9.3-8ka, while in Stelvio Pass area, three different permafrost aggradation periods have 308 been found at 11-9.7ka, 9.3-8ka, and 7.-7.3ka.

4.2.7. Conclusions

Soil micromorphology has been proven as a good tool for past permafrost limit reconstruction. All the profiles are in current non-permafrost areas, with the exception of PS6. We defined the lower limit of Holocene permafrost in Stelvio Pass area at 2228m a.s.l. and in Val Cantone area at 2347m a.s.l., agreeing with the limit of relict permafrost proposed by Guglielmin and Siletto (2000).

Four different podzolization phases have been dated in the study areas: 13.5-11.5ka (I phase), 11-9.7ka (II phase), 9.3-8ka (III phase), and 7.7-7.3ka (IV phase).

Analyzing precipitation and temperature conditions, glacial phases, and the lower boundary of permafrost, it was possible to determine two different permafrost aggradation periods at 11-9.7ka and 9.3-8ka, synchronous to podzolization in Val Cantone. In Stelvio Pass area, instead, three different permafrost aggradation periods synchronous to podzolization have been found at 11-9.7ka, 9.3-8ka, and 7.7-7.3ka.

4.2.8. Acknowledgements

We want to thank the Stelvio National Park for their logistical support of our work in the Stelvio Pass area. We also want to thank PhD Student Jessica L. Raff for the English check on the paper.

4.2.9. References

Antisari L.V., Agnelli A., Corti G., Falsone G., Ferronato C., Marinari S., Vianello G., 2018. Modern and Ancient pedogenesis as revealed by Holocene fire – Northern Apennines, Italy. Quaternary International 467, 264-279.

Bockheim J., Mazhitova G., Kimble J.M., Tarnocai C., 2006. Controversies on the Genesis and Classification of Permafrost-Affected Soils. Geoderma 137, 33-39.

Boeckli, Lorenz; Brenning, A; Gruber, A; Noetzli, Jeannette (2012): Alpine permafrost index map. PANGAEA, https://doi.org/10.1594/PANGAEA.784450, Supplement to: Boeckli, L et al. (2012): Permafrost distribution in the European Alps: calculation and evaluation of an index map and summary statistics. The Cryosphere, 6, 807-820, https://doi.org/10.5194/tc-6-807-2012.

Brewer, R., 1964. Fabric and Mineral Analysis of Soils. John Wiley and Sons, New York, 470 p.

Bullock, P., Fedoroff, N., Jongerius, A., Stoops, G., Tursina, T., Babel, U., 1985. Handbook for Soil Thin Section Description. Waine Research Publications, Wolverhampton, 152 p.

Buntig B.T., 1983. High Arctic Soils Through the Microscope – Prospect and Retrospect. Annals of the Association of American Geographers 73, 609-616.

Burga C.A., 1987. Gletscher- und Vegetationsgeschichte der Südrätischen Alpen seit der Späteiszeit, Denkschritfen der Schweizerischen Naturforschenden Gesellschraft, 101.

Cannone N., Sgorbati S., Guglielmin M., 2007. Unexpected impacts of climate change on alpine vegetation. Frontiers in ecology and the environment 5, 360-364.

Ceriani M., Carelli M., 2000. Carta delle precipitazioni medie, massime e minime annue del territorio alpino della Regione Lombardia (registrate nel periodo 1891–1990). Servizio Geologico, Ufficio Rischi Geologici Regione Lombardia.

D'Amico, M.E., Pintaldi, E., Catoni, M., Freppaz, M., Bonifacio, E., 2019. Pleistocene periglacial imprinting on polygenetic soils and paleosols in the SW Italian Alps. Catena 174, 269-284.

De Coninck, F., Righi, D., Maucorps, J., Robin, A.M., 1974. Origin and micromorphological nomenclature of organic matter in sandy Spodosols. In: Rutherford, G.K., ed. Soil Microscopy. The Limestone Press, Kingston, pp. 263-280.

DiPietro, L.M., Driese, S.G., Goebel, T., 2018. Deposition and pedogenesis of periglacial sediments and buried soils at the Serpentine Hot Springs archaeological site, Seward Peninsula, AK. Catena 170, 204-223.

Dumanski J., Arnaud R.J.St., 1966. A Micropedological Study of Eluvial Soil Horizons. Canadian Journal of Soil Sciences 46 (3), 287-292.

Egli, M., Lessovaia, S.N., Chistyakov, K., Inozemzev, S., Polekhovsky, Y., Ganyushkin, D., 2015. Microclimate affects soil chemical and mineralogical properties of cold alpine soils of the Altai Mountains (Russia). Journal of Soils and Sediments 15, 1420-1436.

ERSAF, 1990. Carta Pedologica della Regione Lombardia a scala 1:250.000.

FAO, 2006. Guidelines for Soil Description.

FAO, 2014. World reference base for soil resources 2014: International soil classification system for naming soils and creating legends for soil maps.

Finsinger W., Tinner W., 2007. Pollen and plant macrofossils at Lac de Fully (2135 m a.s.l.): Holocene forest dynamics on a highland plateau in the Valais, Switzerland. The Holocene 17, 1119-1127.

FitzPatrick E.A., 1993. Soil microscopy and micromorphology. Wiley edition.

Furlanetto G., Ravazzi C., Pini R., Vallè F., Brunetti M., Comolli R., Novellino M.D., Garozzo L., Maggi V., 2018. Holocene vegetation history and quantitative climate reconstructions in a high-elevation oceanic district of the Italian Alps. Evidence for a middle to late Holocene precipitation increase. Quaternary Science Review 200, 212-236.

Guglielmin M., Cannone N., Damis F., 2001. Permafrost-glacial evolution during the Holocene in the Italian Central Alps. Permafrost and periglacial processes 12, 11-124.

Guglielmin M., Siletto G.B., 2000. Carta della Criosfera Regione Lombardia.

Heiri O., Koinig K.A., Spotl C., Berret S., Brauer A., Drescher-Schneider R., Gaar D., Ivy-Ochs S., Kershner H., Leutscher M., Moran A., Nicolussi K., Preusser F., Schmidt R., Schoeneich P., Schworer C., Sprafke T., Terhost B., Tinner W., 2014. Paleoclimate records 60-8ka in the Austrian and Swiss Alps and their forelands. Quaternary Science Review 106, 186-205.

Hormes A., Ivy-Ochs S., Kubik P.W., Ferreli L., Michetti A.N., 2008. Be-10 exposure ages of a rock avalanche and a late glacial moraine in Alta Valtellina, Italian Alps. Quaternary International 190, 136-145.

Karmakar R., Das I., Dutta D., Rakshit A., 2016. Potential Effects of Climate Change on Soil Properties: a Review. Science International 4, 51-73.

Kershner H., Kaser G., Sailer R., 2000. Alpine Younger Dryas glaciers as paleo precipitation gauges. Annals of glaciology 31, 80-84.

Kovda, I., Lebedeva, M., 2013. Modern and relict features in clayey cryogenic soils: morphological and micromorphological identification. Spanish Journal of Soil Science 3, 130-147.

Kovda, I., Sycheva, S., Lebedeva, M., Inozemtzev, S., 2009. Variability of carbonate pedofeatures in a loess-paleosol sequence and their use for paleoreconstructions. Journal of Mountain Science 6, 155-161.

Kovda, I., Goryachkin, S., Lebedeva, M., Chizhikova, N., Kulikov, A., Badmaev, N., 2017. Vertic soils and Vertisols in cryogenic environments of southern Siberia, Russia. Geoderma 288, 184-195.

Laafar, S., Rousseau, L., de Lumley, H., 1995. Evidence of palaeostructures related to freezing through soil micromorphology in Lazaret Cave, Nice (France). Comptes Rendus de l'Academie des Sciences, Serie II, 321, 209-214.

Lauterbach S., Brauer A., Andersen N., Danielopol D.L., Dulski P., Hüls M., Milecka K., Namiotko T., Obremska M., von Grafenstein U., Declakes participants, 2011. Environmental responses to

Lateglacial climatic fluctuations recorded in the sediments of pre-Alpine Lake Mondsee (northeastern Alps). Journal of Quaternary Science 26, 253-267.

Longhi A., Monticelli D., Guglielmin M., 2020. The use of iron chemical analysis of Podzols to date the Late Pleistocene-Holocene deglaciation history of the Central Italian Alps. Journal of Quaternary Science 35, 1021-1035.

Lundström U.S., van Breemen N., Bain D., 2000. The podzolization process. A review. Geoderma 94, 91-107.

Mangini A., 2005. Assessing the variability of precipitation during the Holocene from stalagmite records. Memorie della Società Astronomica Italiana 76, 755-759.

McKeague J.A., 1983. Clay skins and argillic horizons. In Bullock, P.&Murphy, C.P. (eds.), Soil micromorphology, Volume 2, Soil Genesis. AB Academia Publishers, Berkhamsted, 367-387.

Menzies, J., Maltman, A.J. 1992. Microstructures in diamictons - evidence of subglacial bed conditions. Geomorphology, 6/1, 27-40.

Mermut A.R., Arnaud R. J. St., 1981. Microband Fabric in Seasonally Frozen Soils. Soil Science Society of America Journal 45 (3), 578-586.

Murton J.B., 2013. Ice wedges and ice wedge casts in Elias S.A., Mock CJ Encyclopedia of Quaternary Science, Second Edition, Elsevier Amsterdam vol. 3, 436-451.

Murton J.B., Worsley P., Godznik J., 2000. Sand veins and wedges in cold aeolian environments. Quaternary Science Review 19, 899-922.

Musielok L., Drewnik M., Szymansky W., Stolarczyk M., Gus-Stolarczyk M., Skiba M., 2021. Conditions favoring local podzolization in soils developed from flysch regolith – A case study from the Bieszczady Mountains in southeastern Poland. Geoderma 381, 114667.

Notapietro A., De Capitani L., 1985. Contributo alla conoscenza delle plutoniti austridiche dell'Alta Valtellina : il granito del Pizzo Bianco. Rendiconti della società italiana di mineralogia e petrologia 40, 353-363.

Ortu E., Peyron O., Bordon A., de Beaulieu J.L., Siniscalco C., Caramiello R., 2008. Lateglacial and Holocene climate oscillations in the South-western Alps: an attempt at quantitative reconstruction. Quaternary International 190, 71-88.

Pawluk S., Brewer R., 1975. Investigations of Some Soils Developed In Hummocks of The Canadian Sub-Arctic And Southern-Arctic Regions 1. Morphology And Micromorphology. Canadian Journal of Soil Science 55, 301-319.

Ping C.L., Bockheim J., Kimble J.M.,1998. Characteristics of cryogenic soils along a latitudinal transect in Arctic Alaska. Journal of Geophysical Research Atmospheres 103, 28917-28928.

Pissart A.,1969. Le mécanisme périglaciaire dressant les pierres dans le sol. Résultats d'expériences. C.R.Acad.Sc.Paris 268, 3015-3017.

Pitkaranta R., 2009. Pre-Late Weichselian podzol soil, permafrost features lithostratigraphy at Penttilankangas, western Finland. Bulletin of the Geological Society of Finland 81, 53-74.

Rasmussen S.O., Bigler M., Blockley S.P., Blunier T., Buchardt S.L., Clausen H.B., Cvijanovic I., Dahl-Jensen D., Johnsen S.J., Fischer H., Gkins V., Guillevic M., Hoek W.Z., Lowe J.J., Pedro J.B., Popp T., Seiestard I.K., Steffensen J.P., Svensson A.M., Vallelonga P., Vinther B.M., Walker M.J.C., Wheatley J.J., Winstrup M., 2014. A stratigraphic framework for abrupt climatic changes during the Last Glacial period based on three synchronized Greenland ice-core records: refining and extending the INTIMATE event stratigraphy. Quaternary Science Review 106, 14-28.

Rellini, I., Trombino, L., Rossi, P.M., Firpo, M., 2014. Frost Activity and Ice Segregation in a Palaeosol in the Ligurian Alps (Beigua Massif, Italy): Evidence of Past Permafrost? Geografia Fisica e Dinamica Quaternaria 37, 29-42.

Scarciglia F., Terribile F., Colombo C., 2003. Micromorphological evidence of paleoenvironmental changes in Northern Cilento (South Italy) during the Late Quaternary. Catena 54, 515-536.

Schimmelpfenning I., Schaefer J.M., Akcar N., Ivy-Ochs S., Finkel R.C., Schlucter C., 2012. Holocene glacier culmination in the Western Alps and their hemispheric relevance. Geology 40, 891-894.

Sedov, S., Rusakov, A., Sheinkman, V., Korkka, M., 2016. MIS3 paleosols in the center-north of Eastern Europe and Western Siberia: Reductomorphic pedogenesis conditioned by permafrost? Catena 146, 38-47.

Sheinkman, V., Sedov, S., Shumilovskikh, L., Korkina, E., Korkin, S., Zinovyev, E., Golyeva, A., 2016. First results from the Late Pleistocene paleosols in northern Western Siberia: Implications for pedogenesis and landscape evolution at the end of MIS3. Quaternary International 418, 132-146.

Soil Survey Staff, 1993. Soil Survey Manual, United States Department of Agriculture Handbook No. 18.

Steila D., Pond T.E., 1989. The Geography of Soils: Formation, Distribution, and Management. Rowman & Littlefield Publisher.

Stoops, G., 2003. Guidelines for Analysis and Description of Soil and Regolith Thin Sections. Soil Science Society of America, Madison, 184 p.

Stoops, G., Marcelino, V., Mees, F., 2018. Interpretation of micromorphological features of soils and regoliths. Second Edition. Elsevier, Oxford, 1000 p.

Szymanski W., Skiba M., Wojtun B., Drewnik M., 2015. Soil properties, micromorphology, and mineralogy of Cryosols from sorted and unsorted patterned grounds in the Hornsund area, SW Spitsbergen. Geoderma 253-254, 1-11.

Targulian, V.O. and Goryachkin, S.V., 2004. Soil memory: Types of record, carriers, hierarchy and diversity. Revista Mexicana de Ciencias Geológicas, 21:1, 1-8.

Todisco, D., Bhiry, N., 2008. Micromorphology of periglacial sediments from the Tayara site, Qikirtaq Island, Nunavik (Canada). Catena 76, 1-21.

Ugolini F., Corti G., Certini G., 2006. Pedogenesis in the sorted patterned ground of Devon Plateau, Devon Island, Nunavut, Canada. Geoderma 136, 87-106.

Van Ranst E., Wilson M.A., Righi D., 2018. Spodic Materials. In: Stoops, G., Marcelino, V., Mees, F., eds. Interpretation of micromorphological features of soils and regoliths. Second Edition. Elsevier, Oxford, pp. 633-662.

Van Vliet-Lanoë, B., 1988. The significance of cryoturbation phenomena in environmental reconstruction. Journal of Quaternary Science 3, 85-96.

Van Vliet-Lanoë, B., 1998. Frost and soils: implications for paleosols, paleoclimates and stratigraphy. Catena 34, 157-183.

Van Vliet-Lanoë, B., Fox, C.A., 2018. Frost Action. In: Stoops, G., Marcelino, V., Mees, F., eds. Interpretation of micromorphological features of soils and regoliths. Second Edition. Elsevier, Oxford, pp. 575-603.

Vandenberghe J., 2013. Cryoturbation Structures. In: Elias S.A. (ed.) The Encyclopedia of Quaternary Science, vol. 3, pp. 430-435. Amsterdam: Elsevier

Walker M., Johnsen S., Rasmussen S.o., Popp T., Steffensen J.P., Gibbard P., Hoek W., Lowe J., Andrews J., Bjork S., Cwynar L.C., Hugen K., Kershav P., Kromer B., Litt T., Lowe J.D., Nakagawa T., Newnham R., Schwander J., 2009. Formal definition and dating of the GSSP (Global Stratotype Section and Point) for the base of the Holocene using the Greenland NGRIP ice core, and selected auxiliary records. Journal of Quaternary Science 24, 3-17.

4.2.10. Pictures and Tables

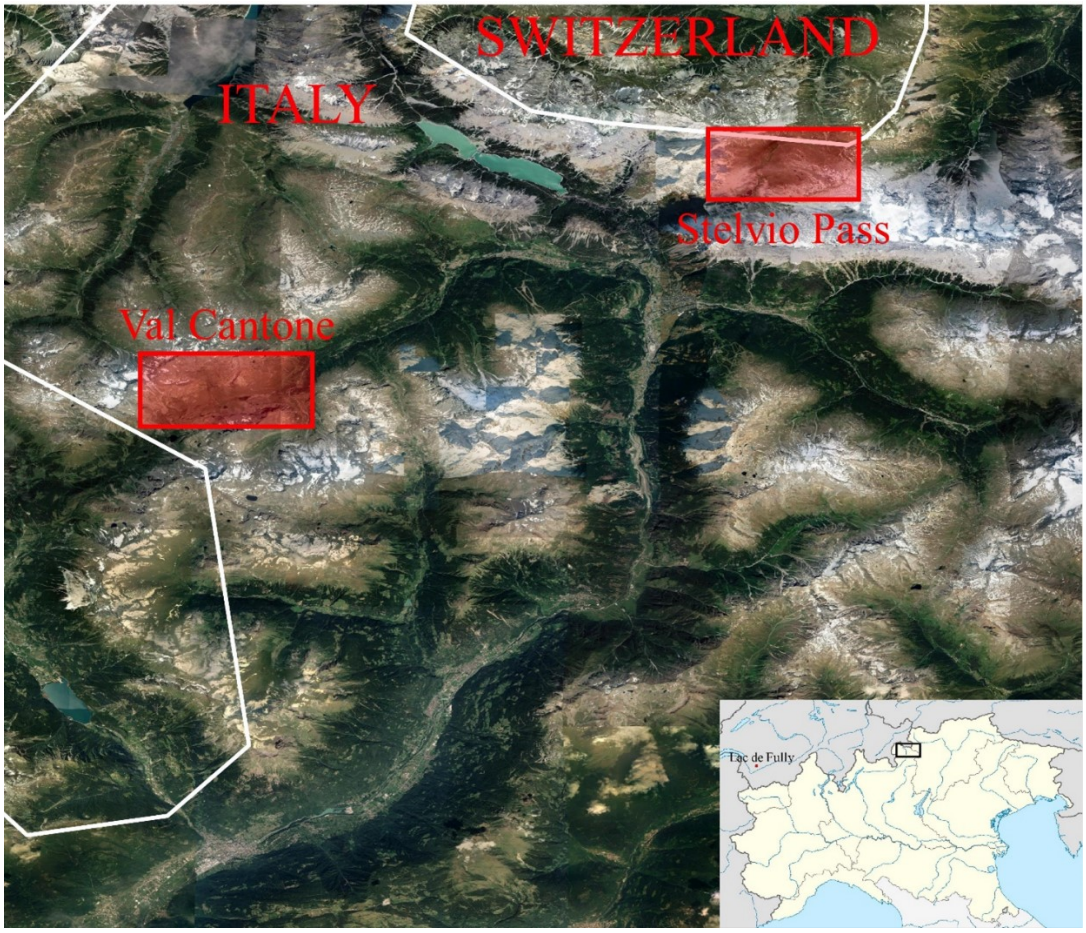

Figure 1: Reference map for site location.

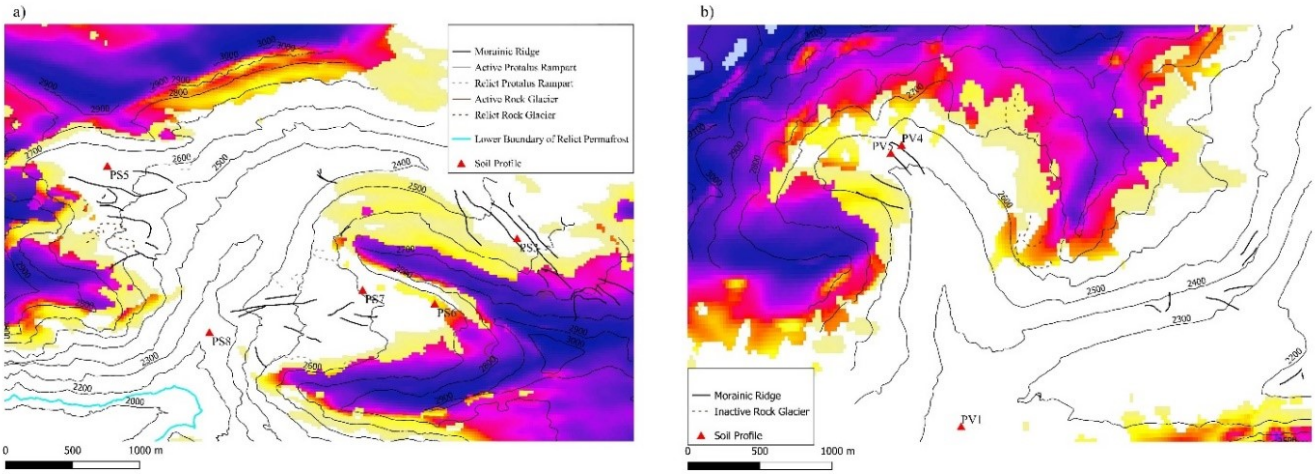

Figure 2: Modern permafrost distribution in Stelvio Pass area (a) and Val Cantone area (b) with APIM model (Boeckli et al., 2012), Relict permafrost distribution (Guglielmin & Siletto,2000), main periglacial and glacial landforms and the location of the profiles here analyzed (red triangles).

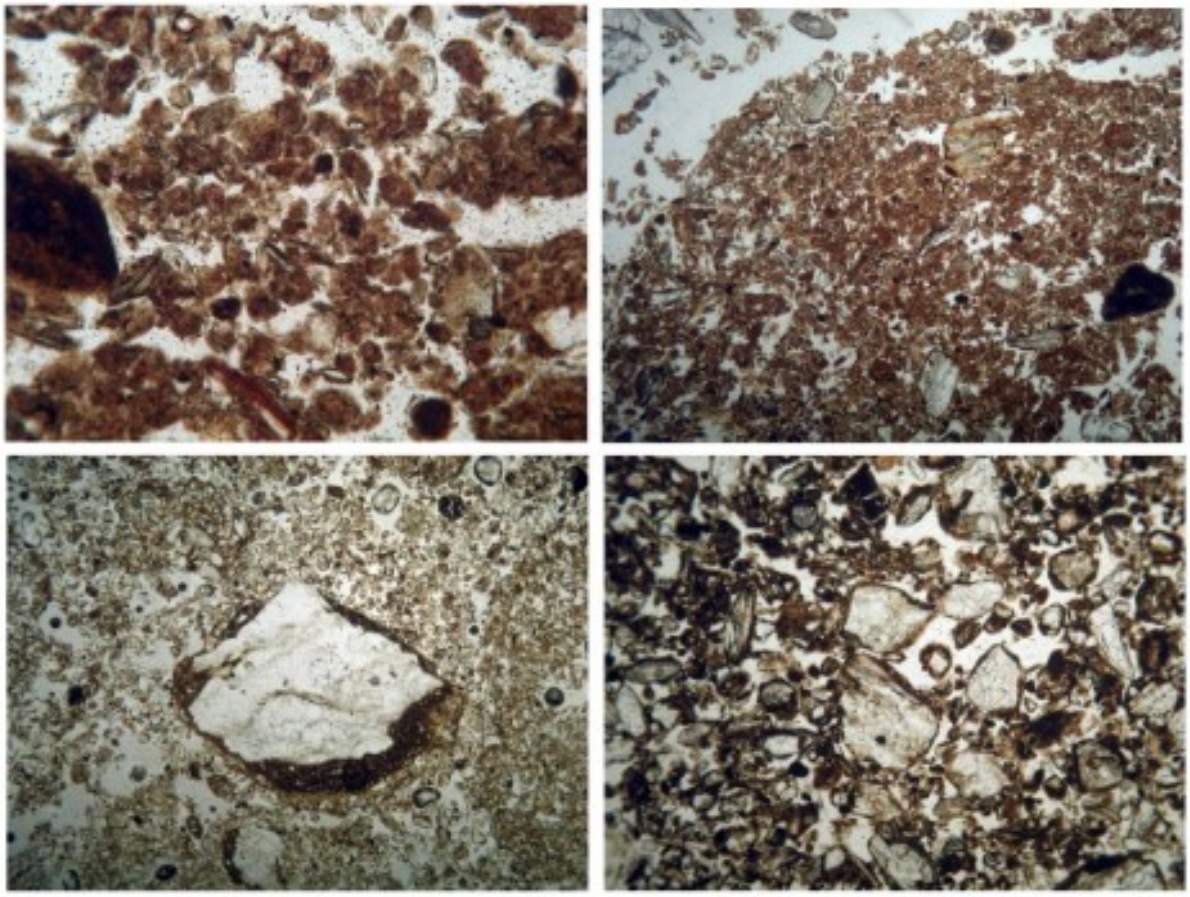

Figure 3a: Val Cantone area more significant micromorphology pictures: 1 - Granular microstructure PV5 PPL 100x; 2 - Coarse subangular blocky ped, formed by coalescence of granules PV4 PPL 16x; 3 - Downturned silt capping PV1 PPL 16x; 4 - Chitogefuric c/f related distribution PV1 PPL 100x.

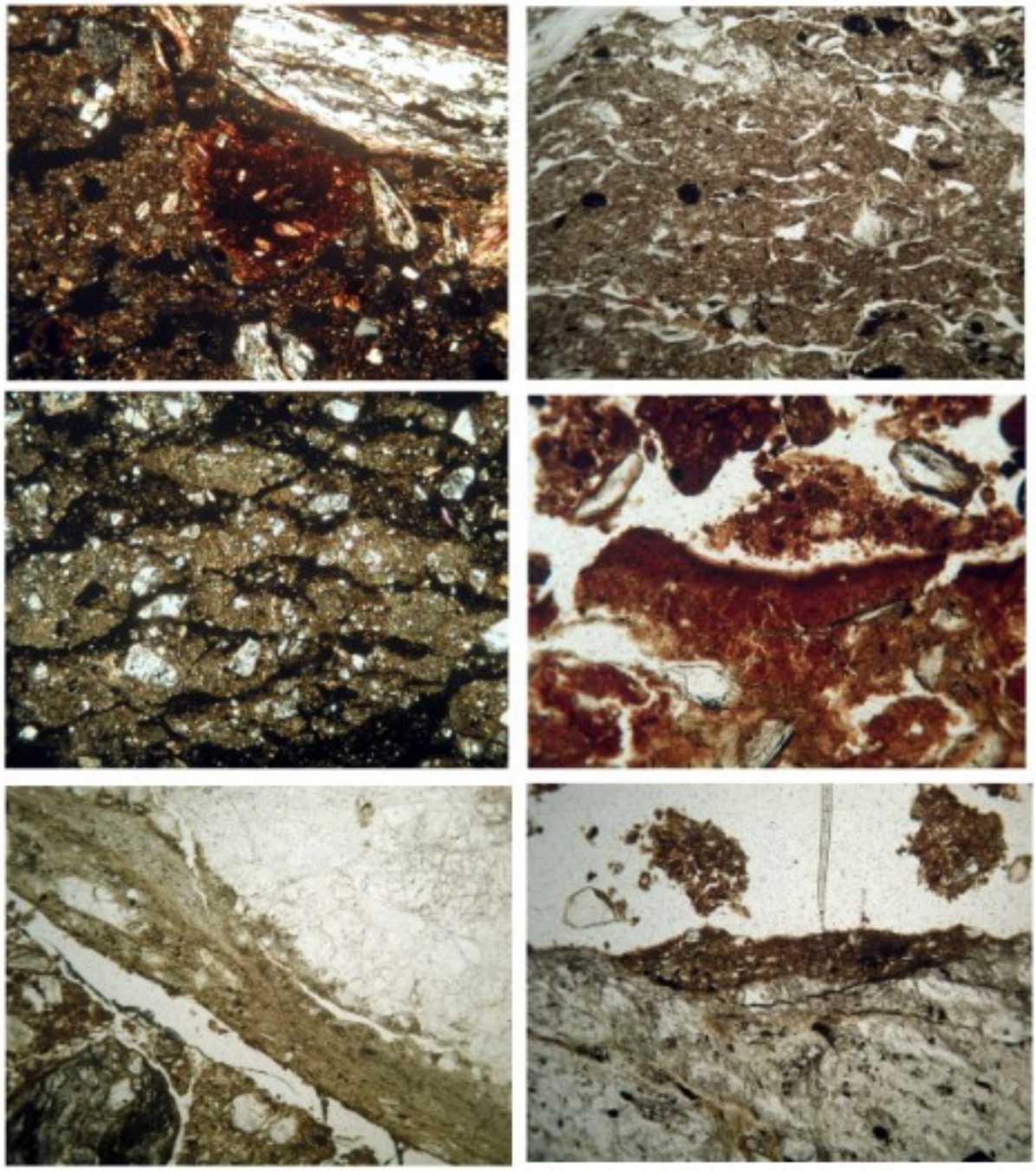

Figure 3b: Stelvio Pass area more significant micromorphology pictures: 1 - Reworked rounded soil fragment PS3 40x; 2 - Lenticular microstructure PS8 PPL 40x; 3 - Lenticular microstructure PS5 XPL 16x; 4 - Coating of monomorphic fine organic material PS8 PPL 100x; 5 - Downturned silt capping PS6 PPL 40x; 6 - Fragmented silt capping PS7 PPL 100x.

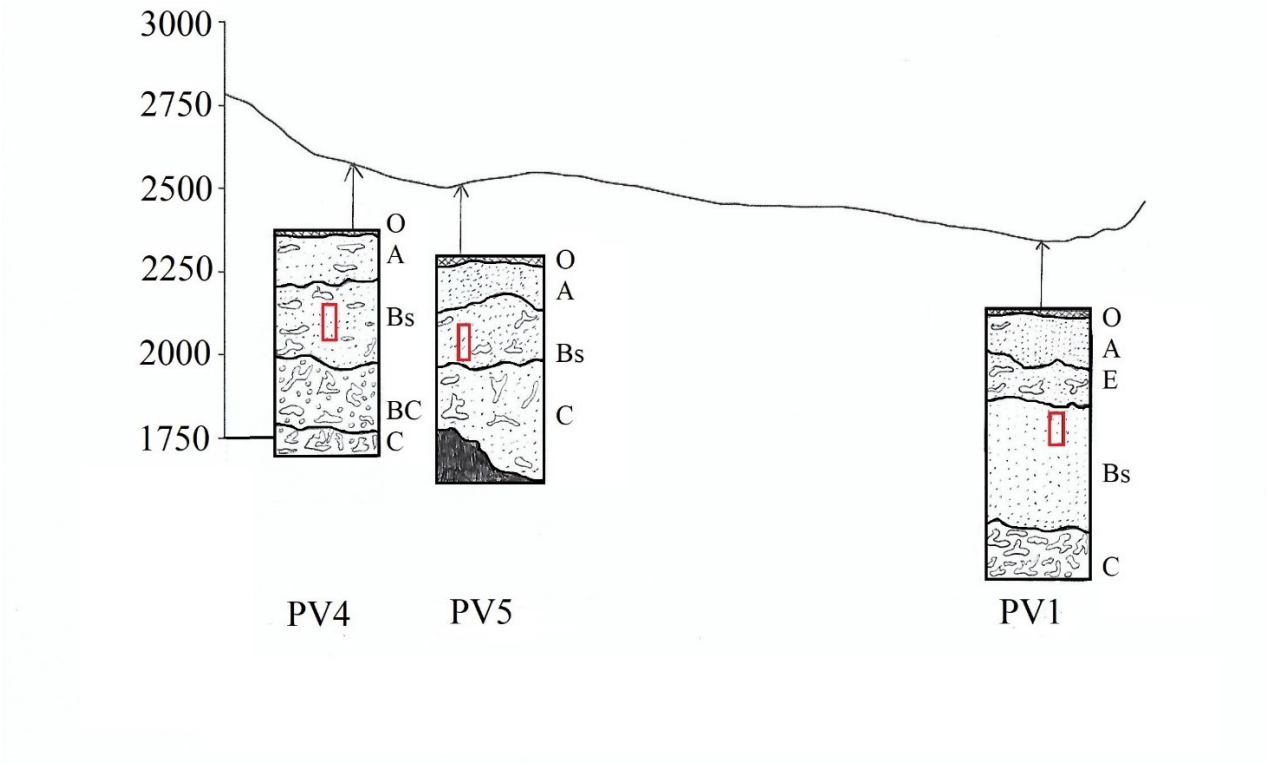

Figure 4: Topographic profile and collocation of the profiles in Val Cantone area.

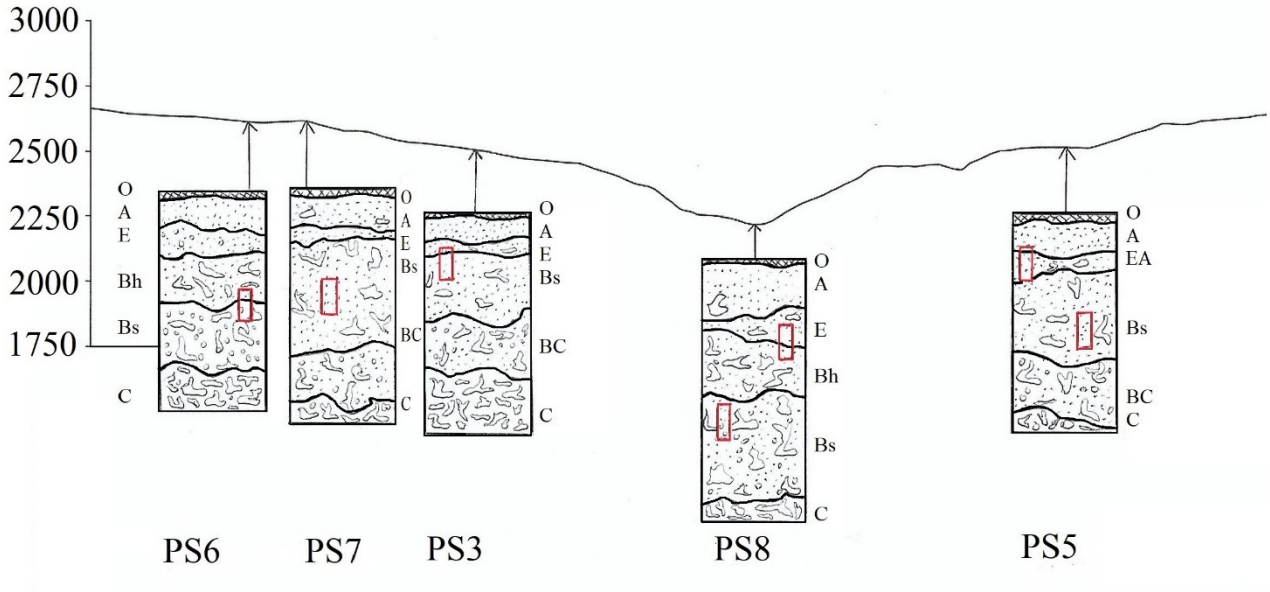

Figure 5: Topographic profile and collocation of the profiles in Stelvio Pass area.

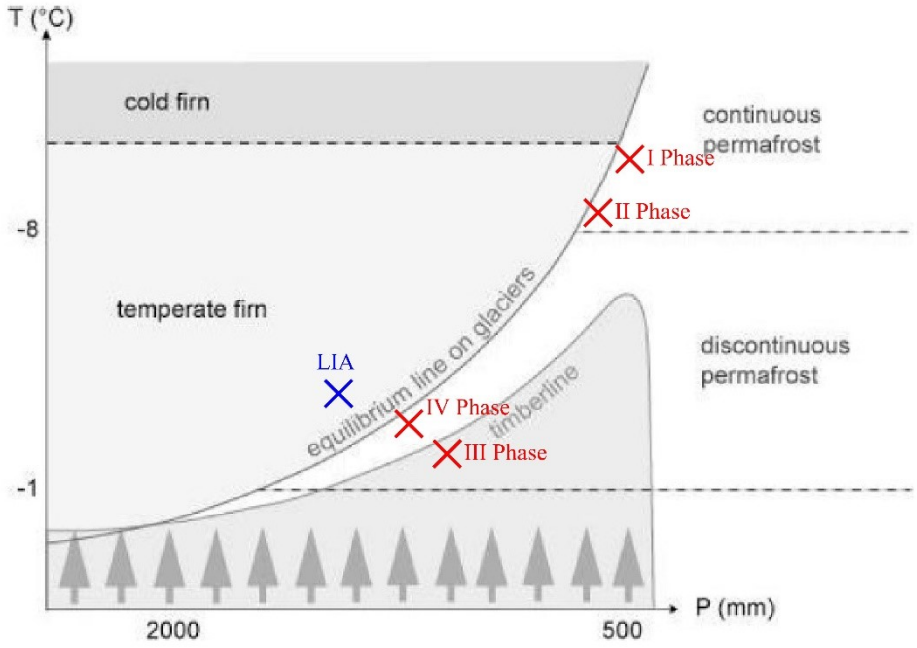

Figure 6: Temperature and precipitation condition during 4 podzolization phases (red x) plotted in the diagram proposed by Haeberli and Burn (2002). Plotted is also the P-T LIA condition calculated at the elevation of IV phase.

Core Site	Elevation m a.s.l.)	Distance (km)	Citation
Silvaplana Lake	1791	50	Furlanetto et al., 2018
Schwarzsee ob Solden	2796	61	Furlanetto et al., 2018; Heiri et al., 2014
Armentarga	2345	70,5	Furlanetto et al., 2018
Oberer Landschitzsee	2076	155	Heiri et al., 2014
Rutor	2594	160	Furlanetto et al., 2018

Table 1: Cores used as proxy for temperature reconstruction, their location and distance from analyzed area, and rescpective citations.

Profile ID	X	Y	Elevation (m a.s.l.)	Aspect (°)	Slope (°)	Vegetational Coverage	Dominant Vegetation	Stoniness	Horizon Sequence	Soil Classification	Solum (cm)
PS3	46.53280	10.43835	2534	274	3	100%	Herbaceous	0%	O-A-E-Bs-B/C-C	Skeletic Podzol	35
PS5	46.53849	10.39837	2610	180	4	80%	Herbaceous	20%	O-A-E-Bs-B/C-C	Albic Podzol	45
PS6	46.5263	10.42936	2630	250	1	75%	Mosses	25%	O-A-E-Bhs-Bs-C	Skeletic Podzol	40
PS7	46.52733	10.42352	2647	301	0	70%	Herbaceous	30%	O-A-E-Bs-B/C-C	Albic Podzol	48
PS8	46.52228	10.40879	2228	356	4	95%	Herbaceous	5%	O-A-E-Bhs-Bs-C	Albic Podzol	56
PV1	46.41917	10.15708	2347	126	0	60%	Herbaceous	40%	O-A-E-Bs-C	Albic Podzol	48
PV4	46.43666	10.15191	2564	160	4	90%	Herbaceous	10%	O-A-Bs-B/C-C	Skeletic Podzol	45
PV5	46.43594	10.15129	2525	141	3	90%	Herbaceous	10%	O-A-Bs-B/C-C	Entic Podzol	25

Table 2: Site and soil description extracted from Table 1 in Longhi et al., 2020. The elevation is given in meters and depth in centimeters.

	Microstructure			**Groudmass**			**Pedofeatures**		
	spheroidal aggregates	**other aggregates**	**microstructure type**	**c/f ratio**	**c/f related distribution**	**organic fine material**	**silt cappings**	**amorphous hypocoatings**	**reworked soil material**
PV1 – Bs	granules crumbs	subangular blocky peds	pellicular grain bridged grain	7:3 (5µm)	chitonic chitogefuric	polymorphic	few (sometimes downturned)	not identified	not identified
PV4 – Bs	Granules	platy subangular blocky peds	granular	2:3 (5µm)	porphyric	polymorphic	very few	not identified	not identified
PV5 – Bs	Granules	not identified	granular	1:1 (5µm)	porphyric	polymorphic	very few (sometimes downturned)	not identified	not identified

PS3 - E(/Bs) top	not identified	subangular blocky peds	subangular blocky	3:7 (5µm)	porphyric	not identified	not identified	not identified	very few
PS3 - (E/)Bs base	granules crumbs	Platy	lenticular	2:3 (5µm)	porphyric	polymorphic	fragmented	not identified	not identified
PS5 - EA(/Bs)	granules crumbs	platy subangular blocky peds	granular	2:3 (5µm)	porphyric	not identified	not identified	not identified	not identified
PS5 – (EA)/Bs	not identified	Platy	lenticular	1:1 (5µm)	porphyric	polymorphic partially monomorphic	very few (sometimes downturned)	very few	not identified
PS6 - Bh(/Bs) top	Granules	not identified	granular	3:2 (5µm)	enaulic	polymorphic	not identified	not identified	not identified
PS6 - (Bh/)Bs bottom	Granules	platy (locally)	granular spongy	1:1 (5µm)	porphyric	polymorphic partially monomorphic	very few (sometimes downturned)	very few (on rock fragments)	not identified
PS7 – Bs	granules crumbs	Platy	lenticular	1:1 (5µm)	porphyric	polymorphic partially monomorphic	fragmented	very few (on rock fragments)	not identified
PS8 - E(/Bh) top	not identified	subangular blocky peds platy (locally)	subangular blocky	1:1 (5µm)	porphyric	not identified	not identified	not identified	not identified
PS8 - (E/)Bh base	granules crumbs	not identified	crumby	2:3 (5µm)	porphyric chitonic (locally)	polymorphic partially monomorphic	not identified	not identified	not identified

PS8 (Bh/)Bs	-	granules crumbs	subangular blocky peds	crumby	2:3 (5µm)	porphyric chitonic (locally)	polymorphic monomorphic	very few (sometimes downturned)	very few (on rock fragments)	not identified

Table 3: Qualitative main micromorphological characteristics of Stelvio and Val Cantone.

Profile ID	Age (ka)	Elevation (m)	Phase	Permafrost Presence	T/P conditions (°C/mm)	-2°C Elevation (m)	Glacier Elevation in the Previous Phase (m)
PV1	12.5± 1.0	2347	I	Yes	-9/525	2093	2700
PV4	10.7± 0.7	2564	II	Yes	-8/575	2112	2350
PV5	9.1±0 .8	2525	III	Yes	-2/975	2597	2450
PS3	9.7±0 .5	2534	II	Yes	-8/575	2112	2340
PS5	12.0± 0.8	2610	I	Yes	-9/525	2093	N.A.
PS6	7.5±0 .2	2630	IV	Yes	-2,4/1000	2569	2380
PS7	8.2±0 .2	2647	III	Yes	-2/975	2597	2340
PS8	10.3± 0.6	2228	II	Yes	-8/575	2112	2228

Table 4: Profiles, elevation, and relative age (from Longhi et al., 2020). Podzolization phase attribution, temperature and precipitation condition during that phase, elevation of the -2°C isotherm, and glacier elevation during the previous phase.

4.3. RECONSTRUCTION OF THE GLACIAL HISTORY AFTER THE LAST GLACIAL MAXIMUM IN THE ITALIAN CENTRAL ALPS USING SCHMIDT'S HAMMER R-VALUES AND CRYSTALLINITY RATIO INDICES OF SOILS.

Quaternary International 558 (2020) 19–27

Contents lists available at ScienceDirect

Quaternary International

journal homepage: www.elsevier.com/locate/quaint

Reconstruction of the glacial history after the Last Glacial Maximum in the Italian Central Alps using Schmidt's hammer R-values and crystallinity ratio indices of soils

A. Longhi, M. Guglielmin *

Department of Theoretical and Applied Sciences, Insubria University, Varese, Italy

ARTICLE INFO

Keywords:
Glacial evolution
Schmidt hammer
Crystallinity ratio index
Late pleistocene
Holocene
Italian central alps

ABSTRACT

Despite the ongoing development of cosmogenic techniques to reconstruct deglaciation and glacial advances, these techniques are not always feasible for logistical and economic reasons.

In this study, we used Schmidt Hammer R-values (SH) and Crystallinity Ratio (CRF) indices of soils, together with a limited number of absolute ^{14}C dates, to outline the glacial evolution of the Gavia Valley. The study area is a sector of the Italian Central Alps with a glacial history that is poorly understood. Methodologically, we found that SH can be successfully applied to Late Pleistocene surfaces younger than 15ka in this Alpine region. The SH method generally underestimates the ages with respect to the CRF indices and the ^{14}C dates. A total of 7 different glacial phases were found in the study area: 14.7ka (I phase), 13.7ka (II phase), 12.2–11.8ka (III phase), 10.2–9.7ka (IV phase), 7.5ka (V phase), 5.5ka (VI phase), 1.9ka (VII phase). These phases are generally consistent with the literature; however, the Little Ice Age was surely less extended respect the other Holocene advances (V and VI phase). This suggests that relatively short climatic variations during the Holocene were locally important.

1. Introduction

Among the different techniques to reconstruct deglaciation and subsequent glacial advances, cosmogenic dating has received the greatest consideration (e.g., Chenet et al., 2016; Moran et al., 2016; Wuthrich et al., 2018; Rolland et al., 2020). However, cosmogenic techniques are not always feasible due to logistical and economic constraints. In this study, we consider the utility of alternative methods like soil dating (e.g., Maejima et al., 2002) or the Schmidt Hammer R-values (e.g., Matthews and Winkler, 2011). Indeed, the Crystallinity Ratio of free iron oxides (hereafter abbreviated CRF) is a well-known age indicator for soils developed on glacial and periglacial features (Arduino et al., 1984; Maejima et al., 2002; Longhi et al., 2020). The Schmidt Hammer R-value provides a metric of the rock weathering rate in order to estimate the relative exposure age of bedrock surfaces (Matthews and Shakesby, 1984; McCarroll, 1989; Goudie, 2006; Shakesby et al., 2006, 2008; Owen et al., 2007; Matthews and Owen, 2010; Matthews and Winkler, 2011; Guglielmin et al., 2012).

In Central-Eastern Alps, the limit of the Last Glacial Maximum (LGM) is placed between 21.1 and 19.1 ka (Ivy-Ochs et al., 2004; Ivy-Ochs, 2015), with more than 80% of the ice volume lost by 18 ka (Ivy-Ochs et al., 2008; Ivy-Ochs, 2015; Wuthrich et al., 2018). A glacial re-advance then occurred around 17 ka, followed by a stabilization at ca. 15.4 ka (Ivy-Ochs et al., 2004; Ivy-Ochs, 2015; Wuthrich et al., 2018). Two other glacial phases have been dated at 13.5–12ka (Kerschner et al., 2000; Bohlert et al., 2011; Ivy-Ochs, 2015) and 11.3–10 ka (Zoller et al., 1998; Ivy-Ochs et al., 2006; Ivy-Ochs et al., 2004).

The last LGM culmination occurred before 17ka in the Eastern Alps (Favilli et al., 2008), while exposure rates of moraine boulders place the LGM at around 24ka in the Maritime Alps (Federici et al., 2016). In the Italian Central Alps, three more recent phases have been identified at 14.6 ka, 11 ka, and 9 ka (Longhi et al., 2020).

In the Gavia Pass area, four glacial phases have previously been identified between the LGM and the Little Ice Age (LIA), dated at 12 ka, 10–9.7 ka, 7-7.5ka, and 5.5 ka, respectively. This suggests different deglaciation patterns at Mt. Gavia Glacier versus Lake Bianco Glacier (Longhi et al., 2020). Lithic industry in the Dosso Gavia area, at 2360 m a.s.l. Indicates that the Alpe Valley was glacier free, at least in the Boreal division (Angelucci et al., 1992). Moreover, in the area close to Lake Nero, there is evidence of more intense periglacial processes and

* Corresponding author.
E-mail address: mauro.guglielmin@uninsubria.it (M. Guglielmin).

https://doi.org/10.1016/j.quaint.2020.08.045
Received 15 June 2020; Received in revised form 28 August 2020; Accepted 28 August 2020
Available online 4 September 2020
1040-6182/

expansion of natural meadows around 7ka (Ravazzi et al., 2004).

The objectives of this study are therefore: a) to reconstruct the glacial evolution of the Gavia Pass area (Italian Central Alps) after the LGM using Schmidt Hammer R-values and Crystallinity Ratio indices of soils, and b) to compare the efficiency of the two dating methods.

2. Study area

The study area surrounds the Gavia Pass area in Upper Valtellina, within the Italian Central Alps (Fig. 1).

The area is located in the Gavia basin, a tributary of Frodolfo Creek, between 2500 m and 3000 m elevation.

Geologically, the area is characterized by orthogneiss, paragneiss, and quartz-phyllites, mostly strongly retrogressed varieties of earlier medium-grade paraschists (Dal Piaz et al., 1988). The valley bottom is mainly rocky with clear evidence of glacial erosion, including roches moutonnées with several ponds in between. The valley sides are mainly covered by ablation till with several moraine ridges deposited by different lateral glaciers. A few rock glaciers and many small periglacial landforms, such as earth hummocks and gelifluction/solifluction lobes, are also present.

The mean annual temperature is between +1 °C and −1.4 °C (Hijmans et al., 2005), and the mean annual precipitation is 1150 mm/year.

3. Methods

3.1. Soil analysis

A total of five soil profiles were dug on top of moraine ridges and classified according to the FAO classification (FAO, 2014).

Standard procedures were followed for the extraction of oxalate (Schwertmann, 1964; McKeague and Day, 1966) and dithionite (Longhi et al., 2020).

Two spoonfuls of 0.06 mm ground soil were pressured to create thin pads and then analyzed with a SEM-EDX system to calculate the total iron content of each sample.

The crystallinity ratio (CRF) was calculated as $CRF = \frac{Fe_d - Fe_o}{Fe_{tot}}$ (Arduino et al., 1984, 1986; Maejima et al., 2002).

The soil ages were calculated according the equation from Longhi et al. (2020):

$$age = 3907*\ln(CRF) + 3508.2$$

Which generates soil ages from the CRF of the B horizon. This equation is the best-fit regression between B-horizon CRF from several podzols and their corresponding ^{14}C (Longhi et al., 2020). The crystallinity ratio of free iron oxides increases with the stage of soil development and has a strong positive correlation with absolute age (Longhi et al., 2020). The selection of a curve derived from the B horizon versus one calculated for the A horizon is related to the possibility of new pedogenesis on the analyzed podzol (Maejima et al., 2002), which could lead to an underestimation of the soil age.

3.2. Schmidt's hammer

In this study, we used a Schmidt-Hammer type N with an impact pressure of 2.207 Nm, which is particularly suited for hard rock (Guglielmin et al., 2012).

In order to avoid potential errors associated with the method, several precautions were taken.

First, we limited our analyses to paragneiss and micaschists. A preliminary analysis was carried out to evaluate the possibility of combining the results of paragneiss and micaschists splitting the stations on each lithology in the same unit and comparing respective R-values. Second, we selected large, flat, horizontal or sub-horizontal surfaces of roches moutonnées, possibly characterized by low roughness, to ensure a homogeneous weathering of crystals over the entire surface (Williams and Robinson, 1983; Owen et al., 2007). Third, measurements were taken in dry conditions during summer to avoid the effects of moisture on the rocks (Sumner and Nel, 2002). Fourth, we intentionally avoided lichen-covered surfaces (McCarroll, 1991). Given the homogeneity of the chosen surfaces, we made 25 readings at each of the 157 roches moutonnées stations, which Matthews and Owen (2010) consider

Fig. 1. Reference map of site location (map data: Google, Maxar Technologies): GV: Gavia Valley.

statistically significant. Moreover, we considered the mean R-values of the 5 highest measurements (Evans et al., 1999; Guglielmin et al., 2012) as the minimal exposure age of each tested surface. Striae orientation on roches moutonnées was also recorded in order to better reconstruct the glacial flow directions.

The availability of four absolute ages (Geoportale Regione Lombardia, 1975–2000; Longhi et al., 2020) allowed to convert the relative R values into calibrated ages (Matthews and Owen, 2010; Guglielmin et al., 2012) and generate a regional calibration curve.

Using the ^{14}C ages, the CRF soil ages, the exposure ages calculated with Schmidt's Hammer R-values, and the geomorphological evidence of glaciation (i.e., the moraine ridges and the striae on the roche moutonnées), different phases of the deglaciation were reconstructed in QGIS 3.16. Recent and modern limits of the glaciers were obtained from the Historical Map of Arrigoni (1840), the Comitato Glaciologico Italiano Bulletin (1952, 1955, 1983, 1985), and from orthophotos (1975, 2000, 2015) provided by Geoportale Regione Lombardia.

3.3. Absolute ages for Schmidt's hammer calibration

Three ^{14}C ages and one historical age were used for the calibration of SH R-values. The first age corresponds to the base of Core RT, drilled in a relict pond dammed by a morainic ridge (Longhi et al., 2020) close to site MGV108 (Unit 4a); this therefore represents its minimal exposure age. After searching for macroremains of terrestrial plants, we found just a single fragment of leaf of *Kalmia procumbens*, which was insufficient material for dating. The age was consequently obtained from bulk sediment including the leaf fragment. The second age corresponds to a paleosol buried in front of a rock glacier located at the base of Corno dei Tre Signori, in the Lake Bianco catchment, and represents the minimal exposure age of Site MGV87 (Unit 2 b). The third ^{14}C age corresponds to the base of Core TBG1 (Longhi et al., 2020) and represents the minimal exposure age of MGV161 (Unit 5 b). At this site, we found the macroremains of a *Kalmia procumbens* leaf and a fragment of *Plantago alpina*. The material was insufficient for dating, so radiocarbon dating was performed on the bulk sediment including the plant fragments. The bulk sediment may have an offset from the true age of deposition (Bertrand et al., 2012) related to the mean residence time of organic matter in soils. Comparison of the ^{14}C ages with the ages obtained via SHR calibration may therefore elucidate the accuracy of bulk-sediment ^{14}C dating.

The historical ages were calculated from overlaying the orthophotos (2000 and 1975, provided by Geoportale Regione Lombardia); this constrain the minimal exposure age of MGV110 (Unit 1a).

4. Results

4.1. Soil description and characteristics

The described soils are Podzols: three of them are Skeletic Podzols while two are Entic Podzols.

None of these were well–developed; the thickness of the A + B horizons ranges between 27 cm (PG6) and 48 cm (PG8). They are also quite coarse (silt + clay <8%) and acidic (pH ranges between 3.64 in PG5-A and 4.65 in PG4-Bs). The CRF content of the soil profiles ranges between 8.61 in PG5 and 21.68 in PG8, corresponding to ages between 11591 and 15809 cal BP (Table 1) based on the B-horizon calibration curves proposed by Longhi et al. (2020).

4.2. Schmidt-Hammer measurements

A total of 157 stations were analyzed, with the results subdivided into 11 units, as shown in Table 2. The stations were chosen only on roches moutonnées and clustered in different geomorphologic units; each unit contained between 2 and 74 stations (Table 2). The geomorphologic units were identified based on the flow directions indicated by the roches moutonnées and the striae, as well as from the geometry of the surrounding moraine ridges.

Table 1
Ages (years Cal BP) calculated from CRF (pure number) according to Longhi et al. (2020) for B horizon of the soils.

Profile	CRF	Ages
PG4	9.49	12035
PG5	8.61	11591
PG6	9.17	11879
PG7	9.90	12230
PG8	21.68	15809

To test the difference in weathering between paragneiss and micaschists in this area, we further examined Unit 7 b, where both lithologies were present in nearly the same percentage. We calculated R25 and its standard deviation on the 30 stations of micaschists and on the 34 stations of paragneiss. Micaschists showed an R25 of 40.83 ± 1.41 while the paragneiss samples had R25 = 40.91 ± 1.75. This result indicates that even if the rocks are differently classified on the geologic map based on mineralogical composition, they have the same weathering rate. Therefore, measurements from both lithologies can be correctly used jointly in the study area.

U1a displayed the highest R values calculated with both methods (R25 = 74.45 ± 0.49; R5 = 77.85 ± 0.49), while the lowest values were found in U11 (R25 = 25.54 ± 0.48 R5 = 31.97 ± 1.61). For the other units, the R25 and R5 gave different values but with the same hierarchical order. Generally, R25 also displayed a lower standard deviation than the R5 measurements; two exceptions are U5b (standard deviation of R25 greater than standard deviation of R5) and U1a (identical standard deviations for R5 and R25; Fig. 2).

4.3. Schmidt-Hammer calibration

Four calibration curves were generated using the R25 and R5 values from the single station closest to the site of the ^{14}C-dated samples (Fig. 3, dashed) and with the mean R25 and R5 values for all stations within in the unit containing the ^{14}C sample site (Fig. 3, thick). All calibration curves display very high R^2 (>0.95). For each calibration curve, the confidence interval was calculated by applying a linear regression between the maximum and minimum of the R-value (R ± Std. Dv.) and the maximum and minimum of the ^{14}C ages.

Among the calibration curves, the best performance is achieved with the mean R25 values of the unit containing the ^{14}C sample (equation 3) because the confidence interval is smaller and the R^2 is highest. This is consistent with the literature, as Shakesby et al. (2006) suggested utilizing a large number of sites and measurements to reduce the error in predicted age. The uncertainty associated with this curve (Table 3) ranges between ± 64 years in Unit 1a and ±688 years in Unit 5 b, increasing as the dated surfaces get older. Compared with other studies (e.g., Shakesby et al., 2006), the errors generated in our study are lower, especially on young surfaces.

4.4. Units exposure age

Using the calibration curve (equation 3), each unit was dated. The results, along with the sample locations, are displayed in Fig. 4.

The most recent exposure age is 1980, obtained for Unit 1a, in the Mt. Gavia Glacier area around 3000 m a.s.l. The oldest exposure age is 15,029 years CalBP obtained for Unit 11, at the confluence of the Dosegù Valley with the Gavia Valley around 2480 m a.s.l. However, Unit 10 has a younger exposure age (14,739 years CalBP) than Unit 11 despite Unit 10's lower elevation of 2250 m a.s.l.

Table 2
R25 and R5 values with their standard deviations in each geomorphological unit.

ID	Number of Station	Mean R. Value (R25)	Std. Dv. (R25)	Top 5 (R5)	Std. Dv. (R5)
1a	2	74.45	0.49	77.85	0.49
2 b	2	68.28	0.11	72.25	0.21
3a	5	56.32	0.75	60.02	1.29
4a	10	52.68	1.94	59.04	2.15
5 b	5	50.98	0.39	57.83	0.22
6 b	4	45.57	0.91	53.15	3.50
7 b	74	39.03	1.61	47.83	2.24
8a	6	36.25	2.56	42.65	2.70
9	40	29.61	1.02	35.42	2.95
10	2	26.48	0.06	32.80	0.42
11	7	25.54	0.48	31.97	1.61

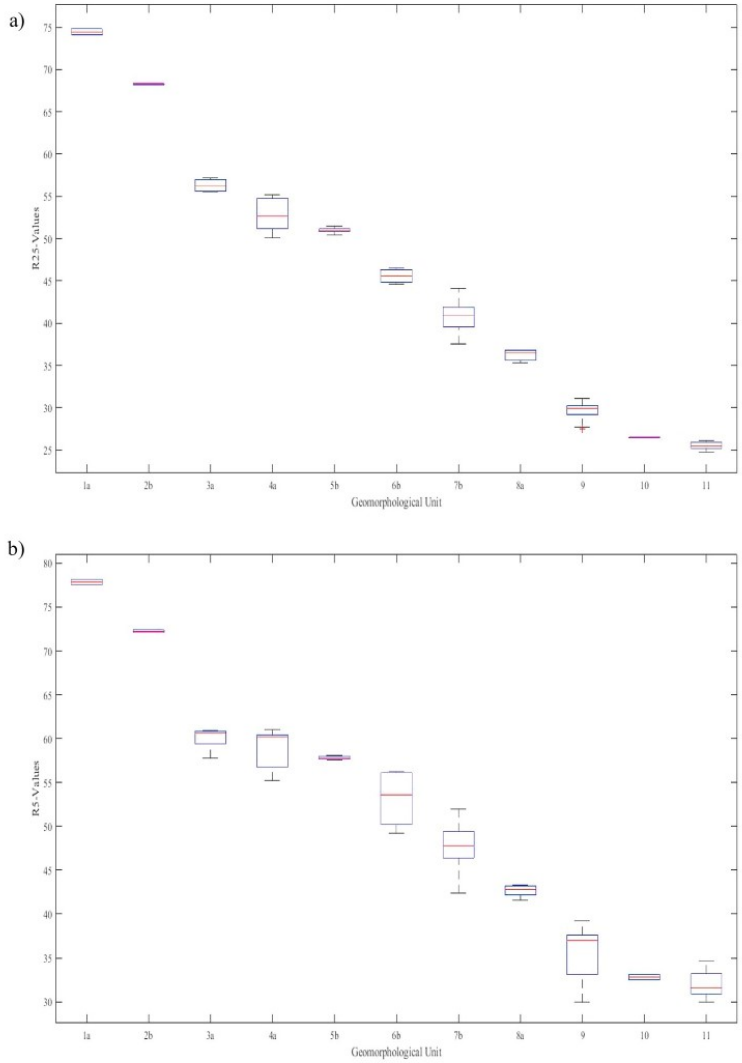

Fig. 2. Box and whisker plots with R25 values (a) and R5 values (b), red line indicates the mean value for each geomorphological unit.

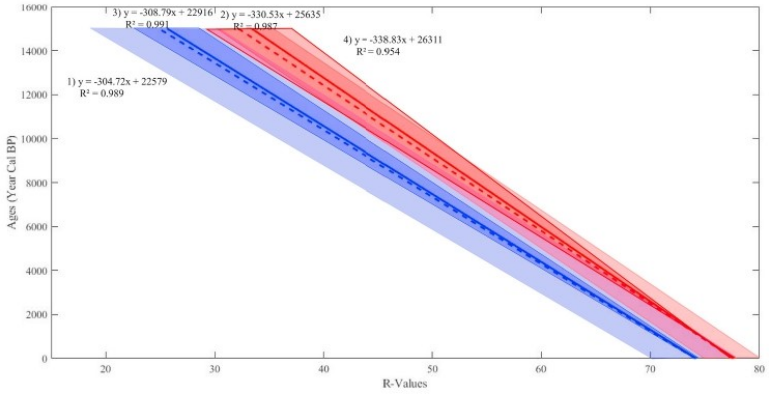

Fig. 3. Calibration curves achieved with R25 (dashed blue-1) and R5 (dashed red-2) values from the sample collected nearest to the ^{14}C sample collection site, and with R25 (thick blue-3) and R5 (thick red-4) values of the geomorphological unit containing the age site, with relative confidence interval.

Table 3
Error associated (years Cal BP) with calibration curve (3). ^{14}C ages are expressed as the mean in years Cal BP with the error associated.

Unit ID	^{14}C Age	Overall Error
1a	1987 AD ±12	±64
2b	1932 ± 70	±228
4a	5040 ± 120	±446
5b	7520 ± 590	±638

4.5. Comparison between Schmidt's hammer and CRF dating methods

In five cases, it was possible to relate the geomorphological units to different dated soils. Soils PG1, PG2, and PG3 are from Longhi et al. (2020), while PG4 and PG8 were collected for this study (Table 4).

The mean ages obtained with CRF are generally older than those obtained with SH, except for PG3/Unit 3a, where both methods produced nearly the same age. The age obtained with CRF represents the minimum age of the morainic ridges weathered to soil. Considering that morainic ridges are deposited when the glacier is advancing and the roches moutonnées are still covered by ice, it is reasonable to obtain younger exposure ages with SH.

^{14}C ages, where available, are closer to the ages obtained with CRF than those calculated with SH. The ^{14}C ages represent the minimum age of the moraine ridges that dammed the ponds and, therefore, it is reasonable to assume that the ponds started to form when the roches moutonnées were still covered by ice.

The small difference between ^{14}C, CRF ages, and SH ages provides evidence that, despite the issues commonly associated with radiocarbon dating of bulk sediment (see Section 2.3), it is reasonable to conclude that the mean residence time of organic matter in soils is negligible for this study area. This is consistent with the findings of Grimm et al. (2009).

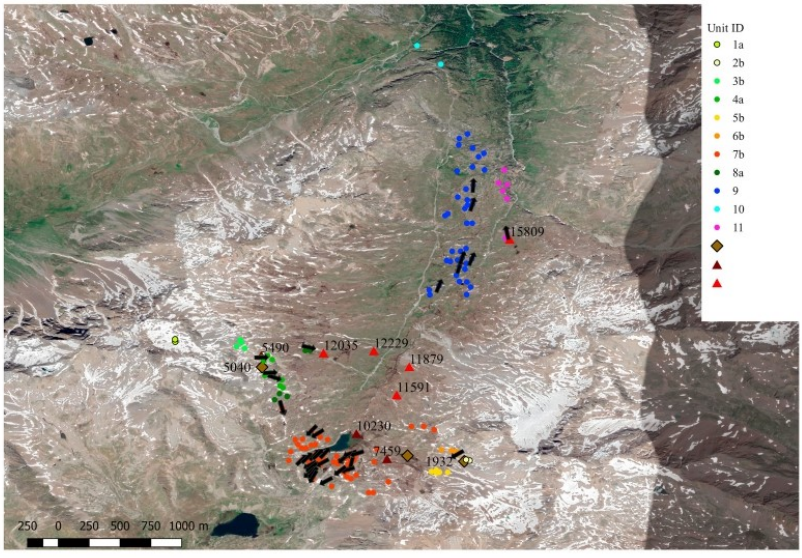

Fig. 4. Location of geomorphological units (Unit ID), striation (black arrows), podzol pits (black triangle from Longhi et al., 2020; red triangle: this paper), and absolute ages (maroon rhombus); (map data: Google, Maxar Technologies). The number of the units is progressive from the younger (1a) to the oldest (11). Unit 11 corresponds to the Dosegù Glacier, whereas Units 10 and 9 correspond to the Gavia Glacier. At Unit 8, the two glacial apparata are a) Mount Gavia and b) Lake Bianco.

Table 4
Comparison between mean ages calculated with CRF (Longhi et al., 2020), SH, and ^{14}C (Longhi et al., 2020) for comparable soil samples.

Soil ID	Unit ID	CRF Age	SH Age	^{14}C Age
PG1	Unit 6 b	10230	8844	–
PG2	Unit 5 b	7459	7173	7520
PG3	Unit 3a	5490	5525	5040
PG4	Unit 8a	12035	11723	–
PG8	Unit 11	15809	15029	–

5. Discussion

5.1. Comparing the SH data with other study sites

Schmidt's hammer has been used in many other studies to reconstruct exposure ages (e.g., Shakesby et al., 2006; Matthews and Owen, 2010; Matthews and Winkler, 2011; Guglielmin et al., 2012). Comparing our curves (Fig. 5) with curves for a similar type of gneiss from the Jotunheimen and Jostedalen regions of Southern Norway (Matthews and Owen, 2010) indicates that the two sites display a similar angular coefficient but a higher intercept. The result is that the Gavia Valley calibration curve produces ages ca. 2ky older than those for Jostedalen.

Although rock properties (e.g., different mineralogy or structure) could cause the differences in R-value, we believe that the climate conditions should also be relevant for defining the weathering rates. In the Gavia Valley, the mean annual temperature ranges between +1 °C and −1.4 °C (Hijmans et al., 2005), and the mean annual precipitation is 1150 mm/year; in Jostedalen, the mean annual temperature and precipitation are 3.7 °C and 1380 mm/year, respectively (Matthews and Owen, 2010). Therefore, it is reasonable to assume a higher weathering rate in Norway due to its higher temperature and precipitation.

Weathering rates calculated via an R-value tend to be lower than those calculated via ^{14}C, particularly for samples older than 5000 cal BP (e.g., White et al., 1998). In our dataset, as shown in Fig. 6, the non-linear curve lies within the confidence interval of the linear relationship (Eq. 3). This indicates that, despite a slight decrease in calculated weathering rate over time, weathering rates calculated using Schmidt's hammer are still within the error of rates obtained by ^{14}C dating.

5.2. The glacial history of the Gavia Pass area and glacier fluctuations in the alps

A total of 7 different glacial phases were found in the area and dated: 14.7ka (I phase), 13.7ka (II phase), 12.2–10.8ka (III phase), 10.2–9.7ka (IV phase), 7.5ka (V phase), 5.5ka (VI phase), 1.9ka (VII phase). Unfortunately, the Little Ice Age was not datable using either method, so we here report the position of the glacier during historical periods (1840 AD, 1927 AD, 1952–55 AD, 1988 AD, and 2015 AD) (Fig. 7a–b).

Earlier than 14.7ka (I phase), the Lake Bianco and Mount Gavia glaciers were joined in a single glacier tongue that flew on the valley bottom at least until the confluence with the Alpe Valley (Unit 10). At that time, the Dosegù Glacier (Unit 11) was already detached from the Gavia Glacier. The position of the terminal moraine of the Dosegù Glacier where the PG8 Podzol was dated therefore may correspond to the Gschnitz II stadial (Burga, 1987). This was also related to the end of the GS-2 event in the INTIMATE stratigraphy (Rasmussen et al., 2014) at the end of the Oldest Dryas division (Iversen, 1954).

Around 13.7ka (II phase), during event GI-1d of the INTIMATE stratigraphy (Rasmussen et al., 2014), when the air temperature cooled, the Gavia Glacier tongue was at around 2380 m a.s.l. (Unit 9). Afterward, enhanced glacier retreat occurred for more than one thousand years, especially on the valley's eastward slope. Then, around 12.3–12.2 ka, Mt. Gavia Glacier advanced on the eastward slope (phase III) to an elevation of 2640 m a.s.l. (Longhi et al., 2020). This glacial phase is therefore referable to the Egesen II stadial (Burga, 1987). This advance is typical for pollen zone III of Youngest Dryas (Iversen, 1954), when the temperature remained low and dry conditions were common in most of the Alps (Kerschner et al., 2000; Walker et al., 2009). At the same time, the westward slope of Lake Bianco was still glaciated, and the Gavia Pass was covered by ice that flowed towards the southwest.

It is also relevant that striae with a trend of 250° (indicating a glacier flowing from Lake Bianco to Gavia Pass), cut another set of striae trending 43° close to the Gavia Pass. This suggests glacial flow from Camonica Valley to Gavia Valley sometime before 10.8 ka.

After that, a more widespread deglaciation occurred until at least 10.2 ka. Lake sediment records from Heiri et al. (2014) indicate a rapid warming event of about 1.5–4 °C during this period. Between 10.2 and 9.7 ka, Lake Bianco Glacier advanced (IV phase) and almost reached the lake with a frontal moraine, dated 10.2 ka at 2610 m a.s.l. and referable the Kromer Valley Glacier advance (Moran et al., 2016; Longhi et al., 2020). In contrast, Mt. Gavia Glacier did not advance during this period.

Both Lake Bianco and Mt. Gavia glaciers advanced synchronously (V phase; Unit- 5 b and 4a) around 7.5ka, although the maximum extent varied. While Lake Bianco Glacier reached 2620 m a.s.l. comparable to its limit during the previous phase, Mt. Gavia Glacier reached only 2700 m a.s.l. This phase could be related to the 8.2 ka cold event identified in the NGRIP δ ^{18}O dataset (Walker et al., 2009, 2012). Alternatively, V

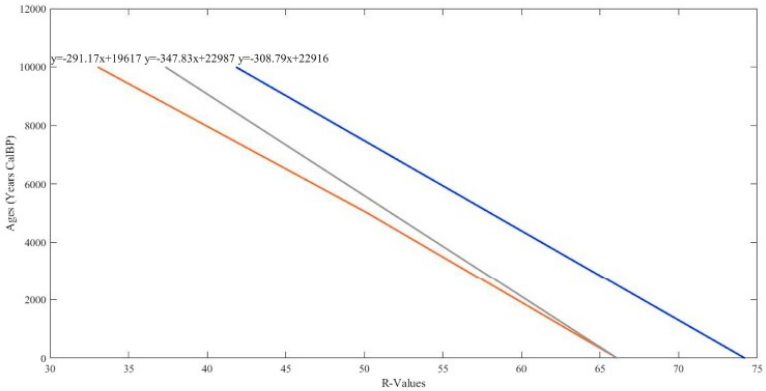

Fig. 5. Different calibration curves for converting R values to age: blue – this study; grey – Matthews and Owen (2010), Jostedalen; orange – Matthews and Owen (2010), Jotunheimen.

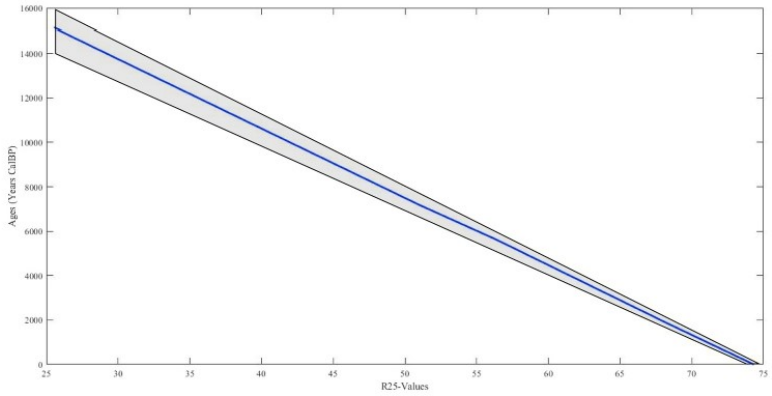

Fig. 6. Non-linear regression (blue line) between R25 values (calculated as the mean of each unit) and ages with confidence interval of (equation 3).

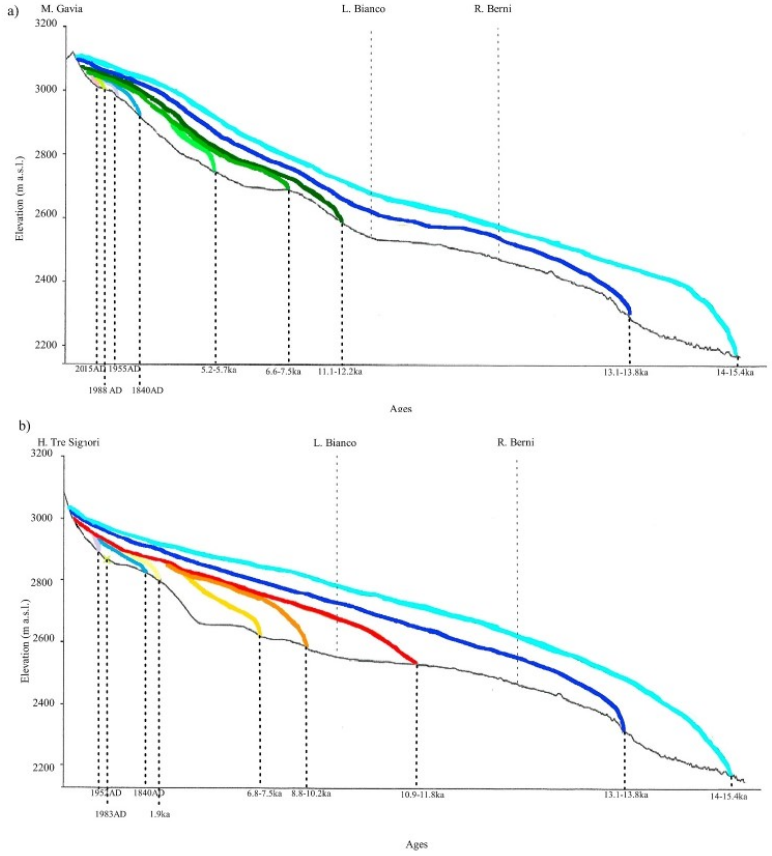

Fig. 7. Glacial evolution of the Gavia Valley and for a) Mt. Gavia Glacier and b) Lake Bianco Glacier. The historical limits were obtained from digitized historical maps (Arrigoni, 1840, and Comitato Glaciologico Italiano, 1961), and using the orthophotos of Regione Lombardia (1975-2000-2015).

phase could correspond to the ~3 °C cooling of summer temperatures between 9 and 7 ka (Ortu et al., 2008), which is supported by pollen analyses in the South Italian Alps and by the general cooling trend in the Alps after 7.6ka (Schimmelpfenning et al., 2012). In the same period, there is evidence of declining *P. cembra* forests, an intensification of periglacial processes, and an expansion of natural meadows in the Lake

Nero region (Ravazzi et al., 2004).

Subsequently, the glaciers shrank dramatically in response to the strong increase in summer temperatures between 7ka and 6.7ka (2 °C). This is independently supported by pollen analyses from the South Italian Alps (Ortu et al., 2008).

Around 5.5ka, there is evidence of a Mt. Gavia Glacier advance (VI phase) which reached 2770 m a.s.l. (Unit 3a). Not far from the study area, Calderoni et al. (1998) dated a period of permafrost aggradation responsible of the formation of some rock glaciers around 2650 m a.s.l. which indicates a cold phase in this region. Moreover, lake sediment records (Ortu et al., 2008; Ilyashuk et al., 2011) suggest a cooling event around 5.2ka. This event likely induced a rapid expansion of the glacier, which is supported by the finding of a mummified prehistoric man in the Ötztaler Alps (the Neolithic Iceman 'Otzi') dated at 5300-5050 Cal BP (Bonani et al., 1994).

Moreover, Lake Bianco Glacier experienced a limited Holocene advance to 2790 m a.s.l. (VII phase) around 1.9ka.

The Little Ice Age is not datable with our methods because there are not bedrock surfaces available within the moraine ridges for either the Mt. Gavia or Lake Bianco glaciers. Historically, Arrigoni (1840) reported the front of the former glacier at 2920 m a.s.l. during the Little Ice Age. The latter glacier reached a lower elevation of 2800 m a.s.l. confirming the asymmetric behaviour of glaciers in the two valleys.

This variable evolution of the two glaciers during the Holocene is probably related to the morphology of the catchments (i.e., smaller area and steeper slopes for Mt. Gavia Glacier).

More favorable conditions within the Lake Bianco catchment were also confirmed between the LIA and the last advance recorded in 1985 AD, when Lake Bianco Glacier reached 2845 m a.s.l. Indeed, based on historical records, Lake Bianco Glacier retreated from 1840 until 1970–83, reaching 2880 m a.s.l. In 1955. The Mt. Gavia Glacier front was 100 m higher (2980 m a.s.l.) during the same year.

It is peculiar that Lake Bianco Glacier was declared extinct in 1985, while Mt. Gavia Glacier was reported to reach 3005 m a.s.l. In 2015. Glacial evolution over the last 30 years is mainly related to the different degree of debris coverage on the two glaciers. The thicker and more continuous debris cover of Lake Bianco Glacier allowed the conservation of more glacier ice, whereas the less extensive debris cover of Mt. Gavia Glacier preserved only a minimal volume of white glacier ice in 2015.

6. Conclusion

The calibration curve produced in this study suggests that SH is a reasonable method of reconstructing exposure ages and glacial history. However, the SH calibration curve is not universal, as shown by a comparison of calibration curves for similar lithologies in Norway and the Mt. Gavia region; the local variation in calibration parameters may be due to site-specific temperature and precipitation.

Our results support the use of SH as an efficient method for dating glacially polished bedrock of Late Pleistocene age until 15 ka in the Mt. Gavia region. However, the SH method generally underestimated the ages when compared to the CRF index of soils and the available ^{14}C dates. This is reasonable because the bedrock samples examined in this study were covered by the glaciers more recently than the soils, which developed on the surrounding lateral or frontal moraine ridges.

A total of 7 different glacial phases were identified and dated for the Mt. Gavia study area: 14.7ka (I phase), 13.7ka (II phase), 12.2–11.8ka (III phase), 10.2–9.7ka (IV phase), 7.5ka (V phase), 5.5ka (VI phase), 1.9ka (VII phase). These phases are generally consistent with the literature (Burga, 1987; Ivy-Ochs et al., 2006; Ivy-Ochs et al., 2004; Longhi et al., 2020). However, a key finding of this study is that the Little Ice Age was surely less extended compared to the Holocene advances. This illustrates the importance of considering relatively short climatic variations when interpreting local Holocene glacial records.

Finally, we recommend further investigation of the occurrence of a different direction of transfluence on Gavia Pass before the Youngest Dryas.

Declaration of competing interest

The authors declare that they have no known competing financial interests or personal relationships that could have appeared to influence the work reported in this paper.

Acknowledgments

We want to thank the Parco Nazionale dello Stelvio for the logistical fieldwork support. We also want to thank Prof. Damiano Monticelli for supporting the chemical analyses of the soils. We finally want to thank PhD Rachel Bain for the English check on the paper. A special thank to the two anonymous reviewers and to the editor that with their suggestions improved significantly the paper.

References

Ivy-Ochs, S., Kerschner, H., Reuther, A., Preusser, F., Heine, K., Maisch, M., Kubik, P.W., Schlüchter, C., 2008. Chronology of the last glacial cycle in the European Alps. J. Quat. Sci. 23, 559–573.

Angelucci, D., Cremaschi, M., Negrino, F., Pelfini, M., 1992. The Dosso Gavia mesolithic site. Gavia valley (sondrio - Italy): environment and peopling during the early Holocene in the Central Alps. Preistoria Alp. 28, 19–32.

Arduino, E., Barberis, E., Carraro, F., Forno, M.G., 1984. Estimating relative ages from iron-oxides/total-iron ratios of soils in the western Po Valley, Italy. Geoderma 33, 39–52.

Arduino, E., Barberis, E., Marsan, F.A., Zanini, E., Franchini, M., 1986. Iron Indexes and clay minerals within profiles as indicators of soil age in Northern Italy. Geoderma 37, 45–55.

Arrigoni, F., 1840. Lombardia: Fisica, Stradale, Commerciale Alla Scala 1/250000. Milano.

Bertrand, S., Araneda, A., Vargas, P., Jana, P., Fagel, N., Urrutia, R., 2012. Using the N/C ratio to correct radiocarbon ages from lake sediments: insight from Chilean Patagonia. Quat. Geochronol. 12, 23–29.

Bohlert, R., Mirabella, A., Plotze, M., Egli, M., 2011. Landscape evolution in Val Mulix, eastern Swiss Alps – soil chemical and mineralogical analyses as age proxies. Catena 87, 313–325.

Bonani, G., Ivy, S.D., Hajdas, I., Niklaus, T.R., Suter, M., 1994. AMS 14C age determinations of tissue, bone and grass samples from the Ötztal Ice Man. Radiocarbon 36, 247–250.

Burga, C.A., 1987. Gletscher- und Vegetationsgeschichte der Südrätischen Alpen seit der Späteiszeit. Denkschritfen der Schweizerischen Naturforschenden Gesellschraft 101, 1–162.

Calderoni, G., Guglielmin, M., Tellini, C., 1998. Radiocarbon dating and postglacial evolution, upper Valtellina and Livignese area (Sondrio, central Italian Alps). Permafr. Periglac. Process. 9 (3), 275–284.

Chenet, M., Brunstein, D., Jomelli, V., Roussel, E., Rinterknecht, V., Mokadem, F., Biette, M., Robert, V., Lèanni, L., Aster team, 2016. ^{10}Be cosmic-ray exposure dating of moraines and rock avalanches in the Upper Romanche Valley (French Alps): evidence of two glacial advances during the Late-Glacial/Holocene Transition. Quat. Sci. Rev. 148, 209–221.

Comitato Glaciologico Italiano, 1961. Catasto dei ghiacciai italiani. Anno Geofisico 1957-1958, vol. III. Consiglio Nazionale delle Ricerche, p. 389.

Dal Piaz, G.V., Del Moro, A., Martin, S., Venturelli, G., 1988. Post-collisional magmatism in the ortler-cevedale massif (northern Italy). Jb Geol. B.A. 131, 533–551.

Evans, D.J.A., Archer, S., Wilson, D.J.H., 1999. A comparison of the lichenometric and Schmidt hammer dating techniques based on data from the proglacial areas of some Icelandic glaciers. Quat. Sci. Rev. 18, 13–41.

Fao, 2014. World Reference Base for Soil Resources 2014: International Soil Classification System for Naming Soils and Creating Legends for Soil Maps.

Favilli, F., Egli, M., Mirabella, A., Sartori, G., Giaccai, D., 2008. High Alpine landscape evolution in Val di Sole (Trentino, Italy) during the Holocene based on charcoal, soil chemistry and mineralogy. Rothenbühler, C. Klimaveränderungen auf der Spur. Samedan 18–37.

Federici, P., Ribolini, A., Spagnolo, M., 2016. Glacial History of the Maritime Alps from the Last Glacial Maximum to the Little Ice Age, vol. 433. Geological Society, London, pp. 137–159.

Goudie, A., 2006. The Schmidt hammer in geomorphological research. Prog. Phys. Geogr. 30, 703–718.

Grimm, E.C., Maher Jr., L.J., Nelson, D.M., 2009. The magnitude of error in conventional bulk-sediment radiocarbon dates from central North America. Quat. Res. 72, 301–308.

Guglielmin, M., Worland, M.R., Convey, P., Cannone, N., 2012. Schmidt Hammer studies in the maritime Antarctic: application to dating Holocene deglaciation and estimating the effects of macrolichens on rock weathering. Geomorphology 155–156, 34–44.

Heiri, O., Koinig, K.A., Spotl, C., Berret, S., Brauer, A., Drescher-Schneider, R., Gaar, D., Ivy-Ochs, S., Kershner, H., Leutscher, M., Moran, A., Nicolussi, K., Preusser, F.,

Schmidt, R., Schoeneich, P., Schworer, C., Sprafke, T., Terhost, B., Tinner, W., 2014. Paleoclimate records 60-8ka in the Austrian and Swiss Alps and their forelands. Quat. Sci. Rev. 106, 186–205.
Hijmans, R.J., Cameron, S.E., Parra, J.L., Jones, P.G., Jarvis, A., 2005. Very high resolution interpolated climate surfaces for global land areas. Int. J. Climatol. 25, 1965–1978.
Ilyashuk, E.A., Koinig, K.A., Heiri, O., Ilyashuk, B.P., Psenner, R., 2011. Holocene temperature variations at high-altitude site in Eastern Alps: a chironomid record from Schwarzsee ob Sölden, Austria. Quat. Sci. Rev. 30, 176–191.
Iversen, J., 1954. The Late-Glacial flora of Denmark and its relation to climate and soil. Danmarks Geologiske Undersøgelse II.række 80, 87–119.
Ivy-Ochs, S., 2015. Glacier variations in the European Alps at the end of the last glaciation. Cuadernos de Investigation Geografica 41, 295–315.
Ivy-Ochs, S., Schafer, G., Kubik, P.W., Synal, H.A., Schluchter, C., 2004. Timing of deglaciation on the northern Alpine foreland (Switzerland). Eclogae Geol. Helv. 97, 47–55.
Ivy-Ochs, S., Kerschner, H., Reuther, A., Maisch, M., Sailer, R., Schafer, J., Kubik, P.W., Synal, H.A., Schlücher, C., 2006. The timing of glacier advances in the Northern European Alps based on surface exposure dating with cosmogenic 10Be, 26Al, 36Cl, and 21Ne. In: Situ-Produced Cosmogenic Nuclides and Quantification of Geological Processes. Geological Society of America Special Paper, vol. 415, pp. 43–60.
Kerschner, H., Kaser, G., Sailer, R., 2000. Alpine Younger Dryas glaciers as paleo precipitation gauges. Ann. Glaciol. 31, 80–84.
Longhi, A., Monticelli, A., Guglielmin, M., 2020. Iron chemical analyses of podzols to date last pleistocene-holocene. A case study in the Italian central Alps. J. Quat. Sci. submitted for publication.
Maejima, J., Nagatsuka, S., Higashi, T., 2002. Application of the crystallinity ratio of free iron oxides for dating soils developed on the raised coral reef terraces of kikai and minami-daito islands, southwest Japan. Quat. Res. 41, 485–493.
Matthews, J.A., Owen, G., 2010. Schmidt hammer exposure-age dating: developing linear age-calibration curves using Holocene bedrock surfaces from the Jotunheimen–Jostedalsbreen regions of southern Norway. Boreas 39, 105–115.
Matthews, J.A., Shakesby, R.A., 1984. The status of the 'Little Ice Age' in southern Norway: relative-age dating of Neoglacial moraines with Schmidt hammer and lichenometry. Boreas 13, 333–346.
Matthews, J.A., Winkler, S., 2011. Schmidt-hammer exposure-age dating (SHD): application to early-Holocene moraines and a reappraisal of the reliability of terrestrial cosmogenic-nuclide dating (TCND) at Austanbotnbreen, Jotunheimen, Norway. Boreas 40, 256–270.
McCarroll, D., 1989. Potential and limitations of the Schmidt hammer for relative-age dating: field tests on Neoglacial moraines, Jotunheimen, southern Norway. Arct. Alp. Res. 21, 268–275.
McCarroll, D., 1991. The age and origin of Neoglacial moraines in Jotunheimen, southern Norway: new evidence from weathering based data. Boreas 20, 283–295.
McKeague, J.A., Day, D.H., 1966. Dithionite- and oxalate-extractable Fe and Al as aids in differentiating various classes of soils. Can. J. Soil Sci. 46 (1), 13–22.
Moran, A.P., Ivy-Ochs, S., Schuh, M., Christl, M., Kerschner, H., 2016. Evidence of central Alpine glacier advance during the Younger Dryas-early Holocene transition period. Boreas 45, 398–410.
Ortu, E., Peyron, O., Bordon, A., de Beaulieu, J.L., Siniscalco, C., Caramiello, R., 2008. Lateglacial and Holocene climate oscillations in the South-western Alps: an attempt at quantitative reconstruction. Quat. Int. 190, 71–88.
Owen, G., Matthews, J.A., Albert, P., 2007. Rates of Holocene chemical weathering, 'Little Ice Age' glacial erosion and implications for Schmidt-hammer dating at a glacier–foreland boundary, Fåbergstølsbreen, southern Norway. Holocene 17, 829–834.
Rasmussen, S.O., Bigler, M., Blockley, S.P., Blunier, T., Buchardt, S.L., Clausen, H.B., Cvijanovic, I., Dahl-Jensen, D., Johnsen, S.J., Fischer, H., Gkins, V., Guillevic, M., Hoek, W.Z., Lowe, J.J., Pedro, J.B., Popp, T., Seiestard, I.K., Steffensen, J.P., Svensson, A.M., Vallelonga, P., Vinther, B.M., Walker, M.J.C., Wheatley, J.J., Winstrup, M., 2014. A stratigraphic framework for abrupt climatic changes during the Last Glacial period based on three synchronized Greenland ice-core records: refining and extending the INTIMATE event stratigraphy. Quat. Sci. Rev. 106, 14–28.
Ravazzi, C., Aceti, A., 2004. The timberline and treeline ecocline altitude during the Holocene climatic optimum in the Italian Alps and the apennines. In: Lithopaleoenvironmental Maps of Italy during the Last Two Climatic Extremes. Explanatory Notes, a C. Antonioli F., Vai G.B., 32nd International Geological Congress, Firenze, pp. 21–22.
Rolland, Y., Darnault, R., Brauscher, R., Bourlès, D., Petit, C., Bouissou, S., Aster team, 2020. Deglaciation history at the Alpine-Mediterranean transition (Argentera-Mercantour, SW Alps) from ^{10}Be dating morains and glacially polished bedrock. Earth Surf. Process. Landforms 45, 393–410.
Schimmelpfenning, I., Schaefer, J.M., Akcar, N., Ivy-Ochs, S., Finkel, R.C., Schlucter, C., 2012. Holocene glacier culmination in the Western Alps and their hemispheric relevance. Geology 40, 891–894.
Schwertmann, U., 1964. Differenzierung der Eisenoxide des Bodens durch Extraktion mit Ammonium-Lösung. Z. Pflanzenernähr Düng Bodenk 105 (3), 194–202.
Shakesby, R.A., Matthews, J.A., Owen, G., 2006. The Schmidt hammer as a relative-age dating tool and its potential for calibrated-age dating in Holocene glaciated environments. Quat. Sci. Rev. 25, 2846–2867.
Shakesby, R.A., Matthews, J.A., Schnabel, C., 2008. Cosmogenic 10Be and 26Al ages of Holocene moraines in southern Norway II: evidence for individualistic responses of high-altitude glaciers to millennial-scale climatic fluctuations. Holocene 18, 1165–1177.
Sumner, P., Nel, W., 2002. The effect of rock moisture on Schmidt hammer rebound: tests on rock samples from Marion Island and South Africa. Earth Surf. Process. Landforms 27, 1137–1142.
Walker, M., Johnsen, S., Rasmussen, S.O., Popp, T., Steffensen, J.P., Gibbard, P., Hoek, W., Lowe, J., Andrews, J., Bjork, S., Cwynar, L.C., Hugen, K., Kershav, P., Kromer, B., Litt, T., Lowe, J.D., Nakagawa, T., Newnham, R., Schwander, J., 2009. Formal definition and dating of the GSSP (Global Stratotype Section and Point) for the base of the Holocene using the Greenland NGRIP ice core, and selected auxiliary records. J. Quat. Sci. 24, 3–17.
Walker, M.J.C., Berkelhammer, M., Björk, S., Cwynar, L.C., Fisher, D.A., Long, A.J., Lowe, J.J., Newnham, R.M., Rasmussen, S.O., Weiss, H., 2012. Formal subdivision of the Holocene series/epoch: a discussion paper by a working group INTIMATE (integration of ice-core, marine and terrestrial records) and the subcommission on quaternary stratigraphy (international commission on stratigraphy). J. Quat. Sci. 27, 649–659.
White, K., Bryant, R., Drake, N., 1998. Techniques for measuring rock weathering: application to a dated fan segment sequence in southern Tunisia. Earth Surf. Process. Landforms 23, 1031–1043.
Williams, R.B.G., Robinson, D.A., 1983. The effects of surface texture in the determination of the surface hardness of rock using the Schmidt hammer. Earth Surf. Process. Landforms 8, 289–292.
Wuthrich, L., Morabito, E.G., Zech, J., Trauerstein, M., Veit, H., Gnagi, C., Merchel, S., Scharf, A., Rugel, G., Christl, M., Zech, R., 2018. Be-10 surface exposure dating of the last deglaciation in the Aare Valley, Switzerland. Swiss J. Geosci. 111, 295–303.
Zoller, H., Athanasiadis, N., Heitz-Waniger, A., 1998. Late-glacial and Holocene vegetation and climate change at palu glacier, bernina pass, grisons canton, Switzerland. Veg. Hist. Archaeobotany 7, 241–249.

4.4. THE GLACIAL HISTORY SINCE THE LAST GLACIAL MAXIMUM IN THE FORNI VALLEY (ITALIAN CENTRAL ALPS). RECONSTRUCTION BASED ON SCHMIDT'S HAMMER R-VALUES AND CRYSTALLINITY RATIO INDICES OF SOILS.

Longhi A.[1] and Guglielmin M.[1*]

[1] Department of Theoretical and Applied Sciences, Insubria University, Varese, Italy.

4.4.1. Abstract

Knowledge about deglaciation after the Last Glacial Maximum (LGM) in the mountain areas of the European Alps is still limited. In this study, we used Schmidt Hammer R-values (SH) and Crystallinity Ratio (CRF) indices of soils, together with historical data, to outline the glacial evolution of the Forni Glacier the biggest Italian glacier until some years ago, from the LGM to the present. The study area is in the Italian Central Alps, which has a well-known history after the LIA but many gaps before. By comparing results from the Forni Glacier and nearby Gavia Pass, we found that weathering rates may differ for the same lithology; therefore, SH requires a local calibration curve. A total of 6 different glacial phases were found in the study area before the LIA: 15ka (I phase), 12.2ka (II phase), 9.5ka (III phase), 4.1ka (IV phase), 3.2ka (V phase), and 1.5ka (VI phase). Comparisons with the Gavia Pass area and with a similar glacier on the northern side of the Alps (Triftjegletscher) indicate that catchment morphology was more important than proximity for controlling Holocene glacial evolution. It was possible to identify the maximum of the LIA expansion in 1810 AD.

Keywords: Glacial evolution, Schmidt Hammer, Crystallinity Ratio Index, Late Pleistocene, Holocene, Central Italian Alps

4.4.2. Introduction

The last glacial maximum (LGM) is set in the European Alps to be spanning from 26.5 to 20 ka (Clark et al., 2009) and represents the last large dominating cold period (Visnjevic et al., 2020). Between 18.1 and 16.9ka a tripartite cold period resulted in a major Alpine glacier advance (Schmidt et al., 2012) and a second shorter and less pronounced cold phase brought another glacier advance around 16.4-16ka (Schmidt et al., 2012).

During the Holocene glaciers throughout the European Alps lost large parts of their mass, following the transition from the Younger Dryas to the Early Holocene (e.g. Ivy-Ochs et al. 2009) and evidence of small-scale Holocene advances was overprinted in many Alpine glacier forefields during the Little Ice Age (Boxleitner et al., 2019).

In the Italian Alps, the last LGM culmination occurred before 17 ka in the Eastern Alps (Favilli et al., 2008), while moraine boulder exposure rates place the LGM at approximately 24 ka in the Maritime Alps (Federici et al., 2016). In the Central Italian Alps, three more recent phases have been identified at 14.6 ka, 11 ka, and 9 ka (Longhi et al., 2020). In the Gavia Pass area, which is not so far from the Forni Glacier, a total of 7 different glacial phases were identified and dated at 14.7 ka, 13.7 ka, 12.2-11.8 ka, 10.2-9.7 ka, 7.5 ka, 5.5 ka, and 1.9 ka (Longhi and Guglielmin, 2020).

The Forni Glacier was the largest Italian valley glacier until its recent shrinkage (Smiraglia, 1989). Consequently, recent fluctuations are well-documented by its moraine apparatus, with post-LIA advances evident in 1904 AD, 1926 AD, and 1981 AD. This glacier has been the subject of numerous papers addressing its energy balance (Fugazza et al., 2016; Senese et al., 2016), post -LIA dynamics (Pelfini and Santilli, 2006; Garavaglia et al., 2010), and cryoconite ecosystems (Pittino et al., 2018; Franzetti et al, 2020). Despite the great knowledge and interest dedicated to the glacier's recent history, almost nothing is known about pre-LIA events due to a significant expansion during the LIA that destroyed the evidence of smaller Holocene advances.

Cosmogenic dating techniques are not always feasible due to logistical and economic constraints, although they have received great consideration in the reconstruction of deglaciation and subsequent glacial advances (e.g., Chenet et al., 2016; Moran et al., 2016; Wuthrich et al., 2018). In this study, we apply an alternative approach suggested by Longhi and Guglielmin (2020) which utilizes soil dating (e.g., Maejima et al., 2002) and the Schmidt Hammer R-value (e.g., Matthews and Winkler, 2011). The Crystallinity Ratio of free iron oxides (hereafter abbreviated CRF) has been demonstrated to be a good indicator of age for soils developed on glacial and periglacial features (Arduino et al., 1984; Maejima et al., 2002; Longhi et al., 2020), and the Schmidt Hammer R-value has been widely used as a metric of the rock weathering. This allows estimation of the relative exposure age of bedrock surfaces (Matthews and Shakesby, 1984; McCarroll, 1989; Goudie, 2006; Shakesby et al., 2006; Owen et al., 2007; Shakesby et al., 2008; Matthews and Owen, 2010; Matthews and Winkler, 2011; Guglielmin et al., 2012; Longhi and Guglielmin, 2020).

The objectives of this study are therefore: a) to reconstruct the glacial evolution of the Forni Glacier (Italian Central Alps) after the LGM using Schmidt Hammer R-values and Crystallinity Ratio indices of soils, and b) to evaluate the effect of subsequent glacial advance on the exposure age of previously exposed roches moutonnée.

4.4.3. Study Area

The Forni Glacier is located in the Central Italian Alps, in Upper Valtellina, within Stelvio National Park (Figure 1).

The area is located in the Frodolfo Basin between 2150 m and 2700 m elevation. Tributary valleys, including the Rosole Valley, the Cedèc Valley, and the S. Giacomo Valley, feed into the main valley. The regional lithology is primarily characterized by chlorite and sericite micaschists and banded paragneiss (ERSAF, 2016). The valley bottom shows clear evidence of glacial activity in the form of striated roches moutonnée. The valley sides are mainly covered by ablation till with several moraine

ridges deposited during different glacial phases. The valley sides are also affected by gravitational processes like landslides and debris flows.

In the upper forefield area, soils mostly correspond to Leptosols (ERSAF, 2012), with very shallow A horizons over a deeper and extremely stony deposit (Pelfini et al., 2014; FAO, 2006). In contrast, the forested lower part of the Forni Valley is characterized by coniferous forest soils (ERSAF, 2012), i.e., Podzols (Duchaufour, 1983; FAO, 2006; Pelfini et al., 2014).

4.4.4. Methods

4.4.4.1. Soil Analysis

In order to select the soil profile locations, we cored the soils with a hand auger to check for the presence of podzols. For each core, the site characteristics (coordinates, elevation, aspect, slope, vegetational coverage, dominant vegetation, and stoniness) and the soil characteristics (horizon sequence, color, texture, structure, characteristics of the boundaries, and eventual cryoturbations) were described following the *Guidelines for soil description* (FAO, 2006).

Only where podzols were identified two soil profiles were dug on top of moraine ridges and classified according to the FAO classification (FAO, 2014).

Standard procedures were followed for the extraction of oxalate (Schwertmann, 1964; McKeague and Day, 1966) and dithionite (Longhi et al., 2020).

Two spoonfuls of 0.06 mm ground soil were compressed into thin pads and then analyzed with a SEM-EDX system to measure the total iron content of each sample.

The crystallinity ratio (CRF) was calculated as $\mathrm{CRF} = \frac{\mathrm{Fe_d} - \mathrm{Fe_o}}{\mathrm{Fe_{tot}}}$ (Arduino et al., 1984; Arduino et al., 1986; Maejima et al., 2002; Longhi et al., 2020).

The soil ages were calculated according to the equation from Longhi et al. (2020):

$$\text{Ages} = 3907 * \ln(\text{CRF}) + 3508.2 \qquad \text{(Eq. 1)}$$

which generates soil ages from the CRF of the B horizon. This equation is the best-fit regression between B-horizon CRF from several podzols and their corresponding ^{14}C (Longhi et al., 2020) calculated in nearby sites in the Central Italian Alps (Stelvio Pass Area, Gavia Pass Area , and Val Viola Area) and can be used also in the study area as the CRF is not dependent of the in situ iron richness. The ages were calculated from the B horizon as well as from the A horizon because of the possibility of new pedogenesis on the analyzed podzol (Maejima et al., 2002), which would generate an underestimation of the soil age.

4.4.4.2. Schmidt's Hammer Measurements

In this study, we used a Schmidt-Hammer type N with an impact pressure of 2.207 Nm, which has been used in several papers to reconstruct deglaciation or glacial evolution globally (i.e. Matthews and Winkler, 2011; Guglielmin et al., 2012; Longhi and Guglielmin, 2020).

To avoid potential errors associated with the method, several precautions were taken.

First, we limited our analyses only to micaschists: this kind of rock is difficult to be used for Schmidt's hammer measurement because of their schistosity. Our selection was imposed by the dominance of this lithology, so attention was paid to maintain the same angle between the measurement surface and the schistosity. Second, we selected large, flat, horizontal, or sub-horizontal surfaces of roches moutonnées, ideally with low roughness, to ensure a homogeneous weathering of crystals over the entire surface (Williams and Robinson, 1983; Owen et al., 2007; Longhi and Guglielmin, 2020). Third, measurements were taken in dry conditions during summer to avoid the effects of moisture on the rocks (Sumner and Nel, 2002). Fourth, we intentionally avoided lichen-covered surfaces (McCarrol, 1991). Given the homogeneity of the chosen surfaces, we made 25 readings at each of the 90 roches moutonnées (called stations). Matthews and Owen (2010) found this sample size to be statistically significant, and Longhi and Guglielmin (2020) demonstrated that this is sufficient data to derive a calibration curve. Striae orientations on roches moutonnées, along with the orientation of the roches moutonnées themselves, were also recorded in order to better reconstruct the glacial flow

directions. The stations were then clustered in 8 different geomorphologic units; each unit containing between 1 and 21 stations, depending on the size and the availability of proper roches moutonnées. The geomorphologic units were identified based on the flow directions indicated by the roches moutonnées and the striae, as well as from the geometry of the surrounding moraine ridges.

The availability of four absolute ages (Geoportale Regione Lombardia, 1981-2000; Pelfini et al., 2014) allowed us to convert the relative R values into calibrated ages and generate a regional calibration curve reported in section 4.3. The number of calibration points was limited by the presence of datable surfaces but recent studies has proposed calibration even with just two calibration points and are assumed possible (Matthews et al., 2020).

Combining the results of the CRF soil ages, the exposure ages calculated with Schmidt's Hammer R-values, and the geomorphological evidence of glaciation (i.e., the moraine ridges and the striae on the roche moutonnées), different phases of the deglaciation were reconstructed in QGIS 3.16. Recent and modern limits of the glacier were drawn from previous glacial reconstruction (Pelfini, 1992; Pelfini et al., 2014), and orthophotos (1950, 1998, 2003, 2007, 2014) provided by Geoportale Regione Lombardia.

4.4.4.3. Absolute ages for Schmidt's Hammer Calibration

Two CRF ages from soil samples, one ^{14}C age from vegetation, and one historical age were used for the calibration of SH R-values (Table 1). The oldest age corresponds to the age of the dated soil PF1 (Fig. 2 and 4), dug on a morainic ridge close to site 44 (Unit 7; Fig.4); therefore, this represents the minimal exposure age of Unit 7 because the soil may have developed some decades after glacier advance. The second age corresponds to the age of PF2 (Fig. 2 and 4), a soil pit opened on a morainic ridge close to site 39 (Unit 6, Fig. 4).In this case, the sample date represents the minimal exposure age of Unit 6. The only ^{14}C date available corresponds to the age of a Pinus cembra log (Pelfini et al., 2014) found close to site 104 (Unit 5) and dated 4117 Cal BP, representing its minimal exposure age.

Finally, the historical age was calculated from overlaying the orthophotos (1998 and 1981, provided by Geoportale Regione Lombardia); this constrains the minimal exposure age of Unit 2.

As suggested by Longhi and Guglielmin (2020), the calibration curve was calculated from the mean of the 25 R-values for all stations corresponding to an absolute age and the confidence interval was calculated by applying a linear regression between the maximum and minimum of the R-values (R±σ) and the maximum and minimum of the absolute ages (Ages calBP± σ). The result was then compared with the curve from Longhi and Guglielmin (2020) to determine eventual differences and to test which was the most accurate one to use in the reconstruction.

4.4.4.4. LIA dating

In the Forni Valley, only Unit 7 and Unit 8 have been ice-free since their first exposure (Figure 4); indeed, the LIA advance covered all the other roches moutonnée until at least 1867 AD (Pelfini et al., 2014). Given this assumption, it is possible to derive a calibration curve with the SH R values of Units 7 and 8:

$$Ages = -325.45*R + 24{,}133 \quad \text{(Eq. 2)}$$

Equation 3 allows us to calculate the R value that would have occurred if the sites were not re-covered by the glacier after their first exposure (Table 6).

Moreover, using the R values of Units 2 and 1, which were only recently exposed after 1981 AD and after 2014 AD, respectively, it is possible to calculate a weathering rate W according to the following equation:

$$W=(R1-R2)/(T1-T2) \quad \text{(Eq. 3)}$$

where R1 is the mean R value for Unit 1, R2 is the mean R value for Unit 2, T1 is the exposure year of Unit 1, and T2 is the exposure year of Unit 2 equal to 0.0053 R/year.

If we then divide the difference between the mean and calculated R values by this weathering rate, we can obtain the ice coverage of Unit 6, Unit 5, Unit 4, and Unit 3 (see Table 6 in discussion).

4.4.5. Results

4.4.5.1. Soil Description and Characteristics

The described soils are Podzols: PF1 is a Skeletic Podzol while PF2 is an Entic Podzol. All profiles data are listed in Table 2.

The thickness of the A+B horizons (solum, *Soil Survey Staff*, 1993) is similar in both profiles and ranges between 45cm (PF2) and 48cm (PF1). They are quite coarse (silt+ clay <5%) and acidic (pH ranges between 3.84 in PF1-A and 4.44 in PF2-Bs). The CRF content of the soil profiles ranges between 8.51 in PF1-Bs and 5.19 in PF2-Bs, corresponding to ages between 9289 (PF2) and 11,263 (PF1) cal BP based on the B-horizon calibration curves proposed by Longhi et al. (2020).

4.4.5.2. Schmidt-Hammer Measurements

A total of 90 stations were analyzed, with the results subdivided into 8 geomorphological units as shown in Table 3. The stations were chosen only on roches moutonnées and clustered in different geomorphologic units; each unit contained between 1 and 21 stations, depending on the size and the availability of proper roches moutonnées (Table 3). The geomorphologic units were identified based on the flow directions indicated by the roches moutonnées and the striae, as well as from the geometry of the surrounding moraine ridges.

Unit 1 displayed the highest R values (R = 74.43), while the lowest values were found in Unit 8 (R = 28.70±0.53). With the exception of Unit 1 (which has only 1 site), the standard deviation is low and ranges between 0.23 (Unit 2) and 1.25 (Unit 7), illustrating the homogeneity of the surfaces within the units (Figure 2).

4.4.5.3. Schmidt-Hammer Calibration

The equation derived by the calibration is

$$\text{Ages} = -318.36*R + 23{,}890, \qquad \text{(Eq. 4)}$$

which has a very high R^2 of 0.99 (Figure 3).

The curve is similar to the one obtained on the same rock type in the nearby Gavia Pass area (*Longhi and Guglielmin*, 2020). However, the erosion rate over roches moutonnées is lower for the Forni Glacier measurements. Given an SH R-value, the corresponding exposure age is higher when calculated with Equation 4.

The uncertainty associated with this curve (Table 4) ranges between ± 137 years in Unit 2 and ±189 years in Unit 7, almost uniform but slowly increasing through time. Compared with other studies (e.g., *Shakesby et al.*, 2006), the uncertainty associated with the present method is lower. Applying the curve from Longhi and Guglielmin (2020), as shown in Table 4, the uncertainty is greater and ranges between ± 9.7 years in Unit 2 and ±468 years in Unit 6.

Therefore, it is preferable to use the new site-specific calibration curve because the maximum error is lower. The ages proposed in this study will be calculated by applying Equation 4.

4.4.5.4. Units exposure age

Each unit was dated using the calibration curve, and the results are displayed in Table 5.

The most recent exposure age is 186 years cal BP in Unit 1. This unit is located at 2550 m a.s.l., close to the current glacier front. The oldest exposure age is 14,792 years Cal BP for Unit 8; the sample was from the highest lateral moraine above the Forni Hut at ~2410 m a.s.l. Only Units 1 and 2 represent historical glacial position, while the exposure ages from Units 3 to 8 indicate that they were deglaciated before the LIA.

4.4.6. Discussion

4.4.6.1. The glacial history of the Forni Glacier

A total of six different glacial phases related to the geomorphological units were found in the area and dated before the LIA: 15 ka (I phase-Unit 8), 12.2 ka (II phase-Unit 7), 9.5 ka (III phase-Unit 6), 4.1 ka (IV phase-Unit 5), 3.2 ka (V phase-Unit 4), and 1.5 ka (VI phase-Unit 3) (Figure 4-Figure 5).

The use of the Schmidt's hammer in geomorphological research as a dating tool on micashists is difficult but is already proved that, given an homogeneity between the same angle between the measurement surface and the schistosity, the results usually show R-values between 2 and 8 points lower than gneiss depending on quartz content (Goudie, 2006). Moreover, the number of calibration points surely is low but was limited by the presence of datable surfaces, and recent studies has proposed calibration even with just two calibration points (Matthews et al., 2020).

Around 15 ka (I phase), the Forni Glacier was much thicker (Unit 8), reaching a minimum thickness of ~300 m above the Forni Hut, the difference in height between the top of the moraine and the Forni Hut. The striae orientations and the morainic ridges at the confluence with the Cedec Valley suggest that the two glaciers were joined, leaving a right lateral moraine above the Forni Hut at ~2430 m a.s.l. On the opposite side of the valley, the San Giacomo Glacier was probably joined too, leaving a left lateral moraine at ~2445m a.s.l. A contemporary moraine can be found above the Forni Alp at approximately 2470 m a.s.l.

Around 12.2 ka (II phase), the glacial tongue was thinner and ended close to the Forni Hut at ~2160 m a.s.l., where the Podzol PF1 was dated (Unit 7). The presence of limestone pebbles in the right lateral moraine at 2280 m a.s.l. supports the interpretation that the Cedèc Valley Glacier was still joined in this phase. The San Giacomo Glacier was also still joined based on the morphology of left lateral moraine between 2460 and 2340 m a.s.l. and the striae orientation over roches moutonnées 33 and 117. A contemporary moraine can be found above the Forni Alp at around 2450 m a.s.l.

Phase III at 9.5 ka represents the Holocene maximum expansion. The glacier reached the valley bottom and deposited a terminal moraine at approximately 2145 m a.s.l. (Unit 6), where Podzol PF2 was dated. Orombelli and Pelfini (1985) reported the Holocene maximum expansion in the same position but dated this event to 2.6 ka using the basal level of a small peat bog dammed by the same terminal moraine; this is considerably younger than our findings. During this period, both Cedèc

Valley Glacier and San Giacomo Glacier detached from the main Forni Glacier and were never joined again.

No further glacial advances were identified before 4.1 ka (phase IV), when Forni Glacier advanced to 2178 m a.s.l and deposited Unit 5 (Figure 5). These findings confirm the glacial advance hypothesized by Pelfini et al. (2014), who found a log buried by till which was dated to 4117 cal BP. Around 3.2 ka (V phase), after a period of strong increase of summer temperature that induced glacial retreat (Ortu et al., 2008), the Forni Glacier advanced to 2190 m a.s.l (Unit 4), while the last detectable pulsation before the LIA is dated 1.5 ka (VI phase) when the glacier reached the valley bottom around 2300 m a.s.l (Unit 3) (Figure 5).

The Little Ice Age is not datable with our methods because all bedrock surfaces covered by the LIA glaciers were exposed during earlier retreats. Payer's (1867) historic iconography places the front of the glacier at 2150 m a.s.l. during the Little Ice Age (Figure 4) in 1867 AD. This is approximately the same position of the III phase 9.5 ka ago.

After the LIA (Figure 5), the glacier had two small advances: one in 1904 AD reaching 2175 m a.s.l., and a second in 1926 AD reaching 2190 m a.s.l. (Pelfini et al., 2014). The glacier then quickly retreated; in 1950 AD, the glacial tongue was already around 2300 m a.s.l. (Orthophoto from Regione Lombardia). In 1981 AD (Pelfini et al., 2014) the Forni Glacier had its "neoglacial" advance and deposited two lateral moraines that were almost joined at 2350 m a.s.l. Afterwards, the Forni Glacier began to shrink rapidly. In only 17 years, the front retreated upward to 2500 m a.s.l. in 1998 (Orthophoto from Regione Lombardia), 2505 m a.s.l. in 2003 AD, 2508 m a.s.l. in 2007 AD, 2512 m a.s.l. in 2014 AD (Pelfini et al., 2014), and finally 2520 m a.s.l. at the time of publication (Google, Maxar Technologies).

4.4.6.2. Glacier fluctuations in the Alps

To better constrain the glacial evolution of the Forni Glacier, we propose a comparison with the glacial history of the nearby Gavia Pass area (*Longhi and Guglielmin*, 2020) and with the glacial

history of the Triftjegletscher (*Kronig et al.*, 2018), a Swiss glacier with the same orientation as the Forni Glacier.

The Forni Glacier's I phase has contemporary deposits in the Gavia Valley (*Longhi and Guglielmin*, 2020). This advance in the pre-Bølling (*Steinemann et al.*, 2020) may be related to the end of the GS-2 event in the INTIMATE stratigraphy (*Rasmussen et al.*, 2014) at the end of the Oldest Dryas division (Iversen, 1954).

The II phase was also identified in the Gavia Valley (Longhi and Guglielmin, 2020) during the Younger Dryas in a climatic phase characterized by cold, dry conditions in most of the Alps (*Kerschner et al.*, 2000; *Walker et al.*, 2009) as documented by the pollen zone III of Youngest Dryas (*Iversen*, 1954). Triftjegletscher boulders and bedrock have been dated around 12 ka (*Kronig et al.*, 2018) and, therefore, also correspond to this phase.

During the subsequent III phase (9.7 ka), only the Gavia Pass Glacier advanced. This occurred between 10.2 ka and 9.7 ka in the Boreal and was related to a cold period after a rapid warming event recorded in Alpine lake sediment (*Heiri et al.*, 2014). Based on the distribution of R values on the roches moutonnee of Unit 6, as well as the development of Podzol PF2 on the Unit 6 terminal moraine at 2145 m a.s.l. (which was previously attributed to the LIA based on iconographic information; *Pelfini et al.*, 2014), it appears that III phase was approximately of the same extent as the LIA. If this is true, then this phase occurred in both the Gavia and Forni areas during the Holocene maximum expansion. However, the LIA advance in the Forni Valley was comparable in size to the III phase glacier, whereas the LIA advance in the nearby Gavia Valley was comparatively localized (*Longhi and Guglielmin*, 2020). Therefore, all post-III phase morainic ridges in the Forni Valley were eroded by the LIA advance, leaving the Schmidt's hammer R values and soil dating as the only methods for reconstructing the deglaciation. A similar behaviour was recorded also on the Triftjegletscher, where the LIA advance was the second-largest Holocene expansion.

The following phases are here hypothesized on the basis of the dated roches moutonnée. The IV phase has no corresponding event in either the Gavia Valley or the Triftjegletscher. The transition at about 4 ka is known for being a complex climatic change period (*Mayewski et al.*, 2004; *Magny et al.*, 2009), and it was characterized by a drying and cooling climate that may be responsible for this advance. Indeed, a well-known "4000 BP event" started approximately 4.4 ka and ended about 3.8 ka (*Perry and Hsu*, 2000; *Drysdale et al.*, 2006; *Magny et al.*, 2009; *Liu and Feng*, 2012; *Pelfini et al.*, 2014).

The V phase was contemporary to the event recorded by the till that buried the soil analyzed by Kronig et al. (2018). This indicates an advance of the Triftjegletscher Glacier sometime after 3.1 ka (*Schneebeli and Röthlisberger*, 1976) that may be related to the 2.8 ka cold event (*Swindles et al.*, 2007; *Wang et al.*, 2013).

The VI phase was the last detectable phase in the Forni Valley, and evidence of corresponding advances is present in both the Gavia Valley (*Longhi and Guglielmin*, 2020) and in Triftjegletscher (*Kronig et al.*, 2018).

The absence of IV phase and V phase in the Gavia Valley is probably related to the global circulation: during the periods winds came mostly from South (*Holzhause et al.*, 2005) and the N aspect of the Forni Glacier may have granted higher precipitation than the E and W aspect of the Mount Gavia Glacier and the Lake Bianco Glacier in the Gavia Valley.

The contrasting extent of the Holocene expansion and the LIA between the Forni Valley and the Gavia Valley is probably related to the morphology of the catchments (i.e., smaller area, steeper slopes, western-eastern aspects, and lower maximum altitudes in the latter). Despite being far from the Forni Valley, the Triftjegletscher is North/North-West facing like the Forni Glacier. The similar glacial history of the Forni and Triftjegletscher glaciers thus supports our hypothesis that catchment morphology is more important than proximity for controlling glacial evolution during the Holocene.

This finding illustrates the importance of considering catchment catchments during glacial reconstruction studies.

It was then possible to determine the age of the LIA maximum as 1810 AD. (Table 6)

After the LIA, the glacier retreated almost continuously, with some small positive fluctuations (Figure 6) in 1904 AD, 1926 AD, and 1981 AD. These are evident in the data from the Comitato Glaciologico Italiano Bulletin (1926 to 2019) and from Pelfini (1992) that deposited the morainic ridges shown in Figure 5.

It is interesting to note that roches moutonnée in Unit 6, which were covered only during the LIA, still display striations, whereas Unit 5, Unit 4, and Unit 3 have no evidence of striation. This observation could be related to the thermal characteristics of the glacier base. If the Forni Glacier was cold-based during the LIA, the older striations on the roches moutonnée would have been preserved. During the following period, the striae on the roches moutonnée in Units 5, 4, and 3 may have been erased by (1) greater volumes of water flowing under the glacier due to warmed climatic conditions and (2) reduced subglacial debris due to different flow pathways. The possibility of the cold Forni Glacier base agrees with recent findings of Francese et al., (2019) even in the current climatic conditions although at high altitude in the accumulation zone.

4.4.7. Conclusion

The calibration curve produced in this study confirms that the SH is a reasonable method of reconstructing exposure ages and glacial history during the Holocene. However, the SH calibration curve is not universal, and even proximal regions with similar lithologies may require different SH calibrations. The reconstruction error that may result from a "universal" curve is shown by comparing the results from this paper with those produced by a calibration curve from the Mt. Gavia region (Longhi and Guglielmin, 2020).

A total of 6 different glacial phases were identified and dated for the Forni area before the LIA: 15 ka (I phase), 12.2 ka (II phase), 9.5 ka (III phase), 4.1 ka (IV phase), 3.2 ka (V phase), and 1.5 ka (VI

phase). Comparing this reconstruction with results from an adjacent area of the Gavia Pass (Longhi and Guglielmin, 2020) and with the glacial history of a similar glacier located on the northern side of the Alps (the Triftjegletscher Glacier; Kronig et al., 2018) suggests that catchment morphology (i.e., area, slope, aspect and maximum altitudes) was more important than proximity in the glacial evolution during the Holocene. For exa-mple, although the Forni Glacier and Triftjegletscher Glacier are located in different sectors of the Alps, their similar catchment morphology caused the LIA expansion to be among the largest recorded during the Holocene. In contrast, the Gavia Pass and Forni Valley are separated by less than 10 km, but the LIA advance in the Gavia Pass was smaller than every other Holocene advance.

Although the LIA glacier was almost equal in extent to the 9.5 Ka phase in the Forni Valley, causing many of the roches moutonnée in the Forni Valley to be re-covered by ice during the LIA, weathering rate calibration allowed us to date the maximum of the LIA expansion to 1810 AD. Additionally, our results suggest that the glacier was cold-based during the LIA.

4.4.8. Acknowledgements

We want to thank the Parco Nazionale dello Stelvio for the logistical fieldwork support. We also want to thank Prof. Damiano Monticelli for supporting the chemical analyses of the soils. We finally want to thank PhD Rachel Bain for the English check on the paper.

4.4.9. References

Arduino E., Barberis E., Carraro F., Forno M.G., 1984. Estimating relative ages from iron-oxides/total-iron ratios of soils in the western Po Valley, Italy. Geoderma 33, 39-52.

Arduino E., Barberis E., Marsan F.A., Zanini E., Franchini M., 1986. Iron Indexes and clay minerals within profiles as indicators of soil age in Northern Italy. Geoderma 37, 45-55.

Burga C.A., Perret R., Zoller H., 2001. Swiss localities of early recognized Holocene climate oscillations: Characterization and significance. Vierteljahrsschrift der Naturforschenden Gesellschaft in Zürich, 146, 65–74.

Clark P.U., Dyke A.S., Shakun J.D., Carlson A.E., Clark J., Wohlfarth B., Mitrovica J.X., Hostetler S.W., McCabe A.M., 2009. The last glacial maximum. Science 325, 710–714.

Chenet M., Brunstein D., Jomelli V., Roussel E., Rinterknecht V., Mokadem F., Biette M., Robert V., Lèanni L., ASTER team, 2016. ^{10}Be cosmic-ray exposure dating of moraines and rock avalanches in the Upper Romanche Valley (French Alps): Evidence of two glacial advances during the Late-Glacial/Holocene Transition. Quaternary Science Reviews 148, 209-221.

Drysdale R., Zanchetta G., Hellstrom J., Maas R., Fallick A., Pickett M., Cartwright I., Piccini L., 2006. Late Holocene drought responsible for the collapse of Old World civilizations is recorded in an Italian cave flowstone. Geology 34,101–104.

Duchaufour P., 1983. Pedologie: 1. Pedogenese et classification, Paris, 59.

ERSAF, 2012. http://www.ersaf.lombardia.it.

ERSAF, 2016, Carta Geologica Foglio 024 – Bormio.

FAO, 2006. Guidelines for soil description. Food and Agriculture Organization of the United Nations, Rome, 109.

FAO, 2014. World reference base for soil resources 2014: International soil classification system for naming soils and creating legends for soil maps.

Favilli F., Egli M., Mirabella A., Sartori G., Giaccai D., 2008. High Alpine landscape evolution in Val di Sole (Trentino, Italy) during the Holocene based on charcoal, soil chemistry and mineralogy. Rothenbühler, C. Klimaveränderungen auf der Spur. Samedan, 18-37.

Federici P., Ribolini A., Spagnolo M., 2016. Glacial history of the Maritime Alps from the Last Glacial Maximum to the Little Ice Age. Geological Society, London 433, 137-159.

Francese RG, Bondesan A, Giorgi M, Picotti S, Carcione J, Salvatore MC, Nicolis F, Baroni C (2019). Geophysical signature of a World War I tunnel-like anomaly in the Forni Glacier (Punta Linke, Italian Alps). Journal of Glaciology 65, 798–812. https://doi.org/10.1017/jog.2019.59

Franzetti A., Pittino F., Gandolfi I., Azzoni R.S., Diolaiuti G.A., Smiraglia C., Pelfini M., Compostella C., Turchetti B., Buzzini P., Ambrosini R., 2020. Early ecological succession patterns of bacterial, fungal and plant communities along a chronosequence in a recently deglaciated area of Italian Alps. FEMS Microbiology Ecology 96, fiaa165.

Fugazza D., Senese A., Azzoni R.S., Maugeri M., Diolaiuti G.A., 2016. Spatial distribution of surface albedo at the Forni Glacier (Stelvio National Park, Central Italian Alps). Cold Region Science and Technology 125, 128-137.

Garavaglia V., Pelfini M., Bollati I.M., 2010. The influence of climate change on glacier geomorphosites: The case of two Italian glaciers (Miage Glacier, Forni Glacier)investigated through dendrochronology. Géomorphologie relief processus environnement 2, 153-164.

Goudie A., 2006. The Schmidt hammer in geomorphological research. Progress in Physical Geography 30, 703-718.

Guglielmin M., Worland M.R., Convey P., Cannone N., 2012. Schmidt Hammer studies in the maritime Antarctic: Application to dating Holocene deglaciation and estimating the effects of macrolichens on rock weathering. Geomorphology 155-156, 34-44.

Heiri O., Koinig K.A., Spotl C., Berret S., Brauer A., Drescher-Schneider R., Gaar D., Ivy-Ochs S., Kershner H., Leutscher M., Moran A., Nicolussi K., Preusser F., Schmidt R., Schoeneich P.,

Schworer C., Sprafke T., Terhost B., Tinner W., 2014. Paleoclimate records 60-8ka in the Austrian and Swiss Alps and their forelands. Quaternary Science Review 106, 186-205.

Holzhauser H., Magny M., Zumbül H. J., 2005. Glacier and lake-level variations in west-central Europe over the last 3500 years. The Holocene 15, 789-801.

Iversen J., 1954. The Late-Glacial flora of Denmark and its relation to climate and soil. Danmarks Geologiske Undersøgelse II.række 80, 87-119.

Kerschner H., Kaser G., Sailer R., 2000. Alpine Younger Dryas glaciers as paleo precipitation gauges. Annals of Glaciology 31, 80-84.

Kronig O., Ivy-Ochs S., Hajdas I., Christl M., Wirsig C., Schlüchter C., 2018. Holocene evolution of the Triftje- and the Oberseegletscher (Swiss Alps) constrained with ^{10}Be exposure and radiocarbon dating. Swiss Journal of Geoscience 111, 117-131.

Liu F., Feng Z., 2012. A dramatic climatic transition at *4000 cal. year BP and its cultural responses in Chinese cultural domains. The Holocene 22(10), 1181–1197.

Longhi A., Guglielmin M., 2020. Reconstruction of the glacial history after the Last Glacial Maximum in the Italian Central Alps using Schmidt's hammer R-values and crystallinity ratio indices of soils. Quaternary International, in press.

Longhi A., Monticelli D., Guglielmin M., 2020. The use of iron chemical analysis of Podzols to date the Late Pleistocene-Holocene deglaciation history of the Central Italian Alps. Journal of Quaternary Science, in press.

Maejima J., Nagatsuka S., Higashi T., 2002. Application of the Crystallinity Ratio of Free Iron Oxides for Dating Soils Developed on the Raised Coral Reef Terraces of Kikai and Minami-Daito Islands, Southwest Japan. The Quaternary Research 41, 485-493.

Magny M., Vannie`re B., Zanchetta G., Fouache E., Touchais G., Petrika L., Coussot C., Walter-Simonnet A.V., Arnaud F., 2009. Possible complexity of the climatic event around 4300–3800 cal. BP in the central and western Mediterranean. Holocene 19, 823–833.

Matthews J.A., Mcewen L.J., Owen G., Los S., 2020. Holocene alluvial fan evolution,Schmidt-hammer exposure-age dating and paraglacial debris floods in the SE Jostedalsbreen region, southern Norway. Boreas 49, 886-904.

Matthews J.A., Owen G., 2010. Schmidt hammer exposure-age dating: developing linear age-calibration curves using Holocene bedrock surfaces from the Jotunheimen–Jostedalsbreen regions of southern Norway. Boreas 39, 105-115.

Matthews J.A., Shakesby R.A., 1984. The status of the 'Little Ice Age' in southern Norway: relative-age dating of Neoglacial moraines with Schmidt hammer and lichenometry. Boreas 13, 333-346.

Matthews J.A., Winkler S., 2011. Schmidt-hammer exposure-age dating (SHD): application to early-Holocene moraines and a reappraisal of the reliability of terrestrial cosmogenic-nuclide dating (TCND) at Austanbotnbreen, Jotunheimen, Norway. Boreas 40, 256-270.

Mayewski P.A., Rohling E.E., Stager J.C., Karlen W., Maasch K.A., Meeker L.D., Meyerson E.A., Gasse F., van Krevel S., Holmgren K., Lee-Thorp J., Rosqvist G., Rack F., Staubwasser M., Schneider R.R., Steig E.J., 2004. Holocene climate variability. Quaternary Research 62,243–255.

McCarroll D., 1989. Potential and limitations of the Schmidt hammer for relative-age dating: Field tests on Neoglacial moraines, Jotunheimen, southern Norway. Arctic and Alpine Research 21, 268-275.

McCarroll D., 1991. The age and origin of Neoglacial moraines in Jotunheimen, southern Norway: new evidence from weathering based data. Boreas 20, 283-295.

McKeague J.A., Day D.H. 1966. Dithionite- and Oxalate-Extractable Fe and Al as Aids in Differentiating Various Classes of Soils. Canadian Journal of Soil Science 46(1), 13-22.

Moran A.P., Ivy-Ochs S., Schuh M., Christl M., Kerschner H., 2016. Evidence of central Alpine glacier advance during the Younger Dryas-early Holocene transition period. Boreas 45, 398-410.

Orombelli G., Pelfini M., 1985. Una fase di avanzata glaciale nell'Olocene superiore, precedente alla Piccola Glaciazione, nelle Alpi Centrali. Rendiconti della Società Geologica Italiana 8, 17–20.

Ortu E., Peyron O., Bordon A., de Beaulieu J.L., Siniscalco C., Caramiello R., 2008. Lateglacial and Holocene climate oscillations in the South-western Alps: an attempt at quantitative reconstruction. Quaternary International 190, 71-88.

Owen G., Matthews J.A., Albert P., 2007. Rates of Holocene chemical weathering, 'Little Ice Age' glacial erosion and implications for Schmidt-hammer dating at a glacier–foreland boundary, Fåbergstølsbreen, southern Norway. The Holocene 17, 829-834.

Payer J., 1867. Die Centralen Ortler-Alpen (Sulden-Gebiet und Monte Cevedale), Peterm. Georg. Mitteil., Ergänzungshelft 18, 1-15, 1 ff., 1 carta topgrafica 1:48000, Gotha.

Pelfini M., 1992. Le fluttuazioni glaciali oloceniche nel Gruppo Ortles-Cevedale (settore lombardo). Universita` degli Studi di Milano. Earth Science Department, PhD thesis IV cycle.

Pelfini M., Santilli M., 2006. Dendrogeomorphological analyses on exposed roots along two mountain hiking trails in the Central Italian Alps. Geografiska Annaler Series A Physical Geography 88(3), 223 – 236.

Pelfini M., Leonelli G., Trombino L., Zerboni A., Bollati I., Merlini A., Smiraglia C., Diolaiuti G., 2014. Rendiconti Lincei 25, 427-437.

Perry C.A., Hsu K.J., 2000. Geophysical, archaeological, and historical evidence support a solar-output model for climate change. PNAS 97(23),12433–12438.

Pittino F., Maglio M., Gandolfi I., Azzoni R.S., Diolaiuti G.A., Ambrosini R., Franzetti A., 2018. Bacterial communities of cryoconite holes of a temperate alpine glacier show both seasonal trends and year-to-year variability. Annals of Glaciology 59, 1-9.

Rasmussen S.O., Bigler M., Blockley S.P., Blunier T., Buchardt S.L., Clausen H.B., Cvijanovic I., Dahl-Jensen D., Johnsen S.J., Fischer H., Gkins V., Guillevic M., Hoek W.Z., Lowe J.J., Pedro J.B., Popp T., Seiestard I.K., Steffensen J.P., Svensson A.M., Vallelonga P., Vinther B.M., Walker M.J.C., Wheatley J.J., Winstrup M., 2014. A stratigraphic framework for abrupt climatic changes

during the Last Glacial period based on three synchronized Greenland ice-core records: refining and extending the INTIMATE event stratigraphy. Quaternary Science Review 106, 14-28.

Schmidt R., Weckström K., Lauterbach S., Tessadri R., Huber K., 2012. North Atlantic climate impact on early late-glacial climate oscillations in the south-eastern Alps inferred from a multi-proxy lake sediment record. Journal of Quaternary Science 27, 40-50.

Schneebeli W., Röthlisberger F., 1976. 8000 Jahre Walliser Gletschergeschichte ein Beitrag zur Erforschung des Klimaverlaufs in der Nacheiszeit. Ph.D. dissertation, University of Zürich, Verlag Schweizer Alpen-Club, Bern, Switzerland.

Schwertmann U., 1964. Differenzierung der Eisenoxide des Bodens durch Extraktion mit Ammonium-Lösung. Z. Pflanzenernähr Düng Bodenk 105(3), 194-202.

Senese A., Maugeri M., Ferrari S., Confortola G., Soncini A., Bocchiola D., Diolaiuti G.A., 2016. Modelling shortwave and longwave downward radiation an air temperature driving ablation at the Forni glacier (Stelvio National Park, Italy). Geografia Fisica e Dinamica Quaternaria 39, 89-100.

Shakesby R.A., Matthews J.A., Owen G., 2006. The Schmidt hammer as a relative-age dating tool and its potential for calibrated-age dating in Holocene glaciated environments. Quaternary Science Reviews 25, 2846-2867.

Shakesby R.A., Matthews J.A., Schnabel C., 2008. Cosmogenic 10Be and 26Al ages of Holocene moraines in southern Norway II: evidence for individualistic responses of high-altitude glaciers to millennial-scale climatic fluctuations. The Holocene 18, 1165-1177.

Smiraglia C., 1989. The Medial Morain of Ghiacciaio dei Forni, Valtellina, Italy: Morphology and Sedimentology. Journal of Glaciology 35, 81-84.

Soil Survey Staff, 1993. Soil Survey Manual, United States Department of Agriculture Handbook No. 18.

Steinemann O., Reitner J.M., Ivy-Ochs S., Christl M., Synal H.A., 2020. Tracking rockglacier evolution in the Eastern Alps from the Lateglacial to the early Holocene. Quaternary Science Reviews 241, 106424.

Sumner P., Nel W., 2002. The effect of rock moisture on Schmidt hammer rebound: tests on rock samples from Marion Island and South Africa. Earth Surface Processes and Landforms 27, 1137-1142.

Swindles G. T., Plunkett G., Roe H. M., 2007. A delayed climatic response to solar forcing at 2800 cal. BP: multiproxy evidence from three Irish peatlands. The Holocene 17, 177–182.

Višnjevic V., Herman F., Prasicek G., 2020. Climatic patterns over the European Alps during the LGM derived from inversion of the paleo-ice extent. Earth and Planetary Science 538, 116185.

Walker M., Johnsen S., Rasmussen S.O.., Popp T., Steffensen J.P., Gibbard P., Hoek W., Lowe J., Andrews J., Bjork S., Cwynar L.C., Hugen K., Kershav P., Kromer B., Litt T., Lowe J.D., Nakagawa T., Newnham R., Schwander J., 2009. Formal definition and dating of the GSSP (Global Stratotype Section and Point) for the base of the Holocene using the Greenland NGRIP ice core, and selected auxiliary records. Journal of Quaternary Science 24, 3-17.

Wang S., Ge Q., Wang F., Wen X., Huang J., 2013. Abrupt climate changes of Holocene. Chinese Geographical Science 23, 1–12.

Williams R.B.G., Robinson D.A., 1983. The effects of surface texture in the determination of the surface hardness of rock using the Schmidt hammer. Earth Surface Processes and Landforms 8, 289-292.

Wuthrich L., Morabito E.G., Zech J., Trauerstein M., Veit H., Gnagi C., Merchel S., Scharf A., Rugel G., Christl M., Zech R., 2018. Be-10 surface exposure dating of the last deglaciation in the Aare Valley, Switzerland. Swiss Journal of Geosciences 111, 295-303.

Zoller H., Schindler C. M., Röthlisberger H. (1966). Postglaziale Gletscherstände und Klimaschwankungen im Gotthardmassiv und Vorderrheingebiet. Verhandlungen der Naturforschungs Gesellschaft Basel 77, 97–164.

4.4.10. Pictures and Tables

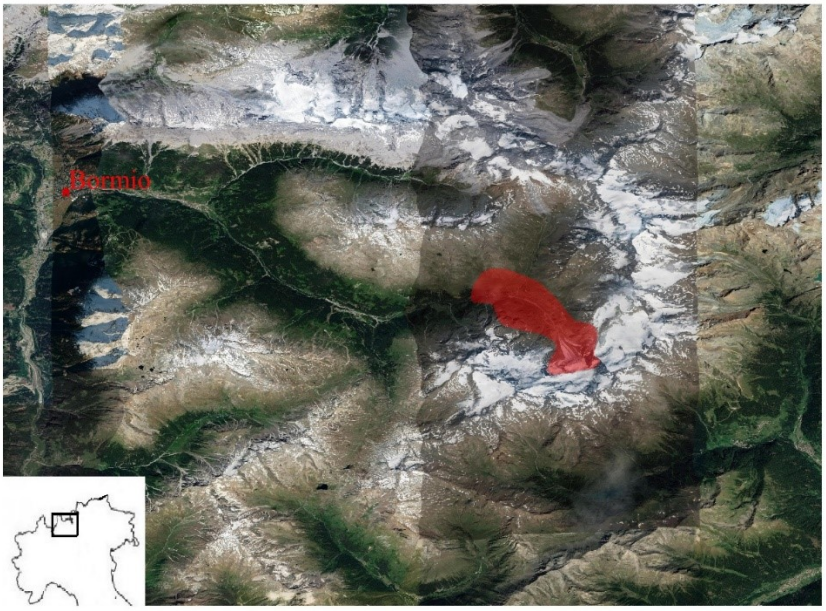

Figure 1: Reference map of site location (map data: Google, Maxar Technologies).

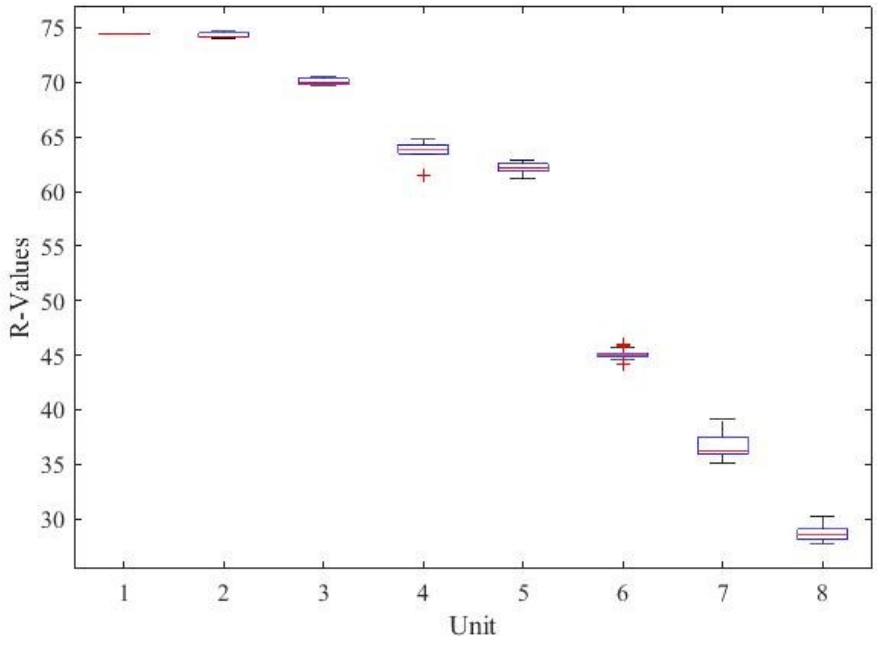

Figure 2: Box and whisker plots with R mean values; red line indicates the mean value for each geomorphological unit.

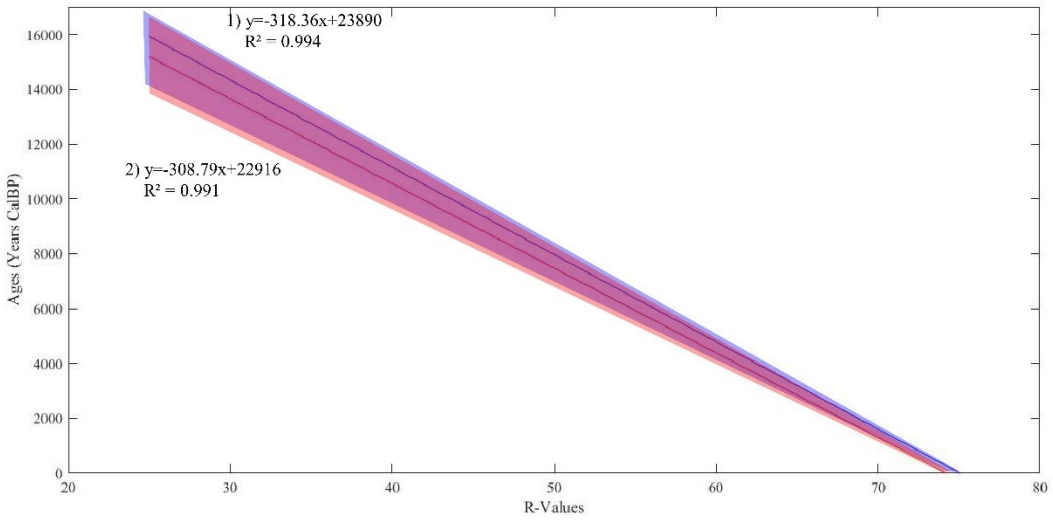

Figure 3: Calibration curve achieved with R mean values (1, blue) and calibration curve from Longhi and Guglielmin (2, red) with relative confidence intervals.

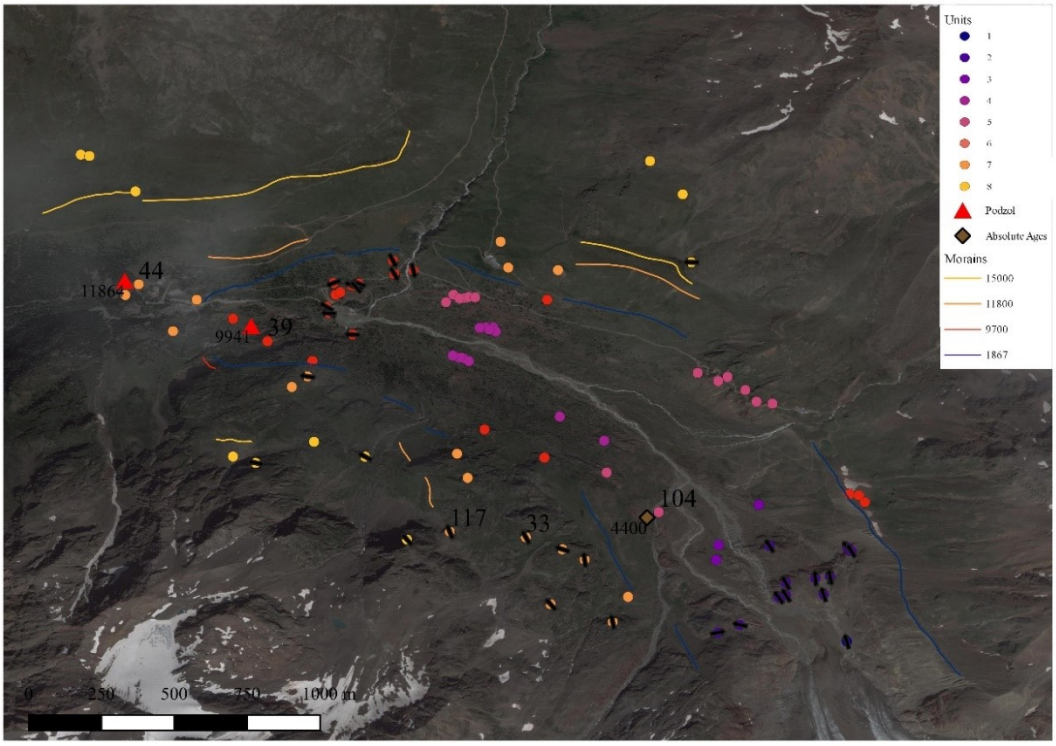

Figure 4: Main glacial features (morainic ridges) of the older three glacial phases and, for comparison, the maximum extent in 1867AD of the Forni Glacier. Colored dots correspond to the different stations where Schmidt Hammer was used, grouped into 8 different units based on their ages. Red triangles are the sites of the dated podzols, and the maroon rhombus is the site of the ^{14}C dated log (Pelfini et al., 2014). Black arrows indicated the orientations of the examined striae.

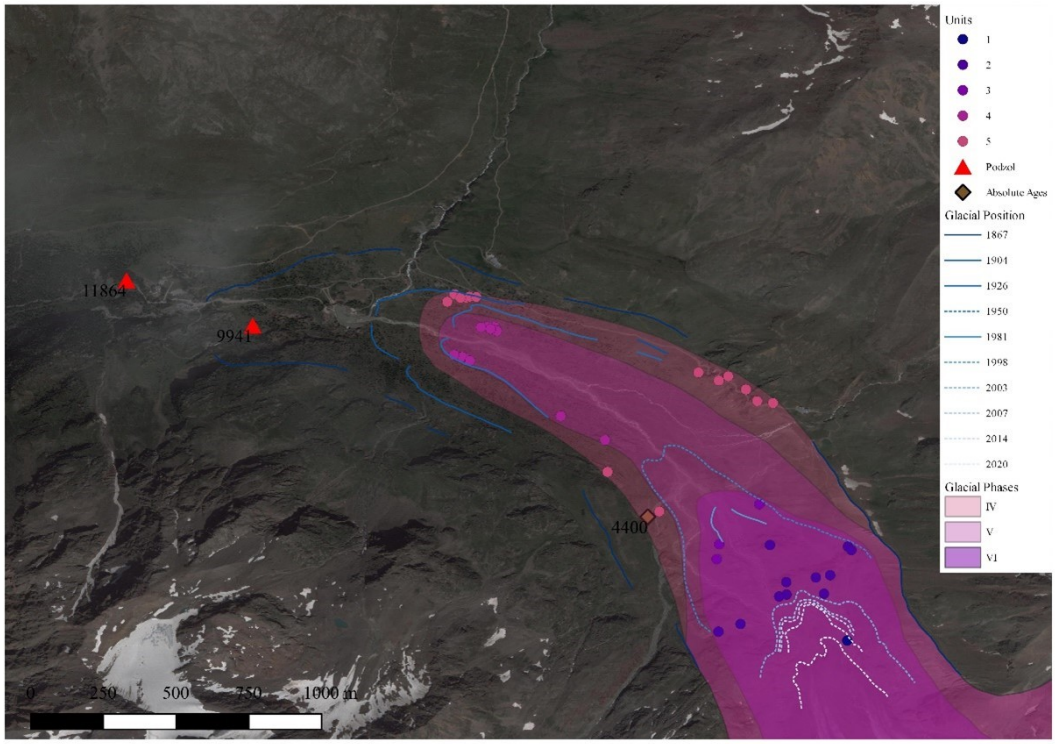

Figure 5: Late Holocene glacial reconstruction of the Forni Glacier. The different violet tones indicate the reconstruction of the IV, V and VI phases based on the Schmidt Hammer values, while the different blue lines indicate the historical reconstruction including the glacial moraines corresponding to the LIA (1867), 1904 AD, 1926 AD and 1981 AD. For the rest of the legend, see Fig. 4.

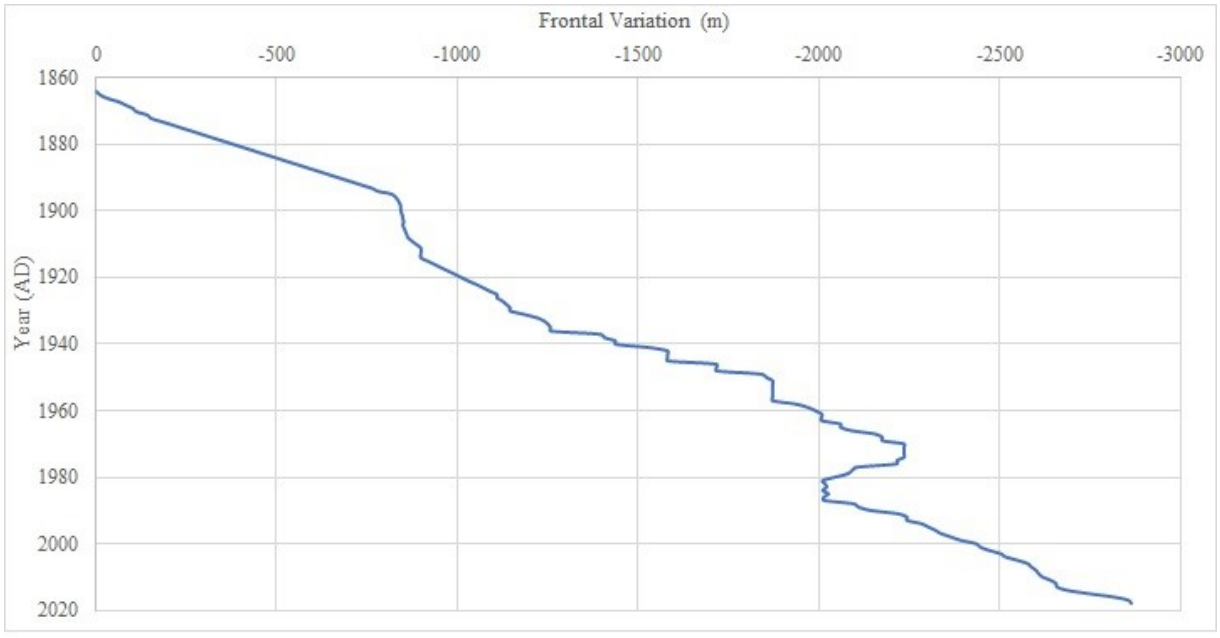

Figure 6: Cumulative frontal glacier variation (Comitato Glaciologico Italiano, 1926 to 2019; Pelfini, 1992) between 1864 and 2019.

Type	Age	Relative Unit
CRF age	11,263	Unit 7
CRF age	9289	Unit 6
^{14}C age	5117 Cal BP	Unit 5
Historical age	1990 AD	Unit 2

Table 1: data used for the calibration, type of data, and relative geomorphological unit.

Profile Id	Horizon	Skeleton	Sands	Silt+Clay	Water Content	pH	LOI	CRF	Ages
PG1	A	34.47	62.94	2.59	26.74	3.84	8.18	N.A.	N.A.
	Bs	40.26	58.88	0.86	15.73	4.18	6.24	8.51	11,263
PG2	A	21.09	76.81	2.1	23.84	4.02	12.89	N.A.	N.A.
	Bs	39.45	55.63	4.92	16.18	4.44	8.11	5.19	9289

Table 2: Soil characteristics. The grain size classes (skeleton, sands, silt+clay), the water content, and the LOI are in % while the pH is in pH unit, CRF is a pure number, and Ages are expressed as years Cal BP. N.A=not analyzed.

Unit ID	Number of stations	R Mean Value	Σ
1	1	74.43	-
2	11	74.28	0.23
3	3	70.07	0.37
4	12	64.98	0.84
5	14	62.12	0.53
6	21	45.05	0.45
7	18	36.65	1.25
8	10	28.70	0.53

Table 3: R mean values with their standard deviations in each geomorphological unit and the number of stations for each unit.

Unit ID	Absolute Age	Overall Error	Error Longhi and Guglielmin (2020)
2	1990 AD	± 137	± 9.5
5	4400	± 141	± 333
6	9941	± 185	± 468
7	11874	± 189	± 137

Table 4: Error associated (years Cal BP) with calibration curve and with calibration curve from Longhi and Guglielmin (2020). Ages are expressed as the mean in years Cal BP.

Unit	R Mean Value	Ages (Years Cal BP)
1	74.43	186
2	74.28	234
3	70.07	1580
4	64.98	3203
5	62.12	4118
6	45.05	9571
7	36.65	12253
8	28.70	14792

Table 5: Geomorphological units, relative R mean values, and calculated exposure ages.

Unit ID	R Mean Value	Calculated R-Value	Calculated Coverage Time	Historical Exposure Age
8	28.70	-	-	-
7	36.50	-	-	-
6	45.05	44.74	57	1867-1904
5	62.12	61.50	116	1904-1926
4	64.98	64.31	126	1926-1950
3	70.07	69.30	144	1950-1981
2	74.28	-	-	1981-1998
1	74.43	-	-	2014-2020

Table 6: Geomorphological units, relative R mean values, calculated R-values, calculated coverage time (years), and historical exposure ages (AD).

4.5.LAKES SEDIMENT ANALYSIS

TBG1 and TBS1 were cored and analyzed to reconstruct environmental and climatic conditions in comparison to the glacial reconstruction. TBG1 was drilled in the deepest point (46.34N, 10.49E, 2657m a.s.l.) of a pond damned by the morainic ridge containing soil profile PG2, in the Gavia Pass area, and its base was dated at 8010-7029 cal. BP (Fig. 18a).

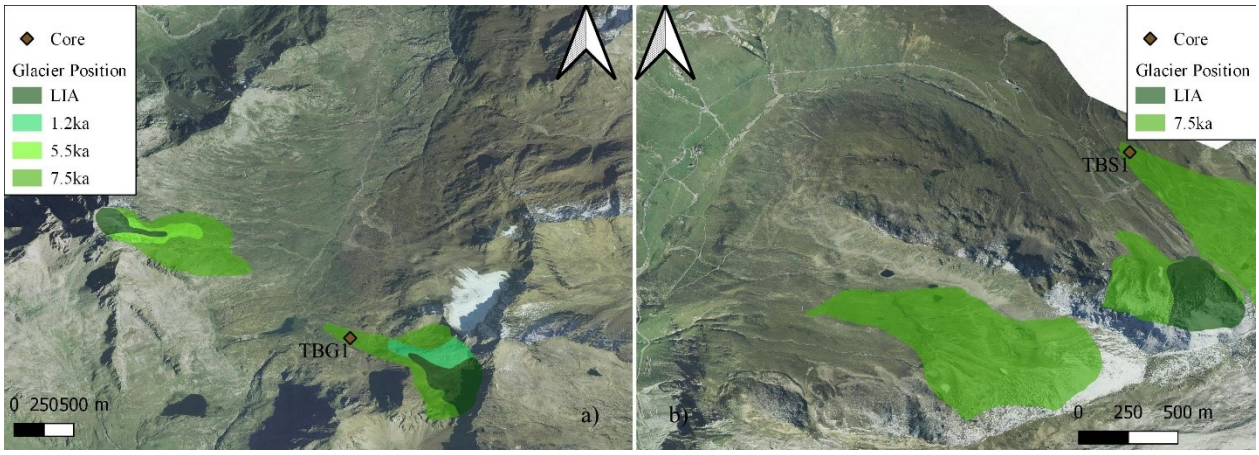

Figure 18: Location of the cores in the Gavia Pass area (a) and in the Stelvio Pass area (b) with glacial position following the cores basal age.

TBS1 was drilled in the deepest point (46.54N, 10.44E, 2565m a.s.l.) of a pond within a depression among some roches moutonées (TBS1) in proximity to profile PS1, in the Stelvio Pass area, and its base was dated at 7271-7125 cal. BP (Fig. 18b).

TBG1 can be divided into 10 stratigraphic units based on particle size distribution (Fig. 19a) and color:

- 164cm-154cm: this basal section is characterized by laminated clays, index of really low current in the basin. The sample TBG1-V was taken for sand mineralogical composition analysis;

- 154cm-151cm: this unit is composed by a paleosoil, indicating that there wasn't sedimentation during this phase but the condition allowed sedimentation. The sample TBG1-U was taken for sand mineralogical composition analysis;
- 151cm-150cm: this small unit indicates a return to low current sedimentation in the basin as it's characterized by laminated clays. The sample TBG1-T was taken for sand mineralogical composition analysis;
- 149cm-150cm: another small paleosoil is present in this section, suggesting another phase of not sedimentation. The sample TBG1-S was taken for sand mineralogical composition analysis;
- 146cm-149cm: this section represents the younger low current sedimentation that left laminated clays in the core. The sample TBG1-R was taken for sand mineralogical composition analysis;
- 134cm-146cm: in this section, the sedimentation is representative of a still low current but higher than before, as the sediment is classified as a silty loam. The sample TBG1-Q was taken for sand mineralogical composition analysis;
- 97.5cm-134cm: in this unit, the sedimentation is representative of a faster current as testified by the loamy sand classification. Three samples (TBG1-N, TBG1-O, and TBG1-P) were taken for sand mineralogical composition analysis;
- 90cm-97.5cm: also this section is classified as loamy sand but more gravel is present, probably indicating a more rainy period, maybe with some extreme event. In this section the sample TBG1-M was taken for sand mineralogical composition analysis;
- 4cm-90cm: in this section a return to the loamy sand is evident. In this section nine different samples (TBG1-B, TBG1-C, TBG1-D, TBG1-E, TBG1-F, TBG1-G, TBG1-H, TBG1-I, and TBG1-L) were taken for sand mineralogical composition analysis;

- 0cm-4cm: this unit represents the real turf of the whole core, its particle size distribution allows to classify it as sand representing the fastest water current phase in the core. In this section the sample TBG1-A was taken for sand mineralogical composition analysis;

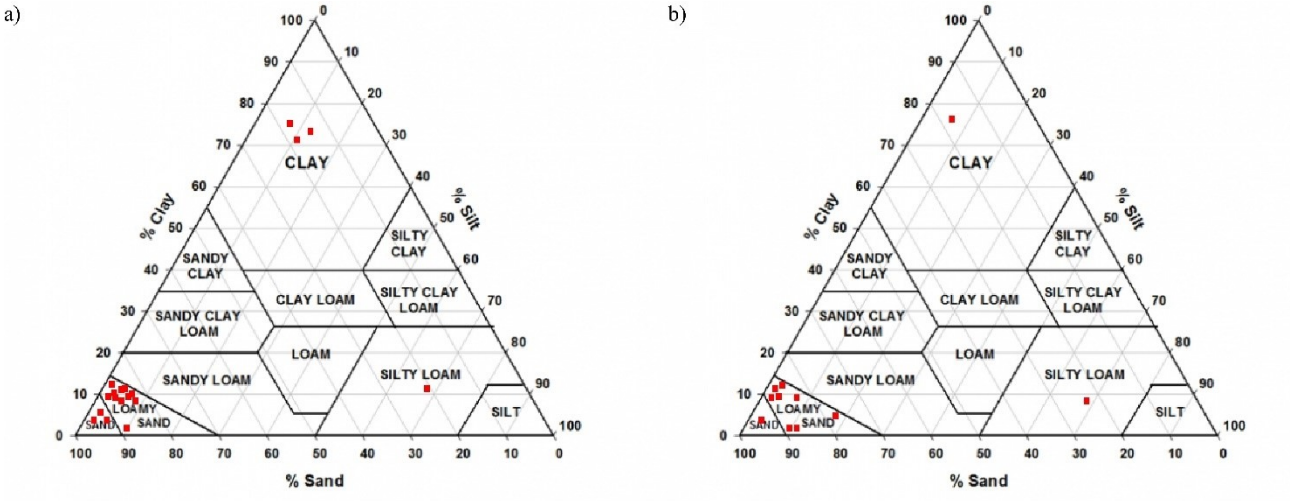

Figure 19: Particle Size Distribution of sample taken for sand mineralogical composition analysis in TBG1 (a) and TBS1 (b).

TBS1 can be divided into 10 stratigraphic units based on particle size distribution (Fig. 19b) and color:

- 106cm-99cm: this section is dominated by laminated clays that are an index of low current sedimentation. The sample TBS1-M was taken for sand mineralogical composition analysis;
- 99cm-94cm: this unit is characterized by loamy sands with a lot of gravel, indicating an extreme rainy event. The sample TBS1-L was taken for sand mineralogical composition analysis;
- 94cm-82cm: here a low current sedimentation is represented by the silty loam classification, but the current was higher than in the first section. The sample TBS1-I was taken for sand mineralogical composition analysis;

- 61cm-82cm: the current increased again in this section as the silt fraction decreases in favor of the sand one. Two samples (TBS1-G, and TBS1-H) were taken for sand mineralogical composition analysis;
- 57cm-61cm: this section is classified as loamy sands but the high presence of gravel suggests an extreme rainy event. The sample TBS1-F was taken for sand mineralogical composition analysis;
- 19cm-57cm: in this section a return to the loamy sand is evident. In this section four different samples (TBS1-B, TBS1-C, TBS1-D, and TBS1-E) were taken for sand mineralogical composition analysis;
- 0cm-19cm: this unit represents the real turf of the whole core, its particle size distribution allows to classify it as sand representing the fastest water current phase in the core. In this section the sample TBS1-A was taken for sand mineralogical composition analysis;

The difference in depth of the two cores suggests a faster mean sedimentation rate in the TBG1 of about 32% more than in TBS1, given almost the same start of sedimentation age.

Besides the turf unit, an upper loamy sand section characteristic of a quite fast current sedimentation interspersed by an extreme event is common in the two cores. Even an underlying silty loam unit seems to be common in both the cores but, while in TBS1 it is overlying an extreme rainy event and a lacustrine clay sedimentation, in TBG1 the situation is more complex. Under the silty loam unit in TBG1, it is represented an alternation between lacustrine sedimentation and pedogenesis that allowed the formation of the paleosoils.

In TBG1 (Fig. 19a) the trend of the LOI and of macroremains can be described by subdividing the core into 7 different sections:

- 164cm-154cm: starting with really low LOI values (9.52%), the trend is increasing and reaching a maximum of 21.29%, evidencing a period of climatic improvement that could have

enhanced the possibility for living beings to increase. Almost no macroremains are found in this section;

- 154cm-130cm: after a small drop that brought the LOI to be close to the beginning of the previous sector (11.06%), the trend starts to increase again to reach a maximum of 33.33% at the end of the section. Macroremains have been found here, especially of Larix decidua, Pinus mugo, and some not identifiable woods;
- 130cm-104cm: in this section, the LOI is pretty stable and the values range from a maximum of 36.30 at 109cm to a minimum of 28.26 at 125cm, indicating a period with no significant variations. Macroremains are at their maximum expression both in diversity and in number, Larix decidua and Pinus mugo disappear, replaced by Juniperus nana and Kalmia sp.;
- 104cm-87cm: the LOI drastically falls from 32.76% to 10.98% in this section, evidencing a worsening of the climatic condition that could make living conditions difficult as the lowering in the number of macroremains supports;
- 87cm-69cm: here the LOI values are stable and indicate a difficult period for life probably due to bad climatic conditions, and the number of macroremains keeps lowering;
- 69cm-34cm: from the low values of the previous section (11.37%), the LOI trend starts to increase and reach a relative maximum of 30.45%, the number of macroremains remains almost the same but Carex sp. increases;
- 34cm-0cm: after a drop to 16.32% in a few centimeters, the LOI starts to increase and from 19cm to the top it remains stable around values of 20%.

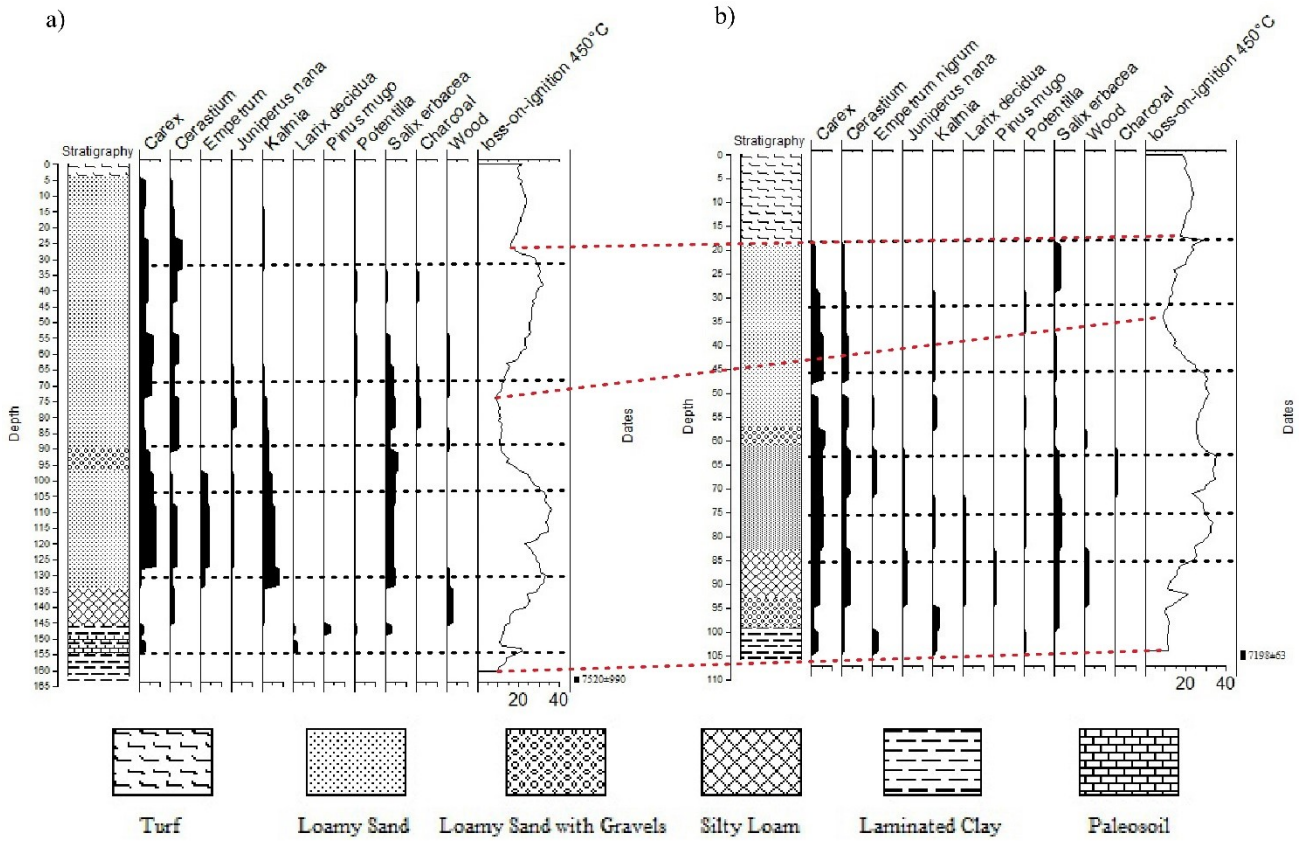

Figure 20: Stratigraphy, macroremains (expressed as number of each species), and LOI (expressed in %) in TBG1 (a) and TBS1 (b).

Even if TBS1 is a shorter core (Fig. 19a), the trend of LOI and macroremains can be described by subdividing the core into 7 sections too:

- 106cm-85cm: from a beginning of really low LOI (9.14%) the trends starts to increase reaching a maximum of 33.64% suggesting a climatic improvement during this period; macroremains number increase too from the bottom to the top of this section and are mostly represented by Pinus mugo, Larix decidua, and Juniperus nana;
- 85cm-76cm: after a small drop, the trend starts to increase again to reach a maximum of 34.28% at the end of the section, just a little higher than in the previous section; the number of macroremains increases a little, Larix decidua are mostly represented in this unit, and the presence of Salix erbacea and of Carex sp. increases;

- 76cm-63cm: the trend of increasing LOI continues in this section but with a slower rate, reaching a maximum of 35.37%; the number of macroremains is stable and no significant variation in the composition can be detected;
- 63cm-45cm: in this section, the LOI is pretty stable and the values range from a maximum of 35.02% at 62cm to a minimum of 28.86 at 53cm, indicating a period with no significant variations; wood macroremains appear here;
- 45cm-32cm: here the LOI values decrease to reach a minimum of 8.98%, even lower than in the first section, indicating a worsening of the climatic condition; the total number of macroremains decreases in this section, and wood macroremains disappear;
- 32cm-19cm: the LOI reverse its trend in comparison to the previous section reaching a peak of 28.32%; the number of macroremains increases;
- 19cm-0cm: a rapid drop brought the LOI to values close to 20% and the trend remained stable from 17cm to the surface.

The section in both cores are not corresponding, but some well known events from the literature can be detected. Dating the base of both cores, it is possible to say that the sedimentation process started approximatively at the same age around 7.5-7.2ka and the LOI values indicate hard conditions for life. These conditions agree with the glacial phase that has been dated in the previous works (*Longhi et al.*, 2020; *Longhi and Guglielmin*, 2020) in both the Gavia Pass area and in the Stelvio Pass area around 7.5ka and with pollen records from high Alpine lakes (*Ortu et al.*, 2008) that support a trend of cooling summer temperatures, with a lowering of about 3°C between 7.9 and 7 ka.

The minimum between LOI values in the two cores, considering as constant the sedimentation rates, should have an age of about 3.4ka. Schimmelpfenning et al. (2012-2014) found evidence a glacial phase in the same period at the Tsidjore glacier, and Denton and Karlèn (1973) suggested a lowering in summer temperatures in Northern Hemisphere due to a decrease in insolation during the boreal summer, corroborating this finding.

The drop in LOI at 24cm in TBG1 and at 18cm in TBS1, considering as constant the sedimentation rates, should have an age of about 1.3ka. In the Gavia Pass area, a glacial phase has been reconstructed at 1.9ka in the previous work (*Longhi and Guglielmin*, 2020), and even in the close Forni Pass area, a glacial advance has been dated at 1.5ka. This glacial advance has been also identified in Triftjegletscher (*Kronig et al.*, 2018), but it was not detected in the Stelvio Pass area but it is conceivable that the expansion was smaller than the LIA, that eroded its traces. The drop in LOI maybe therefore connected to the Göschenen II cold phase (1.6-1.2ka; *Zoller et al.*, 1998). It can not be excluded that this drop may be related to the LIA: analyzing the stratigraphy, the lower section of the two cores has a different sedimentation rate than the upper one, and this may lead to an overestimation of the oldness of this drop.

The span between the bottom of the core and the minimum of LOI may be considered representative of the Holocene Thermal Optimum, characterized by higher summer temperatures than in the pre-industrial period in the medium and high latitudes of the Northern Hemisphere (*Alverson et al.*, 2003). Macroremains supports this hypothesis as their maximum is evident in this period and after the minimum of around 3.4ka, especially the wood ones, suggesting trees existence at high elevation. Charcoals have been been found both in TBG1 and TBS1. In TBG1 they have been found in two different positions: between 80cm and 65cm, and between 40cm and 35cm. The first span is in the middle of a cold phase, it is so unlikely that the charcoal was e result of a natural fire. The second span, instead, is in a period of warming and it is impossible to hypothesize, based only on the position and the climatic reconstruction, if the charcoal is the result of a natural fire or of human activity. In TBS1 charcoals were only found between 70cm and 65cm, in a position attributed to the Holocene Thermal Optimum: it is possible that high temperature and dry condition caused a natural fire, but accurate analysis on the nature of the charcoals are needed for better supporting this hypothesis.

Sample	Quarz %	Feldspar %	Micas %	Amphibolites %	Pyroxene %	Rock Fragment %	Kind of fragment
TBG1-A	83.65	4.81	3.85	0.96	0.00	6.73	gneiss
TBG1-B	86.60	8.25	2.06	0.00	0.00	3.09	gneiss
TBG1-C	88.35	5.83	4.85	0.00	0.00	0.97	gneiss
TBG1-D	91.11	5.56	1.11	0.00	0.00	2.22	gneiss
TBG1-E	81.31	5.61	8.41	1.87	0.00	2.80	gneiss
TBG1-F	86.87	4.04	2.02	3.03	0.00	4.04	gneiss
TBG1-G	84.31	4.90	3.92	3.92	0.98	1.96	gneiss
TBG1-H	87.50	7.69	0.96	0.00	0.96	2.88	gneiss
TBG1-I	85.71	4.46	3.57	2.68	0.00	3.57	gneiss
TBG1-L	89.52	1.90	2.86	3.81	0.00	1.90	gneiss
TBG1-M	86.61	3.57	4.46	4.46	0.00	0.89	gneiss
TBG1-N	81.37	9.80	7.84	0.98	0.00	0.00	-
TBG1-O	88.04	5.43	1.09	3.26	0.00	2.17	gneiss
TBG1-P	86.52	3.37	4.49	2.25	0.00	3.37	gneiss
TBG1-Q	92.94	5.88	1.18	0.00	0.00	0.00	-
TBG1-R	87.91	3.30	2.20	3.30	0.00	3.30	gneiss
TBG1-S	83.67	4.08	8.16	1.02	0.00	3.06	gneiss
TBG1-T	86.81	6.59	3.30	2.20	0.00	1.10	gneiss
TBG1-U	79.59	2.04	7.14	4.08	1.02	6.12	gneiss
TBG1-V	82.76	10.34	2.30	1.15	0.00	3.45	gneiss
TBS1-A	86.81	6.59	5.49	0.00	0.00	1.10	gneiss
TBS1-B	84.31	4.90	3.92	3.92	0.98	1.96	gneiss
TBS1-C	87.10	3.23	4.30	2.15	0.00	3.23	gneiss
TBS1-D	83.33	4.17	8.33	1.04	0.00	3.13	gneiss
TBS1-E	81.31	5.61	8.41	1.87	0.00	2.80	gneiss
TBS1-F	85.05	4.67	3.74	2.80	0.00	3.74	gneiss
TBS1-G	86.24	3.67	4.59	4.59	0.00	0.92	gneiss
TBS1-H	87.10	3.23	4.30	2.15	0.00	3.23	gneiss
TBS1-I	88.17	6.45	3.23	2.15	0.00	0.00	-
TBS1-L	92.77	6.02	1.20	0.00	0.00	0.00	-
TBS1-M	87.78	3.33	2.22	3.33	0.00	3.33	gneiss

Table 2: Mineral composition of cores units.

All units are mainly composed by quartz minerals and the lithic fragments are all composed by gneiss. This may suggest that the glacier flow direction didn't change as the lithology is present in the catchment in both areas. This may be true for TBG1, but a more complex analysis is required on TBS1. As previously demonstrated (Longhi et al., 2020), the Stelvio Pass the Vedretta Piana-Platigliole glacier flew into TBS1 catchment at least until 7.5ka bringing carbonates in a catchment

where they are absent, but no more traces are left in the area. The lower part of TBS1 has got a less acid pH than the overlaying unit, with a change at 98cm that, assuming as constant the sedimentation rate, should have an age of 6.5ka. The change in pH is almost consistent with a change in particle size distribution representative of an extreme event and may mark the end of the transfluence. The absence of carbonate rock fragments is not unexpected, as they dissolve in water and have not reached the bottom in sedimentation, but may have lowered the pH.

5. CONCLUSION

In this thesis, it has been demonstrated how a multidisciplinary approach is needed to understand glacial processes involved in response to past climate change in different and close locations.

The data demonstrated the suitability of the CRF method for dating soils and its potential for use in reconstructing glacial phase boundaries from podzols at high elevations. The CRF calculated on both the A and Bs horizons had a good relationship with absolute age, and the trends were consistent with the results of previous studies (Arduino et al., 1984; Arduino et al., 1986; Maejima et al., 2002) but morphological or pedogenetic processes in the A horizon may lead to errors in calculated age: it was therefore preferable to use equation (2), which was calibrated for the Bs horizon, to date the soils.

The podzol development was very different in the three study areas, despite their similar elevations, suggesting asynchronous glacial advances after the LGM in Stelvio Pass Area, Gavia Pass Area, and Viola Pass Area.

The calibration curve produced in the Gavia Pass Area suggested that the SH is a reasonable method of reconstructing exposure ages and glacial history. However, the SH calibration curve is not universal, as shown by a comparison of calibration curves for similar lithologies in Norway and the Mt. Gavia region; the local variation in calibration parameters may be due to site-specific temperature and precipitation. The best calibration curve is calculated on the R25 calculated on all the sites of every geomorphological unit. The results support the use of SH as an efficient method for dating glacially-polished bedrock of Late Pleistocene age until 15 ka in the Mt. Gavia region even if the SH method generally underestimated the ages when compared to the CRF index of soils and the available ^{14}C dates. This is reasonable because the bedrock samples were covered by the glaciers more recently than the soils, which developed on the surrounding lateral or frontal moraine ridges.

Combining all methods, eleven successive glacial events have been identified and dated before the LIA: 16.7-14.7 ka, 13.7 ka, 12.3-11.8 ka, 11 ka, 10.2-9.5 ka, 9 ka, 7.5ka, 5.5 ka, 4.1 ka, 3.2 ka, and 1.9-1.5 ka. These events were not ubiquitarian, and happened differently in each different study area. In detail, in the Stelvio Pass Area, five successive events have been identified and dated before the LIA: 12.3 ka, 11 ka, 10-9.7 ka, 9 ka, and 7.5ka, while evidence of the LIA is limited to the Scorluzzo N glacier. Two more frontal morainic ridges are present at 2690 and 2710 m a.s.l, with the lower one datable to AD 1590 (Cannone et al., 2003). In this area, a small glacier was documented until AD 1952 (Cannone et al., 2003).

In the Viola Pass Area, four successive events have been identified and dated before the LIA instead: 16.7-14.7 ka, 12.3 ka, 11 ka, and 9 ka.

Moving to the Gavia Pass Area, seven successive events have been identified and dated before the LIA: 14.7 ka, 13.7 ka, 12.2-11.8 ka, 10.2-9.7 ka, 7.5 ka, 5.5 ka, and 1.9 ka, but the evolution was asynchronous between Mt. Gavia Glacier and Lake Bianco Glacier. More favorable conditions within the Lake Bianco catchment were also confirmed between the LIA and the last advance recorded in 1985 AD when the Lake Bianco Glacier was declared extinct, while Mt. Gavia Glacier was reported to reach 3005 m a.s.l. in 2015. Glacial evolution over the last 30 years is mainly related to the different degree of debris coverage on the two glaciers: the thicker and more continuous debris cover of Lake Bianco Glacier allowed the conservation of more glacier ice, whereas the less extensive debris cover of Mt. Gavia Glacier preserved only a minimal volume of white glacier ice in 2015.

Finally, a total of six different glacial phases were identified and dated for the Forni Area before the LIA: 15 ka, 12.2 ka, 9.5 ka, 4.1 ka, 3.2 ka, and 1.5 ka.

Generally, these phases are generally consistent with the literature (Burga et al., 1987; Ivy-Ochs et al., 2006; Hormes et al., 2008; Chenet et al., 2016; Moran et al., 2016; Scotti et al., 2017). However, their extension was very different; this is evidenced by the reduced glacier extent in Val Viola with respect to the previous reconstruction for the Gschnitz II stadial. It is also remarkable that in some

part of this sector of the Central Alps (Gavia Pass area and Stelvio Pass area), the glacial advances around 7.5 ka and 5.3 ka were more extended than during the LIA. In contrast, other alpine valleys had smaller glaciers during these two time periods (Ivy-Ochs et al., 2009). The comparison of the glacial evolution in the Forni Valley with the one in the adjacent area of the Gavia Pass and of a similar glacier located in the northern side of the Alps, the Triftjegletscher (Kronig et al., 2018) showed that the morphology of the catchments (i.e., area, slope, aspect, and maximum altitudes) was more important than proximity in the glacial evolution during the Holocene. Indeed, while in similar glaciers even if located on a different sector of the Alps like the Forni glacier and Triftjegletscher the LIA is the second most expanded glacial phase during all the Holocene, in the adjacent Gavia Pass Area its extent is definitely smaller than every other Holocene advances.

Despite the LIA in the Forni Valley was almost equal to the 9.5 ka in phase and therefore a large part of the roches moutonnées was re-covered by ice during the LIA, it was possible to date the maximum of the LIA expansion in 1810 AD and to underline probably during that time the glacier was cold-based.

Finally, soil micromorphology has been proven as a good tool for past permafrost limit reconstruction. It was possible to define the lower limit of Holocene permafrost in Stelvio Pass area at 2228m a.s.l. and in Val Cantone area at 2347m a.s.l., agreeing with the limit of relict permafrost proposed by Guglielmin and Siletto (2000).

Four different podzolization phases have been dated in the study areas: 13.5-11.5ka, 11-9.7ka, 9.3-8ka, and 7.7-7.3ka. Moreover, analyzing precipitation and temperature conditions, glacial phases, and the lower boundary of permafrost, it was possible to determine two different permafrost aggradation periods at 11-9.7ka and 9.3-8ka, synchronous to podzolization in Val Cantone. In Stelvio Pass area, instead, three different permafrost aggradation periods synchronous to podzolization have been found at 11-9.7ka, 9.3-8ka, and 7.7-7.3ka.

To conclude, it is clear that the glacial evolution of the four close different areas has been different in time and space, even if some similarities have been shown: it is clear that to better reconstruct the glacial evolution of the Alps, more local data are needed. Further investigations are suggested for the comprehension of the occurrence of a different direction of transfluence on Gavia Pass before the Youngest Dryas. More data are also desirable to better analyze the effect of the glacial re-coverage over previously exposed roches moutonnées.

6. ACKNOWLEDGMENTS

I would firstly like to thank my supervisor Mauro through whom this Ph.D. project has been possible, both logistically and scientifically. Mauro follows me from my bachelor thesis, and thanks to him I got all the knowledge I have now.

I also have to thank the referees of this manuscript for their precious help.

My whole family, Erminio, Giancarla, and Giulia must receive my heartfelt thanks, as they supported me even if they can't really understand what a Ph.D. is: you've always been by my side and guided me even in bad times, thank you! A big greeting also to all my grandparents who I am sure would be proud and full of joy for this moment, although they cannot be by my side anymore.

Thanks also to my dear friends Alessandro, Carola, Chiara, Davide, Elisa, Gabriele, Giulia, Maria, Matteo, Paolo, Pietro, Sara, Selena, Silvia, Simone, and Stefano.

The last thank you is for my research group mates Francesco, Giulia, Silvia, and Stefano, which shared their knowledge with me and supported me in fieldwork.

I finally would like to thank the Parco Nazionale dello Stelvio for its logistic support during my movements, without which I would have never met the fantastic people I know in Bormio.

7. REFERENCES

Alverson K.D., Bradley R.S., Pedersen T.F. (eds.), 2003. Paleoclimate, Global Change and the Future. International Geosphere Biosphere Programme Book Series, Springer-Verlang, Berlin, 221p.

Angelucci D., Cremaschi M., Negrino F., Pelfini M., 1992. The Dosso Gavia Mesolithic site. Gavia Valley (Sondrio - Italy): environment and peopling during the early Holocene in the CentraI Alps. Preistoria Alpina 28, 19-32

Arduino E., Barberis E., Marsan F.A., Zanini E., Franchini M., 1986. Iron Indexes and clay minerals within profiles as indicators of soil age in Northern Italy. Geoderma 37, 45-55.

Arduino E., Barberis E., Carraro F., Forno M.G., 1984. Estimating relative ages from iron-oxides/total-iron ratios of soils in the western Po Valley, Italy. Geoderma 33, 39-52.

ASTM, 2007. Standard Test Method for Particle Size Analysis of soil. ASTM D422-63.

Berthel N., Schworer C., Tinner W., 2012. Impact of Holocene climate changes on alpine and treeline vegetation at Sanetsch Pass, Bernese Alps, Switzerland. Review of PaleoBotany and Palynology, 91-100.

Bilzi A.F., Ciolkosz E.G., 1977. A field morphology rating scale for evaluating pedological developments. Soil Sciences 124, 45-48.

Bini A., Buoncristiani J.F., Couterrand S., Ellwanger D., Felber M., Florineth D., Graf H.R., Keller O., Kelly M., Schlüchter C., Schoeneich P., 2009. Swiss federal office of topography, Wabern, Switzerland. Switz. Dur. Last Glacial Maximum 1, 500,000.

Birkeland P.W., 1999. Soils and Geomorphology, Oxford University Press, New York. 3rd edition.

Blume L.J., B.A. Schumacher P.W., 1990. Handbook of Methods for Acid Deposition Studies Laboratory Analyses for Soil Chemistry. EPA/600/4-90/023. U.S. Environmental Protection Agency, Las Vegas, NV.

Boeckli, Lorenz; Brenning, A; Gruber, A; Noetzli, Jeannette (2012): Alpine permafrost index map. PANGAEA, https://doi.org/10.1594/PANGAEA.784450, Supplement to: Boeckli, L et al. (2012): Permafrost distribution in the European Alps: calculation and evaluation of an index map and summary statistics. The Cryosphere, 6, 807-820, https://doi.org/10.5194/tc-6-807-2012.

Bohlert R., Mirabella A., Plotze M., Egli M., 2011. Landscape evolution in Val Mulix, eastern Swiss Alps – soil chemical and mineralogical analyses as age proxies. Catena 87, 313-325.

Bonani, G., Ivy S.D., Hajdas, I. Niklaus T.R., Suter M., 1994. AMS 14C age determinations of tissue, bone and grass samples from the Ötztal Ice Man. Radiocarbon 36, 247-250.

Boxleitner M., Ivy-Ochs S., Egli M., Brandova D., Christl M., Dahms D., Maisch M., 2019. The 10Be deglaciation chronology of the Göschenertal, central Swiss Alps, and new insights into the Göschenen Cold Phases. Boreas 48, 867– 878. https://doi.org/10.1111/bor.12394.

Bullock, P., Fedoroff, N., Jongerius, A., Stoops, G., Tursina, T., Babel, U., 1985. Handbook for Soil Thin Section Description. Waine Research Publications, Wolverhampton, 152 p.

Burga C.A., 1987. Gletscher- und Vegetationsgeschichte der Südrätischen Alpen seit der Späteiszeit, Denkschritfen der Schweizerischen Naturforschenden Gesellschraft, 101.

Cannone N., Sgorbati S., Guglielmin M., 2007. Unexpected impacts of climate change on alpine vegetation. Frontiers in ecology and the environment, 5, 360-364.

Cannone N., Guglielmin M., Hauck C., Muhll D.V., 2003. The impact of recent glacier fluctuation and human activities on permafrost distribution, Stelvio Pass (Italian Central-Eastern Alps). Proceedings of the 8thInternational Conference on Permafrost, Zurich, Switzerland, 21-25 July 2003, 125-130.

Cardassi S.P., 1995. Geologia del Quaternario e geomorfologia della Valle di Trafoi. Master's Thesis, University of Milan.

Ceriani M., Carelli M., 2000. Carta delle precipitazioni medie, massime e minime annue del territorio alpino della Regione Lombardia (registrate nel periodo 1891–1990). Servizio Geologico, Ufficio Rischi Geologici Regione Lombardia.

Clark R., 1994. TORS, ROCK PLATFORMS AND DEBRIS SLOPES AT STIPERSTONES, SHROPSHIRE, ENGLAND. Field Studies, 8, 451-472.

Chenet M., Brunstein D., Jomelli V., Roussel E., Rinterknecht V., Mokadem F., Biette M., Robert V., Lèanni L., ASTER team, 2016. (_^10)Be cosmic-ray exposure dating of moraines and rock avalanches in the Upper Romanche Valley (French Alps): Evidence of two glacial advances during the Late-Glacial/Holocene Transition. Quaternary Science Reviews 148, 209-221.

Comerci V., Capelletti S., Michetti A.M., Rossi S., Serva L., Vittori E., 2007. Land subsidence and Late Glacial environmental evolution of the Como urban area (Northern Italy). Quaternary International 173-174, 67-86.

Dal Piaz G.V., Del Moro A., Martin S., Venturelli G., 1988. Post-Collisional magmatism in the Ortler-Cevedale Massif (Northern Italy). Jb Geol. B.A. 131, 533-551.

Dawson A.G., Matthews J.A., Shakesby R.A., 1986. A catastrophic landslide (sturzstrom) in Verkilsdalen, Rondane National Park, southern Norway, Geografiska Annaler, 68A, 77–87.

de Menocal P., Ortiz J., Guilderson T., Sarnthein M., 2000. Coherent highland low-latitude climate variability during the Holocene warm period. Science 288, 2198-2202.

Dell C.I., 1959. A study of the mineralogical composition of sand in Southern Ontaio. Canadian Journal of Soil Science 39, 185-196.

Denton G.H., Karlén W.H., 1973. Holocene climatic variations: their pattern and possible cause. Quaternary Research 3, 155-205.

Duchaufour P., 1983. Pedologie: 1. Pedogenese et classification, Paris, 59.

Egli M., Lessovaia S.N., Chistyakov K., Inozemzev S., Polwkhowsky Y., Ganyushkin D., 2015. Microclimate affects soil chemical and mineralogical properties of cold-alpine soils of the Altai Mountains (Russia). Journals of soils and sediments 15, 1420-1436.

Egli M., Sartori G., Mirabella A., Giaccai D., 2010. The effects of exposure and climate on the weathering of late Pleistocene and Holocene Alpine soils. Geomorphology 114, 466-482.

Egli M., Wernli M., Kneisel C., Haeberli W., 2006. Melting glaciers and soil development in the proglacial area Morteratsch (Swiss Alps): I. Soil type chronosequence. Arctic, Antarctic, and Alpine Research 38, 499-509.

Egli M., Mirabella A., Sartori G., Fitze P., 2003. Weathering rates as a function of climate - results from a climosequence of the Val Genova (Trentino, Italian Alps). Geoderma 111, 99-121.

ERSAF, 2012. http://www.ersaf.lombardia.it.

Evans D.J.A., Archer S., Wilson D.J.H., 1999. A comparison of the lichenometric and Schmidt hammer dating techniques based on data from the proglacial areas of some Icelandic glaciers. Quaternary Science Reviews 18, 13-41.

FAO. 2014. World reference base for soil resources 2014: International soil classification system for naming soils and creating legends for soil maps.

FAO, 2006. Guidelines for soil description. Food and Agriculture Organization of the United Nations, Rome, 109.

Favilli F., Egli M., Mirabella A., Sartori G., Giaccai D., 2008. High Alpine landscape evolution in Val di Sole (Trentino, Italy) during the Holocene based on charcoal, soil chemistry and mineralogy. Rothenbühler, C. Klimaveränderungen auf der Spur. Samedan, 18-37.

Federici P., Ribolini A., Spagnolo M., 2016. Glacial history of the Maritime Alps from the Last Glacial Maximum to the Little Ice Age. Geological Society, London 433, 137-159.

Gardner W.A., 1986. Water Content. Methods of soil analysis, Part 1: Physical and Mineralogical Methods, American Society of Agronomy, Soil Society of America, 493-544.

Giacomini V., Pignatti S., 1955. Flora e vegetazione dell'alta valle del Braulio con speciale riferimento ai pascoli di altitudine. Fondazione per i Problemi Montani dell'Arco Alpino.

Godwin H., 1962. Half-life of radiocarbon. Nature 195, 984.

Guglielmin M., Worland M.R., Convey P., Cannone N., 2012. Schmidt Hammer studies in the maritime Antarctic: Application to dating Holocene deglaciation and estimating the effects of macrolichens on rock weathering. Geomorphology 155-156, 34-44.

Guglielmin M, 2007. Il Permafrost. Rapporti con l'evoluzione climatica e la dinamica geomorfologica. AIGeo. Insubria University Press.

Guglielmin M., Cannone N., Dramis F., 2001. Permafrost–glacial evolution during the Holocene in the Italian Central Alps. Permafrost and periglacial processes 12, 111-124.

Guglielmin M., Siletto G.B., 2000. Carta della Criosfera Regione Lombardia.

Guglielmin M., Tellini C., 1992. Contributo alla conoscenza dei rock glaciers delle Alpi Italiane. I rock glaciers del Livignasco.(Alta Valtellina, Sondrio). Riv. Geogr. It, 99, 395-414.

Harnois L., 1988. The CIW index: a chemical index of weathering. Sediment Geol 5, 319–322

Hannah G., Hughes P.D., Gibbard P.L., 2017. Pleistocene plateau ice fields in the High Atlas, Morocco. In: Hughes P.D., Woodward J.C. (Eds.) Quaternary glaciation in the Mediterranean Mountains. Geological Society of London Special Pubblications 433. 25-53.

Harden J.W., 1982. A Quantitative Index of Soil Development From Field Descriptions: Examples from a Chronosequence in Central California. Geoderma 28, 1-28.

Harrington C.D., Whitney J.W., 1987. Scanning electron microscope method of rock-varnish dating. Geology 15, 967–970

Harris C., Haeberli W., Vonder Mühll D., King L., 2001. Permafrost monitoring in the high mountains of Europe: the PACE project in its global context. Permafrost and Periglacial Processes, 12(1), 3-11.

Heiri O., Koinig K.A., Spotl C., Berret S., Brauer A., Drescher-Schneider R., Gaar D., Ivy-Ochs S., Kershner H., Leutscher M., Moran A., Nicolussi K., Preusser F., Schmidt R., Schoeneich P., Schworer C., Sprafke T., Terhost B., Tinner W., 2014. Paleoclimate records 60-8ka in the Austrian and Swiss Alps and their forelands. Quaternary Science Review 106, 186-205.

Hijmans R.J., Cameron S.E., Parra J.L., Jones P.G., Jarvis A., 2005. Very high resolution interpolated climate surfaces for global land areas. International journal of climatology 25, 1965-1978.

Hoffmann F.L., Haushofer C., 1872. Karte der Centralen Ortler-Gruppe, 1 : 72.000.

Holzhauser H., Magny M., Zumbuühl H.J., 2015. Glacier and lake-level variations in west-central Europe over the last 3500 years. The Holocene 15(6),789-801. doi:10.1191/0959683605hl853ra

Hormes A., Ivy-Ochs S., Kubik P.W., Ferreli L., Michetti A.M., 2008. Be-10 exposure ages of a rock avalanche and a late glacial moraine in Alta Valtellina, Italian Alps. Quaternary International 190, 136-145.

Huges P.D., Woodward J.C., Gibbard P.L., Macklin M.G., Gilmour M.A., Smith G.R., 2006. The glacial history of the Pindus Mountains, Greece. Journal of Geology 114, 413-434.

Ilyashuk E.A., Koinig K.A., Heiri O., Ilyashuk B.P., Psenner R., 2011. Holocene temperature variations at high-altitude site in Eastern Alps: a chironomid record from Schwarzsee ob Sölden, Austria. Quaternary Science Review 30, 176-191.

Iversen J., 1954. The Late-Glacial flora of Denmark and its relation to climate and soil. Danmarks Geologiske Undersøgelse II.række 80, 87-119

Ivy-Ochs S., Lucchesi S., Baggio P., Fioraso G., Gianotti F., Monegato G., Graf A.A., Akcar N., Christl M., Carraro F., Forno M.G., Schluchter C., 2018. New geomorphological and chronological constraints for glacial deposits in the Rivoli-Avigliana end-moraine system and the lower Susa Valley (Western Alps, NW Italy). Journal of Quaternary Science 33, 550-562.

Ivy-Ochs S., 2015. Glacier variations in the European Alps at the end of the last glaciation. Cuadernos de Investigation Geografica 41, 295-315.

Ivy-Ochs S., Kerschner H., Maisch M., Christl M., Kubik P.W., Schlüchter C., 2009. Latest Pleistocene and Holocene variations in the European Alps. Quaternary Science Review 28, 2137-2149.

Ivy-Ochs S., Kerschner H., Reuther A., Preusser F., Heine K., Maisch M., Kubik P.W., Schlüchter C., 2008. Chronology of the last glacial cycle in the European Alps. Journal of Quaternary Sciences 23, 559–573.

Ivy-Ochs S., Kerschner H., Reuther A., Maisch M., Sailer R., Schafer J., Kubik P.W., Synal H.A., Schlücher C., 2006. The timing of glacier advances in the Northern European Alps based on surface exposure dating with cosmogenic 10Be, 26Al, 36Cl, and 21Ne. In situ-produced Cosmogenic Nuclides and Quantification of Geological Processes. Geological Society of America special paper 415, 43-60.

Ivy-Ochs S., Schafer G., Kubik P.W., Synal H.A., Schluchter C., 2004. Timing of deglaciation on the northern Alpine foreland (Switzerland). Eclogae Geologicae Helvetiae 97, 47-55.

Jackson M.L.; Lim, C.H.; Zelazny, L.W.; 1986. Oxides, hydroxides, and aluminosilicates. Methods of Soil Analysis: Part 1. Physical and Mineralogical Methods, second ed. American Society of Agronomy, Inc., Soil Science Society of America, Inc., Madison, WI.

Jenny H., 1941. Factors of Soil Formation: A System of Quantitative Pedology, 281p.

Kalra Y.P., 1995. Determination of Ph of soils by different methods: collaborative study. Journal of AOAC International 2, 310-324.

Kerschner H., 2009. Gletscher und Klima im Alpinen Spätglazial und frühen Holozän. Schmidt, R., Matulla, C., Psenner, R. (Eds.), Klimawandel in Österreich. Die letzten 20.000 Jahre und ein Blick voraus. Innsbruck University Press, Innsbruck, 5-26.

Kerschner H., Ivy-Ochs S., 2007. Palaeoclimate from glaciers: examples from the Eastern Alps during the Alpine Lateglacial and early Holocene. Global and Planetary Change 60, 58-71.

Kershner H., Kaser G., Sailer R., 2000. Alpine Younger Dryas glaciers as paleo precipitation gauges. Annals of glaciology 31, 80-84.

Kronberg G.I., Nesbitt H.W., 1981. Quantification of weathering of soil chemistry and soil fertility, Journal of Soil Sciences 32, 453-469.

Kronig O., Ivy-Ochs S., Hajdas I., Christl M., Wirsig C., Schlüchter C., 2018. Holocene evolution of the Triftje- and the Oberseegletscher (Swiss Alps) constrained with (_^10)Be exposure and radiocarbon dating. Swiss Journal of Geoscience 111, 117-131.

Lal D., 1991. Cosmic ray labeling of erosion surfaces: in situ nuclide production rates and erosion models. Earth and Planetary Science Letters 104, 424-439

Laustela M., Egli M., Frauenfelder R., Kaab A., Maisch M., Heberly W., 2003. Weathering rind measurements and relative age dating of rockglacier surfaces in crystalline regions of the Eastern Swiss Alps. Proceeding of the 8th International Conference on Permafrost, Zurich, Switzerland, July 2003, pp. 627–632.

Lauterbach S., Brauer A., Andersen N., Danielopol D.L., Dulski P., Hüls M., Milecka K., Namiotko T., Obremska M., von Grafenstein U., Declakes participants, 2011. Environmental responses to Lateglacial climatic fluctuations recorded in the sediments of pre-Alpine Lake Mondsee (northeastern Alps). Journal of Quaternary Science 26, 253-267.

Libby W.F., 1952. Radiocarbon Dating. University of Chicago Press, Chicago.

Longhi A., 2018. Studio degli spodosuoli di alta quota per la ricostruzione della deglaciazione in Alta Valtellina. Università degli Studi dell'Insubria, Master Thesis.

Longhi A., 2015. Studio geomorfologico e geofisico dell'Alta Val Viola. Università degli Studi dell'Insubria, Bachelor Thesis.

Maejima J., Nagatsuka S., Higashi T., 2002. Application of the Crystallinity Ratio of Free Iron Oxides for Dating Soils Developed on the Raised Coral Reef Terraces of Kikai and Minami-Daito Islands, Southwest Japan. The Quaternary Research 41, 485-493.

Malfasi F., 2018. Manipulation experiments for the assessment and monitoring of climate change impacts on vegetation of in alpine and polar ecosystems. Università degli Studi dell'Insubria. PhD thesis XXX cycle.

Matthews J.A., Owen G., 2010. Schmidt hammer exposure-age dating: developing linear age-calibration curves using Holocene bedrock surfaces from the Jotunheimen–Jostedalsbreen regions of southern Norway. Boreas 39, 105-115.

McCarroll D., 1991. The age and origin of Neoglacial moraines in Jotunheimen, southern Norway: new evidence from weathering based data. Boreas 20, 283-295.

McCarroll D., 1989. Potential and limitations of the Schmidt hammer for relative-age dating: Field tests on Neoglacial moraines, Jotunheimen, southern Norway. Arctic and Alpine Research 21, 268-275.

McKeague J.A., Day D.H. 1966. Dithionite- and Oxalate-Extractable Fe and Al as Aids in Differentiating Various Classes of Soils. Canadian Journal of Soil Science 46(1), 13-22.

Mehra O.P., Jackson M.L., 1960. Iron Oxide Removal from Soils and Clay by a Dithionite-Citrate System Buffered with Sodium Bicarbonate. Clays and Clay Minerals, 7, 317-327.

Montrasio A., Berra F., Sciesa E., Mazzoccola D., Mair V., Longhin M., ..., Arzuffi L., 2012. Foglio 024 Bormio. Carta Geologica d'Italia alla scala 1: 50.000.

Moran A.P., Ivy-Ochs S., Schuh M., Christl M., Kerschner H., 2016. Evidence of central Alpine glacier advance during the Younger Dryas-early Holocene transition period. Boreas 45, 398-410.

Mortensen M.F., Birks H.H., Christiansen C., Holm J., Noe-Nygaaard N., Odgaard B.V., Olsen J., Rasmussen K.L., 2011. Lateglacial vegetation development in Denmark – New evidence based on macrofossils and pollen from Slotseng, a small-scale site in southern Jutland. Quaternary Science Review 30, 2534-2550.

Nelson, D.W., Sommers L.E., 1996. Total carbon, organic carbon, and organic matter. Methods of Soil Analysis, Part 2, 2nd ed., A.L. Page et al., Ed. Agronomy. 9:961-1010. Am. Soc. of Agron., Inc. Madison, WI.

Nesbitt H.W., Young G.M., 1989. Formation and diagenesis of weathering profiles. J Geol 97, 129–147

Nesje A., Dahl S.O., 2003. The 'Little Ice Age' – only temperature? Holocene 13 (1), 139-145.

Nicolussi K., Schlüchter C., 2012. The 8.2 ka event--Calendar-dated glacier response in the Alps. Geology 40, 819-822.

Notapietro A., De Capitani L., 1985. Contributo alla conoscenza delle plutoniti austridiche dell'Alta Valtellina : il granito del Pizzo Bianco. Rendiconti della società italiana di mineralogia e petrologia 40, 353-363.

Ortu E., Peyron O., Bordon A., de Beaulieu J.L., Siniscalco C., Caramiello R., 2008. Lateglacial and Holocene climate oscillations in the South-western Alps: an attempt at quantitative reconstruction. Quaternary International 190, 71-88.

Owen G., Matthews J.A., Albert P., 2007. Rates of Holocene chemical weathering, 'Little Ice Age' glacial erosion and implications for Schmidt-hammer dating at a glacier–foreland boundary, Fåbergstølsbreen, southern Norway. The Holocene 17, 829-834.

Paliwal D.P., Thaper H.S., Paliwal G.S., 1984. A simplified seed identification key for nine species of Pinus on the basis of morphological and anatomical characters. Journal of Tree Sciences 3, 134-39.

Pelfini M., Leonelli G., Trombino L., Zerboni A., Bollati I., Merlini A., Smiraglia C., Diolaiuti G., 2014. Rendiconti Lincei 25, 427-437.

Pelfini M., 1992. Le fluttuazioni glaciali oloceniche nel Gruppo Ortles-Cevedale (settore lombardo). Universita` degli Studi di Milano. Earth Science Department, PhD thesis IV cycle.

Pettijohn F. J., 1975. Sedimentary rocks. 3rd ed. Harper and Row, PubI.

Pini R., Ravazzi C., Aceti A., Castellano L., Perego R., Quirino T., Vallé F., 2016. Ecological changes and human interaction in Valcamonica, the rock art valley, since the Last Deglaciation. Alpine and Mediterranean Quaternary 29, 19-34.

Ponti S., 2018. Analysis of the impacts of geomorphological disturbance on alpine and polar vegetation. Università degli Studi dell'Insubria. PhD thesis XXX cycle.

Rasmussen S.O., Bigler M., Blockley S.P., Blunier T., Buchardt S.L., Clausen H.B., Cvijanovic I., Dahl-Jensen D., Johnsen S.J., Fischer H., Gkins V., Guillevic M., Hoek W.Z., Lowe J.J., Pedro J.B., Popp T., Seiestard I.K., Steffensen J.P., Svensson A.M., Vallelonga P., Vinther B.M., Walker M.J.C., Wheatley J.J., Winstrup M., 2014. A stratigraphic framework for abrupt climatic changes during the Last Glacial period based on three synchronized Greenland ice-core records: refining and extending the INTIMATE event stratigraphy. Quaternary Science Review 106, 14-28.

Ravazzi C., Pini R., Badino F., 2014. The latest LGM culmination of the Garda Glacier (Italian Alps) and the onset of glacial termination. Age of glacial collapse and vegetation chronosequence. Quaternary Science Review 105, 26-47.

Ravazzi C., Badino F., Marsetti D., 2012. Glacial to paraglacial history and forest recovery in the Oglio glacier system (Italian Alps) between 26 and 15 ka cal BP. Quaternary Science Reviews 58, 146-161.

Ravazzi C., A. Aceti, 2004.The timberline and treeline ecocline altitude during the Holocene Climatic Optimum in the Italian Alps and the Apennines, in Lithopaleoenvironmental maps of Italy during the Last Two Climatic Extremes. Explanatory Notes, a c. Antonioli F., Vai G.B., 32nd International Geological Congress, Firenze, 21-22.

Reimer P.J., Bard E., Bayliss A., Beck J.W., Blackwell P.G., Bronk Ramsey C., Buck C.E., Cheng H., Edwards R.L., Friedrich M., Grootes P.M., Guilderson T.P., Haflidason H., Hajdas I., Hatté C., Heaton T.J., Hoffmann D.L., Hogg A.G., Hughen K.A., Kaiser K.F., Kromer B., Manning S.W., Nui M., Reimer R.W. Richards D.A., Scott E.M., Southon J.R., Staff A.R.A., Turney C.,

van der Plicht J., 2013. IntCal13 and Marine13 radiocarbon age calibration curves 0–50,000 years cal BP. Radiocarbon 55, 1869–1887.

Renssen H., Seppä H., Heiri O., Roche D.M., Goosse H., Fichefet T., 2009. The spatial and temporal complexity of the Holocene thermal maximum. Nat. Geosci. 2, 411-414.

Rolland Y., Darnault R., Brauscher R., Bourlès D., Petit C., Bouissou S., ASTER team, 2020. Deglaciation history at the Alpine-Mediterranean transition (Argentera-Mercantour, SW Alps) from ^{10}Be dating morains and glacially polished bedrock. Earth Surface Processes and Landform 45, 393-410.

Scapozza C., Ramelli G., 2010. Relative–age dating of rockglacier surfaces with Schmidt hammer in Blenio Valley, Southern Swiss Alps, Thermal state of frozen ground in a changing climate during the IPY. Abstracts from the Third European Conference on Permafrost, Svalbard, Norway, 13–17 June 2010, p. 288.

Schimmelpfennig I., Schaefer J.M., Akçar N., 2014. A chronology of Holocene and Little Ice Age glacier culminations of the Steingletscher, Central Alps, Switzerland, based on highsensitivity beryllium-10 moraine dating. Earth and Planetary Science Letters 393, 220–230.

Schimmelpfenning I., Schaefer J.M., Akcar N., Ivy-Ochs S., Finkel R.C., Schlucter C., 2012. Holocene glacier culmination in the Western Alps and their hemispheric relevance. Geology 40, 891-894.

Schlichtherle H., 1985. Samen und Früchte. In: Strahm C., Uerpmann H.P.S. (eds.) Quantitative Untersuchungen an einem Profilsockel in Yverdon, Avenue des Sports. Freiburg i. Br., 7-43.

Schwertmann U., 1964. Differenzierung der Eisenoxide des Bodens durch Extraktion mit Ammonium-Lösung. Z. Pflanzenernähr Düng Bodenk 105(3), 194-202.

Scotti R., Brardinoni F., Crosta G.B., Cola G., Mair V., 2017. Time constraints for post-LGM landscape response to deglaciation in Val Viola, Central Italian Alps. Quaternary Science Review 177, 10-33.

Scotti R., Brardinoni F., Alberti S., Frattini P., Crosta G.B., 2013. A regional inventory of rock glaciers and protalus ramparts in the central Italian Alps. Geomorphology 186, 136-149. https://doi.org/10.1016/j.geomorph.2012.12.028.

Senese A., Diolaiuti G.A., Verza G.P., Smiraglia C., 2012. Surface energy budget and melt amount for the years 2009 and 2010 at the Forni Glacier (Italian Alps, Lombardy). Geografia Fisica e Dinamica del Quaternario 35, 69-77.

Shakesby R.A., Matthews J.A., Owen G., 2006. The Schmidt hammer as a relative-age dating tool and its potential for calibrated-age dating in Holocene glaciated environments. Quaternary Science Reviews 25, 2846-2867.

Smiraglia C., Diolaiuti G.A.,(Editors) 2015. The New Italian Glacier Inventory. Ev-K2-CNR, Bergamo Publ., 400 pp.

Stone J., 2000. Air pressure and cosmogenic isotope production. Journal of Geophysical Research 105, 23753-23760.

Stoops, G., Marcelino, V., Mees, F., 2018. Interpretation of micromorphological features of soils and regoliths. Second Edition. Elsevier, Oxford, 1000 p.

Stoops, G., 2003. Guidelines for Analysis and Description of Soil and Regolith Thin Sections. Soil Science Society of America, Madison, 184 p.

Sumner P., Nel W., 2002. The effect of rock moisture on Schmidt hammer rebound: tests on rock samples from Marion Island and South Africa. Earth Surface Processes and Landforms 27, 1137-1142.

Tobolski K., Ammann B., 2000. Macrofossil as records of plant responses to rapid Late Glacial climatic change at three sites in the Swiss Alps. Paleogeography, Paleoclimatology, Paleoecology 159, pp. 251-259.

Törnqvist T.E., Rosenheim B.E., Hu P., Fernandez A.B., 2015. Radiocarbon Dating and Calibration. In Handbook of Sea-Level Research, First Edition. Edited by Ian Shennan, Antony J. Long, and Benjamin P. Horton.

Tremblay M.M., Shuster D.L., Spagnolo M., Renssen H., Ribolini A., 2019. Temperatures recorded by cosmogenic noble gasses since the Last Glacial Maximum in the Maritime Alps. Quaternary Research 91 (2), 829-847.

Van Geel B., Mauquoy D., 2007. Plant Macrofossil Methods and Studies: Mire and Peat Macros. Encyclopedia of Quaternary Science 2007, 2315-2336.

Von Blanckenburg F., Willenbring J.K., 2014. Cosmogenic Nuclides: Dates and Rates of Earth-Surface Change. Elements, 10, 341-346.

Walker M.J.C., Berkelhammer M., Björk S., Cwynar L.C., Fisher D.A., Long A.J., Lowe J.J., Newnham R.M., Rasmussen S.O., Weiss H., 2012. Formal subdivision of the Holocene Series/Epoch: a discussion paper by a Working Group INTIMATE (Integration of ice-core, marine and terrestrial records) and the Subcommission on Quaternary Stratigraphy (International Commission on Stratigraphy). Journal of Quaternary Science 27, 649-659.

Walker M., Johnsen S., Rasmussen S.o., Popp T., Steffensen J.P., Gibbard P., Hoek W., Lowe J., Andrews J., Bjork S., Cwynar L.C., Hugen K., Kershav P., Kromer B., Litt T., Lowe J.D., Nakagawa T., Newnham R., Schwander J., 2009. Formal definition and dating of the GSSP (Global Stratotype Section and Point) for the base of the Holocene using the Greenland NGRIP ice core, and selected auxiliary records. Journal of Quaternary Science 24, 3-17.

Wang S., Ge Q., Wang F., Wen X., Huang J., 2013. Abrupt climate changes of Holocene. Chinese Geographical Science 23, 1–12.

Wanner H., Brönnimann S., 2013. Is there a global Holocene climatic mode? PAGES news, 20-1.

Wanner H., Solomina O., Grosjean M., Ritz S.P., Jetel M., 2011. Structure and origin of Holocene cold events. Quaternary Science Reviews 30, 3109-3123.

Westercamp C., Demmelmeyer H., 1997. Blattoberflächen mitteleuropa¨ischer laubgehölze: Leaf surfaces of central European woody plants. Atlas and Keys.

Willenbring J.K., Von Blanckenburg F., 2010. Meteoric cosmogenic Beryllium-10 adsorbed to river sediment and soil: Applications for Earth-surface dynamics. Earth-Science Reviews 98, 105-122.

Williams R.B.G., Robinson D.A., 1983. The effects of surface texture in the determination of the surface hardness of rock using the Schmidt hammer. Earth Surface Processes and Landforms 8, 289-292.

Wirsig C., Zasadni J., Christl M., Akçar N., Ivy-Ochs S., 2016. Dating the onset of LGM ice surface lowering in the High Alps. Quaternary Science Review 143, 37-50. https://doi.org/10.1016/j.quascirev.2016.05.001.

Wuthrich L., Morabito E.G., Zech J., Trauerstein M., Veit H., Gnagi C., Merchel S., Scharf A., Rugel G., Christl M., Zech R., 2018. Be-10 surface exposure dating of the last deglaciation in the Aare Valley, Switzerland. Swiss Journal of Geosciences 111, 295-303.

Zoller H., Athanasiadis N., Heitz-Waniger A., 1998. Late-glacial and Holocene vegetation and climate change at Palu glacier, Bernina Pass, Grisons Canton, Switzerland. Vegetation History and Archaeobotany 7, 241-249.